SECURE, FULL-DUPLEX MULTI-DOMAIN COMMUNICATION NETWORK FOR MARINE ROBOTS

by

Jay Patel

Submitted in partial fulfillment of the requirements
for the degree of Doctor of Philosophy

at

Dalhousie University
Halifax, Nova Scotia
April 2024

To my loving mother, mother-in-law and my family

Table of Contents

List of Tables

List of Figures

Abstract

The underwater channel is a difficult communications medium as its link quality depends on the highly variable seabed and water column characteristics that vary on hourly, weekly, monthly and seasonal scales. One of the thesis objectives is to understand the channel characteristics for data transmission/reception towards development and evaluation of existing or new communication (MAC and routing level) protocols that could better utilize the limited resources within this harsh and unpredictable communications channel. orthogonal frequency-division multiplexing (OFDM)andCDMAare promising physical layer and multiple access techniques for underwater-acoustic sensor networksUW-ASNs as they are: (i) robust to frequency selective fading; (ii) compensate for multi-path effects at the receiver, and (iii) allow receivers to distinguish between signals simultaneously transmitted by multiple devices through a unique code for each transmitting node. Therefore,CDMAincreases channel re-use and reduces packet re-transmissions, which results in decreased energy consumption and increased network throughput. This Ph.D. thesis proposes a communications framework for autonomous co-ordination and networking of marine robot teams from extended (over-the-horizon) ranges to transmit images/information from underwater to above water usingOFDM-basedCDMA. This creates a stack of communication protocols for marine robots that span multiple domains —that is under, on and above the water. Currently, there is no complete protocol stack which spans multiple domains in this way. This thesis proposes an innovativeOFDM-basedCDMAtopology and also presents preliminary results attesting to its effectiveness.

List of Abbreviations and Symbols Used

α	total absorption of sound waves in seawater.
$\eta(t)$	additive Gaussian white noise on the channel at time t.
$\gamma_{(\mathbf{l},\mathbf{f})}$	attenuation in the underwater acoustic channel.
ω_c	the angular frequency of the carrier signal used.
Ψ	unit pulse function.
τ_0	a random time offset used at the receiver.
$A(t)$	locally generated in-phase copy of the transmitted code sequence.
$a(f)$	absorption constant.
$a(t)$	a spreading sequence composed of orthogonal chips.
A/D	analog-to-digital
A_1	the absorption coefficient of Boric acid.
A_2	the absorption coefficient of Magnesium sulphate.
ACDMA	Asyncronous code division multiple access
a_i	an elements of the spreading code.
$a_\rho(t)$	time-variant amplitudes of the ρ^{th} path.
AUV	autonomous underwater vehicle
$\mathcal{B}$	length of the transmitted signal, which is pre-known at the receiver for DSF estimation.
$B(t)$	the de-spread signal.
$b(t)$	information/data signal.
$B_i(t)$	packet from transmitter i at time t.
BER	bit error rate
β_ρ	proportional change per unit time in the observed frequency of a wave, due to the motion of the source or observer (the Doppler effect).
β	doppler scaling factor for the duration scaling in the received signal.

b_j	a sequence of symbols.
$\mathcal{B}'$	estimated length of the received signal after cross-correlation with known preambles and/or post-ambles.
BPSK	binary phase shift keying
B_{symbol}	bandwidth of the symbol.
BW	bandwidth
$\mathcal{C}$	predefined set of orthogonal spreading codes $\{c_1, \ldots, c_n\}$.
$C(t)$	the spreaded the data signal in time.
$c(t)$	code signal.
c	speed of light in a vacuum inertial system.
CDMA	code division multiple access
CFO	Carrier Frequency Offset
CHS	canadian hydrographic service
$c_i(g)$	spreading code selected from a set of orthogonal codes for the g^{th} group.
c_k	Walsh code corresponding to the k^{th} column of the Walsh-Hadamard matrix.
COVE	the centre for ocean ventures and entrepreneurship
CP	cyclic prefix, a sequence of symbols appended at the start of anOFDMsymbol to mitigate intersymbol interference caused by multipath propagation.
CRC	cyclic redundancy check
D	bit data rate.
d	the time domainOFDMsymbol sequence obtained after applying IFFT to $\bar{d}$.
D/A	digital-to-analog
$\bar{d}$	theOFDMdata block in frequency domain after interleaving and before applying IFFT.
DCCL	dynamic compact control language
$\delta(t)$	dirac delta function, representing the impulse in the impulse response.
Δf	frequency spacing in the PN sequence.
Δ_ℓ	output of the de-spreading process for the ℓ-length code in the detection of the received signal.
DFT	discrete Fourier transform
$\widehat{\bar{d}}$	detected data after applying the Fast Fourier Transform (FFT) to the equalized signal.
$\hat{d}_\ell$	detected data after equalization at the ℓ^{th} subcarrier.

DSF	Doppler Scaling Factor, representing the change in frequency and phase of the signal due to the relative motion between transmitter and receiver.
$e_i(t)$	transmitted signal from transmitter i.
ℓ	index within the set $\{1, \cdots, n\}$ used in the despreading process, equivalent to the index of spreading codes.
EM	electro-magnetic
E_s	the energy per symbol.
f	frequency of sound waves in Hz.
f_0	carrier frequency for the OFDM system.
f_1	the frequency term for Boric acid.
f_2	the frequency term for Magnesium sulphate.
f_c	carrier frequency.
f_{chip}	chip frequency.
$f_{c,Rx}$	received carrier frequency.
FDMA	frequency division multiple access
fjåge	Framework for Java and Groovy Agents
$f_{\mathfrak{n}}$	frequency spacing of each sub-carrier affected by doppler induced frequency shift.
f_s	original sampling frequency used at the transmitter.
FSK	frequency shift-keying
f_{symbol}	symbol frequency.
γ	signal-to-noise ratio per symbol.
GEBCO	general bathymetric chart of the oceans
G_ℓ	MMSE equalizer matrix for the ℓ^{th} subcarrier.
$g(t)$	ADC-DAC function representing the filtering and pulse shaping process, approximated as a simple on-off function within the OFDM symbol time.
$h_{ir}(t)$	channel impulse response at time t.
$h_c(t)$	the complex low-pass signal.
$h(t)$	the impulse response of the spectrum-shaping filter.
HH-VBF	hop-by-hop vector-based forwarding
HITL	Hardware-in-the-Loop
H_ℓ	channel matrix for the ℓ^{th} subcarrier.
$H_\ell^{\mathbb{H}}$	Hermitian transpose of the channel matrix for the ℓ^{th} subcarrier.
HPBW	half-power bandwidth

$h(t, \tau)$	time-variant impulse response of the underwater channel model.
IDFT	inverse discrete Fourier transform
IF	Intermediate frequency
$i(g)$	index of the chosen spreading code for the g^{th} group, ranging from 1 to n.
IM	index modulation
I_N	identity matrix of size N.
IoUT	internet of underwater things
ISL	intelligent systems laboratory
JSON	JavaScript Object Notation
k	spreading factor.
K_0	scaling constant.
L	maximum underwater channel tap delay.
l	transmission distance.
LF	low frequency
LFSR	linear feedback shift register
$\hat{\ell}^{(g)}$	index of the detected spreading code for the g^{th} group, selected by maximizing the square absolute value of the correlation output.
LOS	line-of-sight
LPD	low probability of detection
LPI	low probability of interception
M	number of symbols in the M-ary digital modulation scheme.
$\mathcal{M}$	number of PN symbols in the sequence.
$m(t)$	the binary data signal.
$m_p(t)$	preamble.
m	spreading loss with values between 1 & 2.
MAC	medium access control
MAI	multiple access interference
$\mathcal{N}$	length of the PN sequence.
$\mathfrak{n}$	length of the spreading code or the number of possible spreading codes.
N_0	the noise power per unit bandwidth.
NCO	numerically controlled oscillator

NMCM	naval-mine countermeasures
NS2	Network simulator 2
NS3	Network simulator 3
OFDM	orthogonal frequency-division multiplexing
OLS	ordinary least squares
P_1	The pressure term for Boric acid.
$P_1^{(g)}$	first segment identifier for the index of the chosen spreading code in a group.
$P_2^{(g)}$	second segment mapped into a modulated symbol using an M-ary digital modulation scheme.
P_3	the pressure term for pure water.
PASE	python audio spectrogram explorer
PDF	packer delivery flow
P_e	the bit error rate.
PER	packer error rate
PLL	phase locked loop
PN	pseudo-random sequences
P_ℓ	ℓ^{th} symbol time domain PN sequence used as a guard band to avoid intersymbol interference (ISI).
PSD	power spectral density
$Q(x)$	rate at which errors occur in a communication.
QPSK	quadrature phase shift-keying
$r(t)$	ideal received signal.
RF	Radio frequency
ROS	robot operating system
ROS2	robot operating system-2
RRC	root raised cosine
RSSI	received signal strength indicator
$s(t)$	the up-converted signal.
SDOAM	software-defined open architecture acoustic modem
SDR	software defined radio
$s^{(g)}$	modulated symbol for the g^{th} group using an M-ary digital modulation scheme.
$s_i(t)$	spreading code for transmitter i at time t.
σ_n^2	variance of the noise.
s_ℓ	baseband signal for the ℓ^{th} OFDM symbol, including the PN sequence or cyclic prefix and the data symbol.

$\widehat{s_\ell}$	equalized signal at the ℓ^{th} subcarrier.
$S_n(t)$	a baseband signal.
SNR	signal-to-noise
$S_s(t)$	a passband signal.
SSP	sound speed profile
$\underline{S}(t)$	up-converted baseband signal to passband, incorporating the OFDM symbol and carrier frequency adjustments.
SVP	sound velocity profile
T	OFDM symbol time.
$\tau_\rho(t)$	time-variant delays of the ρ^{th} path with Doppler shift.
T_b	symbol rate.
T_c	chip rate.
TCP	transmission control protocol
TDMA	time division multiple access
T_s	symbol duration.
UAN	Underwater acoustic network
UAV	Uncrewed aerial vehicles
UDP	user datagram protocol
$u^{(g)}$	modulated constellation symbols spread over the spreading code, chosen based on the $P_1^{(g)}$ index bits.
$\hat{u}^g$	demodulated symbols for the g^{th} group after despreading the received signal with the detected spreading code.
ULF	ultra low frequency
$\underline{\upsilon}(t)$	passband additive white Gaussian noise (AWGN) affecting the received signal.
USV	Uncrewed surface vehicle
UUV	Uncrewed underwater vehicles
UW-ASNs	Underwater acoustic sensor network
UWAC	underwater acoustic communications
VBF	vector-based forwarding
VBVA	vector-based void avoidance
v_ℓ	noise at the ℓ^{th} subcarrier.
WDS	wireless distribution system
W_n	Walsh-Hadamard matrix of order n.
WOSS	world ocean simulation system

$\mathcal{X}$	transformation matrix used in the detection of frequency domain data symbols.
$\mathcal{X}^{(g)}$	vector representation of the spread sequence for the g^{th} group.
$x^{(g)}$	spread sequence created by spreading the modulated symbol $s^{(g)}$ with the spreading code $c_i(g)$.
$\hat{\mathcal{X}}^g$	estimated vector taken from the interleaved vector $\hat{\bar{d}}_\ell$ corresponding to subgroup g after de-spreading.
$y(t)$	transmitted signal from transmitter.
$\underline{y}_\ell$	received signal at the ℓ^{th} subcarrier after channel and noise effects.
$y(t)$	received passband signal at the receiver, including multipath components and effects of Doppler shifts.
Z_j	a decision statistic.

Acknowledgements

Throughout the writing of this dissertation I have received a great deal of support and assistance.

First and foremost, I would like to thank my supervisor Assoc.Prof. Dr. Mae Seto for her support and expertise through my time at Dalhousie. She not only provided the patient guidance and valuable suggestions but more importantly supported and encouraged me throughout the course. She has my utmost respect and gratitude for understating and believing in me, specially when I was overwhelmed with my family commitment. I would also like to extend my gratitude to my fellow researchers at the Intelligent Systems Lab and MedIT. Their willingness to help, offer suggestions, and engage in fruitful discussions have contributed significantly to the development of my dissertation.

A special thank you goes to Dr. Mandar Chitre and the entire team at Subnero Pvt Ltd for their expertise and valuable suggestions during my research. Their insights have greatly enriched the outcomes of this work.

I would like to acknowledge the financial support provided by Thales R&D, the Irving Chair in Marine Engineering and Autonomous Systems, NSERC CRD, and the Bruce and Dorothy Rosetti Engineering Research Scholarship.

To my friends and family, and especially to my wife, parents, and parents-in-law, I express my heartfelt appreciation for their unwavering support, encouragement, and wise counsel. Their love and understanding have been my pillars of strength throughout this journey. I am forever grateful for their sacrifices and belief in me. Finally, I want to extend my gratitude to my dear mother. Her unconditional love, unwavering encouragement, and countless sacrifices have played an invaluable role in shaping the person I am today. I owe her a debt of gratitude that can never be fully repaid.

Last but not least, I am thankful for the friendship and camaraderie of my friends Joel Lindsay, Franz, and Dr. Ali M. Bassam and all my lab mates. Their stimulating discussions and enjoyable distractions provided much-needed balance and respite from my research. No achievement is accomplished alone, and I am humbled and grateful for the support and contributions of all those who have been part of this journey.

Chapter 1

Introduction

[1]Jay Patel and Mae Seto. "CDMA-Based Multi-Domain Communications Network for Marine Robots". In Proceedings of the 14th International Conference on Underwater Networks & Systems (WUWNet '19). Association for Computing Machinery, New York, NY, USA, Article 9, 1–2. doi: https://doi.org/10.1145/3366486.3366520, [73].

1.1 Overview

Almost 75 % of the Earth is covered by water in the form of oceans, seas, lakes, rivers, basins, ponds, etc. To perform underwater environmental monitoring, ocean engineering, marine research and disaster prevention, it is critical that the underwater environment be characterized. This is still a critical area of research [80]. The military, industry and scientific research communities acknowledge this as evidenced through the rapidly emerging field of,internet of underwater things (IoUT). Such characterization is to achieve optimal underwater sensing and communications. Underwater communications is the focus of this thesis.

Four types of conventional communication systems exist in the underwater domain based onelectro-magnetic (EM), optical, magnetic induction and acoustic modalities. The propagation of vibrations (pressures) generated by a sound (acoustic) source through the air, or other media like water, is referred to as an acoustic wave.

Acoustic waves are the most feasible modality for underwater sensing and communication [101] compared to optical and electromagnetic (EM). From the research and development of maritime military, commercial and scientific activities, underwater acoustic sensor networks (UW-ASNs) have progressed rapidly in recent years.UW-ASNsare used in submarines, deep-sea manned submersibles, underwater wireless robots, remote control telemetry, data acquisition of seabed-based equipment, etc (Figure1.1). The underwater acoustic channel is a difficult communications medium due to its high spatio-temporal variability. Its channel characteristics can vary on the order of seconds, minutes, hours, days, months and seasonally.

Underwater communication mostly uses pressure waves (acoustics) to propagate signals through the water. Acoustic waves travel faster in denser media as closer neighboring particles can more rapidly propagate a signal (disturbance) passing through. For example, there are about 800 times more particles in a bottle of water than in the same bottle filled with air. Consequently, acoustic waves travel much faster in water (1500 m/s) than they do in air ($c \simeq 340$ m/s). For example, in room temperature freshwater, sound travels 4.3 times faster than it does in air at the same temperature [96].

The thesis contributions create advanced capabilities for robots to collaborate across domains. As defined in this thesis, domains consist of underwater, surface and above-water. Figure1.1depicts multiple uncrewed underwater vehicles (UUV) performing a collaborative underwater survey towards the common goal of localizing a target (not shown). They relay their findings to an uncrewed surface vehicle (USV), which coordinates them and relays their collaborative findings to an uncrewed aerial vehicle (UAV).

To achieve the underwater communications portion, it is necessary to characterize and understand theUUVs' communications performance for a given underwater channel as a function of water depth (at source and receiver),sound velocity profile (SVP), bottom type

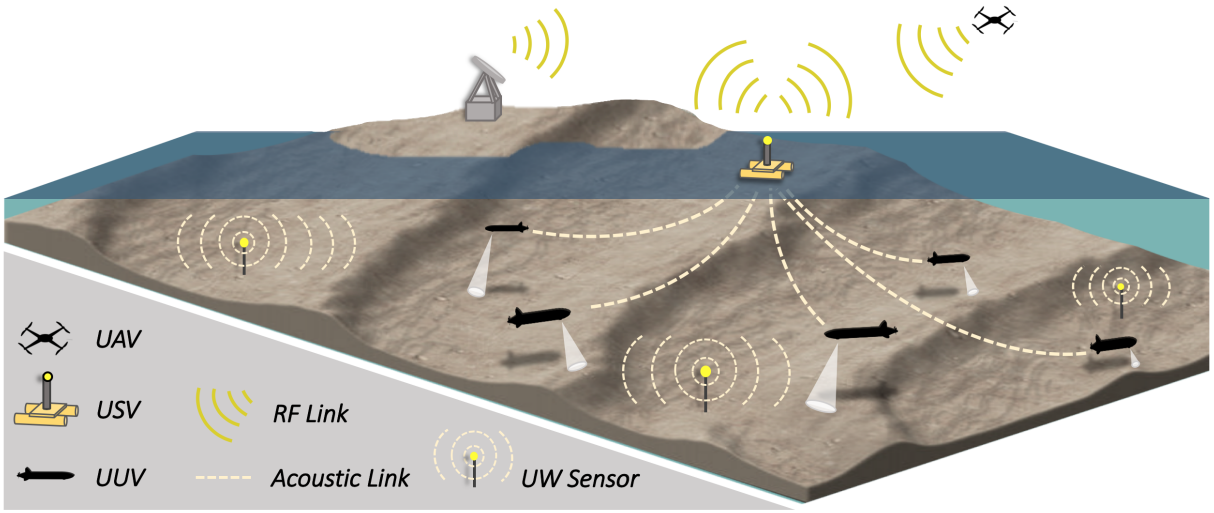

Figure 1.1: A heterogeneous system consisting ofUUV,USVandUAVrobotic platforms to support multi-domain collaborative sensing and communication nodes from below to above-water (and vice versa), relaying information acoustically from the underwater sensor UUVs to/fromUSV. From theUSVthe information is further relayed with traditional RF or satellite to a an over-the-horizon base station via aUAV[73].

(e.g. sand, silt, mud, etc.) and bathymetry [76] at a minimum. These environmental characteristics drive the underwater communication channel's performance. Equally important are signal parameters like its carrier frequency, bandwidth, and pulse characteristics [11] in this channel.

As the interest is in networked collaborative robotic platforms hosting communications (and sensing) nodes,UW-ASNsare discussed next.

1.2 Introduction to the Underwater Acoustic Channel andUW-ASNs

Generally, in communications a channel is the signal path in the medium from transmitter to receiver. For the underwater acoustic case, the channel is the path(s) taken by an acoustic signal in the underwater environment to its intended receiver. Several such paths are shown for a signal from transmitter to a receiver in Figure1.2.

Knowledge of channel characteristics make it possible to predict the channel effect (e.g. attenuation) on the received signal. Additionally, insight into channel characteristics that impact data transmission are essential for the development and evaluation ofmedium access control (MAC)and routing level protocols (a thesis objective). These protocols govern how to best utilize the channel. This is especially important in the harsh and

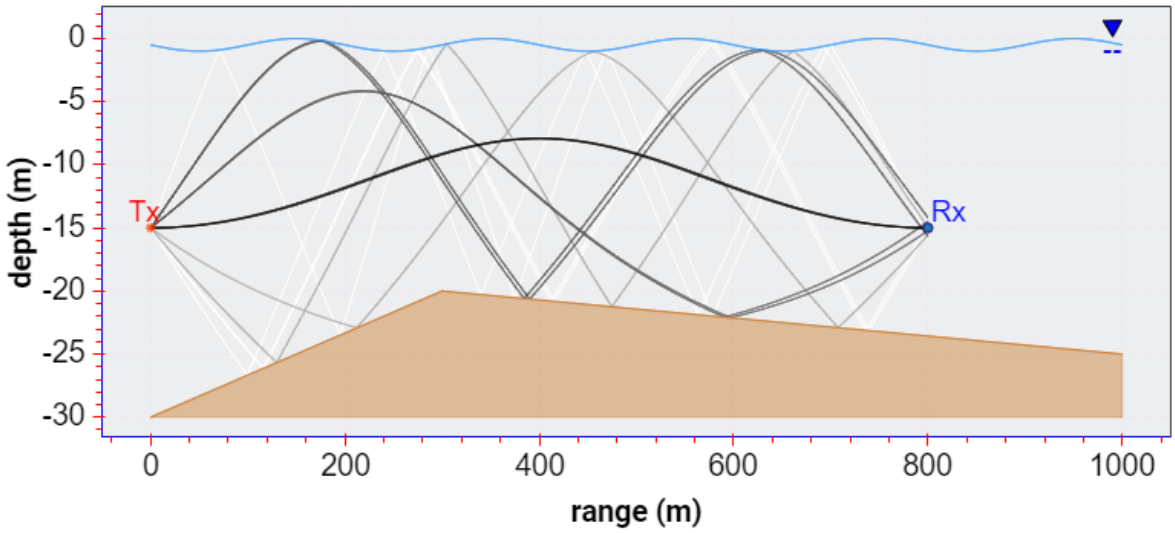

Figure 1.2: Representation of plane wave acoustic rays (normal to surface of constant phase fronts) propagating from a transmitter to a receiver in shallow water. Note, the acoustic wave traverses multiple paths to arrive at the receiver as it reflects from the (orange) seabed as well as a time-varying free surface (blue).

uncertain underwater environment which is challenged by the factors highlighted in the next section.UW-ASNs[58] can consist of sensors integrated onUUVs (also known as autonomous underwater vehicle (AUV)) andUSVs. Such vehicles could collaborate with above-water robots likeUAVs to perform, for example, collaborative monitoring tasks. Since these multi-domain vehicles collaborate, they must communicate. A use case is to transmit findings from the underwater robot network to above-water locations / operators / decision-makers or to transmit above-water instructions, underwater (Figure1.3). For theUUVandUSV, for which theUSVmust relay for the submergedUUV,MAC and routing level protocols become important, and play an essential role in underwater communications due to the unique challenges of this environment. They ensure efficient utilization of limited bandwidth (especially underwater), promote energy conservation by minimizing long propagation delays to some extent, and avoid data loss from signal collisions. In the dynamic underwater environment, marked by changing sea states, currents, and the mobility of nodes, routing protocols maintain effective data paths. Additionally, they adapt to complex and variable acoustic communication channels driven by factors such as temperature, pressure, salinity, sound speed profile and depth. The integration of these protocols is pivotal for efficient and reliable data exchange betweenUUVs,USVs, and other entities, supporting collaborative tasks and enabling the transmission of underwater findings to above-water locations, as well as the delivery of above-water instructions underwater.

UW-ASNsare built around key systems that are briefly introduced next.

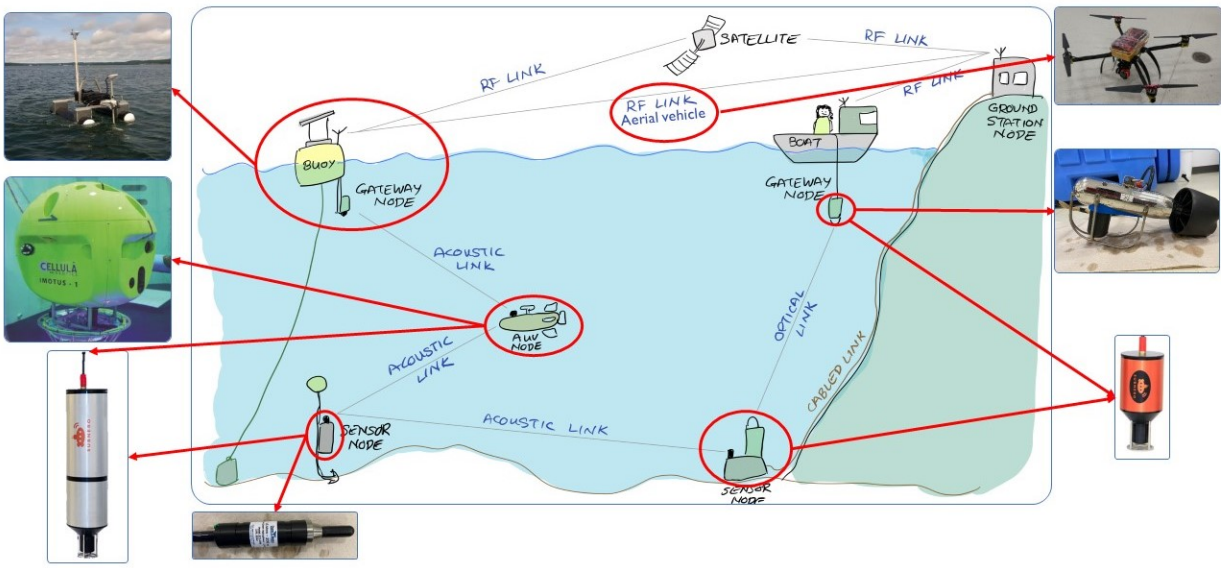

Figure 1.3: The network architecture of multi-vehicle collaboration above and below water, partially adopted from [9].

Through the efforts of decades of ocean engineering research, most underwater acoustic communication systems are now digital and include transmitter-receiver (transceiver) transducers, encoders / decoders, modulators/de-modulator and the acoustic channel itself, as shown in Figure1.4[101]. M. Stojanovic et al. [85] describes the basic functions of each component in such systems.

- **transmitter-receiver (transceiver) transducers**: These tranduce electrical signals into acoustic ones (in the transmitter), and vice versa (in the receiver). They essentially serve as the interface between the communication system and the water medium.
- **encoders / decoders**: Encoders convert information into signals that can be transmitted through the medium. On the receiving side, decoders convert or recover these signals back into their original form.
- **modulator / demodulator**: The modulator changes the characteristics of a carrier signal based on the information to be transmitted. This is performed so the receiver, equipped with a demodulator, can recover the original signal.
- **acoustic channel**: This refers to the underwater environment between transmitter and receiver through which the acoustic signals travel. Its characteristics, including temperature, salinity, pressure,SVPand motions, greatly affect the propagation of the signals.
- **digital-to-analog (D/A)andanalog-to-digital (A/D)converters** : digital-to-analog (D/A) converters are used in the transmitter to convert the digital signal

that has been generated into an analog signal that can be transmitted through the acoustic channel. analog-to-digital (A/D) converters in the receiver do the reverse, converting the analog signal received into a digital signal that can be processed and decoded.

- **amplifiers and filters**: amplifiers and filters play crucial roles in both the transmitter and receiver sections. In the transmitter, an amplifier boosts the signal power to ensure its propagation through the medium, while filters shape the signal, keeping it within the desired frequency range. Conversely, at the receiver, an amplifier enhances the weak received signals for easier processing and decoding. Meanwhile, filters help eliminate any unwanted signals or noise outside the required frequency range.

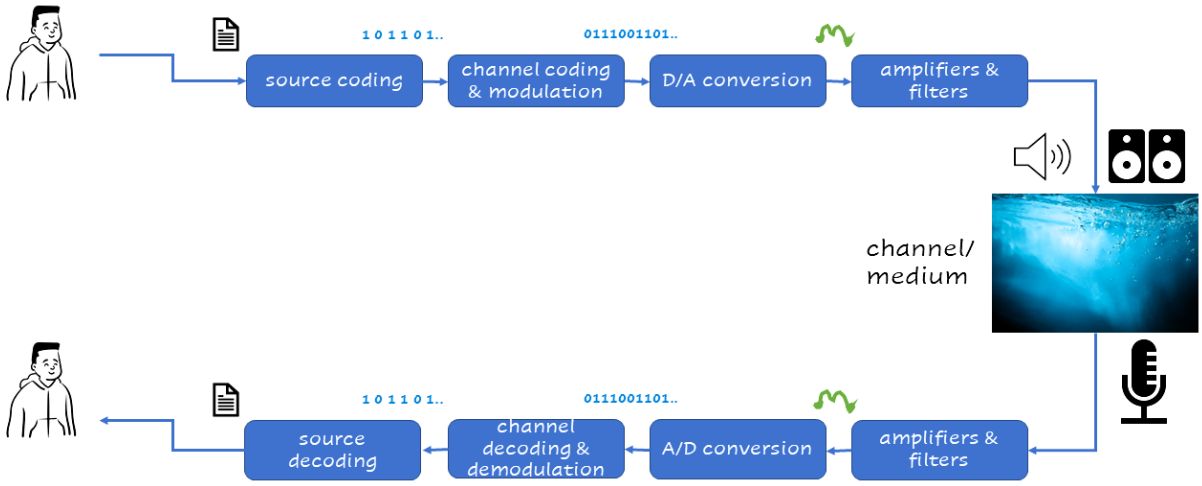

Figure 1.4: Typical structure and components of a full-duplexUW-ASNsdigital communications system.

Despite the extensive research and development to date, there are still fundamental challenges to design and implement underwater acoustic communication systems that are comparable in performance to their above-water counterparts. These include:

1.frequency and range dependent attenuation;

2.multi-path due to the rapidly time-varying (i.e. low channel coherence time) nature of the channel;

3.susceptibility to Doppler effects;

4.limitedbandwidth (BW), and

5.acoustic ambient noise.

1.2.1 Frequency and Range Dependent Attenuation

A notable challenge in the propagation of underwater acoustic signals is the range and frequency dependent attenuation. These are caused by the conversion of acoustic energy into heat, geometric spreading and absorption (among others). The attenuation is captured in Thorp's model [88–90]. Figure1.5aplots the attenuation as a function of distance (range) and Figure1.5bshows the half-power bandwidth (HPBW) for select frequencies relevant in underwater communication systems. From these, it can be seen that for long distance communications, the use ofultra low frequency (ULF)andlow frequency (LF)are advised as they suffer less attenuation. However, there is a trade-off to communicating withLFto achieve greater range and better reliability at the cost of bandwidth and data rate.

The other key factor that influences underwater acoustic communication is frequency-dependent attenuation. Frequency dependent attenuation in an underwater acoustic channel results from the loss of acoustic energy in the form of heat which is absorbed by the channel. The loss ($\gamma_{(\mathbf{l},\mathbf{f})}$) is describe by Eq.1.1

$$\gamma_{(\mathbf{l},\mathbf{f})} = K_0 * l^m * a(f)^l \tag{1.1}$$

such that K_0 is a scaling constant, l is the transmission distance, $a(f)$ the absorption constant and the exponent m describes the spreading loss with typical values between 1 and 2, indicating cylindrical ($m = 1$) or spherical ($m = 2$) spreading loss models [12,96].

Eq.1.2describes the seawater absorption coefficient at frequency f(kHz) [12] and is written as the sum of chemical relaxation processes and absorption from pure water (Figure1.6):

$$\overbrace{\alpha}^{\substack{\text{total}\\ \text{absorption}}} = \overbrace{\frac{A_1 P_1 f_1 f^2}{{f_1}^2 + f^2}}^{\substack{\text{boric}\\ \text{acid contribution}}} + \overbrace{\frac{A_2 f_2 f^2}{{f_2}^2 + f^2}}^{\substack{\text{magnesium}\\ \text{sulphate contribution}}} + \overbrace{P_3 f^2}^{\substack{\text{pure}\\ \text{water contribution}}} \tag{1.2}$$

such that α is the total absorption coefficient of seawater at frequency f(kHz); A_1, A_2, are the amplitude coefficients and P_1,, P_3 are the pressure dependencies for the boric acid, magnesium sulphate, and pure water contributions, respectively, while f_1, f_2 are the relaxation frequencies for the boric acid and magnesium sulphate contributions, respectively.

1.2.2 Multipath Effects

Underwater acoustic communications are heavily impacted by multipath propagation due to reflections, scattering, and refractions from the sea surface and seafloor as shown

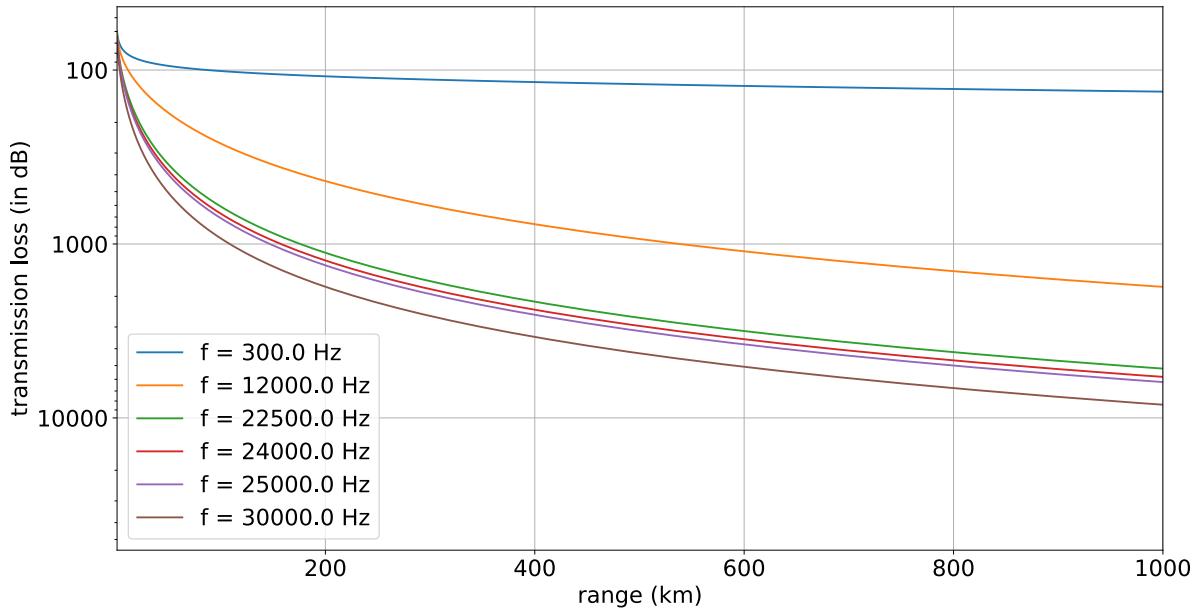

(a)

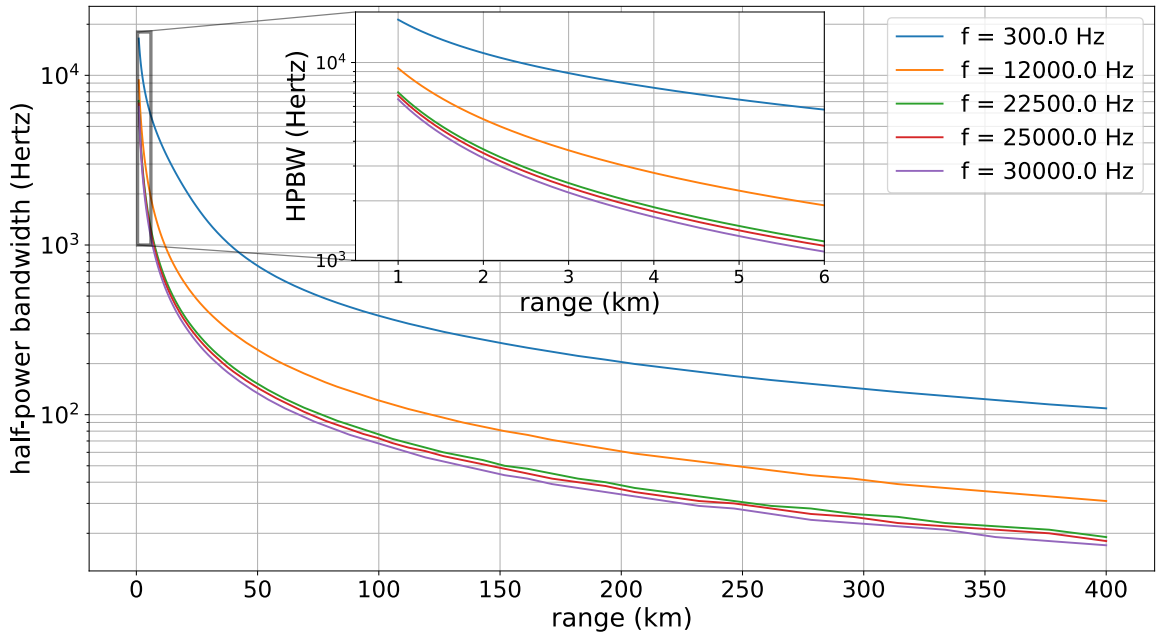

(b)

Figure 1.5: Properties of underwater acoustic propagation varies with signal carrier frequency: (a) range-dependent transmission loss and (b)HPBW. Note the relationship between theHPBWand frequency, with respect to range. For a range $\leq$ 17 km, theHPBW is better for lower frequencies ($\leq$300 Hz) than for higher ones within the same range. The inset picture in Figure1.5bhighlights theHPBWfor frequencies of interest in this thesis for a range of $\leq$ 6 km (Adapted from [11]).

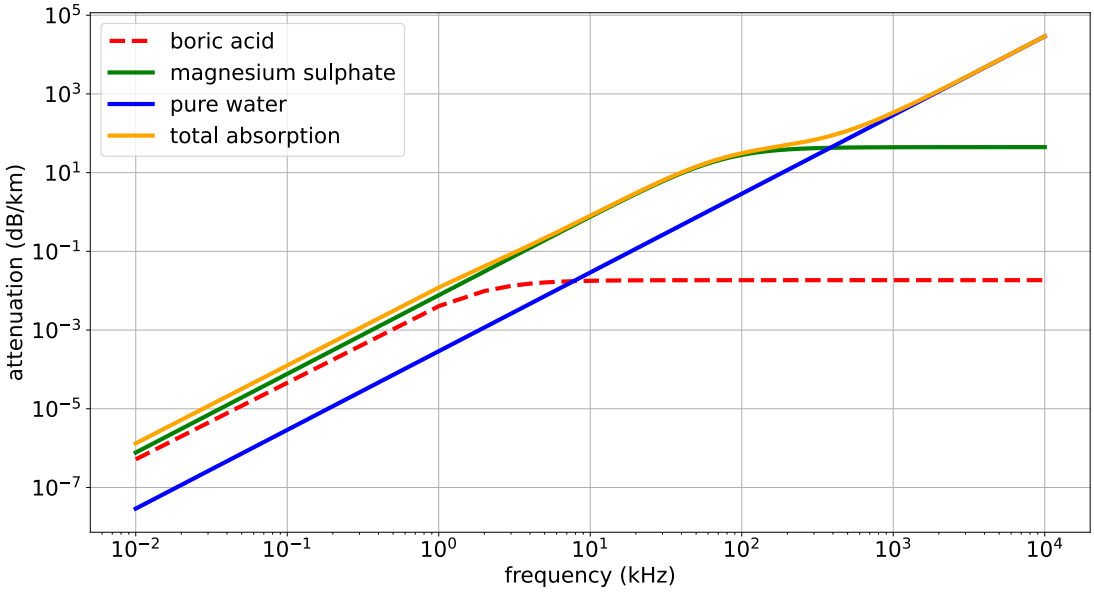

Figure 1.6: The relative contribution of dissolved oceans salts (boric acid, magnesium sulfate, and pure water) on the absorption of underwater acoustic energy with signal carrier frequency, ranging from 0.01 to 10,000 kHz. For the case shown, the water has a salinity of 35, temperature of 10 ℃, pH level of 7.8, and a depth of 500 meters. Note, magnesium sulphate at higher frequencies contributes the largest attenuation due to absorption. The total absorption (yellow) is also plotted, (re-generated from Ainslie and McColm, 1998 [12]).

in Figure1.2. Multipath is particularly pronounced in shallow horizontal channels and cause fading and phase-shifting of the transmitted signals, significantly complicating signal processing at the receiver. While multipath is a common in bothRFand underwater communication, it is considerably more severe in the latter due to two factors. Firstly, the underwater environment often contains multiple reflections between interfaces unlike in terrestrialRFcommunications. Finally, the speed of underwater acoustic signals is significantly lower (around 1500 m/s) compared to electromagnetic waves in free space. This much lower speed exacerbates multipath delay spread, even with minor path differences, which imposes substantial limitations on the transmission speed and quality inunderwater acoustic communications (UWAC)s [101].

1.2.3 Doppler Effects

Underwater environments present additional challenges like Doppler shifts which are due to the relative velocity between transmitter and receiver being a notable percentage of the speed of sound. These shifts are particularly prominent in marine robotic networks, where the robots are mobile. Doppler shifts can cause a change in signal frequency at the receiver, leading to potential misinterpretation of the signal. Misinterpretation may then lead to errors in decoding, thus reducing the reliability and performance of the communication system [16,17,80].

1.2.4 Limited Bandwidth

As previously discussed, lower frequencies propagate further underwater. Consequently, the communication carrier frequencies typically used are in the range of 10 - 60 kHz to achieve greater ranges. However, bandwidth scales with the carrier frequencies as they are usually 20% of the carrier frequencies [21,46]. For the WHOI Micro-Modems initially used in this thesis, their 25 kHz carrier frequency results in a bandwidth of about 5 kHz. This is quite low compared to above-water RF carrier frequencies that are in the MHz and GHz due to higher supported carrier frequencies. Consequently, there is little bandwidth for underwater transmissions.

1.2.5 Underwater Acoustic Ambient Noise

Noise is generated by uncorrelated sources and interference inherent in devices and channels in a communication system [101]. Physical noise is created by water currents, breaking waves, thermal agitation, and other natural oceanographic phenomena. Biological noise arises from marine life activities, such as the movements and vocalizations of fish, whales, and other underwater organisms.

It is also generated by anthropogenic sources like underwater blasting, military sonars, underwater construction, ships. As shown in Figure1.7, from 20 - 500 Hz the primary contribution to the underwater acoustic ambient is shipping. In the range of 500-100,000 Hz, the underwater acoustic ambient is mostly due to spray and bubbles associated with breaking waves. At frequencies above 100,000 Hz, the underwater acoustic ambient is fairly broadband and dominated by the random motion of water molecules (thermal noise) [32]. Since then, the ocean acoustic ambient has increased by 3 dB per decade. While device noise also impacts system performance, it is typically orders of magnitude less than the external dominant underwater noise sources in the channel.

A high underwater ambient is a challenge to underwater acoustic communications as it provides a substantial noise floor communication systems must transmit and receive through. The signal-to-noise ratio underwater is generally not high, leading to communication errors and reducing the overall system performance. Therefore, insight and mitigation of such noise sources are vital to the development of efficient and reliable underwater acoustic communication systems.

The most dominant challenges for the proposed network addressed in the thesis are frequency and range dependent attenuation, Doppler effects and the acoustic ambient.

Given the above outlined challenges of underwater acoustic propagation it is recommended that, as much as possible, data from underwater sensors collected byUUVs be data-reduced on-board into information so they can be transmitted off theUUVwith much less bandwidth given there is not much available bandwidth to begin with.

This brief introduction to the underwater acoustic channel and its challenges provides

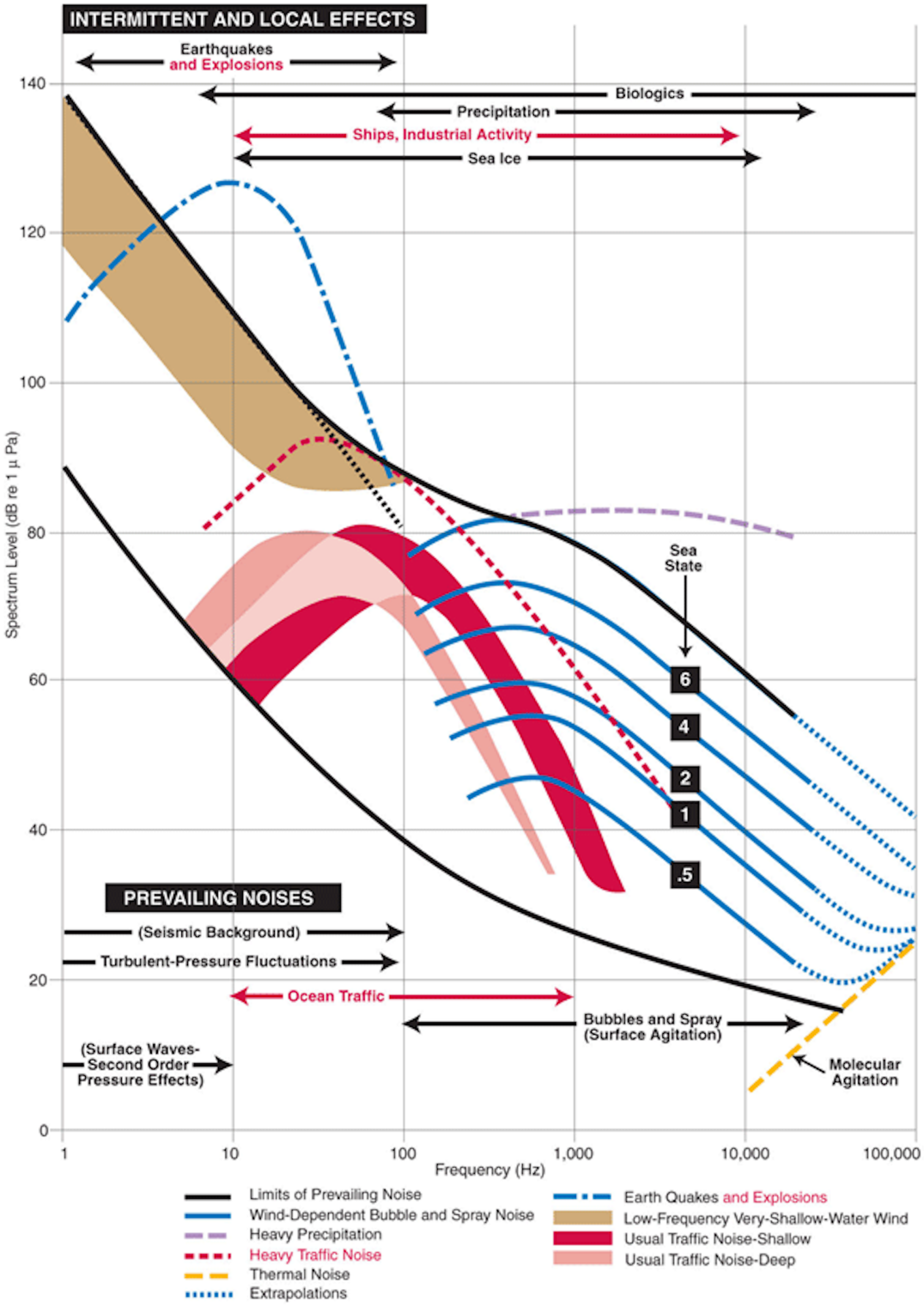

Figure 1.7: General acoustic levels of ocean ambient acoustic noise over different frequency bands in 1962 (Wenz curves —1962) [32].

the backdrop for the next sub-section which presents the motivation and direction for the thesis work.

1.3 Background and Motivation

OFDM-based code-division multiple access (CDMA) is proposed as a protocol to support networked heterogeneous collaborating marine robots which are mobile collaborative communication nodes. While CDMA use above-water is fairly established, it is not really used underwater.

A challenge to deploy the proposed multi-domain network is the development of aMAC protocol that spans domains that are under, on, and above water. Underwater and above-water networks have very different environmental communication challenges to contend with.CDMAis a promising physical layer and multiple access technique for underwater sensor networks since it: i) is robust to frequency-selective fading; ii) compensates for multi-path effects at the receiver by exploiting Rake filters [34], which collect the transmitted energy distributed over multiple rays [34,36,78,82]; iii) optimally uses the underwater channel and has bandwidth for multiple receiver nodes since it can distinguish multiple signals, embedded within a single signal —results in higher update rates; iv) generates signals resilient to ambient noise and thus achieves a higherSNRratio, and v) encodes the embedding in (iii) to provide a level of security by controlling access through unique random access codes for each node. For these reasons,CDMAincreases channel re-use and reduces packet re-transmissions, which ultimately results in decreased energy consumption. This has the hallmarks of a good protocol for multi-domain marine communications.

To efficiently utilize the limited underwater channel bandwidth, it is proposed that an OFDM-basedCDMA-based communication protocol be studied to evaluate how well it addresses the multi-domain challenges of the overall network configuration. This thesis will develop an underwater OFDM-basedCDMAprotocol which allows its mesh nodes to communicate on the same shared channel. As well, the thesis create a framework for autonomous co-ordination and networking of marine robot teams to transmit information (and images) to and from the underwater and above-water domains. In this context,user datagram protocol (UDP)is favored overtransmission control protocol (TCP)for data transfer. This choice is motivated by lessons learned from the UNMANNED WARRIOR 2016 Exercise [6], an international scientific trial, where the use ofTDMAled to sub-optimal bandwidth utilization. With the proposedCDMAprotocol, it is expected that full channel bandwidth can be simultaneously used for multiple signals, enhancing bandwidth efficiency and reducing transmission delays.

To address the problem statement, there are four primary objectives and areas of study:

1. develop a process model to predict environmental conditions given available a priori information (e.g. seasonal sound velocity profile);

2.design and implement an underwaterCDMAnetwork simulation testbed which captures/mimics the environmental (channel) conditions and serve as a development environment for the aforementioned novel protocols;

3.design and implement aCDMAnetwork configuration for software-defined acoustic modems, and

4.relaying the above-waterCDMAand underwaterCDMAnodes.

Spread spectrum systems, however, have inherent resistance to Doppler effects. Unlike other multiplexing techniques,CDMAallows all users to use the entire bandwidth concurrently. Each user has a unique code or key, which is used to modulate their signal. The receiver then uses this code to demodulate the signal and extract the original data. This process, combined with the spread spectrum nature ofCDMA, mitigates the effects of Doppler shifts to some extent. The spread spectrum feature ofCDMAalso makes it resistant to multi-path propagation effects, which are common in underwater communications.

By employing anOFDM-basedCDMAcommunication protocol, this research aims to overcome the challenges imposed by Doppler shifts, further enhancing the reliability and efficiency of underwater communications. The robustness ofCDMAto Doppler shifts and other underwater channel impairments makes it a promising technique for the efficient and reliable transmission of data in marine robotic networks.

1.3.1 Motivation

The transmission of information from distributed teams of marine robots at ranges beyond the horizon from their support ship, to the support ship (or shore-based station), is of interest to the ocean industry. The support ship monitors and manages the robot teams' efforts and objectives. These teams consist of marine robots that are under (UUV), on (USV), and well-above (UAV) the water. For transmission of information from underwater to above-water (and vice versa), a reliable established link is needed between them. The information (in situ processed sensor data) must be transmitted off theUUV to an underwater receiver that has an above-water expression and could re-broadcast/relay in-air. It is very difficult to directly transmit acoustically through the air-water interface – especially from the water side. There are several possible solutions. AnUSVwith an integrated underwater acoustic receiver and an in-air radio could provide such above- and below-water relaying (Figure1.3). The merits of this method are evaluated against other possibilities, next.

One way to transmit theUUVinformation above-water is for theUUVto surface and broadcast from the water surface. While easy to implement, there are disadvantages. Firstly, frequent surfacing and subsequent diving adds mission overhead and takes time – especially when operating in deep water. During the surfacing and diving, theUUVis not performing its task (e.g., survey). Secondly, surfacing adds uncertainty to the submerged UUVlocalization. While theUUVcould reduce its position error on the surface with

a GPS calibration, when it spirals back down to depth, especially in deep water, this compromises the dead-reckonedUUVposition through constant heading changes (when dead-reckoned position errors grow rapidly). The position error growth is slower if anUSV assists the at-depthUUVs' position based on theUSV's known GPS position and its range and bearing from the submergedUUV(s) [82]. This assumes anUSVcould be deployed to begin with. Finally, when surfaced, theUUVmay not have enough broadcast power to repeatedly transmit its information far (e.g. to the ship or a satellite). Alternatively, it is possible, depending on sea state, for theUUVto transmit low bandwidth information to a satellite from the surface. Due to the difficulty (and cost) in securing a satellite connection at sea level, this is not performed regularly during a mission. It is preferable to keep the underwayUUVoperating at-depth without frequently ascending/descending for mission efficiency andUUVpositioning reasons. Below and above water marine robots can autonomously coordinate and network to enable this assistedUUVnavigation and localization.

1.3.2 Contributions and Significance

The contributions of this research are as follows:

1. a novel OFDM-basedCDMAUDPunderwater protocol for environments impacted by severe multi-path and incorporates underwater acoustic channel characterization towards more accurate predictions of channel behaviour and node placements;

2. a network of both stationary and mobile communication nodes (e.g.UUV) – both, can transmit to mobileUSVnodes which further relay above-water to anUAVnode;

3. in-water verification of a multi-domain heterogeneous marine robot collaborative network, and

4. development of a complete protocol stack using OFDM-basedCDMA, which spans multiple marine domains such as underwater, on-the-water, and above-water.

1.3.3 Novelty

The novelty in the proposed Ph.D. thesis is a complete protocol stack, using OFDM-basedCDMA, which spans multiple marine domains such as underwater, on-the-water and above-water. It builds on earlier work [6] withTDMAin a network to link 11 marine robots for a collaborative underwater mission. Metrics will be constructed to assess the efficacy of CDMAoverTDMAin terms of the timeliness of the transmitted information, effectiveness of the mission, bandwidth achievable, and security.

From an optimization perspective, this research achieves mission efficacy through the following: security, timeliness, and bandwidth.

Security is deemed the foremost priority achieved throughCDMAencoding which inherently adds a layer of security and resilience against jamming and unauthorized access,

This is unavailable in standardTDMAsystems. A metric of security could be the difficulty in defeating the encoding. Following security, timeliness is prioritized and discussed next.

Timeliness is measured by the ability to transmit the data as soon as it is available, as opposed to buffering or queuing it for transmission (embodying just-in-time engineering) as in the case ofTDMA, where one node completely occupies the channel all the time. This is facilitated by the PN encoding inCDMA(described later). InCDMAmultiple nodes can concurrently use the channel all the time. A measure of timeliness could be the maximum number of nodes concurrently supported before performance degrades. For example, if 5 nodes could be supported, this would scale to a 5 $\times$ improvement in timeliness. Following on timeliness, efficient bandwidth use is prioritized.

CDMAefficiently uses bandwidth since multiple nodes can concurrently use the channel. The bandwidth of standard systems likeTDMAtypically are around 20 % of the f_c, which amounts to 4-5 kHz for carrier frequencies of 25 kHz. In contrast, the implementation of software-defined modems usingCDMAare not restricted by this and could almost span 100% of the centre frequency. A measure of bandwidth efficiency could scale near-linearly with centre frequency.

These 3 factors directly contribute to mission effectiveness and especially so in the case where larger mounts of information must be transmitted between nodes.

This proposed OFDM-CDMA network will be implemented and initially tested with hardware-in-the-loop simulators for a minimum of 3 marine robots, followed by in-water tests in a controlled environment then finally, in-water testing in an unstructured one.

1.4 Ph.D. Thesis Outline

The outline of the rest of this thesis is as follows.

Chapter 2: Background & Literature Review This chapter presents a comprehensive review of the influential and incremental developments in underwater communications that contributed to the scientific direction of this thesis. It explores the fundamental theories underlying secure communication underwater systems, discusses their merits and demerits, and identifies research gaps that motivate the work conducted in this thesis.

Chapter 3: Methodology The methodology pursued to design and develop the communication system is described. It covers simulation techniques and the development process, outlining the steps to achieve the research objectives. This also includes computer simulations, hardware-in-the-loop testing and presents results of the developed system usingNS3.

Chapter 4: Experiments The initial in-water testing conducted in a controlled environment is described. It provides a complete and detailed explanation of the experimental setup, including the equipment used, experimental protocols, and measurement techniques.

Chapter 5: Results and Discussion The results from experimental verification are compared with the simulations. It thoroughly discusses the results, analyzes the performance of the system, and compares it against established benchmarks as well. Additionally, it includes the results from the Dalhousie University Aquatron tank (controlled in-water environment) trials and in-water testing atCOVEand St. Margaret's Bay, providing insight into the system's performance in real-world scenarios.

Chapter 6: Conclusion This chapter summarizes the results presented in Chapter 5. It discusses the implications of the findings, identifies strengths and limitations of the proposed system, and explores potential avenues for further development. Finally, this chapter presents the author's recommendations for future research directions based on the main findings, suggests potential areas of focus to build upon the work presented in this thesis.

Appendices The appendices contain supplementary information, such as detailed technical specifications, additional experimental data, and supporting figures and tables.

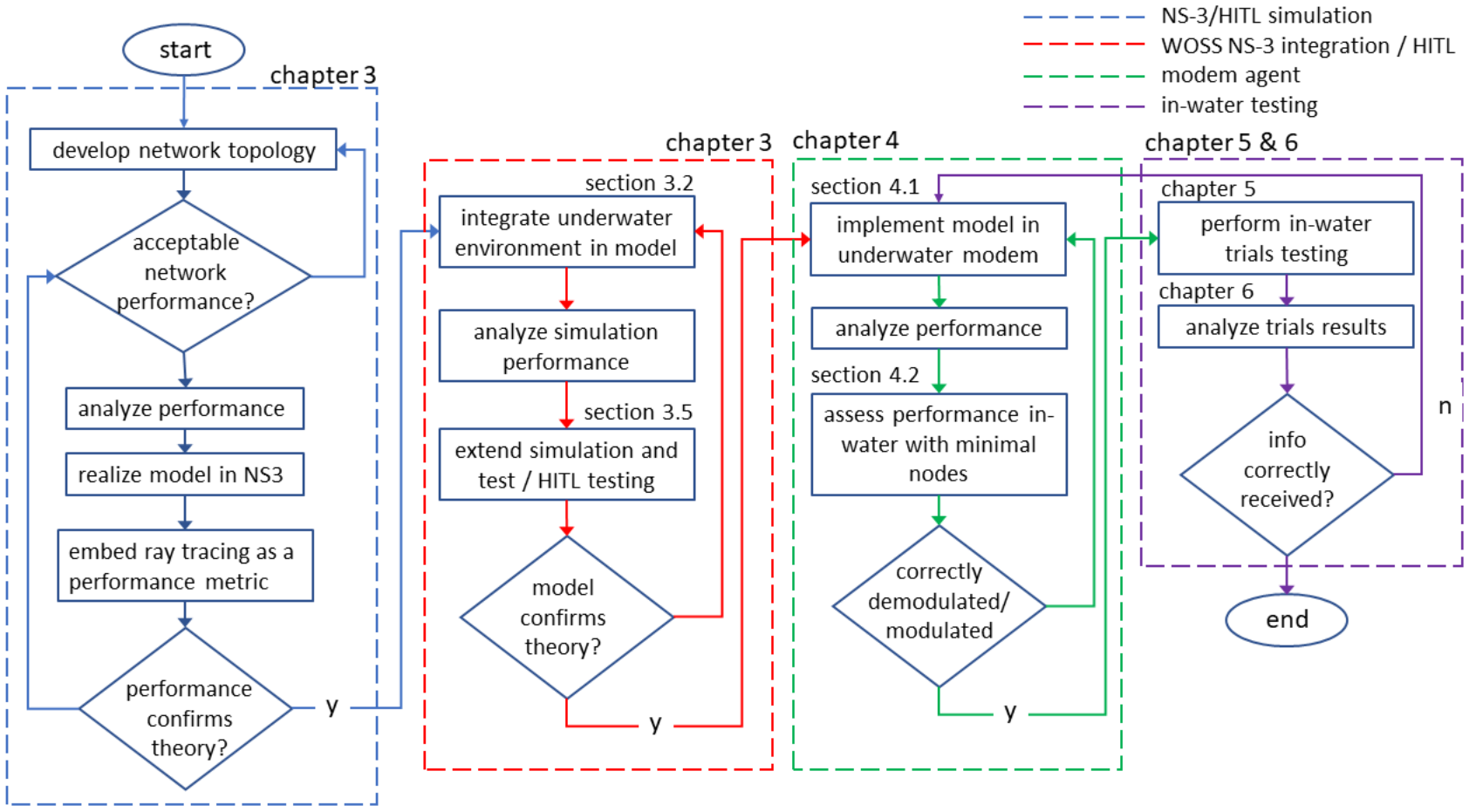

Figure 1.8: Overview of the thesis from simulations to to indoor Aquatron Pool Tank Tests (controlled environment) and in-water testing at COVE and St. Margarets Bay(unstructured environment).

Chapter 2

Background & Literature Review

The previous chapter described the challenges posed by underwater acoustic channels. It also introduces the potential of Code Division Multiple AccessCDMAas a solution for cross-domain communications. With this as background, this chapter2describes the robotic platforms that host the communication nodes across 3 domains and describes some use cases.

This chapter investigates the limitations of existing routing protocols for underwater networks, including their limited scalability, energy inefficiency, and the complexity of dynamic topology adaptation. The potential ofCDMAto address these challenges is explored, with a focus on its ability to accommodate multiple concurrent broadcasts, optimally use the underwater channel, and provide a level of security.

Then, this chapter presents a review of the relevant literature that motivated this thesis. The integration of above-water (in-air radio frequency (RF)) components into the multi-domain network usingCDMAcommunications is also discussed. WhileRFCDMA is not a novel research area, its integration with the water surface domain presents new opportunities for exploration. The chapter also identifiesNS3[3,91] and Unetstack [95], with Unetpy [52], as suitable tools for the thesis analysis and simulations.

The it concludes by setting the stage for the Methodology in Chapter3which describes how the identified challenges, and thus thesis objectives, will be met. The goal is to develop a robust and efficient underwater communication system through a combination of theoretical insights, experimental verification, and the application of emerging technologies. This chapter, therefore, serves as a foundation for the research, providing the necessary background and motivation for the thesis discussed in the previous Chapter1.

2.1 Mobile Communication Nodes

The history of underwater acoustics, networking and wireless technologies has taken many forms over the years. During the 20^{th} century, information gathering, processing, and distribution was the dominant interest [78]. Moving into the 21^{st} century, networking and wireless technologies emerged as the dominant focus. This thesis contributes to these areas.

Some applications of underwater communications include:

- underwater environment data collection for weather monitoring;
- underwater oil exploration;
- undersea pollution monitoring;
- disaster prediction;
- scientific underwater exploration;
- harbor protection;

- natural resource exploration for exploitation;
- deep-sea archaeology;
- study of marine phenomena;
- oceanographic studies, and
- detection of undersea objects (e.g., salvage, recovery, mines, etc.).

Multi-domain marine robot collaborations leverage on-board sensors and data analysis from heterogeneous robots to monitor and interpret the environment. These heterogeneous marine robots are described next.

1. **Uncrewed Underwater Vehicles (UUVs)**:UUVs operate below the water surface and are thus designed to navigate without GNSS and endure high pressures at significant depths. Therefore, they are tasked to underwater survey and recovery missions. Their powering is from the on-board batteries they carry. Their operating speeds are typically between 1 - 6 knots. They are integrated with sonar or chemical sensor payloads for data collection tasks related to environmental monitoring or detection of specific targets. Their communications while submerged is predominantly through underwater acoustics.

2. **Uncrewed Surface Vehicles (USVs)**: Operating on the water surface,USVs can carry larger payloads (than UUVs) as they are supported by buoyancy and have longer endurance thanUUVs as their powering can be from on-board batteries or air-breathing engines. In multi-domain operationsUSVs often act as communication relays betweenUUVs and above-water platforms like support ships, satellites or aerial assets. This ability is particularly important in situations where near real-time decision making is needed for tasks like marine mammal detection or innaval-mine countermeasures (NMCM)operations. Their communications above-water is through conventional RF.

3. **Uncrewed Aerial Vehicles (UAVs)**: Large areas can be quickly surveyed by UAVs, as they can achieve 40 knots travel, for a plan view of the operation zone. Fast communication relays can be served by them or they can carry out high-level surveillance tasks. In tracking marine mammals, for example, continuous visual tracking from above can be provided byUAVs whileUUVs collect acoustic data from below, creating a more comprehensive picture of an animal's activity or behaviors. Their communications is through conventional RF above-water and underwater acoustics below-water.

UUVs integrated with sonar sensors are used in underwater surveys and inspections for offshore structures, downed aircraft, displaced underwater pipelines, underwater mines, and hydrothermal vents to name a few. Such missions benefit from collaborations with USVs and UAVs. These missions are briefly described next to build the case for multi-domain robotic collaboration.

1. **Underwater recovery of downed aircraft**: The sea floor can be scanned byUUVs using side-scan sonar to localize wreckage. The UUV's communication range can be extended byUSVs (acting as relays) and the overall operation can be monitored from above byUAVs which can relay crucial information to support ship(s) in near real-time.

2. **Naval mine countermeasures (NMCM)**: Potential seabed mines can be detected byUUVs integrated with side-scan sonar systems. If a suspected mine-like object is detected from the processed sonar imagery and subsequent analysis, this information can be rapidly relayed to the support ship or command center viaUSVs andUAVs, to make informed decisions about the likelihood it is a mine and whether it merits neutralization.

3. **Survey hydrothermal vents**: The high pressure and temperatures near hydrothermal vents can be tolerated byUUVs to collect data or water samples, while near-continuous communication between theUUVs and support ships / scientists can be ensured by theUSVrelay. Surface conditions and the operational status of theUSVs can be monitored byUAVs and reported to support ships that are well beyond the horizon.

4. **Track marine mammals**: Acoustic vocalizations of marine mammals can be detected and logged byUUVs andUSVs integrated with hydrophones and underwater arrays. Aerial surveys of the animals' surface behavior can be streamed byUAVs. A more comprehensive understanding of the animals' behavior can be achieved with all 3 robot types collaborating on their monitoring.

UUVs now possess the on-board intelligence (autonomy) to process or reduce in-situ sensor measurements into information – which requires less bandwidth to transmit. This information is of limited value until it is transmitted off theUUVto a ship- or land-bound operator,UAV, underwater network, etc. to be used. As previously discussed, acoustic signals provide the best range and bandwidth underwater, but they are limited still compared to in-airRFtransmissions because of the underwater environment. Underwater acoustic signal propagation is characterized by latency, poor signal-to-noise, multi-path, Doppler-shifting, high attenuation, low carrier frequency and by extension, low bandwidth. These challenges also mean the connection to a network may be intermittent at best [76, 78,85]. It is not easily possible to transmit acoustically through the air-water interface. The information must be transmitted off theUUVto an underwater receiver which has an above-water expression and could re-broadcast in air. AnUSVwith an integrated underwater acoustic receiver and an in-air radio could perform such relaying. The merits of this method is evaluated against other possibilities, next.

Communications between distributed submergedUUVteams to/from beyond the horizon from/to their support ship, or shore-base station, is relevant to collaborating marine robots operations. It is difficult to secure a satellite connection at sea level so this is not performed regularly during a mission. It is preferable to keep the underwayUUV(s) operating at-depth without frequently ascending/descending for mission efficiency andUUV

positioning reasons. Below- and above-water marine robots that autonomously coordinate and network can enable this capability [73].

The transmissions between marine robots can consist of sensor data, information (reduced sensor data), own position, operational status, commands or mission updates, environmental data (or information), and, in some cases, processed data like images or detection alerts.

Considering the unique capabilities and potential synergies offered by multi-domain robot collaborations, effective underwater communication becomes ever more critical. This introduces a myriad of challenges, particularly due to the limitations of underwater acoustic communication. Issues such as limited bandwidth, latency, and susceptibility to environmental influences underscore the need for robust, innovative solutions. Consequently, the primary objective of this thesis is to design, implement, evaluate, and test the feasibility of a full-duplex underwater acoustic network (UAN) for multi-domain collaboration between marine robots. Such a system would serve as a key enabler, fostering enhanced collaboration and more efficient execution of complex multi-domain marine operations like those mentioned earlier.

Underwater communication presents unique challenges compared to above-waterRF. The most difficult nodes are the underwater ones on mobile robots or even at fixed locations which communicate acoustically. They are limited in bandwidth, range, and low coherence times, meaning link quality varies rapidly and spatio-temporally. Particularly,UANlinks, given their desired long range, are susceptible to severe multi-path spreading, significant distortions, range and frequency-dependent attenuation, and Doppler effects as shown in Figure2.1and summarized in Table2.1. Doppler effects, which change the frequency of an acoustic signal due to the relative motion between transmitter and receiver, can introduce significant errors in communications.

However, recent emerging advancements are improving the efficiency and reliability of underwater communications. For instance, full-duplex communication systems [57] can somewhat manage and correct these effects, allowing for more reliable and efficient communications.

Table 2.1: Comparison of key communication parameters between above-water (RF) and underwater (acoustic) communications. Highlighted are the substantial differences in link delay, propagation delay, packet size, data rate, and successful transmission time – the inherent challenges with underwater acoustic communications [22,35].

medium	**link delay**	**propagation delay**	**packet size**	**data rate**	**successful transmission time**
above-water	100 m	0.33 μ sec	100 byte	10 kbps	0.08 sec
underwater	100 m	0.29 sec	100 byte	10 kbps	0.3713 sec

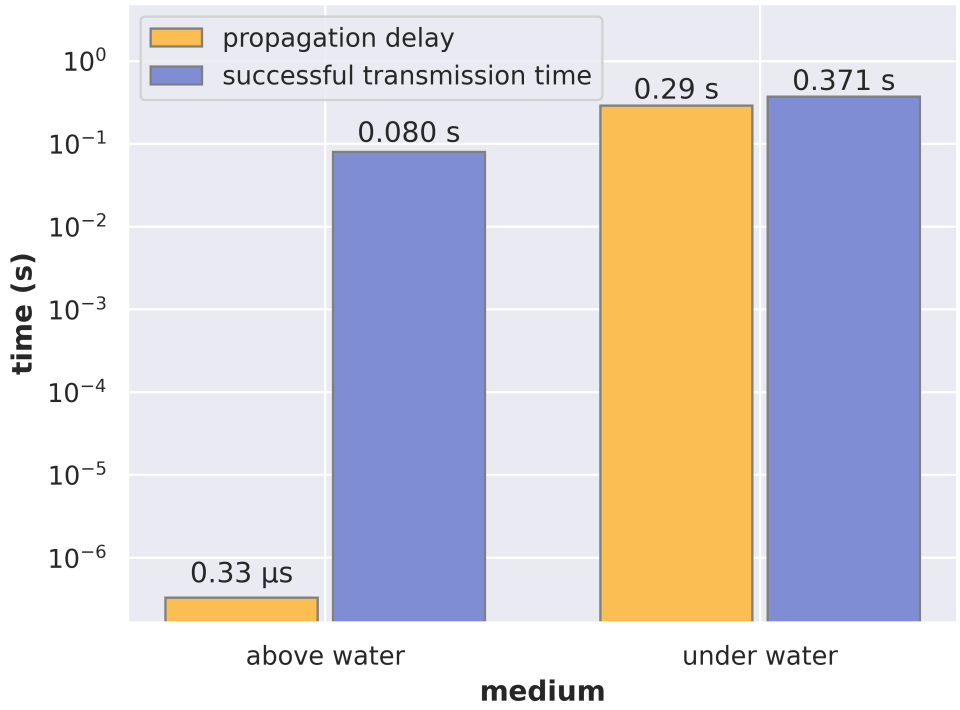

Figure 2.1: Comparison of propagation delay and successful transmission time using CS-MA/CA protocol based packet transmission for above and under water. Propagation delays underwater are significantly greater which highlights the challenge in underwater communications.

To date, most underwater modems operate in half-duplex mode which adapts to the negative impact of latency and delay while using one channel for transmission with a unique carrier frequency. In contrast, full-duplex systems use two separate channels, uplink and downlink, with two different frequencies to mitigate long propagation delays. This is a much more efficient use of the channel, but for various reasons, it has not been considered for underwater.

Now, full-duplex communication has become feasible underwater due to technological advances and insight into the unique challenges posed by the underwater environment. These advances include the development of sophisticated signal processing techniques and the use of multiple channels with different carrier frequencies. This allows for concurrent transmission and reception of signals, reducing the impact of long propagation delays – a major challenge in underwater communications. Furthermore, advances in hardware and algorithms have enabled better mitigation of interference, a critical factor in enabling full-duplex operations [78].

2.1.1 Background

In a communication network, it is crucial to manage how multiple devices access the communication medium which is where multiple access control (MAC) protocols come into play.MACprotocols dictate how data is transmitted between multiple points or nodes over shared channels. This is especially important in multi-domain communication networks (like those that include under- and above-water nodes) where there might be many devices, each needing to communicate without interference. By dictating how these devices access the network and manage communications,MACprotocols ensure efficient, reliable communication across different domains.

2.1.2 Multiple Access Control Protocols

MAC protocols are common in mobile wireless networks where more than one mobile user, subscriber, or local base station shares the same communication medium simultaneously – regardless of multiple transmissions that may originate from different locations. There are three basic classes of multiple access techniques:

1.frequency division multiple accessFDMA;

2.time division multiple access (TDMA); and

3.code division multiple access (CDMA).

CDMAis very effective inRFwireless networks, primarily because it allows many users to simultaneously utilize the same frequency band. Each user's signal is assigned a unique code, to distinguish it from others' and thus permit simultaneous communications. This is a notable advantage overFDMAorTDMAsystems, which require either distinct frequency bands, or time slots, respectively for each user. Moreover,CDMA, due to its spread spectrum nature, accommodates a considerable number of users within a given band, making it especially beneficial in densely populated areas.CDMAis also resistant to interference and jamming, offering improved communication quality even in challenging conditions, and enhances security due to its controlled channel access through unique codes. The scalability and flexibility ofCDMAnetworks further ease the addition of new users without requiring infrastructural changes. Lastly, the incorporation of power control techniques optimizes the transmission power of each user, which reduces interference and increases battery life of mobile devices, makingCDMAan efficient and reliable choice in RFwireless networks. Consequently, it is widely used for in-air wireless communications. If similar robust performance and advantages can be achieved with its application to underwater acoustic channels, then the new design and development of underwater networks can leverage some of this proven performance inRFwireless networks [18].

2.1.3 Code Division Multiple Access

CDMAis a channel access method which is spread-spectrum for multiple access. It deliberately spreads a signal's bandwidth uniformly over a larger range of frequencies than the

signal's actual bandwidth to give the perception of noise or randomness. This is achieved with pseudo-random (pseudo-random sequences (PN)) codes, which are the fundamental units of the spreading code used to modulate the transmitted signal. These codes operate at a faster rate than the transmitted signal, with each individual code element known as chips, given by Eq.2.1,

$$f_{chip} = \times f_{symbol}. \tag{2.1}$$

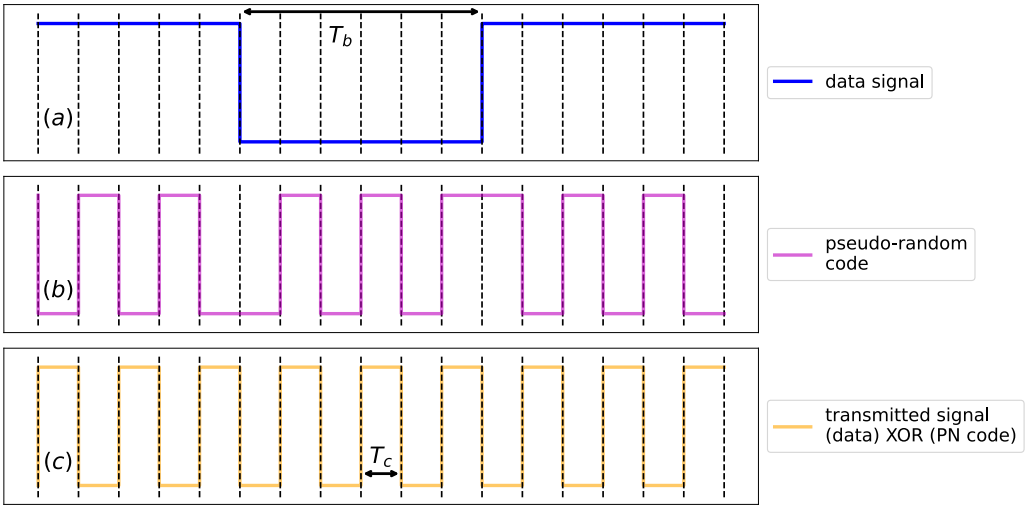

Figure 2.2: Steps to generate aCDMAsignal: (a) the unmodulated signal with symbol rate T_b; (b) the pseudo-random code to differentiate each node's part of the signal, and (c) the transmittedCDMAsignal, generated from a logical X-OR (exclusive-OR) operation between the unmodulated signal in (a), and the pseudo-random code of (b). As shown, the chip rate of the pseudo-random code and transmitted signal is T_c.

The chip rate of the code is the number of pulses per second (chips per second) the code is transmitted, or received, at. The chip rate is larger than the symbol rate, meaning one symbol is represented by multiple chips (Figure2.2). This ratio is the spreading factor (k) or processing gain, given by Eq.2.2, i.e.:

$$\text{spreading factor } (k) = \frac{T_c}{T_b}. \tag{2.2}$$

CDMAmultiplexes multiple nodes to transmit concurrently on one channel. This means two communicating nodes are allocated the entire spectrum all the time. Multiple nodes share a range of bandwidths over different frequencies.CDMAemploys the concept of spread-spectrum and a coding scheme, whereby each transmitter is assigned a unique code, so multiple nodes (e.g.UUVs) can be multiplexed over one physical channel. In contrast, time division multiple access (TDMA) divides access by time where two communicating

nodes are allocated all of the spectrum for part of the time.

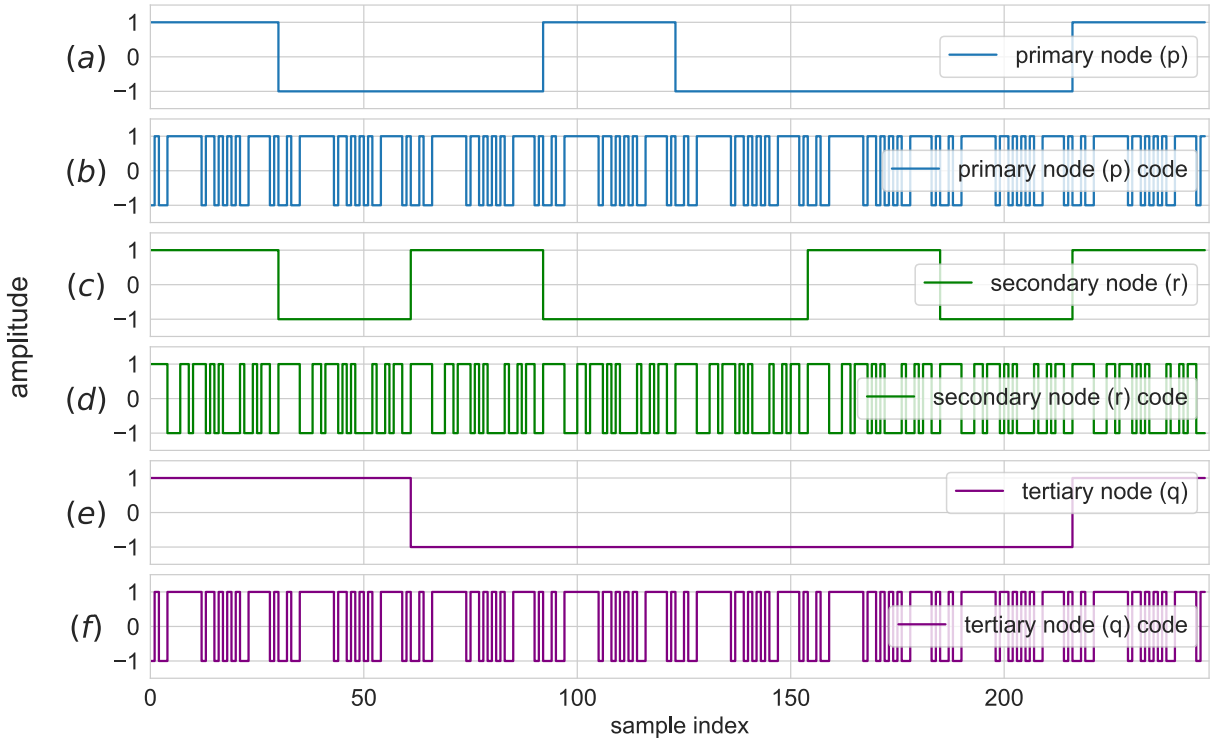

Figure 2.3: CDMA signals and their corresponding pseudo-random sequences (PN) codes for three different nodes, where each signal is spread with its unique PN code: (a) the primary node's signal and (b) the primary node's PN code. The secondary node's signal and code are depicted in (c) and (d), respectively. Finally, the tertiary node's signal and code are shown in (e) and (f), respectively. In all plots, the abscissa is the sample index and the ordinate is the signal amplitude. Note, these allows multiple signals to be transmitted concurrently over the same frequency band, thereby improving the efficiency of spectrum usage and increasing the capacity of the communication system.

Similarly, frequency division multiple access (FDMA) divides access along frequency bands where two communicating nodes are allocated part of the spectrum all of the time. CDMAis a form of spread spectrum signaling since the code modulated signal has a higher bandwidth (Eq.2.3), than the un-modulated signal [64]:

$$\begin{aligned} B_{\text{symbol}} &= \frac{1}{f_{symbol}} \\ &= \frac{1}{f_{chip}}. \end{aligned} \tag{2.3}$$

As an illustrative example, 3CDMAnodes are applied to GPS satellite communications. Their performance is based on the X-OR logic to determine whether a 0 or 1 is transmitted

[99]. Figure2.3shows how a spread spectrumCDMAsignal (also known as composite signal (FigureC.1)) is generated from a sequence of bits and the node's chip. A signal of pulse duration T_b is X-OR'd with the transmission code of pulse duration T_c. The relationship $\frac{T_c}{T_b}$ between the two is the aforementioned spreading factor (k) or processing gain which drives the upper limit for the total number of nodes (e.g.,UUVs) supported concurrently by a base station.

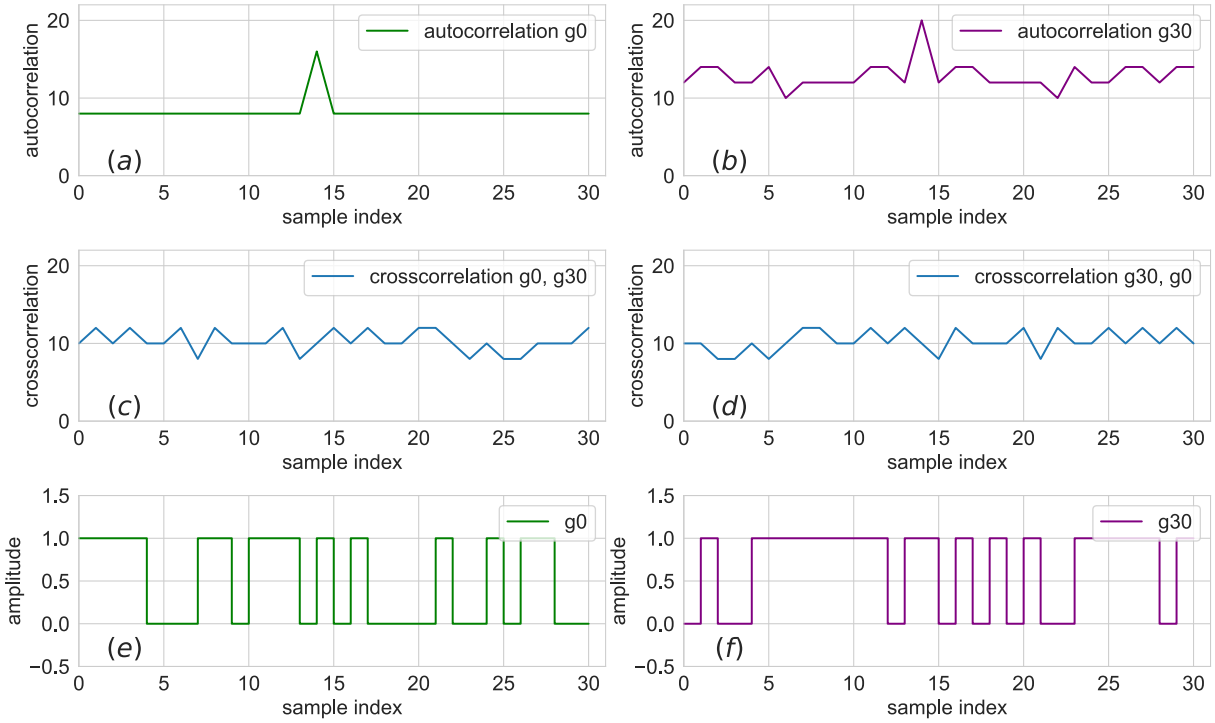

Figure 2.4: Auto-correlation and cross-correlation of two PN codes ($g0$ and $g30$) in the CDMA system: (a) auto-correlation of $g0$ code shows a peak with zero lag, indicating high correlation with itself; (b) auto-correlation of $g30$ code, also shows a peak with zero lag; (c) cross-correlation between $g0$ and $g30$ codes, show low correlation which means good orthogonality properties; (d) cross-correlation between $g30$ and $g0$, confirming their low mutual correlation; (e) amplitude of $g0$ code, and (f) amplitude of $g30$ code. The good cross-correlation properties of the two PN codes minimizes interference between node signals.

In aCDMAnetwork, each node employs a unique code, or a set of codes, to modulate its signal (Figures2.3,2.4,2.5,2.6). These codes vary based on whether the signal and its pilot, a reference signal used for synchronization, are transmitted at the same or different frequencies. This can translate to the use of a single code for both signal and pilot channels, or distinct codes when transmitted at different frequencies. The selection of these codes drives these systems' design and subsequent performance. Well-known code techniques such as Hadamard and Gold [40], predominantly used inCDMA, are also utilized for Asyncronous code division multiple access (ACDMA). Optimal performance is achieved

when there is sufficient separation between the signals of nodes, a scenario referred to as multiple access interference (MAI).

Generally,CDMAis subdivided into two basic categories based on the type of spreading codes used:

- synchronous orthogonal codes or
- asynchronous usingPN.

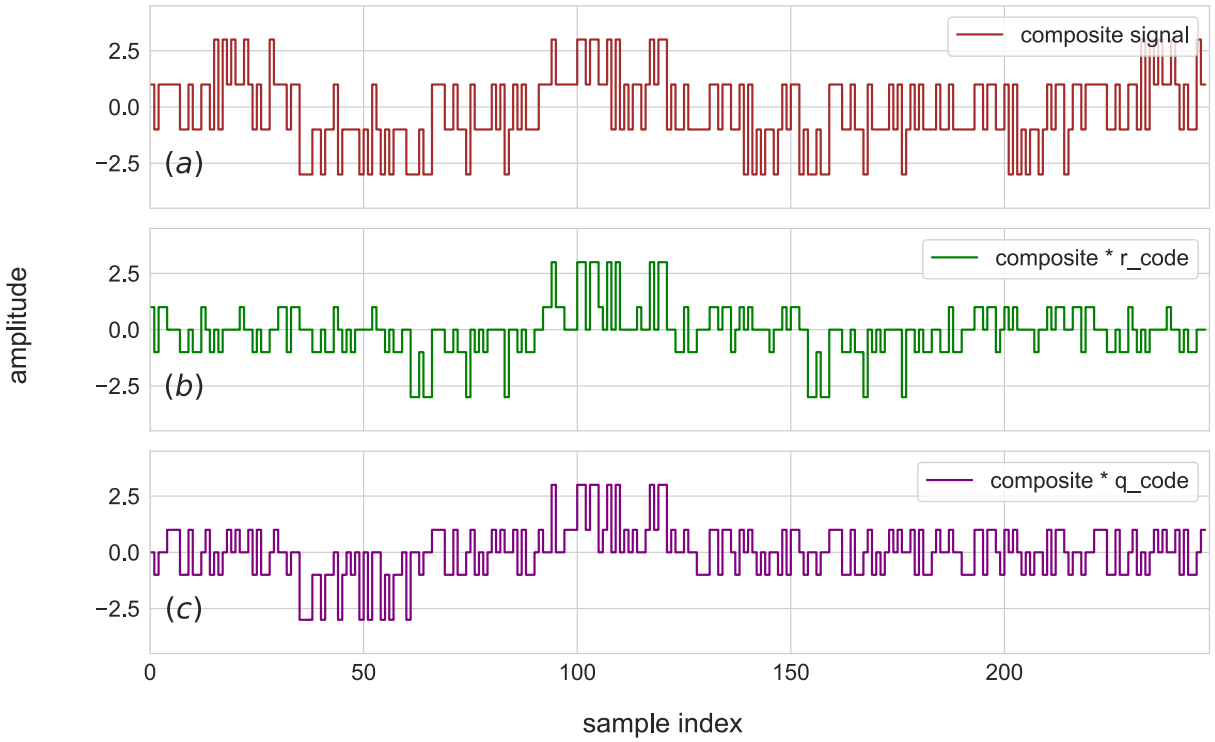

Figure 2.5: Composite signals in a CDMA system: (a) the composite signal from aggregating signals from all three nodes; (b) the composite signal after multiplication with the secondary node's PN code, a vital step in signal recovery and, (c) the composite signal after multiplication with the tertiary node's PN code. Each plot's abscissa is the sample index and each ordinate represents amplitude. Note, that the successful recovery of the signal for a specific node is achieved by multiplying the composite signal with the node's unique PN code, demonstrating the effectiveness of CDMA technique to distinguish signals from different nodes.

ACDMAlinks are used when the mobile (transmitter) to the base communication cannot be coordinated with sufficient precision, due to the mobility of terminals. This has implications —as the chip code needs to have good properties at the instant when the signal is received and when the signal is delayed. A first approach would design a

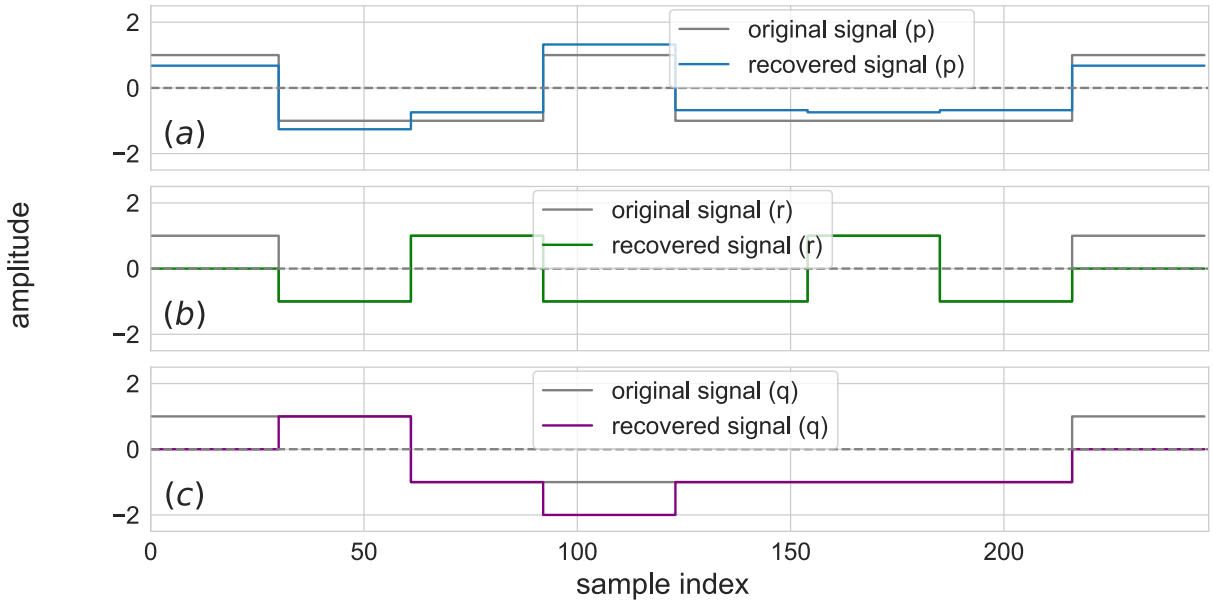

Figure 2.6: The original (modulated) and recovered (demodulated) signals of the three nodes in the example CDMA system. The original signals were successfully recovered from the composite signal by de-spreading them with the corresponding pseudo-random code: (a) the original and recovered signals for the primary node; (b) similarly for the secondary node, and (c) for the tertiary node.

system orthogonal, at all times ideally, to eliminate interference and allow clear signal separation; however, this is impossible mathematically. Therefore, aPNcode with the desired balance, run, and correlation properties with the auto-correlation ideally an impulse function, meaning it is close to zero for all non-zero time shifts. This helps in signal detection and synchronization (Figure2.4). APNcode is a binary sequence which appears random but can be reproduced deterministically. ThesePNcodes are used to encode and decode the signal from asynchronousCDMAnodes in the same way as orthogonal codes with synchronous nodes. ThesePNsequences are statistically correlated, and the sum of a large number ofPNsequences results inMAIwhich is approximated by a Gaussian noise process in the absence of the near-far problem [1] (extracted from the Central Limit Theorem [2]). If all nodes have the same power, then one can approximate the variations of theMAIas white noise which is directly proportional to the number of nodes. In other words, unlike synchronousCDMA, the signals from other nodes appear as noise to the signal-of-interest and interfere slightly with the desired received signal in proportion to the number of nodes. These signals from other nodes in theACDMAare received as broadband noise which reduces the gain of the process. Since each node generatesMAI, controlling the signal strength is a key issue withCDMAtransmitters [64].

[1] Problem is based on the receiver detecting a strong signal which subsequently makes it impossible for it to detect a weaker signal.

[2] Central Limit Theorem states, in very general terms, that the distribution of the sum of random variables tends to a normal distribution when the number of variables is very large.

CDMAhas advantages, shown in Table2.2[1], over other access methods likeTDMA andFDMA[53] for underwater applications:

1.efficient use of channel bandwidth;

2.flexible allocation of resources (nodes);

3.anti-jamming (secure), and

4.resistant to interference (secure).

Table 2.2: Comparison ofTDMA,FDMA, andCDMA.

Parameter	**TDMA**	**FDMA**	**CDMA**
definition	divides the signal into different time slots; each node is assigned a different time slot.	divides the bandwidth into different frequency bands; each node is assigned a different frequency band	each node is assigned a unique code to communicate over the entire spectrum at all times
bandwidth	all nodes share the same frequency but have different time slots	each node has a different frequency band	all nodes use the entire spectrum
interference	inter-symbol interference can occur	cross-talk can occur	can experience interference from all other users
spectral efficiency	less efficient than CDMA.	less efficient than CDMA.	more efficient due to the use of spread spectrum technique.
complexity	less complex than CDMA	less complex than CDMA	more complex from use of unique codes and need for power control
flexibility	less flexible	less flexible	more flexible and can accommodate more nodes per kHz of bandwidth

The basics ofCDMAand its advantages for underwater communications are described in more detail next.

2.2 Basics of CDMA

The fundamental principle ofCDMAwill be illustrated through an example [71] and also illustrated in AppendixC. The bit data rate, D, represents the rate of the signal. Each bit is divided into k chips using a fixed pattern which is unique for each node (or e.g.,UUV), referred to as the *node's code*. Consequently, the channel has a chip data rate of $k \times D$ chips per second. If $k = 6$. It is convenient to represent a code as a sequence of 1's and -1's.

In practice, theCDMAreceiver filters the contribution from other users or they appear as noise. However, if many users compete for the channel, or if the signal power of one competing signal is much higher (due to it being physically closer to the receiver (the *near/far* problem), the system may break down.

Therefore, it is recommended to use DS-CDMA, which uses orthogonal codes[3]. For two m - bit codes - $x_1, x_2, x_3, \ldots, x_m$ and $y_1, y_2, y_3, \ldots, y_m$ their cross correlation is shown in Eq.2.4,

$$= \sum_{i=1}^{m} x_i \cdot y_i = 0. \tag{2.4}$$

For example: $x = [0, 0, 1, 1]$ and $y = [0, 1, 1, 0]$. The 0's are mapped -1, and 1's remain as they are. The cross-correlationis calculated as in Eq.2.5and consequently:

$$\begin{aligned} x &= [-1, -1, 1, 1] \\ y &= [-1, 1, 1, -1] \\ &= [1 - 1 + 1 - 1] = 0. \end{aligned} \tag{2.5}$$

The product of two m-bit codes may not be zero for every pair of signals even when the average over many pairs of such signals is zero. Such random signals are said to be near-orthogonal to emphasize that their products are zero in the mean but not identically zero for all individual signal pairs [18].

After signal transmission, the receiver coherently demodulates to de-spread the spread-spectrum signal with a locally generated code sequence. To achieve the de-spreading, the receiver must not only know the code sequence used to spread the original signal, but also synchronize the locally generated code sequence with the received signal. This synchronization must be accomplished at the beginning of the reception and maintained until the entire signal is received. The synchronization/tracking block performs this operation shown in FigureC.9. After de-spreading, a data-modulated signal is the outcome, and after demodulation the original signal is recovered [18].

[3]A pair of codes is said to be orthogonal if the cross correlation is zero.

2.2.1 System Development

This section briefly describes the system implemented in the thesis. It starts with a high level description of the organization of the transmitter, receiver and channel to the components in the system block diagram shown in Figure1.4, then a more detailed analysis.

Ideally the system consists of several transmitters that communicate with a common receiver through a common channel (Figure2.7). Communications with the common receivers can be carried out with each transmitter using a bandwidth set by its associated chip code [64].

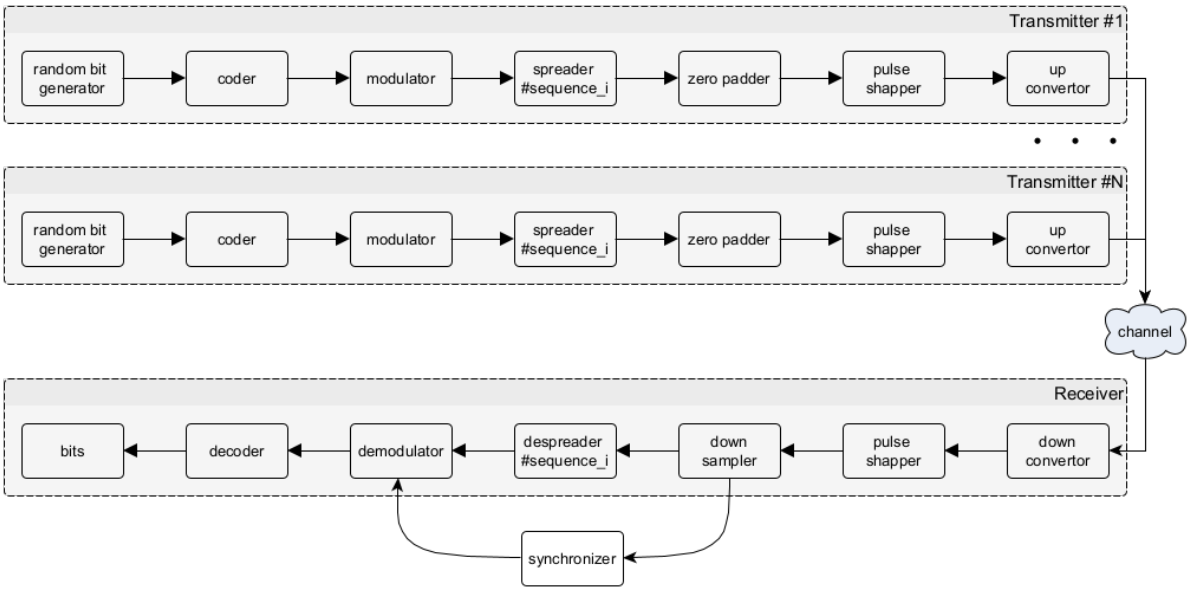

Figure 2.7: General structure ofCDMAcommunication system [64]

The modulation process generates abinary phase shift keying (BPSK)modulated signal by combining the data bits with a code sequence. The signal generator generates the signal from the data bits, and the resulting signal is then modulated using the code sequence. This modulation generates a spread spectrum signal with a wider bandwidth than standard modulation techniques. To maintain conciseness, this mentioned example and necessary figures have been relocated to appendixC.2.1. FigureC.6illustrates theCDMABPSK modulator.

To demodulate the spread spectrum signal and recover the original data, the receiver needs to de-spread the signal. The receiver generates its own code sequence that matches the transmitted code sequence and adjusts its phase to be in-phase with the received sequence. This process removes the spreading effect. FigureC.7depicts theCDMABPSK demodulator.

However, the receiver faces two challenges. Firstly, it needs to run at a high sample rate to accommodate the signal. Secondly, it is difficult to recover and synchronize the code

sequence when it is imposed on the actual signal. It is easier to recover and synchronize the code sequence when the signal is in the baseband.

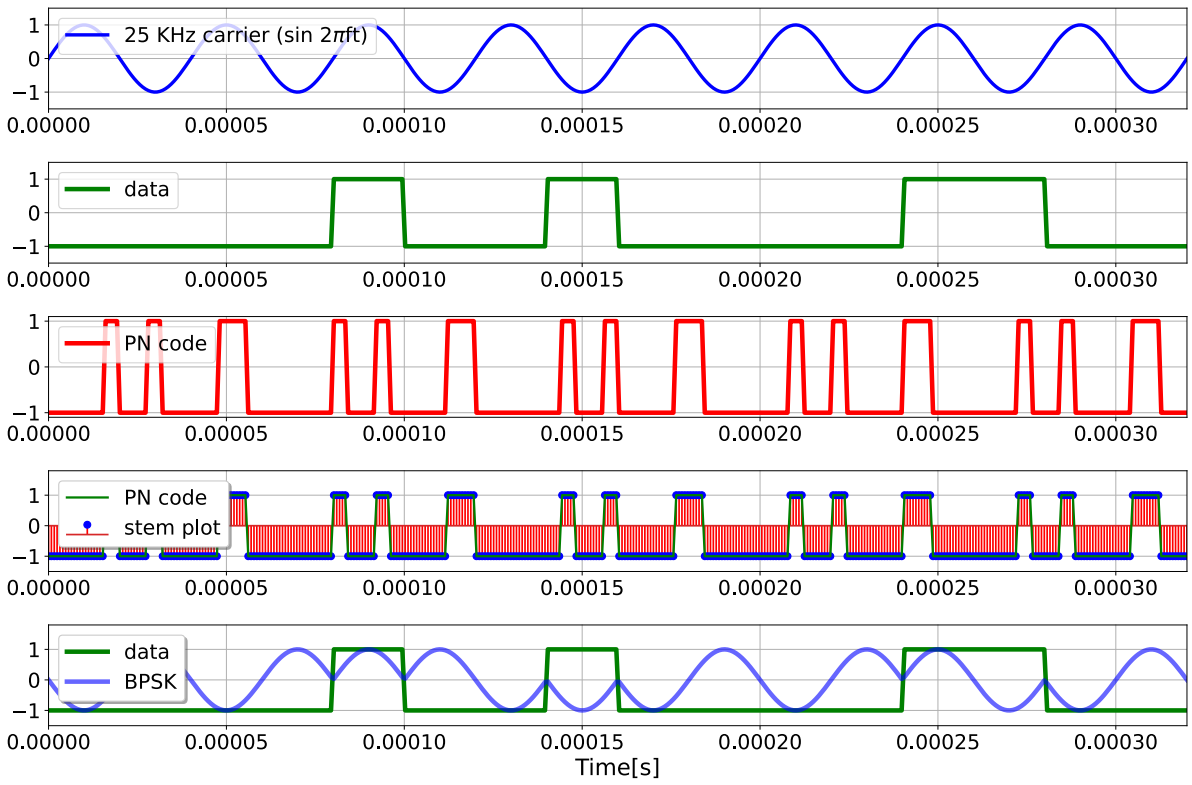

Figure 2.8: Generation of a CDMA BPSK signal: (a) 25 KHz carrier wave used for modulation; (b) generated random data; (c) generated pseudo-random (PN) code sequence in red, (d) representation of the PN code as a stem plot along with the PN code in green, and (e) the final CDMA BPSK signal, showing modulation of the carrier wave by the PN code. This figure highlights the phase shift in the signal, visible as blips in the sine wave, every time the signal changes from 1 to 0 or vice-versa, illustrating the use of BPSK modulation.

To address these challenges, a better receiver topology is proposed. The spread spectrum signal is down-converted to the baseband using a common quadrature down-converter, where it is easier to recover the code sequence. Once the signal is in the baseband, the receiver synchronizes its own code sequence generator with the received code sequence. The receiver undergoes an acquisition phase, searching for the correct phase alignment with the received code sequence. Once the alignment is achieved, the receiver enters the tracking mode. The tracking mode uses correlators to measure the energy of the de-spreaded signal and continuously corrects the code sequence generator's phase. FiguresC.8andC.9 illustrate the spread spectrum receiver in acquisition and tracking modes, respectively.

After the de-spreading process, the receiver applies a costas loop-like structure to recover the I and Q bit streams. The receiver further includes time recovery blocks, such as a Gardner time error detector and a PI controller (optional), to recover the correct bit rate. The output of the receiver provides the recovered data, where each bit can be identified as 0 or 1.

As an illustrative example, a 25 KHz (Figure2.8) carrier for modulation is used. The transmitted signal usesBPSK, then the signal is changed by phase shift of $\pi = 180°$ while it turns from 1 to -1, which can be achieved by multiplying the carefully constructed PN with the carrier. This works because a $sin(x) \times (-1) = sin(x - 180°)$, in other words it is exactly a 180 degree phase shift. This appears as blips in the sin wave every time the signal changes from 1 to 0 or visa-versa. For clarity, Figure2.8zooms into one spot as it is difficult to decipher since the carrier runs three orders of magnitude faster than the PN.

On the receiver side, if the entire process is reversed and theroot raised cosine (RRC) filter is applied at the received signal, at the correct phase and time, with the correct code, the correct up-sample code can be recovered as shown in Figure2.9

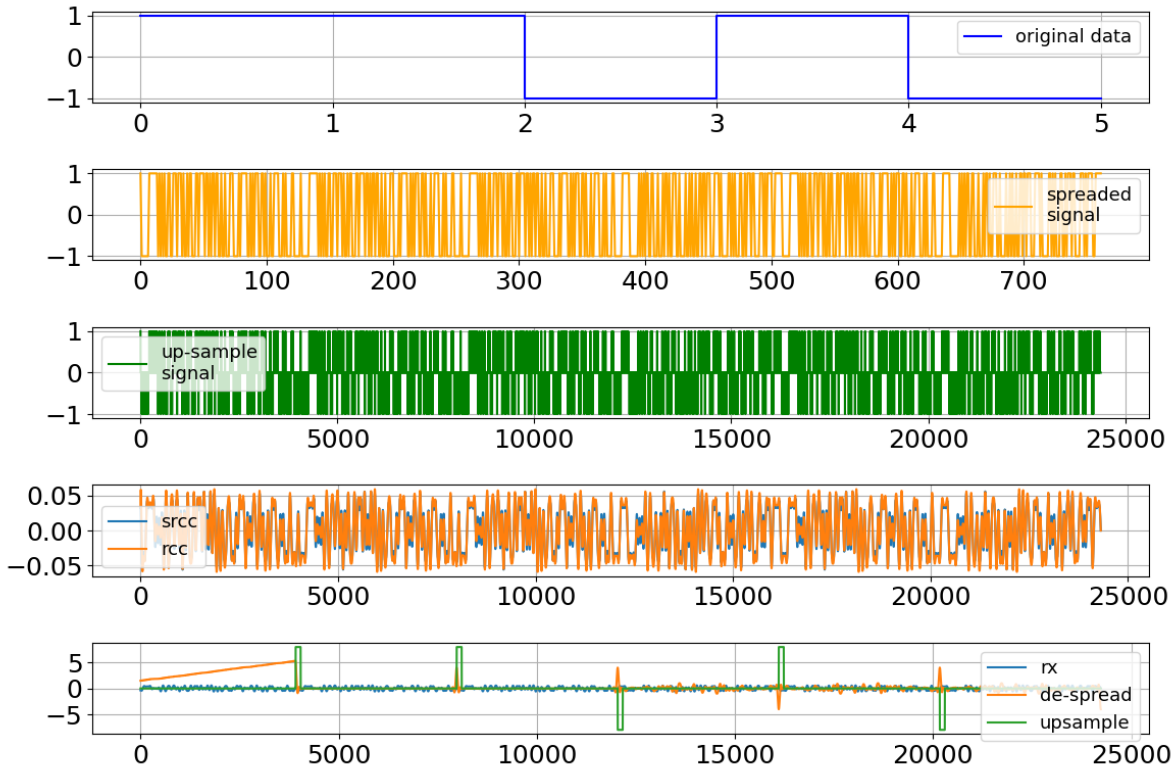

Figure 2.9: CDMA BPSK signal recovery

The established structure has proven effective for in-air communications. The thesis objective is to design and verify a similar structure for underwater communication. This

objective raises further research questions such as: how does an underwater robot communication network differ from an in-air one?

Another significant aspect to consider is the environmental factors that have the greatest impact on the underwater communications channel. Insight into these factors is essential to design and operate such systems effectively. A comprehensive case study addressing this topic is available in reference [76].

As previously discussed, anthropogenic and natural activities contribute to the underwater acoustic ambient (Figure1.7). There is world-wide concern on the impact of anthropogenic activities on marine life and efforts to mitigate adverse impacts are underway. Addressing these concerns is outside the scope of this thesis. However, it is important to examine how the underwater acoustic ambient negatively impacts performance of communication systems and how such impacts could be addressed during the design stage of underwater communication systems.

Furthermore, the overall mission objective is to transmit information collected from the underwater domain by underwater robot networks to surface robots (USVs) for relaying above-water or to send above-water instructions to the underwater robot network. To address this objective, it is crucial to investigate how information from the underwater domain can be relayed to the above-water domain. Additionally, understanding the constraints and requirements of integrating these two distinct communication modalities is necessary.

Bandwidth limitations pose a significant constraint in the underwater communications channel compared to the above-water in-air one, greatly impacting data transmission. To overcome this challenge somewhat, the user datagram protocol (UDP) packet transmission is used underwater, which saves bandwidth by minimizing control messages and message ordering. The trade-offs and implications of usingUDPtransmission are considered. There are many other factors like this to consider with practical implications on the underwater communication systems design.

2.3 Literature Survey

In the literature, there is work towards underwaterMACprotocols for marine robot and sensor networks over the last decade [34,36,78,82]. Due to the somewhat unpredictable frequency-dependent underwater channel, existingMACprotocols do not work well in this harsh environment. As discussed previously, the underwater acoustic channel is characterized by limited bandwidth, range dependent attenuation and extensive propagation delays (low sound speeds) making it problematic as a communication channel (Figure1.2). This variable link (as manifest in the channel coherence time) depends on local environmental parameters that vary with the hour, day, month and season. As mentioned earlier, insight into channel transmission characteristics is essential to the development and evaluation ofMACand routing level protocols that better utilize the limited resources within the unpredictable communications channel.

Specific papers that impacted the direction and content of this thesis are highlighted next.

UW-ASNsare used for ocean sensing and monitoring [58,78] in addition to communications. Underwater acoustic network protocols are usually designed for specific deployment scenarios and link properties. Their network structure differs from conventional RF-based networks. The performance of their communications networks were analyzed using analytical modeling, computer simulations, hardware-in-the-loop tests [35,54,97] and finally field trials. The work described by the authors is based on computer simulations to prepare for hardware tests however, they did not do any hardware tests themselves. This paper provided a comprehensive background on theNS3UANmodule which was eventually used in this thesis.

2.3.1 Simulation and experimentation platforms for underwater acoustic sensor networks: advancements and challenges [58]

This paper provides a brief analysis of various commercially available simulators along with their pros and cons and provides components to develop simulation and experimentation platforms. As well, there is a comprehensive survey report based on some typical criteria, useful guidelines for researchers on choosing suitable platforms for computer simulation in accordance with their requirements. This paper provided solid insights of simulation tools available for underwater acoustic sensor networks and led the work in this thesis towards theNS3simulator.

2.3.2 Analysis of Simulation Tools forUW-ASNs[68]

Presented, is an in-depth analysis of variousUW-ASNssimulation tools along with the performance comparison and key features associated with them. The paper also assists researchers to select the best available tool and highlights research directions to inherit advanced features in UWSN simulators to perform advanced real-time underwater simulations. This work redirected the thesis' research to specific tools to design underwater acoustic networks inNS3.

2.3.3 A CDMA-based Medium Access Control for Underwater Acoustic Sensor Networks [78]

AMACprotocol was proposed for anUW-ASNs. There are only a few contributions that address CDMA schemes, at the physical layer only, for frequency-selective fading channels. This was a transmitter-basedCDMAscheme for deep water (> 100 m) communications which was not affected by multi-path. There was little discussion on the use of this in shallow waters which would be more severely affected by multi-path. Another technique uses upwelling to enhance the underwater communications range using m-ary frequency shift keying. It provides design configuration parameters needed to designCDMA

the communication physical layer for the underwater domain. Most of the thesis parameters are adapted as per this paper. The authors provided a half-duplex configuration usingCDMAwhich was the starting point for the thesis towards developing a full-duplex solution.

2.3.4 Comparative Analysis of Routing Protocols for Under-Water Wireless Sensor Networks [49]

A performance analysis of three classical location-based routing protocols (namely, vector-based forwarding (VBF),hop-by-hop vector-based forwarding (HH-VBF), andvector-based void avoidance (VBVA)) for underwater wireless sensor networks in terms of three critical performance metrics was presented. The metrics are energy consumption, end-to-end delay, and packet delivery ratio. This study provides excellent candidates for underwater routing protocols that the thesis will draw on. This research highlighted a strong candidate for routing in the acoustic domain which was used for performance comparisons with the proposed thesis algorithm as it is a state-of-the-art routing method.

2.3.5 Embedded Systems for Prototyping Underwater Acoustic Networks: the DESERT Underwater Libraries On-Board the PandaBoard and NetDCU [24]

The focus was on the process to transferNetwork simulator 2 (NS2)simulations on embedded computer boards like PandaBoard and NetDCU. The authors also provide support information on how to install NS, NS-Miracle libraries and DESERT Underwater libraries. This provides emulation platform studies for real-time underwater embedded systems. They are good platforms to emulate underwater communication systems. These libraries were an initial starting point for the network emulation in this thesis.

2.3.6 The World Ocean Simulation System - WOSS [41]

Presented is a C++ framework,WOSS, which is mostly a wrapper around the BELLHOP [41] Acoustic Toolbox. Its objective was to model channel power delays or frequency attenuation profiles based on accurate representations of the propagation phenomena described by the physics of underwater propagation.WOSSis a multi-threaded framework which can integrate any existing underwater channel simulator with environmental data and provides as output a channel realization represented with the aforementioned channel profiles.WOSSwas integrated in the thesis to make the environment more realistic by using aSSPand bathymetry data [76] for Bedford Basin (Halifax, Nova Scotia) which is one of the thesis venues for at-sea testing.

2.3.7 UnetStack: An Agent-based Software Stack and Simulator for Underwater Networks [30]

Until now most of the underwater modems/nodes [9] operate in the half-duplex configuration with low overhead and high packet loss. This paper presents a groovy-based UnetStack [30] discrete-event simulator which is capable of full-duplex underwater operations. The authors used a software-in-the-loop simulator. It uses a desktop computer sound card to transmit and receive sound and also to design and debug the complex communication protocols. After careful analyses, their communications stack can be directly ported to real-time underwater modems to test the proposed thesis communication stack. This open up new possible opportunities in the underwater domain likesoftware defined radio (SDR). This is the heart of the thesis research from hardware point-of-view.

2.4 Baseband Signal Processing with UnetStack [29]

Most widely used underwater modems are not re-configurable, which is not cost effective or easily adaptable to other protocols – especially experimental ones. There are expensive commercially available software-defined modems that can cost up to £80k and likely more. The authors proposed a software-in-the-loop simulator which uses computer sound cards to transmit and receive data for development purposes [29]. This software-in-the-loop simulator led the thesis to develop a custom basebandCDMAsignal using a custom physical agent (encodes the messages into aCDMAspread spectrum one) which uses UnetStackFramework for Java and Groovy Agents (fjåge)[37]. Unetstack integrates well with Python tools and BELLHOP [20]. The authors use UnetStack to integrate above and below-water communications on a passive buoy. Their baseband arbitrary waveform generation capability used by the author was adopted for the thesis.

2.5 Robust Index Modulation Techniques for Underwater Acoustic Communications [80]

In the exploration conducted by Qasem, the details of enhancing underwater acoustic communication through hybridizing OFDM-CDMA are described through the deployment of an X-transform time-domain synchronous index modulation orthogonal frequency-division multiplexing spread spectrum (IM-OFDM-SS) methodology. This methodology infuses index modulation into the spread spectrum, and is shown to significantly augment the system's energy efficiency with PN codes as CP. A notable reduction in the peak-to-average power ratio (PAPR), alongside an amplification in spectral efficiency—pivotal metrics, for underwater communications—is seen. Qasem's work was targeted standard underwater communication systems. The innovative approach proposed in Qasem's thesis resonates with the overarching objectives of better modulation techniques pursued in this research.

The methodologies adopted in this thesis are aligned with the broader narrative of

advancing underwater communication technologies through innovative signal processing. Serving as a critical reference point, Qasem's work provides insights into how a hybrid OFDM approach is possible at least in principle. This thesis is different from the work of Qasem in that CP and custom preambles as well as advanced filtering are completely different from Qasem's. This thesis also complements Qasem's with an implementation using innovative software-defined underwater modems in addition to rigorous simulations.

2.5.1 Design Challenges

The design of underwater communication systems face the following challenges:

- **limited routing protocols:** Existing routing protocols are suitable for a small number of nodes and are primarily designed for symmetric networks. In contrast, underwater networks often have asymmetric and dynamic connections due to variable underwater conditions. Additionally, most existing protocols are not designed to scale to a large number of nodes, which limits their applicability for large-scale underwater sensor networks. The development of efficient and scalable routing protocols specifically designed for the underwater environment is a significant research challenge.

- **signal routing overhead:** Routing processes in underwater networks often require significant signal overhead, which refers to the additional data that must be transmitted with the actual data for the purpose of routing. This includes control messages for route discovery, route maintenance, and error handling. In the bandwidth-limited underwater environment, this signal overhead can consume a significant portion of the available bandwidth, thereby reducing the network's data transmission capacity. Reducing signal routing overhead is a key challenge in the design of underwater communication systems.

- **energy consumption:** Underwater sensor nodes are typically battery-powered so have limited energy resources. Some routing protocols may have high energy consumption due to frequent control message exchanges, complex computations, or long transmission ranges. The difficulty to access nodes for battery replacement or recharging once they are deployed underwater further exacerbates this energy constraint. Therefore, designing energy-efficient protocols and mechanisms is a crucial challenge in underwater sensor networks.

- **complex topology adaptation:** Adapting to dynamic network topologies in the underwater environments is complex for several reasons. Firstly, the environment itself is quite dynamic with variable water currents, temperatures, and salinity levels, which affect acoustic signal propagation. Secondly, the nodes in the network may be mobile (e.g., integrated on underwater vehicles or marine animals), leading to a constantly changing network topology. Lastly, the inherent delay and limited bandwidth of underwater communication makes it difficult to obtain real-time information on the network topology.

Background and Literature Review Discussion

The challenges encountered in underwater communication systems are numerous and complex. Unique obstacles inherently presented by the underwater acoustic channel include attenuation (scattering and absorption), high acoustic ambient, long propagation delay, multi-path fading, limited bandwidth, low data rate, and difficulties in node deployment. Such difficulties include the physical challenge of deploying devices underwater, the requirement for precise placement to ensure effective coverage, the potential impact of water currents and marine life on node positioning, and challenges to maintain and service deploy nodes among others. The design and operation of underwater communication and sensing systems are significantly impacted by these issues.

The underwater acoustic channel challenges manifest in the routing protocols designed for underwater networks. These challenges encompass limited scalability, energy inefficiency, and the complexity of dynamic topology adaption.

UnlikeTDMA[6],CDMAaccommodates multiple concurrent broadcasts. This more optimally uses the underwater channel and at a much higher update rate with the nodes. CDMAachieves this multiplexing multiple broadcasts into a spread spectrum signal which also has the collateral benefit of making the acoustic signals resilient to noise resulting in a higher signal-to-noise ratio. Each node has a unique code for a particular receiver to extract its components from the spread spectrum signal to reconstruct its signal. This also affords some security within the network.CDMAis scalable to some extent with increase numbers of nodes/underwater robot team members. Underwater communications latency and intermittent connectivity leads to variations in the network group membership. While consistent membership is desired, underwater propagation conditions do not always permit that. Underwater communications forUUVorUSVfavoursUDP[78] communications which has less emphasis on hand-shaking (to acknowledge received messages) or ordering of received signal packets –TDMAis a popular implementation of this. OFDMA/CDMA are emerging options for underwater communications with advantages that address the underwater autonomous system challenges mentioned earlier and will be explored in this thesis. They will be considered for coordination and networking of robot teams distributed over extended ranges.

The above-water (in-airRF) component of the multi-domain network will useCDMA communication as well.RFCDMAhas received much attention so is not a research focus for this thesis. However, there are contributions in its integration with the surface domain.

This thesis is entitled: “Secure, Full-Duplex Multi-Domain Communications Network for Marine Robots”. Its contributions emphasize networked nodes across domains, necessarily more efficient bandwidth use, ability for concurrent transmission and reception, resilience to noise and interference, and network security.

A review of state-of-the-art tools suggests thatNS3and UnetStack [95] are reasonable thesis starting points for the analysis and simulations. This will be incorporated into the methodology.

To address these challenges and harness the potential of underwater communications requires the implementation of a well-thought-out methodology. In the next section, Chapter3, the proposed methodology will be presented, with the aim to address the identified challenges in this chapter and realize the thesis objectives. Development of a robust and efficient underwater communication system is the primary focus, achieved through the integration of theoretical insights, experimental verification, and emerging technologies. Chapter3comprehensively outlines the methodology to encompass discussions on the theoretical foundations, experimental setup, data collection, and analysis techniques applied in this thesis. It serves as a cohesive and interconnected component of this thesis – Chapter3 establishes a transition between the identified challenges and the practical implementation of the research.

Chapter 3

Methodology

[1]J. Ross, J. Lindsay, E. Gregson, A. Moore, J. Patel and M. Seto. "Collaboration of multi-domain marine robots towards above and below-water characterization of floating targets", 2019 IEEE International Symposium on Robotic and Sensors Environments (ROSE), Ottawa, ON, Canada, 2019, pp. 1-7, doi: 10.1109/ROSE.2019.8790419, [82].

[2]Jay Patel, Mae Seto. "CDMA-based multi-domain communications network for marine robots", J Acoust Soc Am 1 October 2020; 148 (4_Supplement): 2510. doi: https://doi.org/10.1121/1.5146976, [74].

[3]Jay Patel, Mae Seto. "Underwater channel characterization for shallow water multi-domain communications", Proc. Mtgs. Acoust 9 September 2020; 40 (1): 070014, doi: https://doi.org/10.1121/2.0001316, [76].

[4]J. Patel and M. Seto. "Live RF Image Transmission using OFDM with RPi and PlutoSDR", 2020 IEEE Canadian Conference on Electrical and Computer Engineering (CCECE), London, ON, Canada, 2020, pp. 1-5, doi: 10.1109/CCECE47787.2020.9255670, [75].

This chapter outlines and describes the methodology to achieve the thesis research objectives, described in Chapter1, and as informed by Chapter2. The objective is again aCDMA-based communications network for autonomous marine (robotic) systems that spans underwater, water surface and above-water which is novel. This is a problem with a large scope so the research contributions focus on the underwater nodes with only basic implementation for the surface and aerial nodes.

With that in mind, the methodology undertaken is as follows:

1.simulations based on theory to explore concepts that inform and refine;

2.hardware-in-the-loop (HITL) simulations towards more efficient and de-risked solutions;

3.implementation on real systems; and

4.in-water verification on real systems.

The theoretical analysis and simulations yield a nominal design for the network. Then, the next step is to realize the designed system in a hardware-in-the-loop (HITL) simulator. This efficiently tests new designs and de-risks the implementation on a platform and ultimately reduces the in-water testing needed. Then, the design is in high readiness for the in-water experimental test and verification phase which is performed in stages. It starts with tests in controlled environments like the indoor underwater tanks at the Dalhousie University Aquatron Facility. Then, the in-water test and verification progressed to less structured underwater environments off the jetties at the Centre for Ocean Venture Enterprises (COVE; Dartmouth, Nova Scotia). The final stage of in-water test and verification occurred in the uncontrolled environment at St. Margaret's Bay (Head of St. Margaret's Bay, Nova Scotia).

The detailed methodology depends on resources like software tools as well as hardware systems. The methodology scope is grounded in what is accessible for both as well as the time available. The thesis timeline was adversely impacted by the global pandemic among other circumstances. Due to the novelty of the research, it was also necessary to create custom testbeds and interfaces.

Given the thesis objectives, to start, the next section briefly introduces the available hardware and software tools thought relevant to the thesis objectives as well as the marine autonomous systems that will host the nodes of this novelCDMAnetwork.

3.0.1 Underwater Modems for In-Water Test and Verification

Several underwater modems were considered based on what was accessible to the Lab. The Woods Hole Oceanographic Institution (WHOI, Woods Hole, Massachusetts) Micro-Modem 2 (MM2) was the starting point for the thesis. MM2's use time-division multiple access (TDMA) modulation. As mentioned in Chapter1,TDMAis currently widely-used for marine robot collaborations across multiple domains since they are relatively easy to

design and implement. The Lab is familiar with these state-of-the-art modems and has used them successfully for a while. However, it was deemed difficult to convert them to CDMA. Therefore, software-defined underwater modems became a better fit for the thesis objectives since they could accommodate any custom/CDMAprotocols. The Subnero modems [9] were identified to meet the requirements to develop and verify aCDMA-based communications network.

In principle, theCDMAprotocol offers greater advantages overTDMAandFDMA. CDMAis a reliable proven technique for in-air communications which adds an extra layer of security to the communication system at the cost of increase system complexity. This enables the ability to transmit sensitive information securely through an underwater channel. However, it is just emerging underwater due to its receiver design and operational (tight regulation on transmitting power) complexities. To date, state-of-the-art underwaterCDMAsystems are only half-duplex [78]. One objective of the thesis is full-duplex CDMAcommunications for multi-domain marine robots.

For the in-water implementation, test, and verification of theCDMAnetwork, the Subnero M-25 series [57] software-defined underwater modems (Singapore) were selected. These modems types are still emerging and not yet widely used even in the research community.

Underwater software-defined modems are the preferred choice as it is possible to design and build new communications protocols with them. Modems which can natively support UnetStack [95] (discussed later) on their firmware, are desired. UnetStack has many good development tools - one of which is hardware-in-loop-simulation (HITL) with the modem. TheHITLcan simulate theUUVkinematics and communications between the robots. Such flexibility and customizability is necessary to develop communication networks for collaborative mobile marine robots. These software-defined modems also support Python APIs and custom baseband arbitrary waveform transmission. This is significant as there are available Python tools and utilities for basic modem functions making it easier to focus on the research aspects.

With this decision made, the underwater channel models and network design tools were considered given standard (no extraordinary memory or processing requirements) desktop and laptop computers for the simulations, design, and analysis.

3.0.2 Channel Models and Network Design

The open literature on underwater communications yields a variety of models for the physics of underwater acoustic propagation. A common one is the BELLHOP module in the Acoustics Toolbox [5] which is a ray-tracing analysis that predicts acoustic pressure fields in underwater environments. As the distance between nodes are kilometers or more apart, the water depths considered are orders of magnitude greater than the transmission wavelengths, and the transmission carrier frequencies are relatively high (10's and 20's of kHz), a ray-tracing treatment (and thus BELLHOP) is a valid underwater channel

modelling tool for the thesis.

For network design, Network Simulator 3 (NS3, [3]) is a network simulator initially used to design the CDMA-based multi-domain network. The World Ocean Simulation System (WOSS[41]) is a framework that integrates underwater channel environmental information with existing underwater channel simulators like theNS3. TheGEBCO2019 Database [38] contains bathymetry at 100 m resolution to integrate with the underwater acoustic channel model. These models and design tools work with the WHOI MM2 and Subnero M-25 series underwater acoustic modems. However, there are tools that work exclusively with the Subnero M-25 series that are promising in their research and development capability which are discussed next.

Unetstack [95] is the interface to develop, test and deploy Unetstack-based modems like the Subnero M-25. Additionally, Unetpy [52,94] is an open-source Python API which is compatible with Unetstack. The custom developed pysubacoustic module, was designed and developed in this thesis, to communicate with the Subnero modem across the Unetpy API. As part of the thesis work, contributions were made to the Unetpy API [94]. The pysubacoustic module confirmed the Unetpy APIs functionality with the Lab's existing Subnero M-25 series underwater modems.

Additionally, an above-water testbed was developed to facilitate test and development of underwaterCDMAagents. This is itself a contribution of a valuable tool others can use within Unetstack. How this was achieved is described next.

Unetstack's UnetAudio services [48] is a software defined open architecture acoustic model (SDOAM) which enables users to use their computer as a proxy for an underwater acoustic modem within the limitations of the computer sound card. The sound card performs the digital signal processing (DSP) as well as the digitizing and concurrent logging of the transmitted and received signals (operating full-duplex). Computer sound cards only sample up to 22 kHz bandwidth which is just short of the 25 kHz required for the thesis. Nonetheless, this feature is significant to the thesis as it offers a convenient method to test prototypeCDMAagents in an above-water environment prior to in-water testing and verification. Ultimately, it reduces the in-water tests needed. Once developed, the computer is replaced with an embedded processor like the Raspberry PI integrated with an USB sound card. This testbed also works with a user dashboard to, for example, reconfigure modem parameters or evaluate performance during run-time.

The custom developed dashboard provides real-time signal stream plotting and critical information on the communication system's performance. This testbed dashboard was designed and implemented based on the Plotly [77] python module. It was designed and implemented for the testbed and also configurable to be used for field-testing with UnetStack-based Subnero modems like the M-25 series used in the thesis. The testbed and associated dashboard will be made accessible to all underwater acoustic developers and is in itself, a contribution.

For the integration of the in-airCDMAcommunication component, this chapter explains how data transmitted from underwater nodes/sensors are relayed to the surface node using traditionalRFmethodologies or software-defined in-air modems (radios) like ADALM PlutoSDR [33]. The use of GNURadio [39], Unix piping system, sockets and ROS2enables the information to go across multiple domains.

In addition to the modems, support equipment like over-the-side hydrophones, power supplies, acoustic sources, analyzers, conductivity-temperature-depth sensors,A/Dconverters, etc. were also used. Boats and RHIBS supported the in–water verification as required. Implementation on the robotic platforms is the next stage after completion of the thesis objectives and is out-of-scope for this thesis. The marine robotic platforms the CDMAnetwork will ultimately be hosted on will be discussed next as it provides context and fortifies the use case.

3.0.3 Marine Multi-Domain Autonomous Systems – Concept of Operations

Collaboration between marine robots that span multiple domains create new capabilities for research, military and commercial end-users for ocean observation, timely military situational awareness, or commercial surveys and prospecting [6], respectively. Therefore, the requirement that drove this thesis was for secure, full-duplex, high bandwidth communications across domains for collaborating marine robots.

The thesis objective is to investigate the efficacy of underwater communication systems based onCDMAdeployed on collaborative robotic platforms across multiple marine domains (Figure3.1). These domains encompass underwater, surface, and above-water environments and therefore networkUUV(Figure3.2a),USV(Figure3.2b) andUAV(Figure 3.2c) platforms, respectively. Each of these robotic platforms is a mobile communications node. Note, the USV has 2 nodes – an underwater and an above-water one.

While the integration of the novel network onto the marine robots was not the first focus of the thesis, the network implementation considers the robotic platforms.ROS2is the defacto publish-subscribe architecture on-board modern autonomous robots.ROS2consists of robotics algorithm libraries, simulators, and middleware. This *pub-sub* architecture facilitates creating the many decoupled processes required to operate advanced autonomous systems. The novel development here is to useROS2to facilitate communications between multiple robots which each host communications nodes. This results in a more seamless integration of the communications network with the robots where the novel communication nodes are integrated into theROS2robotic architecture. The concept of operations is that a support ship monitors and manages the robot teams' efforts and objectives.

The proposed solution to transmit underwaterUUVinformation above-water is to use USVs as communication network nodes. TheseUSVs have underwater acoustic modems

(below the waterline) which receive underwater acoustic transmissions from theUUVand then re-broadcasts them usingRFradios above-water. This in itself is not new [78]. As the USVis at sea level it is difficult for it to transmit extended ranges in-air since its horizon is only $6 \sim 7$ km. It is proposed to periodically deploy and recover anUAVfrom the ship to monitor the robot team ofUSVs andUUVs and to relay their information to the ship and the ship's updated commands to the robot team.

With theUAVrelayed information on the robot team's telemetry and status, the shipboard operators can monitor, assess, re-task or aid in the robot team's survey and inspection objectives. TheUAVrelayed information on the survey or inspection would be used by the ship. It is of course possible for theUUVon the surface to transmit directly to a low altitudeUAVif theUAVknows where and when theUUVsurfaces.

Given the discussion on physical layer systems (underwater modems), underwater acoustic models and network design tools, the thesis methodology is refined as follows:

1. Develop an underwater communications channel model that captures environment parameters like sound-speed profile, bathymetry, and seabed cover. The aim is to predict the performance of the communication system given the environmental characteristics in the underwater channel. This will be achieved with BELLHOP.

2. Design aCDMA-based network topology that meets the requirements of security, high

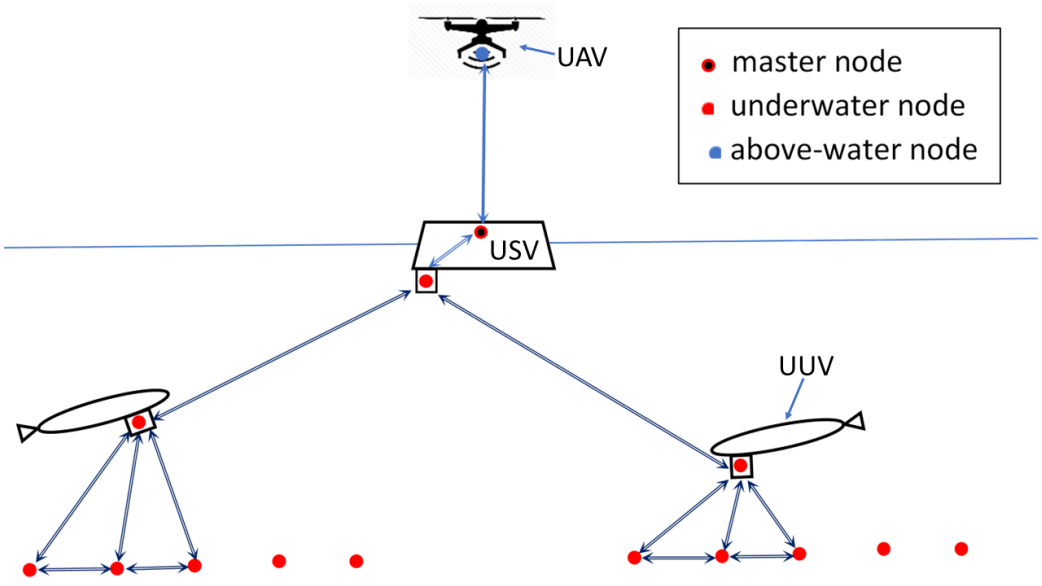

Figure 3.1: Architecture for the marine sensor network with nodes deployed on heterogeneous robotic platforms. The network comprises autonomous marine platforms includingUUVs,USVs, andUAVs, as well as stationary underwater sensors. TheUSVrelays messages between the underwater (UUV) and above-water domains (USV, UAV). This configuration enables efficient and robust data collection in multiple marine environments, facilitating a range of oceanographic research, military and commercial applications [56,76].

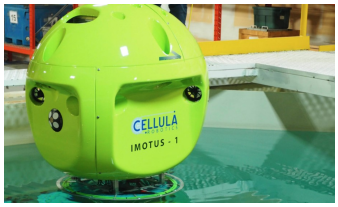

(a)

(b)

(c)

Figure 3.2: Robotic platforms that host nodes in the research: (a) IMOTUS hover-capable UUVhosts an underwater node; (b) ISL high-buoyancyUSVhosts an underwater and above-water node, and (c) ISL marinized PelicanUAVhosts an above-water node. These nodes are networked to securely transmit data from the underwater to above-water remote location to enable near real-time decision-making and coordinated autonomous communications [56,82].

bandwidth, and full-duplex communications with nodes operating across multiple domains. This will be achieved withNS3,WOSSandGEBCOto start.

3. Implement theCDMA-based network topology using software-defined modems and radios, followed by an evaluation of the network's performance across the multiple domains in a structured laboratory environment. This will use Unetstack with its associated Unetpy interface and UnetAudio Services.

4. Perform in-field testing of the designed and implemented CDMA-based multi-domain network. This will use the Subnero M-25 series modems for the underwater nodes and the software-defined PlutoSDR radios for the in-air nodes. The testing will involve deploying the network in a real-world marine environment, conducting communication tests under various conditions, and collecting data for further analysis. Based on the results, necessary refinements will be made to the network design and implementation, followed by a final round of testing to validate the performance of the refined network.

These steps contribute to understanding the efficacy ofCDMA-based underwater communication systems and their applicability for collaborative robotic platforms operating in multiple marine environments. The following sections will describe these 4 steps in turn starting with the underwater channel model.

3.1 Underwater Acoustic Channel Model

A question from the background and literature review was to determine the important underwater channel parameters that drive performance. Underwater acoustic channel models are specific to the environment and vary with the sound velocity profile, slant range, seabed bottom type, water depth and bathymetry (Figure3.3) between the source and receiver. Therefore, prior to a deployment, it mitigates risk and reduces the in-water trials time, to perform simulations of the mission with communications nodes in as realistic a

channel model as possible. Predictions of the communication system's performance, as a function of the channel's characteristics, informs mission parameters like available bandwidth, achievable range between transmitter and receiver, data rate, optimal depths to deploy transmitter and receiver, and network topology. Such simulations provide insight into the communication system's performance for given channel conditions.

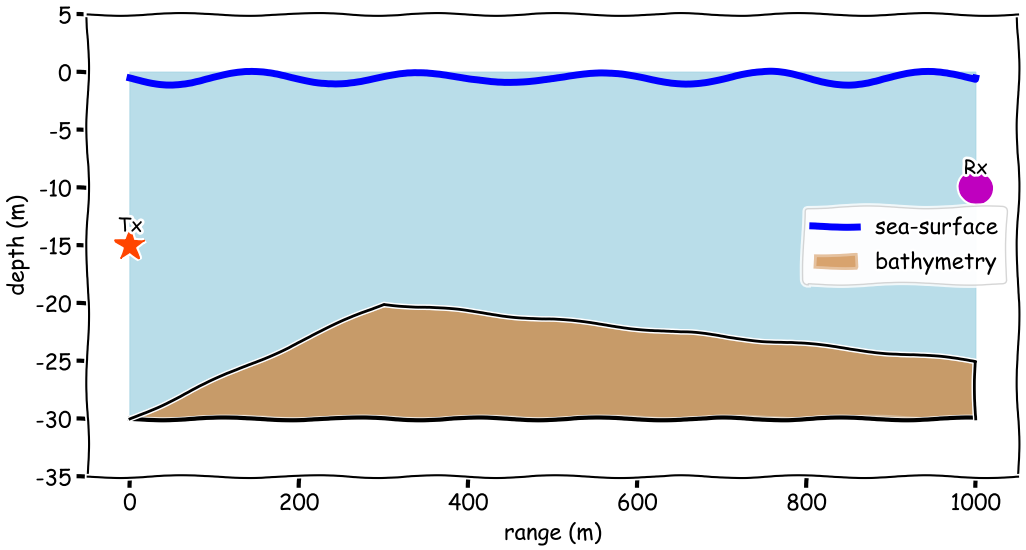

Figure 3.3: Basic components of an underwater acoustic channel: sea surface, bathymetry, and an acoustic transmitter (Tx) and receiver (Rx). The sound speed profile is an important component (not visualized).

It is proposed that BELLHOP be embedded in the channel estimation model. BELLHOP produces relevant predictions like ray-paths (Figure3.4a), transmission loss (Figure3.4b), eigen-rays (Figure1.2), and time-of-arrivals (Figure3.4c) as time-series. This is based on inputs for the acoustic presence of the water surface, bottom boundaries (bathymetry), sound speed profile (SSP), seabed absorption, receiver and transmitter array depths, etc. The BELLHOP embedding is convenient and makes the channel model more streamline for analysis.

For the underwater channel, Thorp propagation [91] andWOSS[41] are initially used as they are natively supported byNS3. Thorp approximation accounts for frequency dependent attenuation due to absorption and spreading (Eq.1.1) as a function of range. The BELLHOP module of the Acoustic Toolbox [5] channel simulator is more sophisticated and used to predict transmission loss, and thus transmission ranges, between transmitter and receiver.

Bedford Basin (Halifax, Nova Scotia) is an inland body of water used for marine robot and underwater communication testing by the Lab. Its depth varies from $0 - 60$ m. Its sound speed profiles have been measured by the Lab (Figure3.5) and its bathymetry is

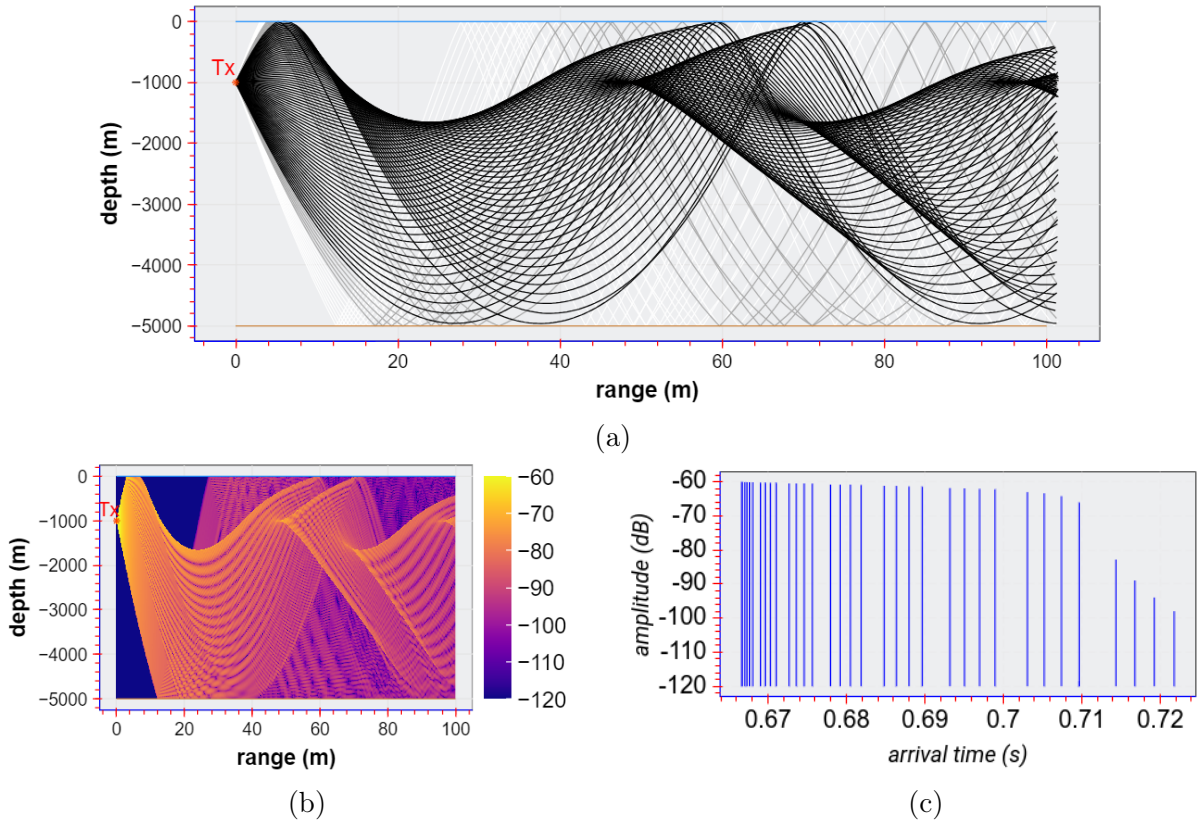

Figure 3.4: The BELLHOP Acoustic Toolbox [5] used in the thesis predicts: (a) ray-tracing propagation of sound wave paths far from a source; (b) transmission loss from signal attenuation with distance, and (c) relative ray arrivals to show temporal distributions of acoustic energy. These predictions are critical to design and optimize underwater acoustic communication systems to perform optimally given the underwater channel.

known to within a 5 m resolution (Figure3.6). Given the detailed environment information of the Basin as an underwater acoustic channel, it is used as a test environment for modelling.

With the underwater acoustic channel model and a sample environment defined, the next step is to address the design and implementation of the CDMA network that will operate within this modelled channel.

3.2 Design of Novel Marine Multi-Domain Network

This section addresses how to develop and implement a multi-domain marineCDMA communication network that incorporates the underwater path. The work-flow for the network design is shown in Figures3.7(tool selection), Figure3.8(modelling).

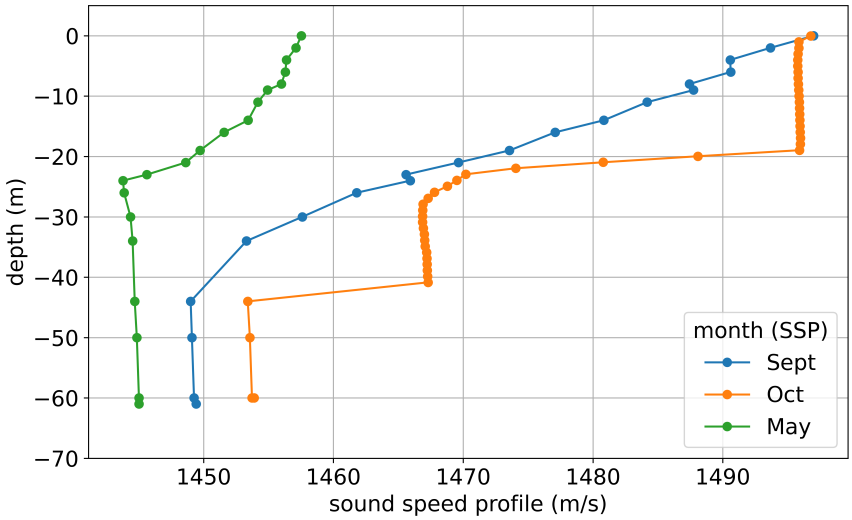

Figure 3.5: Sound speed profiles for Bedford Basin (Halifax, Nova Scotia) as a test environment for this thesis. Its sound speed profiles vary with the season and directly impact the underwater acoustic channel and thus communications performance betweenUUVs and the submerged part of theUSV. It is important to consider the sound speed profile in network planning and operations [67].

Red boxes represent problems or challenges. They are mapped to green boxes which are possible solutions that are not themselves without challenges. This outlines the process that lead to decisions on tools and solutions for the thesis.

To start, a thesis challenge was to explore how to securely communicate information from underwater to above-water (surface domain) then to a remote base station (and vice versa). This is challenging given the underwater channel's limited bandwidth and acoustic ambient.

3.2.1 Underwater CDMA Network

The state-of-the-art in multi-environment marine autonomous systems communications uses conventional in-airRFradios above-water which patches to an underwater acoustic modem on anUSVrelay with anRFradio. Usually, the underwater acoustic communications modulation isTDMA, where eachUUVor node is allocated one cyclic time slot for transmission.TDMAdoes not scale well with increased number of nodes. With many nodes in a network, long intervals elapse before a node (UUV) can report its position, status or other information. As well, the potential for interference increases with number of nodes. Other communications protocols and access controls will be explored in the proposed work with marine environment considerations for robots that span multiple

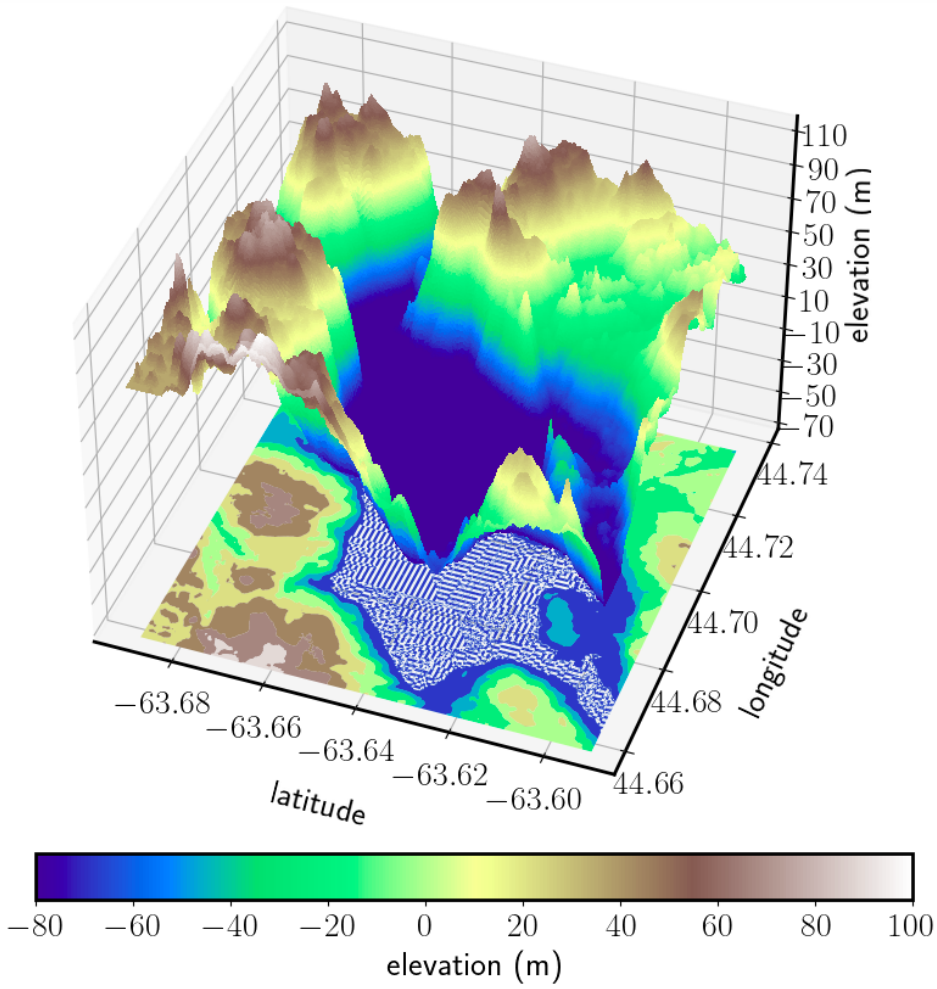

Figure 3.6: Bathymetry of Bedford Basin (Halifax, Canada) which is an environment for in-water testing. Simulations in this thesis use Bedford Basin to test models on network operational range and transmission loss betweenUUVs and theUSV.

domains.

The underwater branch of the network cannot be developed like a conventionalRF one (Figure3.17, discussed later). In general, the three techniques to analyze network performance are:

1.analytical modeling;

2.simulations, and

3.real-time physical measurements.

For the first two techniques, simulations are a feasible approach for this analysis, initially.

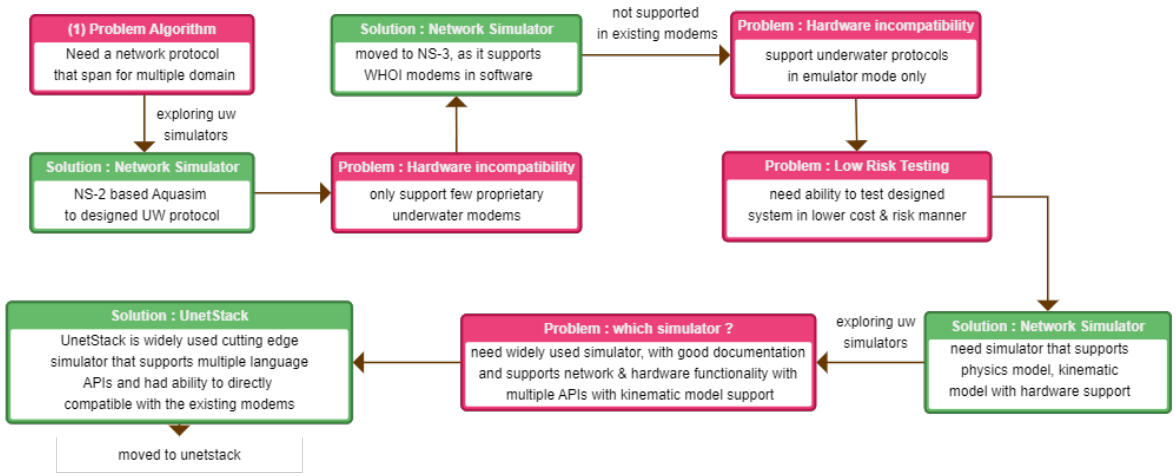

Figure 3.7: Decisions that justify selection of Unetstack over NS3 for network modelling. This starts with the original problem (upper left) and solutions followed by subsequent problems that lead to Figures3.8.

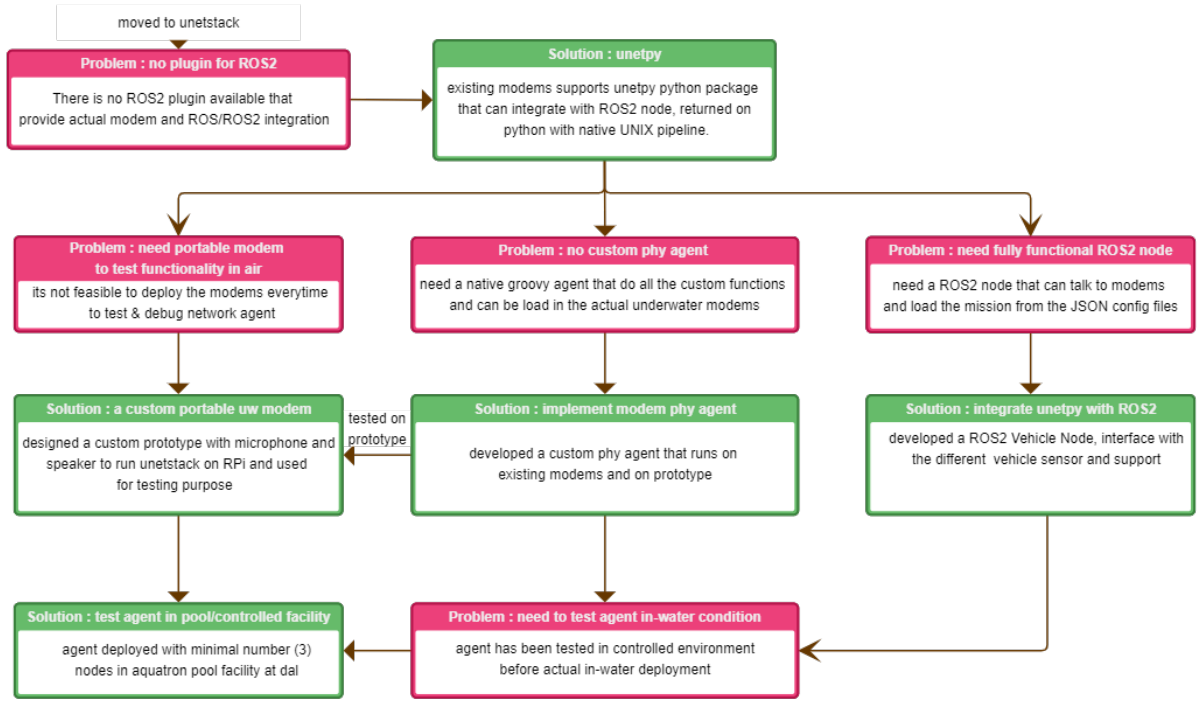

Figure 3.8: Continuation of the decision process from Figure3.7, This decision branch focuses on implementation of the proposed system with UnetStack and integration with the real-time robot/modem using ROS2. This continues in Figure3.9(in-water testing)

Initially,NS2and Aquasim [8,86] were explored as candidate underwater network simulators. Due to their lack of hardware support (restricted to a few proprietary underwater modems) and maintenance, the newerNS3integrated with theWOSSframework, was

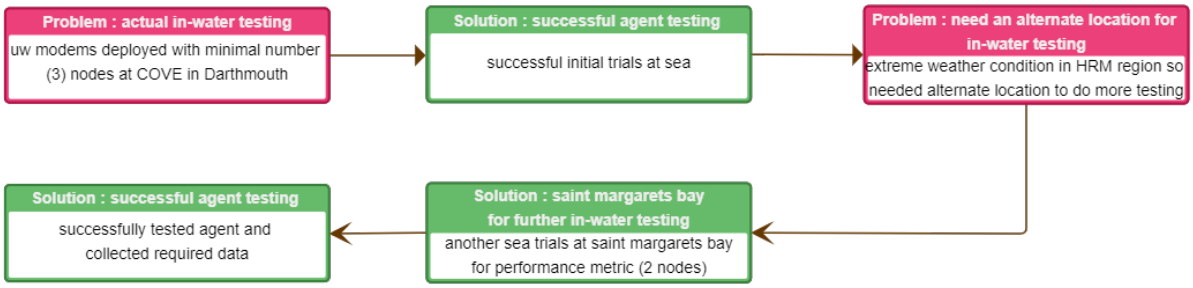

Figure 3.9: Outdoor in-water strategy to verify the marine CDMA network.

selected to work initially with the WHOI underwater Micro-Modems.

Table 3.1: Communication system parameters to capture in the underwater channel model. These impact receiver and transmitter performance like the network's operational range and bandwidth as a function of environmental conditions.

parameter	**channel 1**	**channel 2**
	source inputs	
number of sources	1	1
carrier frequency (Hz)	25000	25000
source depth (m)	10	3
water depth (m)	200	20
launching angle	45	60
	receiver input	
receiver depth (m)	1.8	1.8
receiver ranges (km)	[0 6]	[0 6]
number of receiver depths	201	201
number of receiver range	501	501
number of beams[a]	0	0
	additional options	
method of interpolation	CVW	CVW
type of media	A*	A*
type of information required[b]	R	R

[a] zero indicate BELLHOP automatically calculates the number of rays required,
[b] choose R for rays, E for eigen-rays, C for coherent acoustic pressure.

UWA communications is needed for multi-domain collaborative marine robotics missions that require transmission of control commands, sensor data / information and shared situational awareness from above to below water and vice versa.

To predict the performance of a communication system, the underwater channel model from Section3.1, sound speed profile and Table3.1parameters are needed. The predictions

are needed prior to deployment for: 1. a priori insight towards adaptations to channel characteristics; 2. guidance on optimal placement of marine robots; 3. estimates on parameters for link budget calculation, and 4. most importantly, an estimate on the communications network range. This is illustrated through a use case discussed next.

A non-responsive floating target is at the horizon (6 km) in Bedford Basin (Figure3.6) where water-depth varies from 0 - 60 m. A collaboration ofUUVand USV are deployed from a ship to investigate and the UUVs must communicate underwater with the USV. The UUV nodes are not always in range, and do not need to communicate with each other all the time (Figure3.14). It depends on the mission that is underway (e.g., coordination, collaboration, surveying, etc). The following assumptions were made: (1) 25 kHz carrier frequency (4-5 kHz bandwidth) for underwater acoustic modems integrated on theUUVs and submerged part of theUSV; (2) measured ambient noise at 73 dB; (3) sea bottom sound-speed $\simeq$ 1450 m/s; (4) a sound speed profile (SSP) is available through a sound speed drop or seasonal measurements (Figure3.5) [67], and (5) for link budget calculations, monitor transmission loss (TL), with 60 dB identified as the critical threshold based on theUUVs' underwater modem operating characteristics.

From the above five assumptions the network operational range can be estimated. Then, the amount of data reduction needed for the on-board sensor measurements, control signals and mission information to communicate betweenUSVandUUVcan be determined.

Table3.1highlights the necessary channel parameters to model. Figure1.3is a simulation example with a multi-domain autonomous ocean observation network with four nodes: fixed sensors, mobileUUVs, mobileUAVs, and the fixed surface node (USV) which hosts the master node. The master node (USV) relays the underwater sensor measurements to theUAVvia radio frequency (RF) communications. This example focussed on the UWA links specifically, evaluating the communication networks' operational range.

To achieve the maximum communications range the following are considerations:

channel environment: sound velocity profile, bathymetry and water depth (inherent to the channel)

systems operations: carrier frequency, slant range, surface proximity (operationally driven).

Figure3.10shows a typical channel condition betweenUUVandUSV, the achieved network operational range for a given sound velocity profile, and proximity to the near surface. Given the carrier frequency and chosen transmission loss threshold, the achievable range betweenUUVandUSVwas determined to be $<$ 1.5 km. This underscores that channel sound velocity profileSVP, slant range between theUUVandUSVand near-proximity to the surface must be captured in the model. This verifies the BELLHOP Acoustic Toolbox channel predictions for oneUUVand oneUSVnode to evaluate the achievable range given transmission loss between two nodes and thus the required number

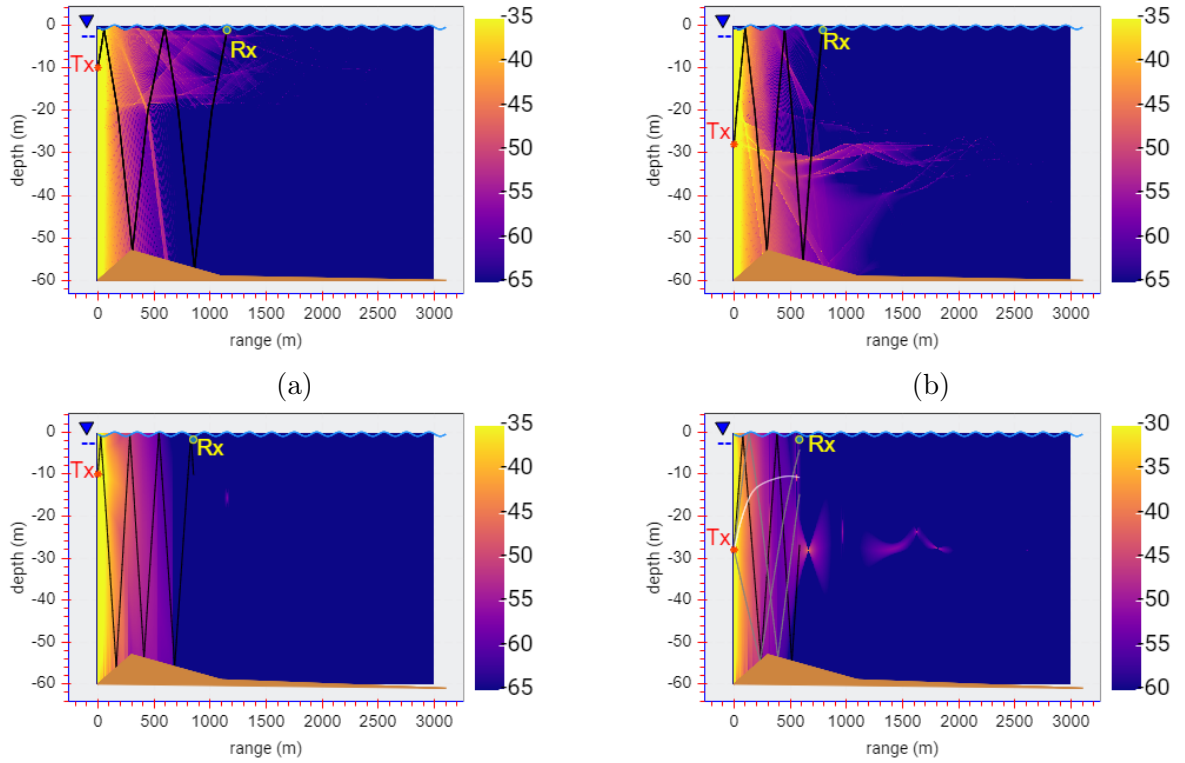

Figure 3.10: For an USV underwater node at 1.8 m depth which must communicate with a submerged UUV, the achieved range depends on the maximum acceptable transmission loss (60 dB), carrier frequency (25 kHz), and sound speed profile (Figure 3.5 and UUV depth. (a) and (b) both have the Oct (winter) SSP with UUV depths of 10 m and 28 m, respectively with achieved ranges of 1150 m and 790 m, respectively. (c) and (d) both have the May (spring) SSP at UUV depths of 10 m and 28 m, respectively with achieved ranges of 850 m and 580 m. These BELLHOP simulations show a shallower UUV depth yields a greater range when one node must be on the surface. For the same UUV depth, the winter SSP yields greater range. These examples are relevant to collaborating underwater nodes which is relevant to this thesis.

of UUV/USV) nodes to achieve the total mission range.

There has been a fair bit of development in UAN simulators [3,15] and emulators [24] at the time of the study. Based on a review, NS3 was selected as an appropriate simulator as it has the required capabilities for this thesis like cross-layer protocol development and specific UAN [91] tools to design the network topology.

The UAN tool in NS3 is the proposed one to develop the UW-CDMA. At the time of the study, NS3-v 3.30 supports TCP/IP and UDP. The proposed UW-CDMA network to develop would model from the channel to the application layers (Figure 3.12), incorporate

BELLHOP (viaWOSS[41,42]) and account forUUVkinematics. Notably,NS3has multi-threaded functionality [102] compared to other network simulators. In this framework, Rake receivers [34] are considered since they are efficient forCDMAand make effective use of the multi-path propagation characteristics. The packet contains a header and its data which is spread by pre-defined unique random codes assigned to each node (Figure3.11).

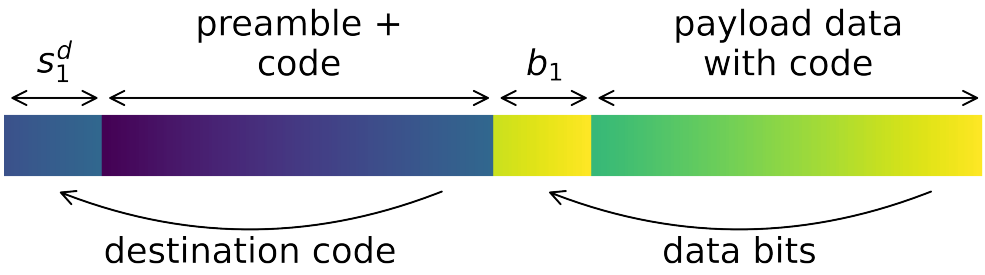

Figure 3.11: Packet format used modified from [34]).

NS3also estimates the channel's impulse response ($h(t)$), signal-to-noise ratio (SNR), and other performance measures. This information can be used to adapt the transmission strategy to the current channel conditions, improving the performance and reliability of the whole communication system.

The next sub-section describes how these described modelling tools will be integrated into a larger framework to address the thesis objectives.

3.2.2 Software Framework

The software framework is a construct or framework which integrates all the communication systems' components that includes the underwater and above-water stacks. The underwater stack is discussed next.

To start, the underwater stack was based on an underwater network stack inNS3, a discrete-event network simulator. Unlike traditional TCP/IP stacks used in terrestrial networks, the proposed stack is designed to handle the unique challenges of underwater communications networks, like high latency, low bandwidth, and high error rates. This stack's application, transportation and routing,MAC, and physical layer (acoustic modems) are discussed next.

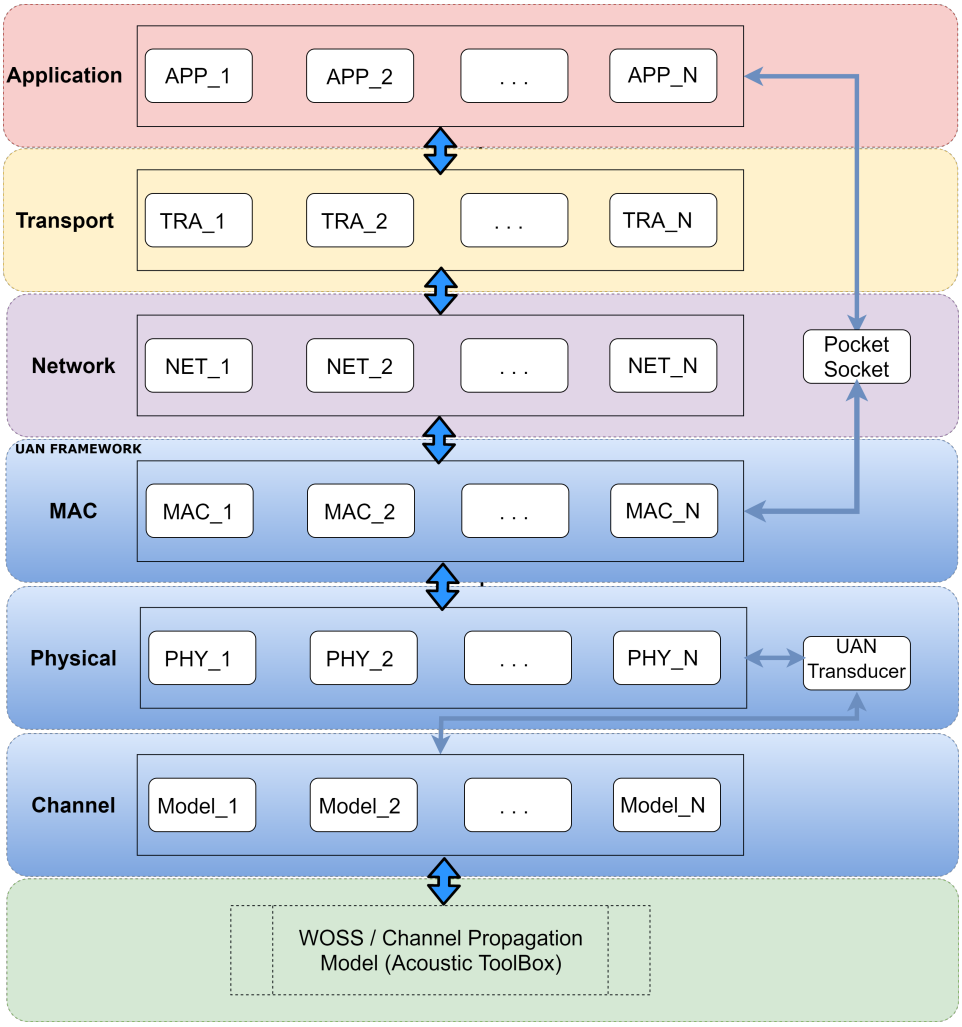

Figure 3.12: The stack to simulate the proposedCDMAprotocol using theUANtool in NS3. This framework models the entire communication process from the channel to the application layers. It integrates the BELLHOP ray-tracing model viaWOSSand accounts forUUVkinematics. This complete end-to-end approach allows for a realistic simulation of underwater communication systems. Note however, that not all layers of the stack are involved in every operation.

Underwater Stack

Application Layer

WithNS3simulations, the generated packets may not contain information bits, but they have a packet header with packet state information. Generally, in simulations, network transmit/receive success rates can be predicted with probabilistic models [102]. The packet header also has acyclic redundancy check (CRC)bit which verifies at the end of the transmission whether a packet was successfully received. The transport and routing

layers play significant roles in managing the unique challenges of underwater communication, ensuring that data is transmitted reliably and efficiently, adapting to the dynamic environment.NS3's transportation and routing layers are discussed next.

Transportation and Routing Layers

NS3has API support for the transportation and routing layers which are fairly straight forward to use. The proposed stack will use standard IPv4 andUDPprotocols [91] which are customized with parameters for theUANframework.UUVposition is tracked through theNS3UUVkinematic models. Static routing protocols, which use pre-defined routing information, is used for the routing layer to relay information to the next hop for the transmission.

The Medium Access Control (MAC) layer's primary function is to control how networked devices gain access to the medium and permission to transmit. Given the unique characteristics of underwater environments, such as long propagation delays, high error rates, and limited bandwidth, theMAClayer's role becomes even more critical.

MAC Layer

As mentioned earlier, in a shared communication medium like underwater, multiple nodes may attempt to transmit data simultaneously, leading to inter-symbol collisions. TheMAClayer protocols manage access to the medium, to avoid such collisions and improve overall network efficiency. For instance, this thesis'MAClayer is a combination of ALOHA [4,91] andCDMAtechniques. Given the limited bandwidth in underwater communications, the available spectrum must be efficiently used. TheMAClayer protocols ensure the channel is optimally used, balancing the need to avoid collisions with that to maximize throughput, consequently, there is no packet acknowledgment given the limited available bandwidth. Devices used in underwater communication, such asUUVs or sensors, often operate with power constraints. TheMAClayer contributes to energy efficiency by managing when devices go into a low-power sleep mode and when they need to be active for transmission or reception. In some instances, theMAClayer adapts the network to evolving underwater conditions. For instance, if a node moves, or if environmental conditions change, theMAClayer can adjust its protocols to maintain efficient communication.

Physical Layer

The physical layer in underwater communication systems manage the transmission and reception of data over the medium, modulates and demodulates the signals, detects and corrects errors, characterizes the communication channel, and manages energy use. It plays a fundamental role in ensuring data can be reliably transmitted and received in the challenging underwater environment. The physical layer in this framework uses a cross-layer approach for request-to-send (RTS), which contains the destination address. This is different from traditional TCP/IP stacks where RTS is handled at the MAC layer. For the thesis, the physical layer is realized in the form of an underwater acoustic modem. For

shorter data, the *uwlink* agent is the physical layer for UnetStack and provides reliable datagram delivery [93].

The transmitted signal, $e_i(t)$ (Eq.3.1), such that $B_i(t)$ is the packet from transmitter, **i**, and $s_i(t)$ is the spreading code for transmitter **i** (Figure2.7) is:

$$e_i(t) = B_i(t)s_i(t). \tag{3.1}$$

The received signal from all underwater nodes is defined as:

$$= \sum_{i=1}^{K} e_i(t) \circledast h_{ir}(t) + \eta(t) \tag{3.2}$$

such that r_i is the sum of the contributed signals from each node, i. This is the convolution of the transmitted signal $e_i(t)$ and channel impulse response $h_{ir}(t)$; $\eta(t)$ is additive Gaussian white noise on the channel and K is the total number of underwater network nodes. When node i is not transmitting, $\mathbf{r_i(t)}$ is logically set to zero. The channel model is based on that of [34] which uses the the Rake receiver principle where in the event of multiple receivers, the one with the strongestSNRis chosen.

With the underwater stack identified, the next step is to develop a methodology to study a multi-domain network of autonomous marine robots (Figure3.1) to communicate using the developedCDMAprotocol. To start, this could be set-up inNS3with two types of communication nodes: fixed and mobile ones. The mobile ones would be integrated on UUVs andUSVs. As theUSVis in a unique position in the water column between above and below water, it hosts the master node which controls the distribution and movement of all network nodes. In this way, theUSVmaster node can relay messages from underwater (UUV) to above-water (UAV(or some other above-water node) and vice versa. This is more complex than a homogeneous set of nodes in one domain. How the network will be designed and then simulated is described next.

3.2.3 Justify Choice of CDMA

The proposed UW-CDMA network was tested with a 15-nodes example, described below, and compared against the UAN geo-routing aware MAC protocol, UW-GOAL [91], supported inNS3. This comparison serves as a performance measure for the proposed CDMA framework and justifies the choice of the CDMA protocol.

First, create a network of 15 communications nodes of which: 3 are under, or on, the water (2-UUVs, 1-USV); 1 is above-waterUAV(not shown), 1 node is the master (hosted on theUSV), and the other 10 are underwater stationary nodes (e.g. deployed seabed instruments, arrays, etc.). The master node communicates bi-directionally with the mobile sensor nodes (2UUV, 1USV, 1UAV). The submerged stationary sensors communicate

bi-directionally with eitherUUVor amongst themselves. 14 of the 15 nodes are integrated with sensors. The 15^{th} is the master node on theUSVused for relaying. TheUSVcould also have been a sensor node but not for this case. All nodes are transceivers.

Next, construct the marine robot network with theUANmodule and generate the code which uniquely identifies each node. Subsequently, establish the interface, which encompasses the acoustic links facilitating inter-node communication (Figure3.1and Figure1.1). All nodes, except the master andUAVones, collect sensor data (e.g., conductivity or temperature). The master node relays the underwater sensor payload measurements to the UAVvia anRFlink. Finally, the collected stationary sensor data is encoded and transmitted to the master node via theUUVs' nodes. The simulation parameters are shown in Table3.2and the steps in Figure3.13.

Table 3.2: The framework to design the proposed CDMA-based multi-domain communications network of autonomous marine robots utilizing the NS3 framework with IPv4 as the TCP/IP model.

parameter	**value**
data rate	512 b/s
center frequency	25 kHz
transmission bandwidth	5 kHz
TCP/IP model [a]	IPv4
packet error rate model	ns3::UanPhyPerNoCode
signal noise model	ns3::UanPhyCalcSinrDefault
acoustic propagation model	ns3::UanPropModelThorp
acoustic propagation speed	1500 m/s
mobility model	RandomWalk2Dmobilitymodel [b] (speed: 2 $\sim$ 4 m/s)
energy model	Acousticmodemenergymodel (Tx: 50$\sim$80 W Rx/Idle: 160 mW, sleep:6 mW)
payload of DATA	64 Bytes
# of data packets / block	60
number of nodes	3–20, nodes are randomly deployed
sink node position	(1000, 1000, 0) m
source node position	(0, 0, 200) m

[a] framework uses the default TCP/IP support module from the coreNS3 for terrestrial communications, while underwater communications utilize the UDP protocol, [b] directions are chosen randomly.

As mentioned earlier,WOSSis a framework which integrates environmental channel characteristics like bathymetry,SSPand, sediment type with an underwater channel simulator, likeNS3or others, to predict network performance.WOSSandNS3are natively integrated soNS3automatically expects theSSPand bathymetry.SSPs for a region are obtained from in-water casts or archived seasonal profiles. Bathymetry can come from

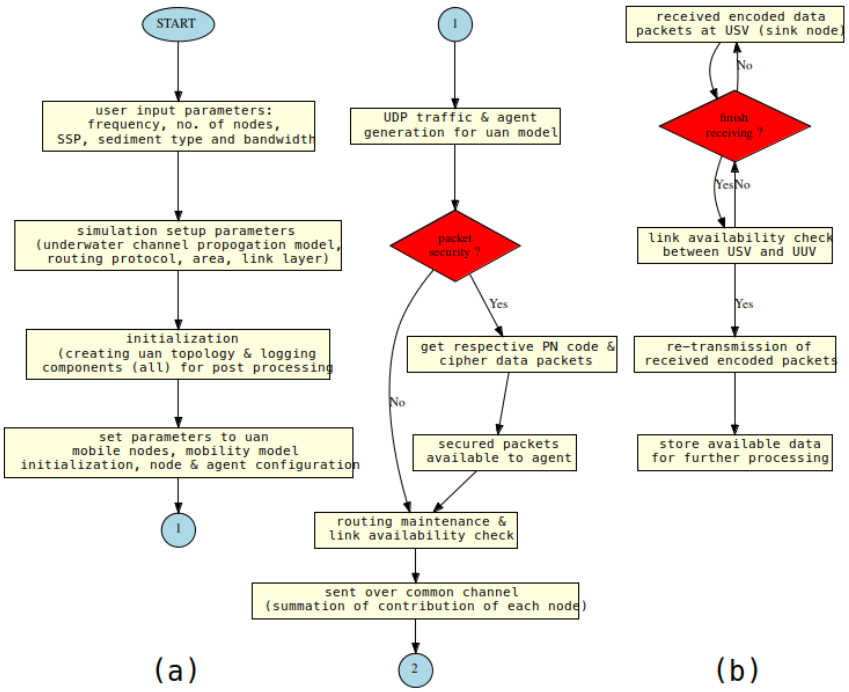

Figure 3.13: The steps to carry out an NS3 simulation. Shown is the communication process within the multi-domain network of autonomous marine robots: (a) transmission of encoded signals from mobile nodes (UUV,USV,UAV) to the master node, and (b) reception of these signals at the master node from the mobile nodes.

GEBCO(100 m resolution) or sources like thecanadian hydrographic service (CHS)(2 m resolution). Visualization tools were implemented for the integratedWOSS/CHS-NS-3 simulator to assess the impact of node deployment and mobility on performance as shown in Figure3.14.

TheNS3multi-threading functionality means parallel processing could be applied to the USV master node to improve network simulation performance (though it was not applied here). TheUANWOSS[41,42] channel model calculates the channel's impulse response. Each node is assigned a unique pre-defined code known to the master node. Adaptations were made to embed theUUVdepth as a thirdNS3parameter, in addition to theSSPand geo-referenced bathymetry (from eitherCHS(2 m resolution) orGEBCO2019 Database (100 m resolution)). OtherNS3inputs include the node deployment location and mobility (UUV velocities).

Once the bathymetry is extracted, BELLHOP acoustic model simulations were performed for the frequency band around the carrier frequencies (25 kHz). This generates a BELLHOP environment object, times-of-arrival, as well as ray-tracing data for post-processing and verification to evaluate network performance. With all this,NS3could support WHOI MicroModem physical channel simulations usingfrequency shift-keying (FSK)andquadrature phase shift-keying (QPSK)modulations.

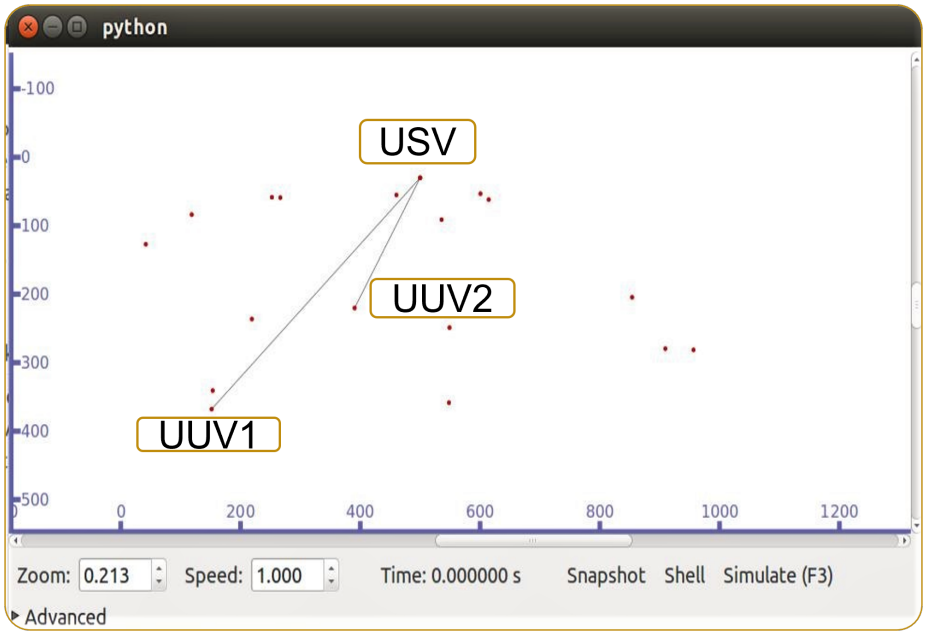

Figure 3.14: AnNS3simulation of the multi-domain network of autonomous marine robots. Note multiple UUVs deployment and mobility are coordinated through the master node hosted on theUSV. The 10 dots are stationary underwater nodes like seabed instrumentation, arrays, etc. that are part of the network.

Such simulations were performed for a variety of node mobility and deployment configurations like: list (equi-distant on a line); grid (even $x - y$ spacing); random rectangle (4 nodes in a rectangular configuration with unknown central location); random arc (nodes not necessarily equi-distant and with unknown central location), and uniform arc position (nodes equi-distant on an arc) (Figure3.15). All simulations were for the Bedford Basin bathymetry (Figure3.6) andSSPin Figure3.5.

User-supplied scripts in the 2D NetCDF data format are required to extract:

- bathymetry measurements fromGEBCOgiven a GPS coordinates (lat/long) and 15 seconds arc (2 km) of measurement in the desired direction, and
- bathymetry, sediment andSSPmeasurements from theCHSmeasurements,SSPcan also be directly defined in theWOSSmodule.

The end-to-end delay (EED) performance results are depicted in Figure3.16(a). In UW-GOAL, a longer wait time before sending a data packet is employed to avoid collisions, resulting in longer end-to-end delays, particularly when the nodes are randomly distributed. In contrast, the proposed framework utilizes the entire channel's bandwidth to transmit multiple signals, each assigned a unique pre-assigned code to the receiving node. This efficient utilization of the channel reduces the end-to-end network delay, enhancing

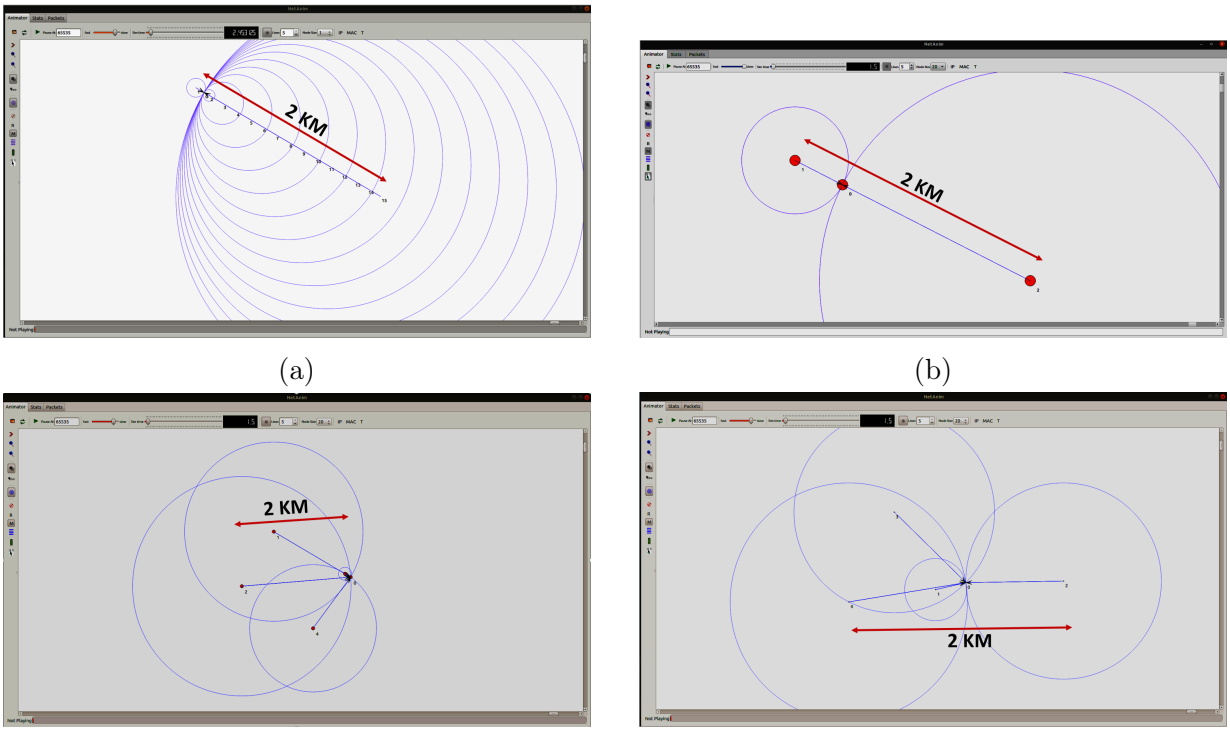

Figure 3.15: Various node deployment configurations and their relative spacing used in theNS3andWOSSintegrated simulations to study their impact on network performance. The configurations depicted are: (a) list position with 15 nodes; (b) list position with 2 nodes; (c) grid position with 5 nodes, and (d) random arc position with 5 nodes.

communication efficiency.

Energy consumption with increasing node numbers is shown in Figure3.16(b). As expected, transmitting nodes consume more power compared to receiving/sink nodes. It is noted that underwater acoustic networks typically have limited energy per node.

In the UW-GOAL protocol, transmitting nodes broadcast data packets to their immediate neighboring nodes, and receiving nodes with higher priority forward the received data packets. However, unstable links in underwater sensor networks often result in higher packer error rate (PER), making it challenging to receive data packets reliably. The proposed framework, on the other hand, employs a collective decoding mechanism where nodes collectively decode data packets from multiple sending nodes. The network throughput, defined as the number of received packets per unit time, and thepacker delivery flow (PDF), defined as the total number of transmitted packets normalized by the total number of received packets, are shown in Figures3.16(c) and3.16(d), respectively. Both the proposed framework's throughput andPDFoutperform UW-GOAL's.

Unfortunately, to design a real-world underwater communications system,NS3falls short in several key areas. It only offers support in emulation mode, this means it cannot

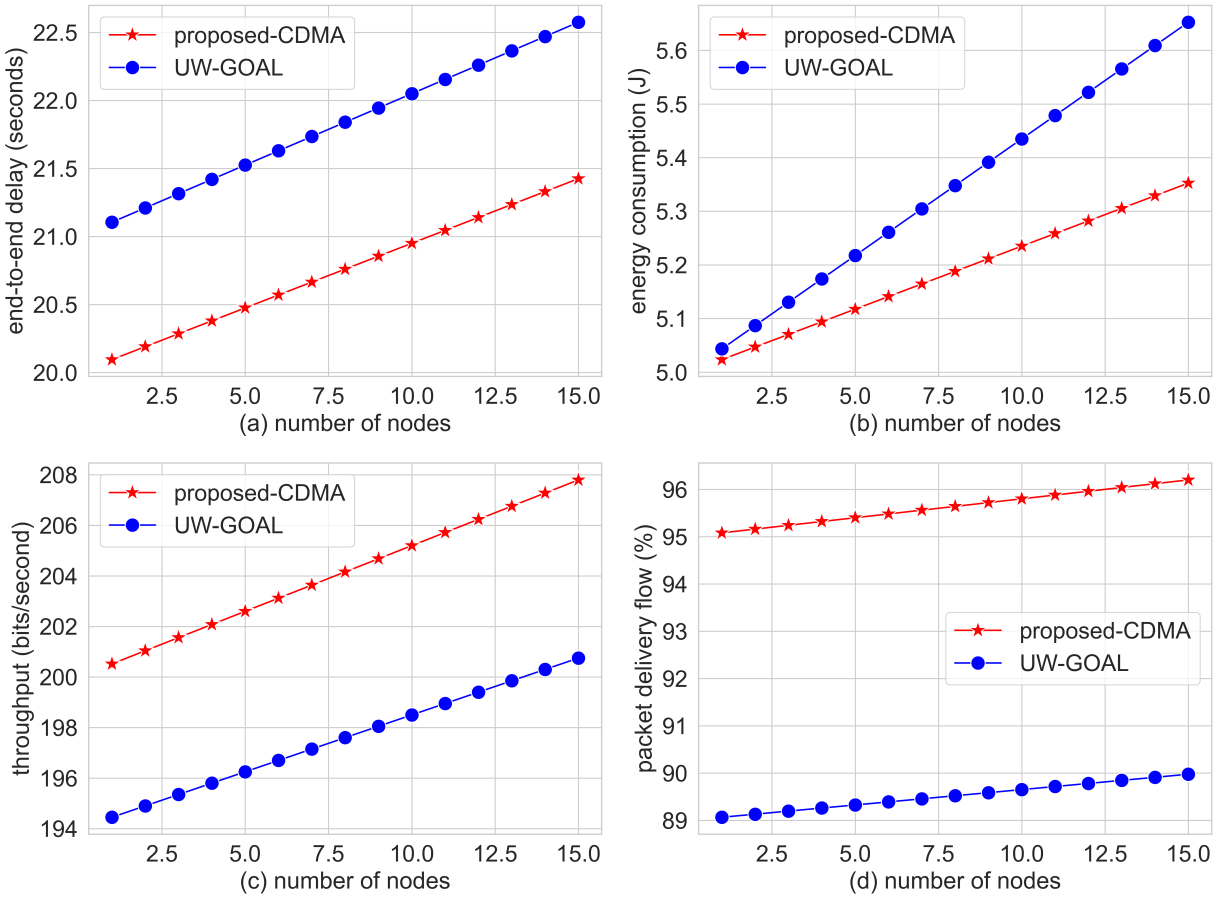

Figure 3.16: Simulated performance comparison of the proposed CDMA against the existing UW-GOAL protocol with increase node numbers: (a) the CDMA framework reduces end-to-end delay by approximately 1 second; (b) energy consumption in the CDMA framework is 0.2 Joules less at 15 nodes, enhancing energy efficiency; (c) throughput in the CDMA framework is 5 bits per second higher, suggesting improved data transfer rates; and (d) the packet delivery flow in the CDMA framework is 6% higher overall, indicating better network performance. These findings demonstrate the superior performance of the proposed CDMA framework over the UW-GOAL protocol for underwater acoustic networks.

model commercially-available proprietary modems (Table 1 from [81]). The state-of-the-art in underwater acoustics emphasizes simulators that reproduce underwater modem functionality on the modem itself and in the air simply and easily. This requirement highlighted NS3's limitations: not only its inability to model commercial modems but also the fact that developedNS3code cannot be ported to any hardware. Bespoke hardware options which runNS3code were unavailable for this research. On the other hand, UnetStack stands out. Agents developed in UnetStack can be created on a computer and directly loaded onto any UnetStack-based underwater modem, which the lab currently possesses. Its direct compatibility with existing modems, support for real hardware, versatility in integrating with

real-time robot/modem systems throughROS2, and ease for controlled environment in-water testing makes UnetStack the superior choice for this research, marking a clear shift in preference fromNS3.

3.3 Comparison of traditional TCP/IP stack and UnetStack

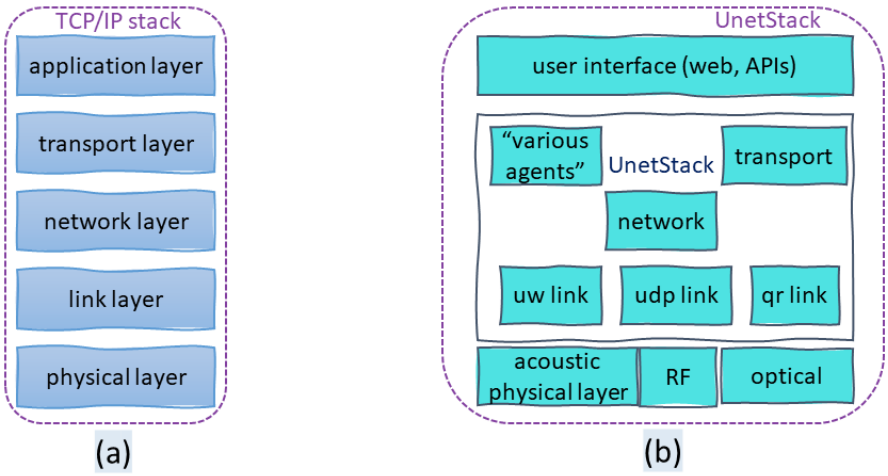

Figure 3.17: Comparison of TCP/IP Stack and UnetStack. (a) TCP/IP stack consists of five hierarchical layers: physical, data link, network, transport, and application. Each layer has a role in the process to transmit data over a network. (b) UnetStack is organized into three main layers: physical layer; a stack of agents which include the data link (or MAC layers) and network layer, and the user interface layer (web/APIs). These layers address the unique underwater communication challenges. Therefore, Unetstack was selected to model the modem function in the communications channel.

The traditional TCP/IP stack is a hierarchical protocol stack that consists of five layers: physical, data link, network, transport, and application (Figure3.17). Each layer has a specific role towards the process to transmit data over a network. The physical layer is responsible for the transmission of data, the data link layer manages the physical and logical connections to the devices, the network layer handles the routing of data, the transport layer ensures reliable transmission, and the application layer is where the network applications operate [3].

In contrast, UnetStack (Figure3.18), a software stack specifically designed for underwater communications, presents a software-defined architecture. UnetStack is organized into agents, where each agent is responsible for a specific task in the communications process. These agents can be categorized into three main components (Figure3.17): physical layer; stack of agents which include the data link (MAC layer) and network layer, and the user interface layer provides access to web/modem APIs [93].

The physical layer in UnetStack is similar to the traditional TCP/IP stack and is responsible for data transmission and reception. However, given the unique challenges of underwater communications, like latency, limited bandwidth, and high error rates, the physical layer in UnetStack includes capabilities specifically designed to handle these challenges. For some of the short burst data, *uwlink* agent can also provide reliable datagram delivery. The agent stack, in UnetStack coordinates access to the communication medium among multiple nodes. It includes mechanisms for collision avoidance and detection, which are crucial in the underwater environment where the propagation delay is significant. The Unetstack network layer routes data packets from the source to destination node. Unlike the TCP/IP stack, which uses static routing protocols, UnetStack supports dynamic routing protocols and thus can adapt to the changing underwater environment.

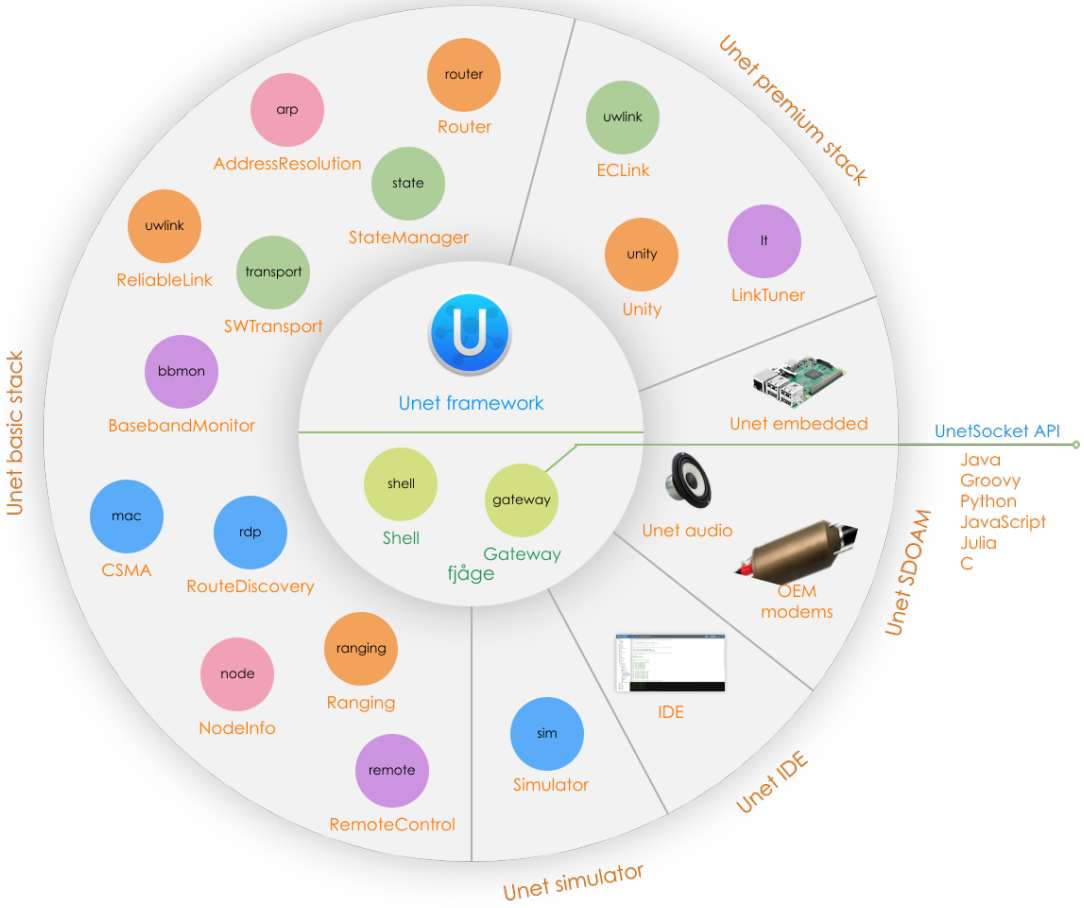

Figure 3.18: Overview of UnetStack, illustrating the key parts of the Unet system including the Unet Framework, Basic Stack, Premium Stack, Simulator, IDE, and Unet audio, which together provide the necessary services, functionality, and interfaces to develop, simulate, test and deploy Unets [93].

In addition to these layers, UnetStack also includes a framework layer that provides services like transport protocols, file transfer protocols, and remote agent invocation. These services are designed to simplify the development of underwater communication applications.

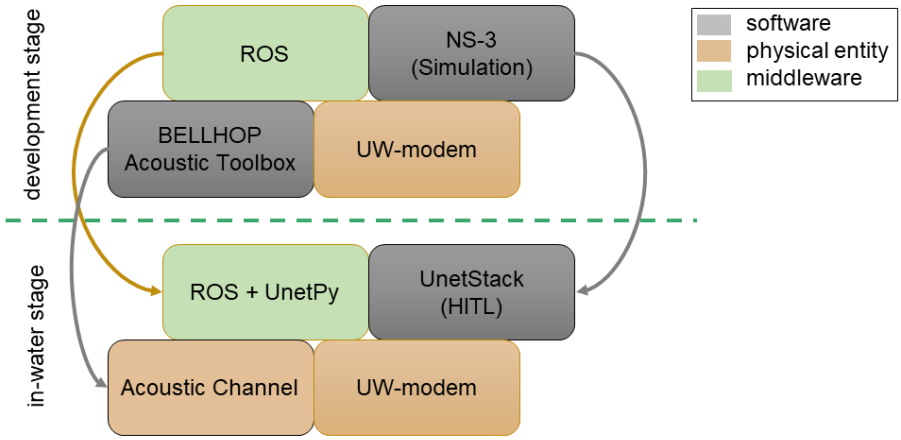

Figure 3.19: The UUV hardware-in-the-loop (HITL) simulator integrates hardware, software and middleware. ThisHITLsupports, matures and de-risks efficient testing of hardware integration prior to integration on the UUV and subsequent in-water deployment. HITLtesting also serves to reduce the in-water testing necessary.

In summary, while the traditional TCP/IP stack and UnetStack both provide a layered architecture for network communications, UnetStack has features and services that specifically address the unique underwater communications challenges. This makes UnetStack a suitable choice for the proposed underwater communication system. UnetStack (Table 1 from [65]) is compatible with the lab's Subnero M25 series modems [9,28] and more suitable for the thesis (Table3.3). UnetStack also has the UnetAudio services [93] which is quite useful to develop any kind of protocol. UnetStack is a collection of technologies to extend communication networks underwater. The Unet consists of many Unet nodes (e.g. underwater sensor,UUVs, gateway buoys, ground stations, and boats/ships that generate, consume or relay data over a variety of links such as acoustic, RF, Wired, Satellite, etc [93,95].

In the transition from the development to the in-water stage, the thesis modelling was refined (Figure3.19) to resemble a UnetStack hardware-in-the-loop (HITL) simulator for two underwater nodes (e.g.UUVs orUSV). AnHITLsimulator integrates the tools instantiated in software for most importantly, a hardware board, which emulates anUUV.

TheHITLmethodology is efficient and de-risks hardware (UUV) integration prior to integration on the vehicle. Theintelligent systems laboratory (ISL)accesses two IVER3

Table 3.3: Comparison of Subnero and WHOI MicroModems against desired thesis specifications and performance metrics. The Subnero modem better fulfills the requirements and was thus selected for the thesis work to implement the proposed CDMA-based underwater communications system.

			Better Performance	
thesis parameter	**Subnero**	**WHOI**	**Subnero**	**WHOI**
software-defined	✓	×	✓	×
data rate	15000 bps	80-5400 bps	✓	×
frequency	18-32 KHz	0-25 KHz	✓	×
modulation	PSK-OFDM, FH-BFSK, FSK	FSK,PSK, No OFDM support	✓	×
power consumption	< 4 W (Rx mode, nominal) < 80 W (Tx mode, max.) < 60 W (Tx mode, avg.)	4 W Rx Mode ∼60 W Tx Mode ∼81 W Tx Mode	✓	×
co-processor	delivered with NVIDIA Jetson	separate purchase	✓	×
software interface	USB, RS232, I^2C (for external sensors)	RS232, no USB support	✓	×
operating range*	3-6 km	3-6 km		
JANUS compatibility	supported	need to develop	✓	×
API support	Java, Groovy, Python, C, MATLAB, JavaScript, Julia, JSON/TCP, Interactive User Interface	no additional API support, can not re-configure	✓	×
FEC	LDPC (up to 1/6 rate code); JANUS (1/2 rate convolution code)	JANUS (1/2 rate convolution code)	✓	×
ranging	precision 0.1 m	precision 0.1 m		
documentation	development is documented	not very much	✓	×
Doppler resilience	± 4 knots or better	± 2 knots	✓	×
arbitrary waveform transmission and recording	passband and baseband	passband	✓	×
onboard storage	32 GB	not available	✓	×

* nominal, depending on channel conditions

HITLemulators which use theROS2middleware for this purpose. The emulators support a serial interface that allows for waypoint-based control (Figure3.20). It is beyond the scope of the thesis to integrate the developedCDMAnetwork onto theUUVs.

However, theUUVemulators lack a payload andROSinterface to integrate to the vehicle. To overcome this, a vehicle interface for underwater communications must be developed. This means creating a process to send and receive messages acoustically across networked vehicles using thedynamic compact control language (DCCL), which marshalls object-based messages, particularly for networks with extremely low throughput links [83, 84] such as marine robot networks.

The author's contributions to the underwater communications interface paved the way for further exploration ofHITLmethodologies with the aim to develop and test the communication protocol to a fairly mature level prior to in-water deployment. This will be considered in future work.

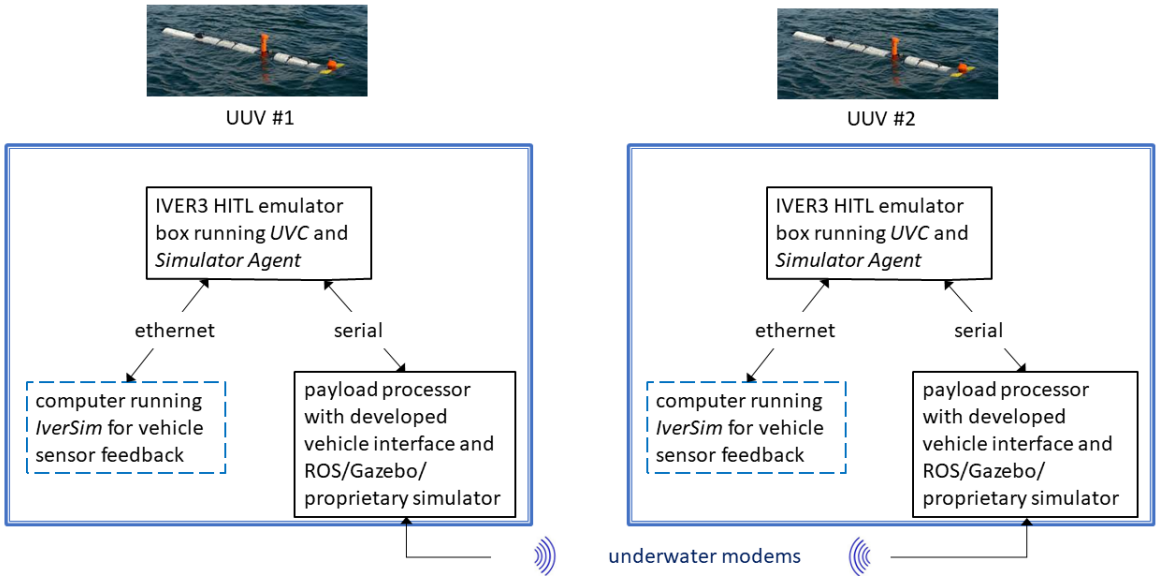

Figure 3.20: The end-to-end communication system forUUVHITLsimulation. Note the integration of OEMUUVsoftware (UVC and Simulator Agent) with the thesis-developed payload communications capabilities via a hardware board from a vehicle.

This approach greatly de-risks and matures the underwater communications prior to in-water deployment and thus reduces the in-water time required. The access to in-water deployments was curtailed for 2 years during the global COVID-19 pandemic. A different set of tools are required to estimate the channel response of the system. Previously C++ basedWOSS[42] was used to automate the BELLHOP process, now the ARLPY [20] underwater toolbox, developed by Dr. Mandar Chitre and his ARL Lab team, is chosen to perform the BELLHOP ray-tracing analyses for this thesis. A few test cases were investigated with aSSP(Figure3.5) and bathymetry (Figure3.6) [45] to verify that both the old (WOSS) and new (ARLPY) interfaces work as intended.

Figure3.21shows a test case with transmitter and receiver at depths of 50 m and 20 m below the water surface (Figure3.21a), respectively and eigen rays from transmitter to receiver (Figure3.21b). The position of the transmitter and receiver are important parameters of the underwater acoustic communications channel as the SSP varies with depth. This agrees with the earlierNS3simulations. The focus of the thesis is < 100 m depth (shallow water conditions).

In another test case, the transmitter is at 4 m depth and the receiver depth varies from 1 m to 8 m (Figure3.22a). Its ideal channel response, pure received signal and Fourier analysis of the channel impulse response are shown in Figure3.22, respectively.

The multi-frequency channel response in Figure3.23a is over a range of depths from 1 m to 8 m at a distance of 200 m between transmitter and receiver. Such test cases are also

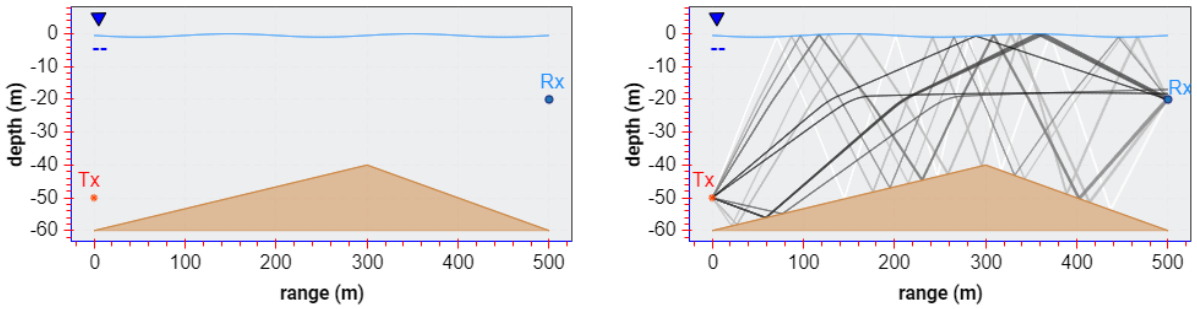

(a) the underwater environment (env)

(b) the eigen rays for the given underwater env

Figure 3.21: Underwater acoustic simulations using Arlpy. (a) The underwater environment with the transmitter and receiver at depths of 50 m and 20 m, respectively, (b) The eigen rays from transmitter to receiver, demonstrate the variability in the channel's behavior at different depths. These predictions shows how an understanding of underwater environments and eigen rays impact acoustic simulations, and the importance of considering them in the design of underwater communication systems.

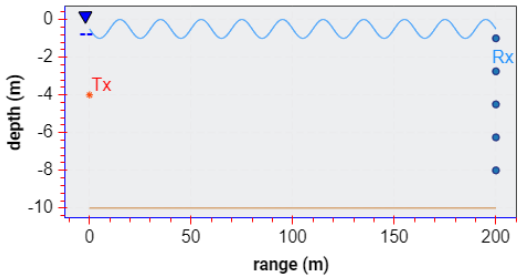

(a) Transmitter at 4 m depth and receiver depth varies from 1 to 8 m

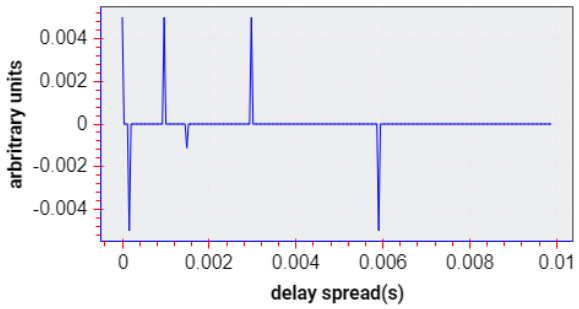

(b) snapshot of the ideal channel response

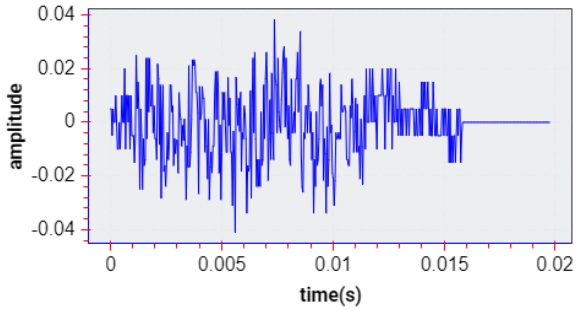

(c) pure received signal

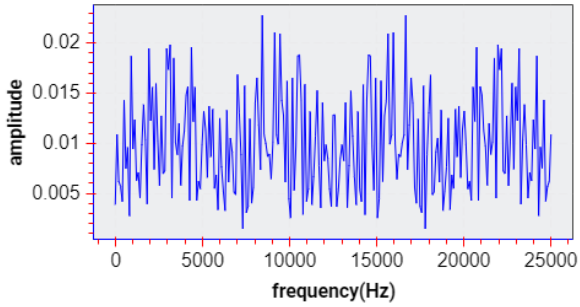

(d) FFT of the given impulse response of the channel

Figure 3.22: A simulation with the Python-based Arlpy module using BELLHOP: (a) varying receiver depths; (b) ideal channel response; (c) pure received signal, and (d) the power spectral density of the channel's impulse response. This provides insight into the channel's behavior and characteristics, which are crucial to understand the underwater communication performance.

explored to find the optimum depth to the transmitter and receiver for the given channel at the time [76].

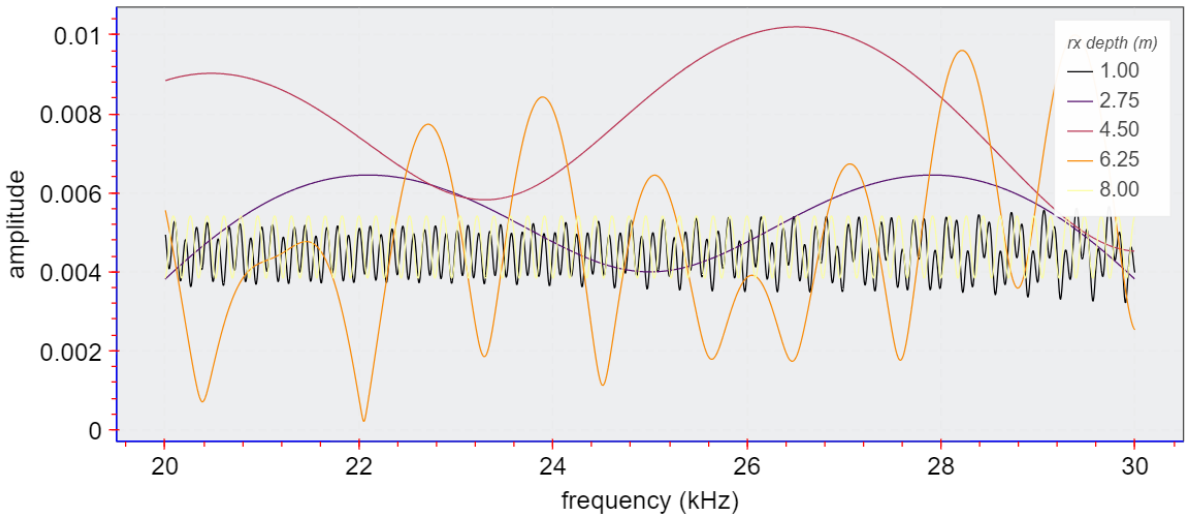

(a)

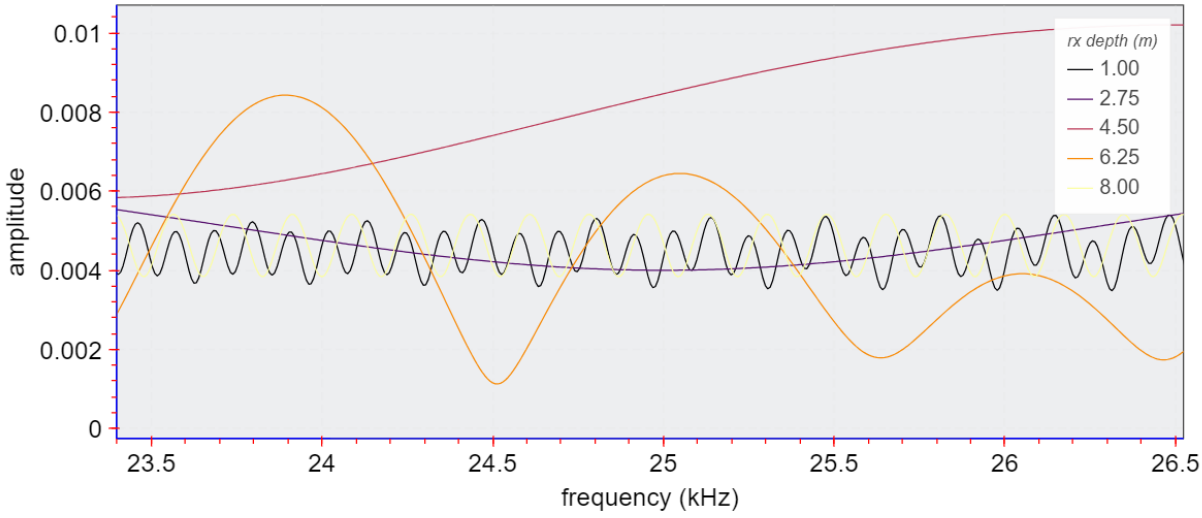

(b)

Figure 3.23: Determine optimum transmitter and receiver depths for a given channel at 200 m range. Depictions of multi-frequency channel response under varying conditions: (a) response for a range of receiver depths from 1 m to 8 m and a fixed receiver range of 200 m, and (b) zoomed-in of (a) focussing on carrier frequency range of interest. These visuals validate hypotheses regarding optimum transmitter and receiver depths under specific channel conditions, as explored in prior studies [56,76].

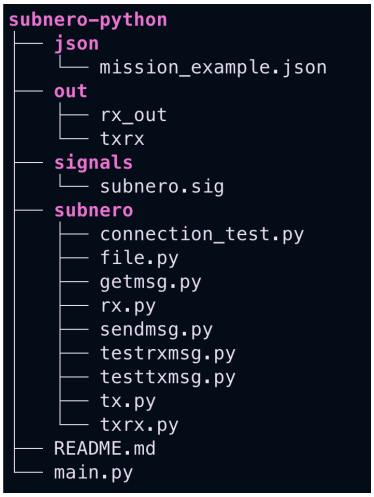

Figure 3.24: Directory structure of the pysubacoustic module developed using the unetpy APIs to test the unetpy APIs functionality with the Subnero M25 series underwater modems. This module allows missions to be loaded as JSON files above-water and performed step-by-step, enabling tasks like baseband signal transmission and reception, text messaging, and file transmission.

3.4ROS2and pysubacoustic module

ROS/ROS2is a set of software libraries and tools used to develop robot control and deliberation software [69]. These are large libraries of well-vetted robotics algorithms, simulators, and middleware [69].

TheROS2middleware provides the ability to create decoupled processes that interact through public interfaces. A ROS node (distinct from a communications node) encapsulates a process or function inROS2(not always true, but sufficient to understand work within this thesis). The public interfaces can either be in the form of publish-subscribe (pub-sub) messages or service-client services. Messages are passed over topics which are given a unique string identifier domain-wide withinROS2.

Before any deployment, the Subnero Python module (Figure3.24) is designed and developed using the unetpy APIs to test the functionality and Unetpy APIs with the Lab's Subnero M25 series underwater modems. The module is based on the contributions in [20,94] and designed so a mission can be loaded in the module as aJavaScript Object Notation (JSON)file. The mission is performed step-by-step with tasks like transmit baseband signal, receive baseband signal, transmit-received baseband signal, sendmsg(text), file transmission, etc.

This is used to develop aROS2interface node for both the Subnero surface and standalone-submerged nodes. ThisROS2interface node can also be configured seamlessly withUUVs like the REMUS 100, IVER3, etc. The node is designed to operate in

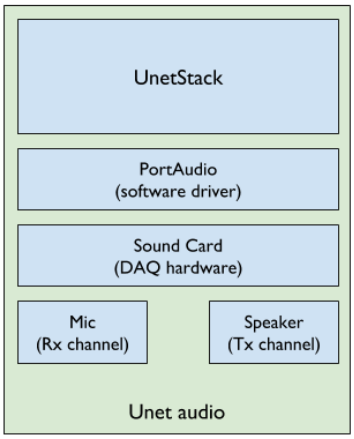

Figure 3.25: Architecture of Unet audio, a software-defined open architecture acoustic modem (SDOAM) which enables a computer with a sound card, speaker and microphone to be an acoustic modem to transmit and receive in-air acoustic signals [48]. This computer-based modem is a testbed to design and test acoustic modulation schemes for above or below-water in the thesis work.

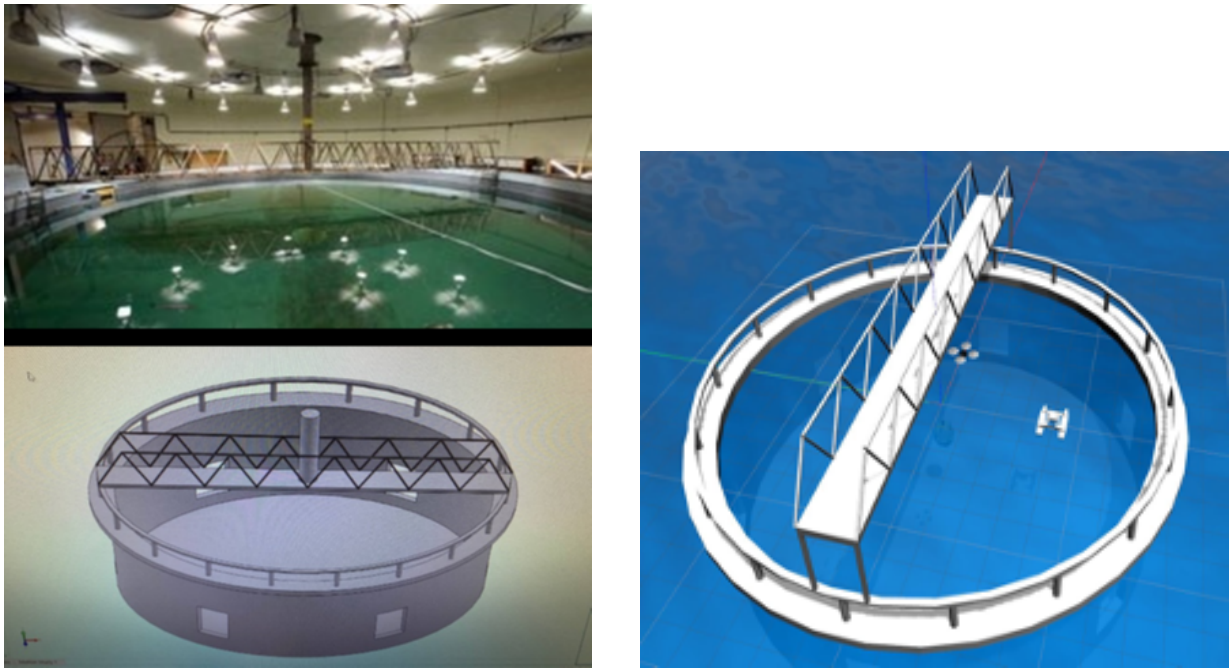

(a) (b)

Figure 3.26: Controlled indoor underwater tank studies at the Dalhousie University Aquatron Facility: (a) top image – photograph of the 15 m diameter Pool Tank, bottom image – solid model of the Pool Tank [82]. (b) Graphic of the three marine robots collaborating at the Pool Tank to test path-planning and data flow reduction requirements for networking multi-domain robots.

full-duplex mode for optimal performance.

A custom physical agent [72] was developed using UnetStack and its functionality tested using the UnetAudio services [93]. This is one of the software-defined open-architecture acoustic modems (SDOAM) built in the thesis with UnetStack. Ultimately, it is possible to convert computers with sound cards into an in-air acoustic modem to act as a proxy for the designed underwater modem. The computer's sound card (or any sound card integrated with the computer) along with its speaker and microphone become the transceiver (Figure3.25) to transmit and receive data or signals as instructed by the user [48]. This significantly reduces the in-water testing needed to develop an underwater modem.

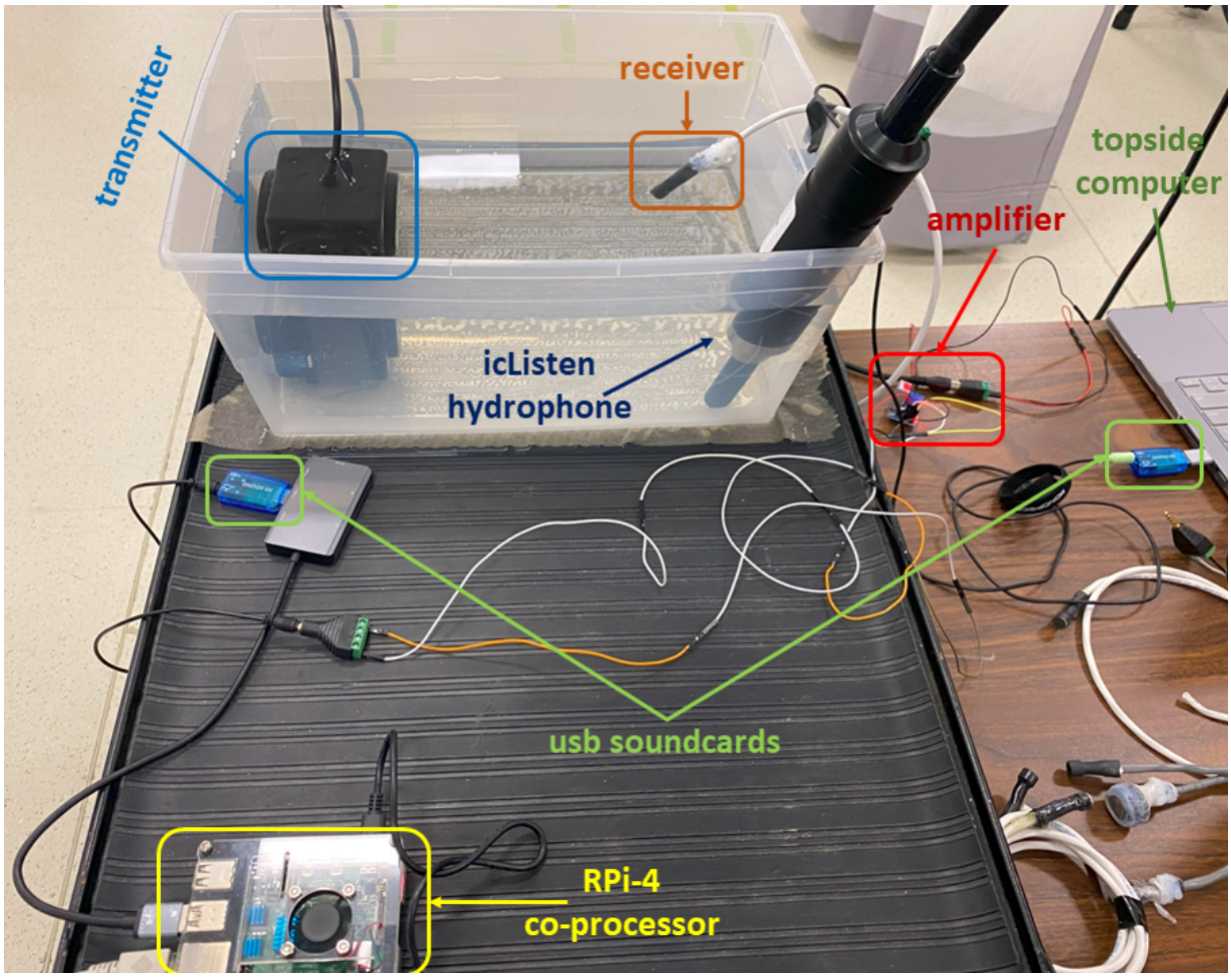

Figure 3.27: Prototype miniature full-duplex underwater modem with a Raspberry Pi-4 co-processor, computer sound card, amplifier, underwater speaker and UnetStack for transmission, and a custom-made, potted microphone receiver for reception. The modem operates at a test frequency of 12 KHz, due to the sampling limitation of the sound card. Once the agent is validated on this prototype, it is ready to deploy on Subnero M25 series modems to test in both controlled and uncontrolled environments.

A prototype underwater modem was developed (based on [60], modified for custom application with custom receiver) in this thesis (Figure3.27) to run UnetStack on a Raspberry Pi co-processor with an external sounds card and underwater speaker as the transmitter. A small commercial microphone was custom potted as the receiver. An amplifier was applied to the external sound card to amplify the audio signal before the underwater receiver. Note the audio signal produced is mono channel, but could be used in dual channel mode. The modem can also operate in full-duplex mode. The custom agent that drove this modem was tested at only 12 KHz in-air due to sampling limitations on a conventional sound card. This modem was used as a proxy for early stage test and development of the CDMA protocol for an underwater node. Once the agent was fully tested on the prototype modem, it was loaded in the Subnero M25 series modems. Then, the agent is in a high state of readiness to test in controlled environments like the Aquatron Pool Tank (Figure3.26) and/or uncontrolled environment like Bedford Basin.

To facilitate online debugging of the communication system, a plotly [77] dashboard was created for UnetStack to plot the live signal streams and provide the critical information about the communication system's performance (discussed in later chapters).

As discussed in3.4, a custom dashboard was used to monitor and debug the live signals during the experiment. The dashboard (Figure3.28) is accessible to all devices connected to the same router in the network.

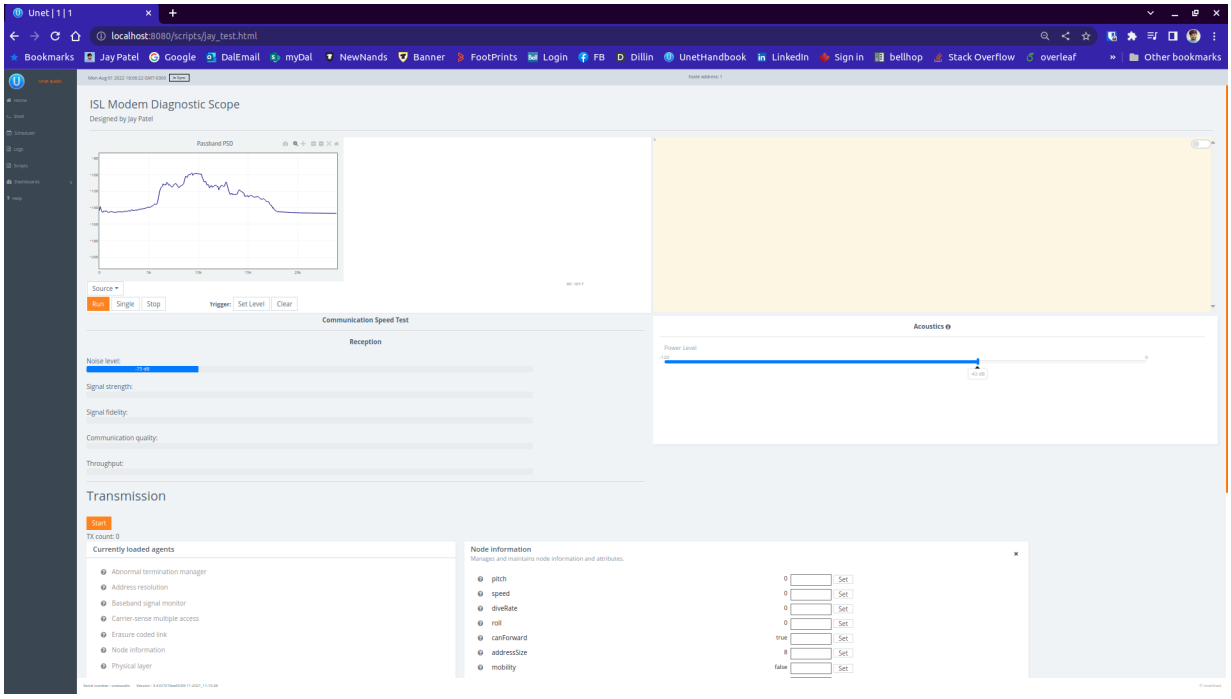

Figure 3.28: The custom developed dashboard to monitor and debug live signals from the underwater network nodes during trials in semi-controlled and uncontrolled environments.

Given the design and simulation methodology described in this chapter, the next Chapter will discuss how the proposedCDMA-based network topology is implemented and tested in both controlled and uncontrolled environments.

Chapter 4

Implementation and Experimentation

[1]J. Lindsay, J. Ross, Seto, M., E. Gregson, A. Moore, Patel, J. , and R. Bauer. "Collaboration of Heterogeneous Marine Robots Toward Multidomain Sensing and Situational Awareness on Partially Submerged Targets", in IEEE Journal of Oceanic Engineering, vol. 47, no. 4, pp. 880-894, Oct. 2022, doi: 10.1109/JOE.2022.3156631, [56].

[2]Jay Patel, Ali Bassam, Mae Seto. "Multi-UUV object detection, localization and tracking with secure, full-duplex communication networks", Proc. Mtgs. Acoust 20 June 2021; 44 (1): 070037, doi: https://doi.org/10.1121/2.0001510, [72].

This chapter outlines and describes the implementation, test and verification experiments to evaluate the performance and reliability of the designed underwater communication network, as described in Chapter2, and informed by Chapter3. This communications network is to be applied to autonomous marine systems in real-world marine conditions – which is novel. This communications network problem has a large scope so the test and verification focuses on the underwater nodes with only basic implementation for the in-air and above-water (surface) nodes.

The implementation of the CDMA-based communications network is discussed first (section4.1). Then, the test and verification experiments are staged as follows:

4.2Initial test and verification in a controlled environment at the Dalhousie University Aquatron Pool Tank to explore concepts and refine the system.

4.3In-water test and verification in a semi-controlled environment off the jetties at the COVE to assess the system's performance under less-controlled conditions.

4.4In-water verification in an uncontrolled environment (St. Margaret's Bay) to evaluate the system's robustness and reliability in an operationally relevant environment.

The results from basic tests that advance the communication system development from one stage to the next are discussed in this Chapter. Detailed presentation and discussion of advanced testing will be more fully addressed in the following Chapter5.

4.1 CDMA Communications Network Implementation

4.1.1 Robot Operating System

The preferred open source robotics middleware for implementation is the Robot operating System (ROS). ROS can also simulate the communications between the multiple robots in the mission (Figure3.19). AlthoughROSis not an operating system but a collection of software frameworks for robot software development, it provides services designed for a heterogeneous computer cluster such as hardware abstraction, low-level device control, implementation of commonly used functionality, message-passing between processes, and package management.

The network nodes are integrated through theROSmiddleware.ROSwas the selected middleware since the communications system is integrated as another robotic subsystem on a marine robot. The version ofROSused wasROS2(Foxy Fitzroy distro).ROSnodes are software constructs that are integrated with the hardware modems or radios. The integration of thisROSsoftware and modem or radio hardware constitutes a network node as presented to this point in the thesis.

ROShas a publish-subscribe architecture. Topics / messages are published and subscribed byROSnodes as the method to communicate. This level of abstraction facilitates easy design and testing by decoupling the hardware and software. It also increases code

use and portability so that the network nodes developed are not for a specific brand or type of marine robot. It assumes the hardware devices have software interfaces which is now quite common.

AROSpackage was developed to interface the CDMA network nodes with the modem / radio hardware to the detail described above. This package serves as an interface so the modems and radios know when and what to communicate and how to interpret what is received.

In aROSimplementation example where the above-water (UAV) network node transmits commands or information to the underwater (UUV) network nodes, this occurs as follows. The above-waterUAVnetwork node is instantiated as aROSnode which encodes theUUVcommands or information in the previously mentioned custom format asROS topics / messages. It then encodes them in a form that is suitable for in-air RF transmission then publishes it to the network. The radio node is instantiated as aROSnode that subscribe to this topic / message and transmits it into the air.

The in-airUSVnetwork node is instantiated as aROSnode that subscribes to the radio topics / messages and then demodulates and filters it then publishes it to the network. TheUSVunderwater network node is instantiated as aROSnode that subscribes to the USV's in-air topics / messages and encodes them in a form that is suitable for underwater modem transmission then publishes it. A modem node on the USV subscribes to these USVunderwater topic / message and transmits the topic / message from the modem into the water. The reverse happens when underwater network nodes transmit information to the above-water node.

Figure4.1shows how the underwater network nodes, instantiated asROSnodes, communicate.

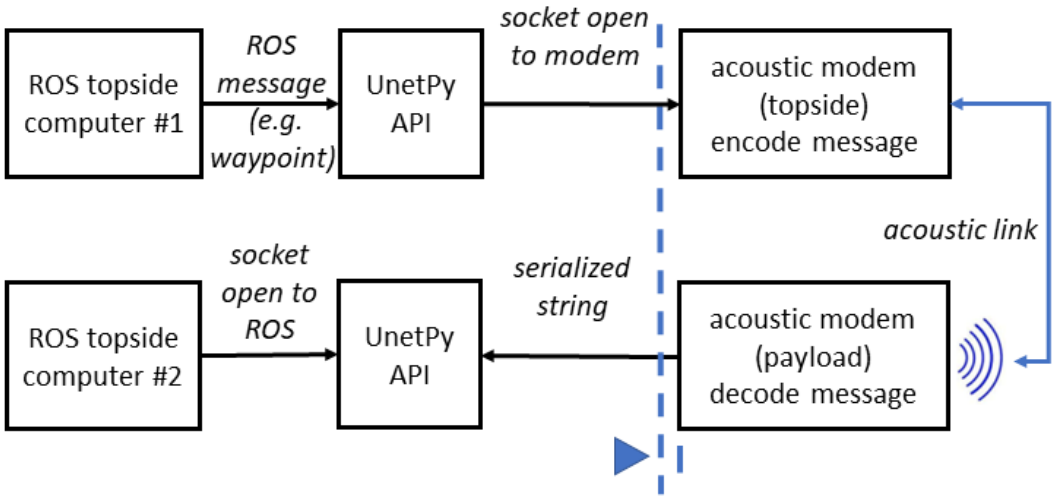

Figure 4.1: The work flow for communications betweenROSnodes

4.1.2 Implementation of Communication System Underwater

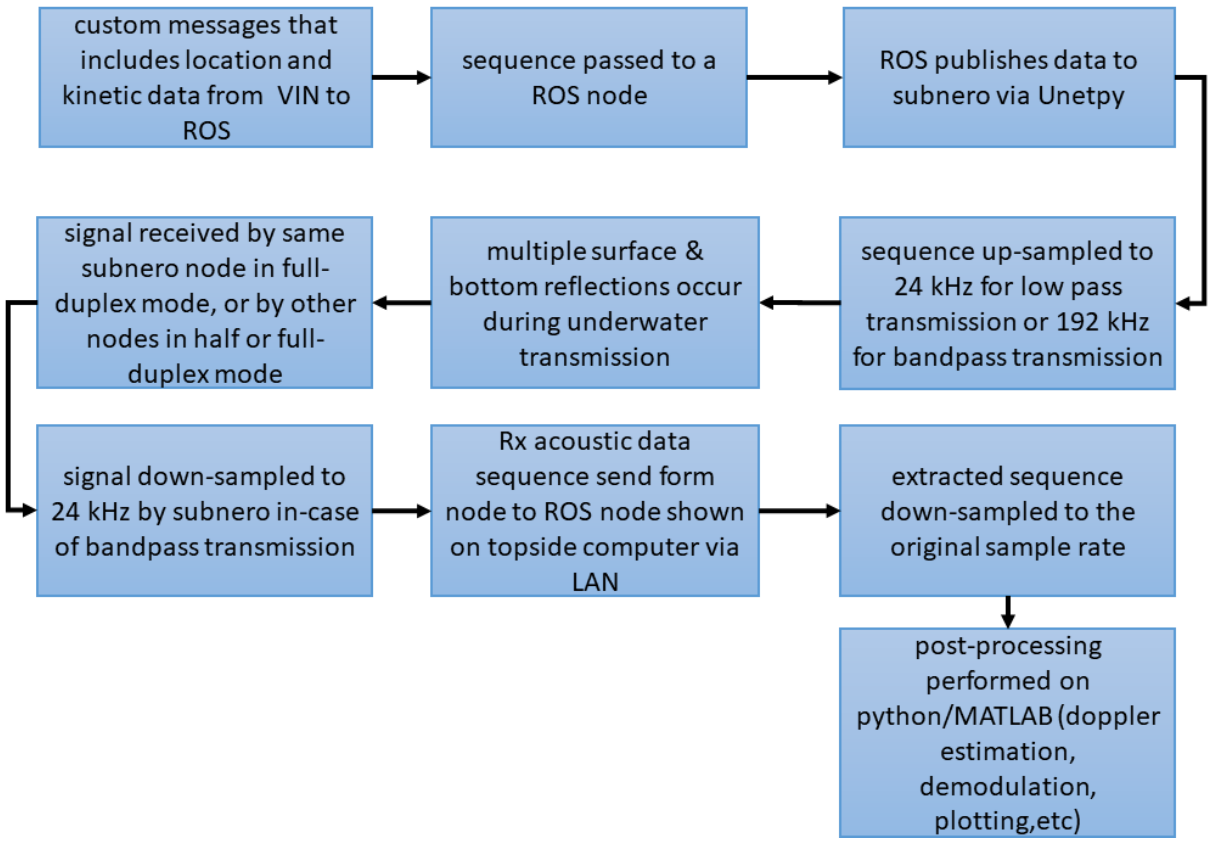

Figure 4.2: Description of the full communication system currently employed.

This section briefly describes the implemented system (Figure4.2). As shown, the system starts with a high level description of the transmitter, receiver and channel components and in later stages, a more detailed analysis.

The underwater nodes' modems can be configured in either half- (Figures4.3) or full-duplex (Figure4.4) modes. The modems can be configured to operate in full duplex mode (which is a thesis objective and a novel development beyond the previously mentioned TDMA modulations) where they transmit and receive concurrently.

Channel Doppler Mitigation

The Doppler effects in a channel are relevant as these communication systems are deployed onUUV,USV, andUAVwhich are mobile. Doppler effects are more pronounced in the underwater branch of the communication system. Channel Doppler effects can be mitigated by pre-pending pilots, in the form of preambles, in the raw baseband signal.

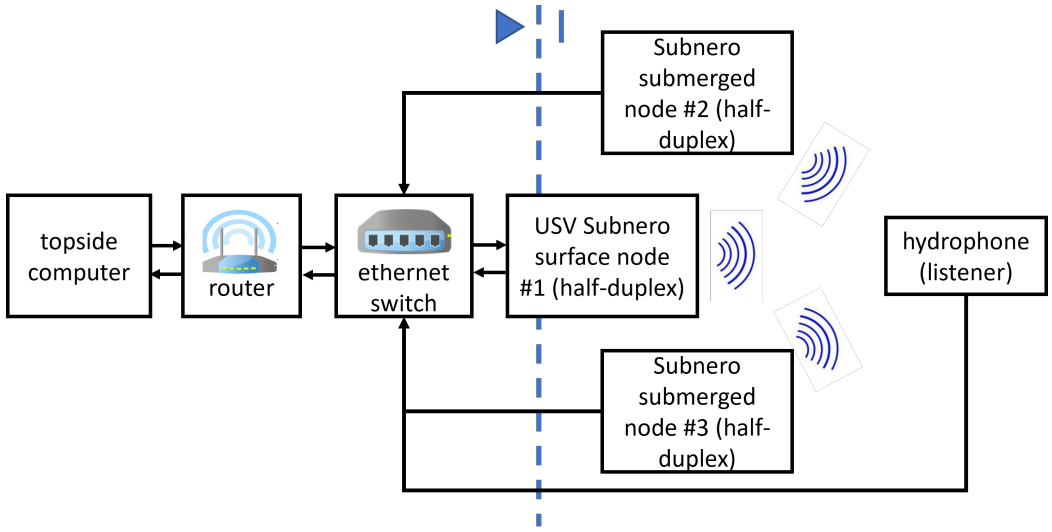

Figure 4.3: The communication systems' three underwater nodes configured in half-duplex mode with Subnero modems. Half-duplex is what is typically used underwater. The proposed communication system can replicate what is typically done by others.

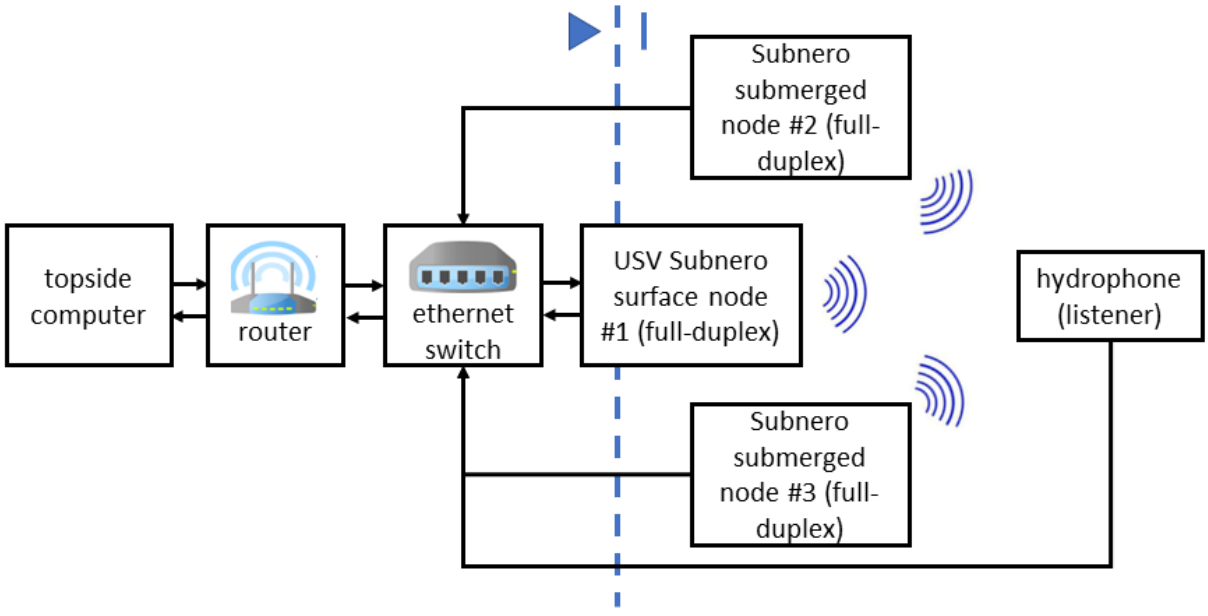

Figure 4.4: An underwater communication system configured in full-duplex mode. This is a novel communications mode for underwater nodes developed in this thesis.

The modems can transmit raw digital signals like binary base band signals. This is relevant to the proposed communications channel as it accommodates the lower bandwidth communication systems for underwater channels.

N-point, in this case $N = 64$, preambles are pre-pended to the baseband signal to estimate the channel Doppler effects. Therefore, auto-correlation peaks will occur every 64 samples as the peak is the starting point for a sequence within the preamble. All Subnero modems have a maximum of 1024 points however, only 1022 points are accessible (2 samples reserved for a checksum). Therefore, the last sequence in the auto-correlation output will only be 62-points long – slightly smaller than the other sequences (Figure4.5).

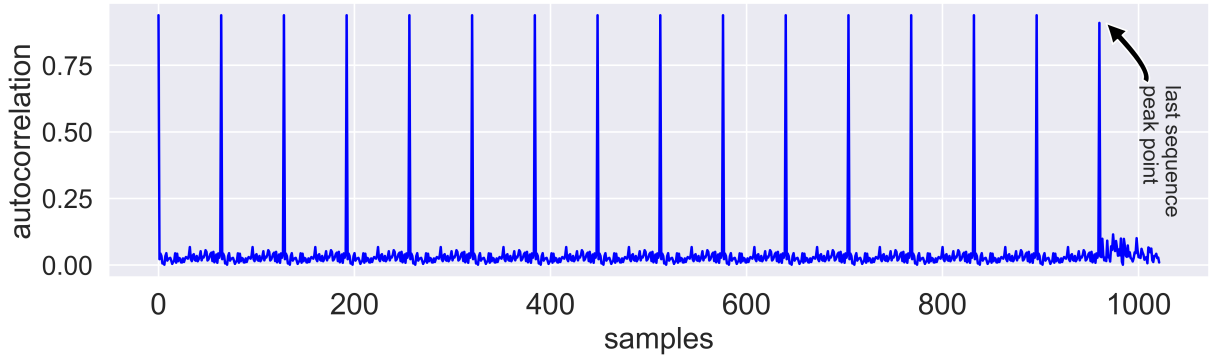

Figure 4.5: A method 2 (Doppler mitigation) example. The custom preamble auto-correlation selected is a shift orthogonal comb-type PN sequence [16]. This preamble is pre-pended to the raw baseband signal. The first 15 individual sequences in the preamble are 64-points long. The 16^{th} sequence is 62-points long yielding a total preamble length of 1022 points (modem limit). This illustrates the auto-correlation properties of the custom preamble selected to pre-pend to the baseband to mitigate channel Doppler and to identify a received signal as the intended one.

Note, the illustration in AppendixC.3is for an ideal case where the signal is not affected by ambient noise or other environmental factors. The Subnero modems use agents to adapt to the environment to minimize channel Doppler effects. These agents can be the default Unetstack ones (not discussed) or user-customized ones.

There are two user-customized methods to change the default Subnero modem preamble. The customized preamble could be:

1. integrated as part of the transmitted signal by pre-pending to the raw baseband (Figure4.6)

2. assigned to a control channel which is pre-loaded with the preamble while the data (raw baseband signal) is assigned to another channel (Figure4.5).

The advantage of method 1 is its simplicity. The advantage of method 2, over method 1, is that the preamble can also be used to detect the raw baseband signal. Tests were

conducted using both methods. For example, Figure4.6is an example of method 1 where a standard signal like an $m-$sequence (240-sample long hyperbolic up sweep or a 1023-chirp $m-$sequence with 50% bandwidth) is the preamble.

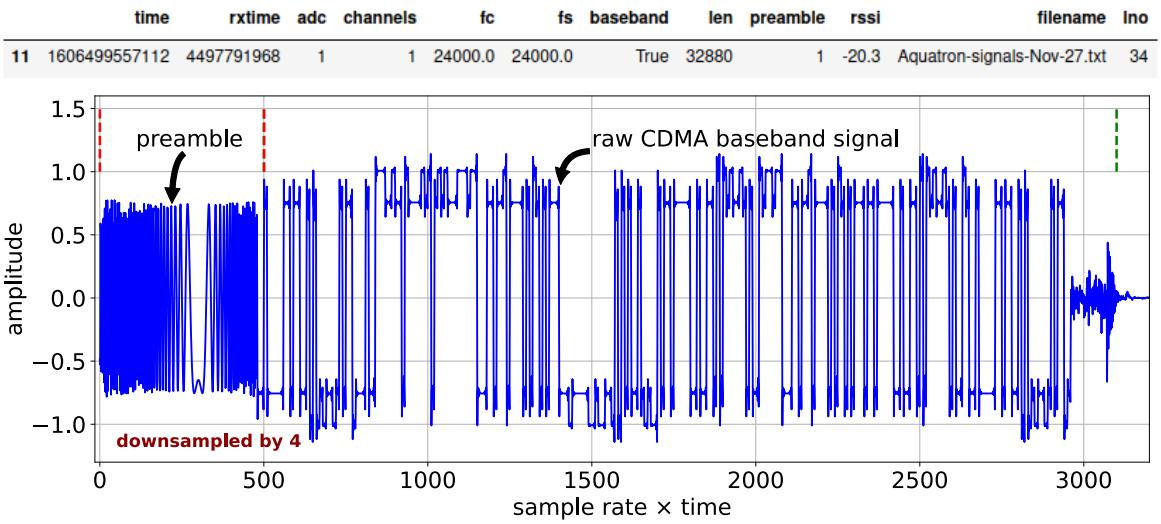

Figure 4.6: A method 1 (Doppler mitigation) example where the custom CDMA signal consists of a pre-pended m-sequence preamble to the raw baseband signal as *received* by a single modem in full-duplex mode. Note theRSSIis -20.3 which is strong. This Subnero modem was submerged to a depth of 2 m (mid-water column).

A custom shift orthogonal comb-type PN sequence type [16] was selected. This preamble was selected because it is fairly lightweight in size and has shown promise for mobile underwater network nodes. Therefore, this custom preamble is pre-pended to the baseband signal.

Compared to method 1, method 2 can actively determine the start of the raw baseband signal in the transmission (after the termination of the preamble). Figure4.5is an example of a custom preamble correlation using method 2.

Given the raw baseband signal has been Doppler compensated (to some extent), the other components of the transmitted signal, $y(t)$, are described next.

Transmitted Signal

Transmitted signal, $y(t)$, consists of four components – preamble, raw baseband signal, code-signal (raw baseband X-OR with the PN code), and a high-frequency carrier signal. The transmitted signal can therefore be described in: Eq.4.1and shown in FigureC.13,

$$y(t) = \ sin(2\pi f_c t) \times c(t) \times m_p(t) \tag{4.1}$$

such that f_c = carrier frequency (25 kHz), $c(t)$= code-signal, $m_p(t)$= preamble and raw baseband signal.

After the transmitted signal is received at the receiver, the extracted signal, $b(t)$ is obtained by frequency demodulation and filtering to remove the carrier signal:

$$b(t) = c(t) * m_p(t) \tag{4.2}$$

such that $m_p(t)$ is now only the raw baseband signal as the modem receiver removes the preamble at this stage. From Eq.4.1and4.2the code-signal was de-spreaded at the receiver to extract the raw baseband signal.

This concludes the implementation of the communication system underwater branch with the three underwater nodes. The next subsection describes implementation for above-waterCDMAbranches with theUAVin-air andUSVin-air and underwater network nodes. While the thesis contributions are in the underwater branch the implementation of other branches are included for completeness and to show it is possible to integrate CDMA protocols across domains.

4.1.3 Implementation of Comms System Above-Water Branch

The implementation for the above-water branch of theCDMA-based communication system is described in this section. The implementation shows that it is possible to integrate it with the underwater network nodes through theUSVin-air network node. The above-water branch underwent basic verification but this was not pursued to controlled, semi-controlled or uncontrolled environments as it is not expected to be a problem.

Once data from theUSVunderwater network node is relayed to the USV in-air node, theUSVin-air node can further relay the data (e.g.CDMAraw baseband signal) through traditional RF methods. Developed in this thesis is a solution with software-defined radios like the ADALM PlutoSDR [33]. In the above-water or aerial domain, bandwidth is not a significant concern to relay low bandwidth underwater signals. There are mature tools available for above-water software-defined radios, such as GNURadio [39]. With the tools and services available inROS, UNIX piping systems and socket programming, the information received from one domain (e.g. underwater) can be relayed via PlutoSDR to the above-water domain and subsequently post-processed at the base station. This hypothesis was verified previously in the Lab's collaborative work [82]. The transmission of above-water audio and images was previously explored [70,75].

For above-water experiments, the real-world tests were performed in the Industrial, Scientific, and Medical (ISM) bands only. For simulations, a carrier frequency of 25 KHz was used in GNURadio. There is an existing module of GNURadio by Achilleas Anastasopoulos [27], developed for the older GNURadio version 3.7. The main contribution for the in-air branch of the multi-domain CDMA communications system is to port this module to the latest GNURadio version 3.8 (Figure4.8). It was not straight-forward how to transmit messages from the non-GNURadio source, ZMQ push node, developed forROS2. The

ZMQ push node converts messages from ROS to GNURadio and those messages are processed in the gr-cdma module [27] and transmitted over air using the audio sink gnuradio block/PlutoSDR (Figure4.7) [75].

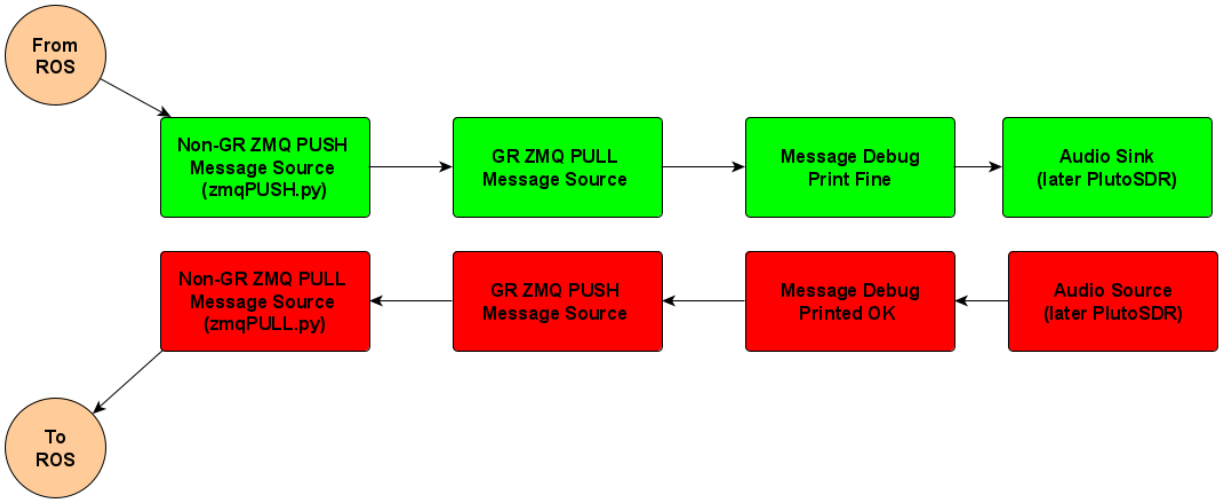

Figure 4.7: Integration ofROS2/ZMQ with GNURadio to operate with the ADALM PlutoSDR. Shown, is the work-flow to relay information from underwater to above-water. It includes the conversion of message types fromROS2to GNURadio with the ZMQ push node. This message is then processed in the gr-cdma module and transmitted using the audio sink GNURadio block/PlutoSDR. On the receiver side, the process is reversed, and the decoded message is converted back toROS2via a ZMQ pull node with further processing at the USV in-air network node.

On the receiver side, the process is reversed and decoded messages are pushed toROS2 via the ZMQ pull node and those messages are processed at the USV in-air network node.

In tests and verification with the PlutoSDR in the ISM band, it is noted there is appropriate buffer and gain as the PlutoSDR expects samples between -2^{14} and $+2^{14}$, not the -1 and $+1$ of some traditional SDRs (Figure4.9).

While the thesis research focused primarily on the underwater branch, the above-water branch was adequately developed to transmit or relay information immediately upon receipt of messages from the underwater branch (specifically, the USV underwater network node).

While the received data could be decoded for internal ROS management this was not performed as the USV in-air node will not act on the information. Therefore, and in the interest of maintaining the data's integrity, it is forwarded to the above-water node, as-is.

The following sections describe the test and verification experiments in controlled and uncontrolled environments for the designed CDMA-based communications network.

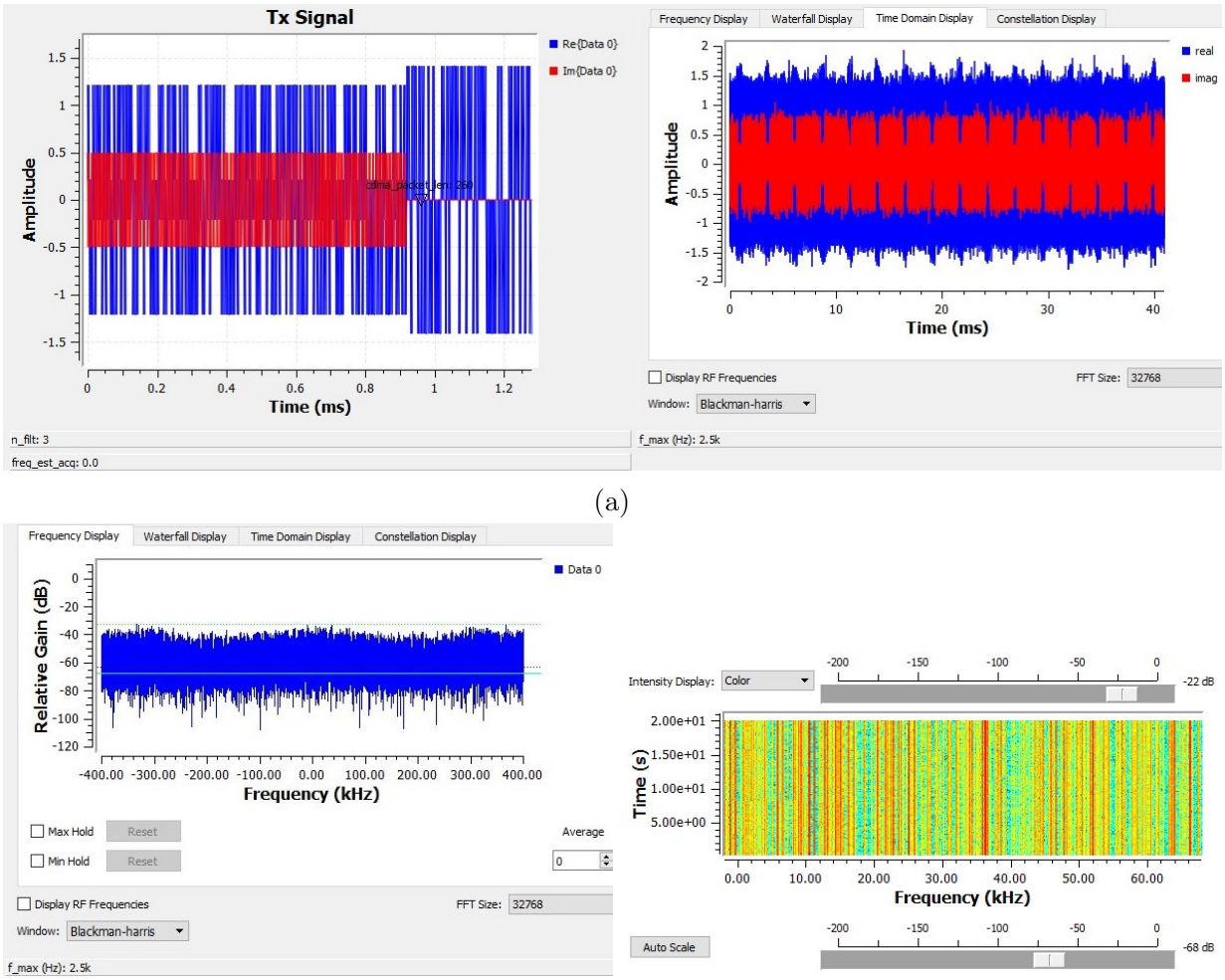

Figure 4.8: Example of transmitted CDMA signal using the GNURadio module: (a) starting from left, first few seconds of complex signal in the time domain and to right entire duration of the complex signal considered; (b) power spectral density analysis over the first 20 ms, and (c) spectrogram over the first 20 ms. The need for appropriate buffer and gain adjustments for PlutoSDR transmissions in the ISM band is due to specific sample range requirements.

4.2 Test and Verification in a Controlled Environment

Within the Aquatron Pool Tank the end-to-end functionality and correctness of the integrated communications system (hardware and software) and configuration of the software-defined modems, andCDMAwaveforms developed (e.g., spreading factor, carrier frequency, signal gains, both baseband and pass band signals, deployed modem depths, response to underwater acoustic ambient, etc.) were verified. As well, what could be tested and verified is the necessary processing of the modem signals that includes filters, power spectral densities and time-frequency power distributions.

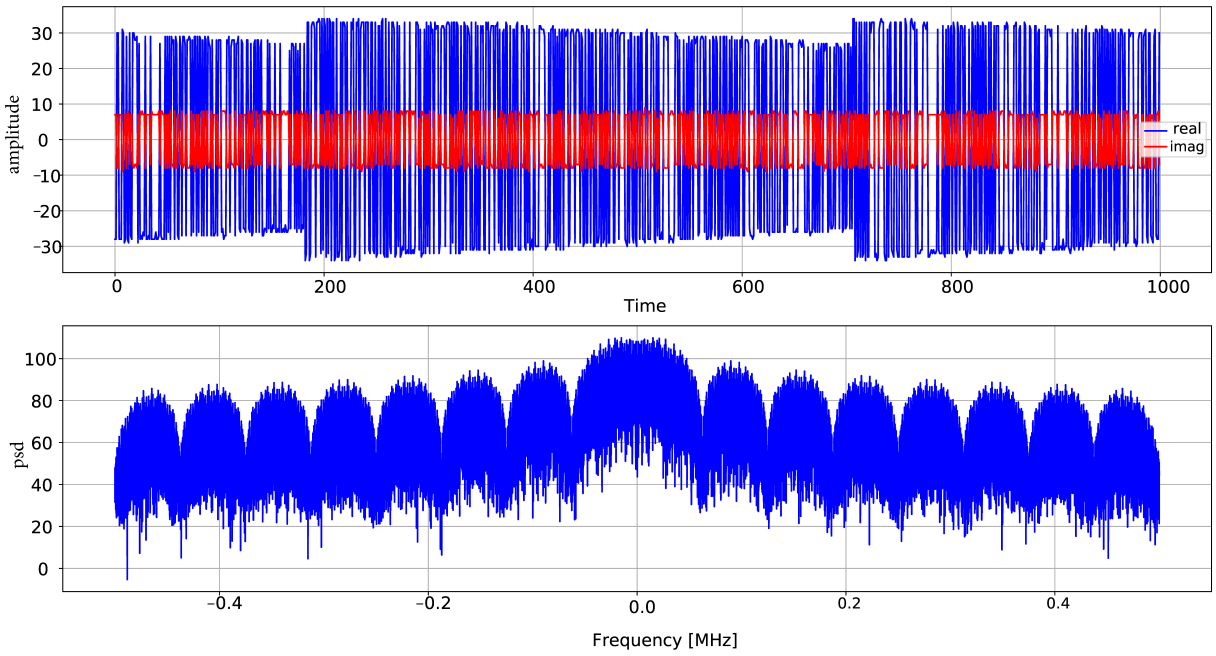

Figure 4.9: CDMA signal received via PlutoSDR, represented in both time and frequency domains, assuming close proximity between the transmitter and receiver.

The intent is to make the communications network more mature to decrease risk and increase its readiness for testing in a semi-structured environment.

4.2.1 Experimental Setup (Aquatron Pool Tank Facility)

To test the proposed network topology, a minimal number of communication nodes, which represent implementation on a marine robot network, would be deployed in-water for static tests (i.e., they are not in motion). The three transceiver robot nodes represent 2× UUVs and 1× USV. The experimental set-up is shown in Figure4.10.

The two underwater network nodes (UUV), which are deployed mid-water column, are shown as

- submerged node # 2 (UUV)
- submerged node # 3 (UUV).

Again, theUSVhas two network nodes – an underwater and a floating in-air one. The USV's underwater network node is shown as "USVsurface node # 1" which communicates with the two underwaterUUVnetwork nodes.

A deployed passive hydrophone provides an independent measure of incoming and outgoing signals between the nodes. These hydrophone recordings are processed to provide

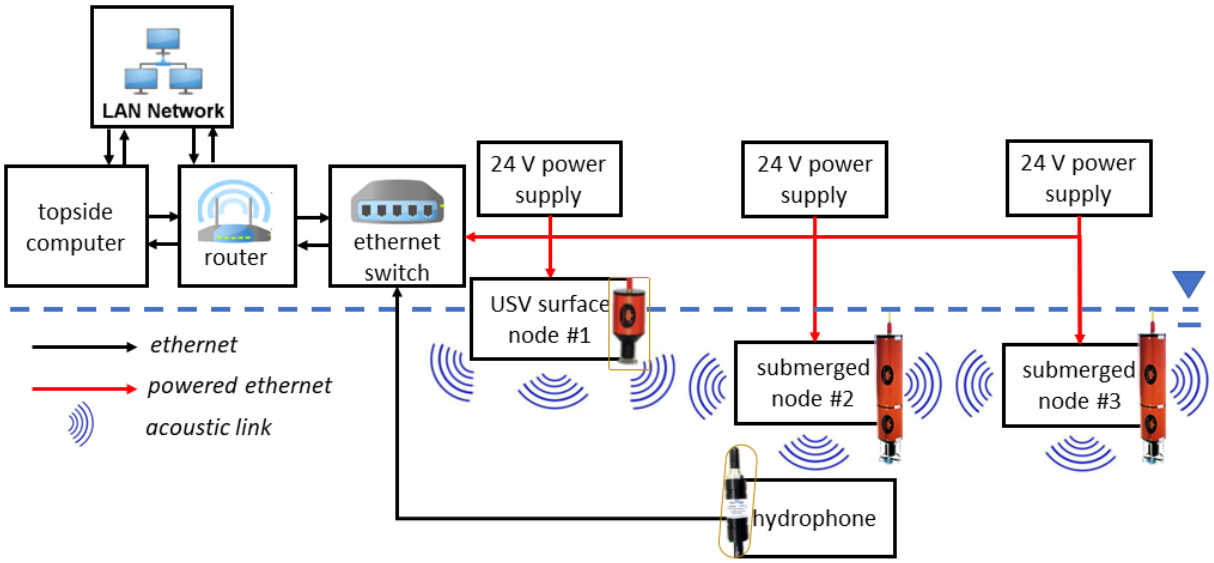

Figure 4.10: The experimental setup for the Aquatron Pool Tank (controlled environment test and verification) for the underwater branch of the proposedCDMA-based communications system (in-air and above-water nodes not shown.)

power spectral densities and time-frequency distributions (spectrograms) of the transmitted and received signals between these three nodes. This processing yields information on signal bandwidth and power which are criterion and performance measures the network is evaluated against. All three nodes are networked and thus accessible to any device (e.g. modem, hydrophone, support laptops, etc.) in the network. The transmitted/received signals encode messages with the robot's pose (latitude, longitude, heading, and depth) as well as its speed. For example, an encoded message would be: T-44.6488N,63.5752W,35.5,271.4,45.5) [71].

TheUSVunderwater node is further integrated to a software-defined PlutoSDR radio which represents the in-air node to communicate with theUAV. In this final configuration, theUSV's underwater node communicates with the submergedUUVs and its floating in-air node communicates with anUAValoft. With this communication system on theUSVit is able to relay under- and above-water messages in both directions.

The requirement for the research is unique where theUSV's in-air network node must have a line-of-sight range $\geq$ 10 km as this is the range of the underwater nodes and the UAVabove-water network node would be at some altitude above sea level. The information that needs to be relayed in-air by theUSVincludes the quantities in the example encoded message above. It can also include an unknown mobile underwater target's state. It can also be processed UUV orUSVsensor data that needs to be conveyed to an above-water station. Conversely, this station may transmit commands for theUSVandUUVto execute. In this way, these collaborative network nodes can increase the mission range to well over-the-horizon (Chapter 1 - Figure1.3).

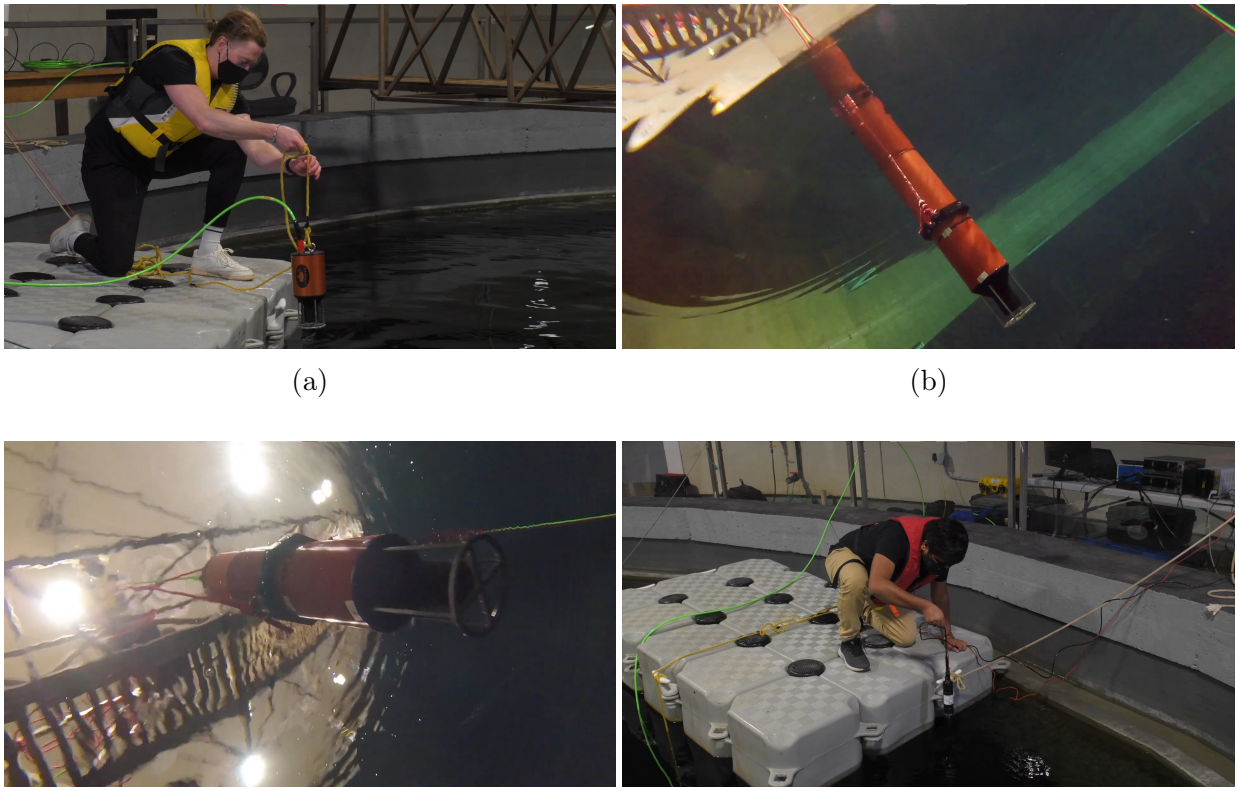

(a) (b)

(c) (d)

Figure 4.11: Deployment of underwater network nodes in the communications network (based on Subnero modems) in the Aquatron Pool Tank (controlled environment test and verification): (a)USVsurface node # 1; (b) Subnero submerged node # 2; (c) Subnero submerged node # 3, and (d) iCListen OceanSonics hydrophone.

To fulfill the thesis requirement for an innovative network modulation which has improved bandwidth use, security, and full-duplex capabilities, underwater software-defined modems were used as it is possible to design and build new communications protocols with them. Such modems which can natively support UnetStack [95] in their firmware, are desired. UnetStack has the necessary development tools for this thesis – one of which is hardware-in-loop-simulation with the modems themselves. Unetstack can simulate the UUVkinematics and emulate the communications between the UUVs. Such flexibility was necessary to develop the communications network for collaborative mobile marine robots. Unetstack-compatible software-defined modems also support Python APIs and custom baseband arbitrary waveform transmission. This is significant as there are Python libraries and utilities that can be leveraged for basic modem functions making it easier to focus on the research aspects.

Previously generated and newly designedCDMAwaveforms (FigureC.1) can be used with the developed Python tools [71]. UnetStack runs on the top-side computer (laptop in Figure4.10) which is integrated within the same network that theUSV's andUUVs' nodes are in.

The following equipment and tools (Figure4.11) were used for the above-mentioned in-water verification:

- PC (Linux) with Python2, Python3 and UnetStack
- 1x - floating Subnero UW-Modem (Subnero modem WNC-M25MSS3)
- 2x - submerged Subnero submerged nodes 1 and 2 (Subnero modem WNC-M25MSN3)
- 1x - iCListen HF Smart Ocean Sonics hydrophone 200 m depth (SC2-ETH)
- 1x - sound velocity profiler (CastAway-CTD E767-CA-CTD)
- 1x - router and 1x network switch
- 3x - 24 V DC power supply

Figure4.12is a photograph that shows all three underwater network nodes (Subnero modems) deployed in the Aquatron Pool Tank. Figure4.13shows an experiment where the USVunderwater node (top terminal) transmits five messages at a near-constant frequency to the two submerged UUV nodes (two terminals on the bottom). The two UUV underwater network nodes successfully received four of the five custom message which includes location, kinematic and geometric data. TheUSVunderwater node suffered a dropped packet (second of the five transmissions) due to a buffer overflow which manifests as a "false" in theUSVunderwater node's terminal. These dropped packets occur when the network link is congested.

Figure4.14shows the processed results of what the hydrophone monitored and corroborated for the setup in Figure4.12and the experiment detailed in Figure4.13. The PSD(Figure4.14(top)) over the 2-minute experiment showed large amplitudes (to the point where the auto-scaling could not keep up) in the frequencies around 25 kHz. This is expected as the carrier frequency for the signals (messages) was 25 kHz. The spectrogrm in Figure4.14(bottom) corroborated, as a function of time, that the highest levels received were at 25 kHz (in red). It also shows the four signals that made it into the water-column and were received by the hydrophone. The approximate time (labelled "missing") where the dropped signal 2 (out of 5) would have been is highlighted.

The results from the controlled environment test and verification in the Aquatron Pool Tank verified the correctness of the developed and researched modem functions, transmittedCDMAunderwater network node signals, the underwater branch of theCDMA communications system, and developed software processing tools.

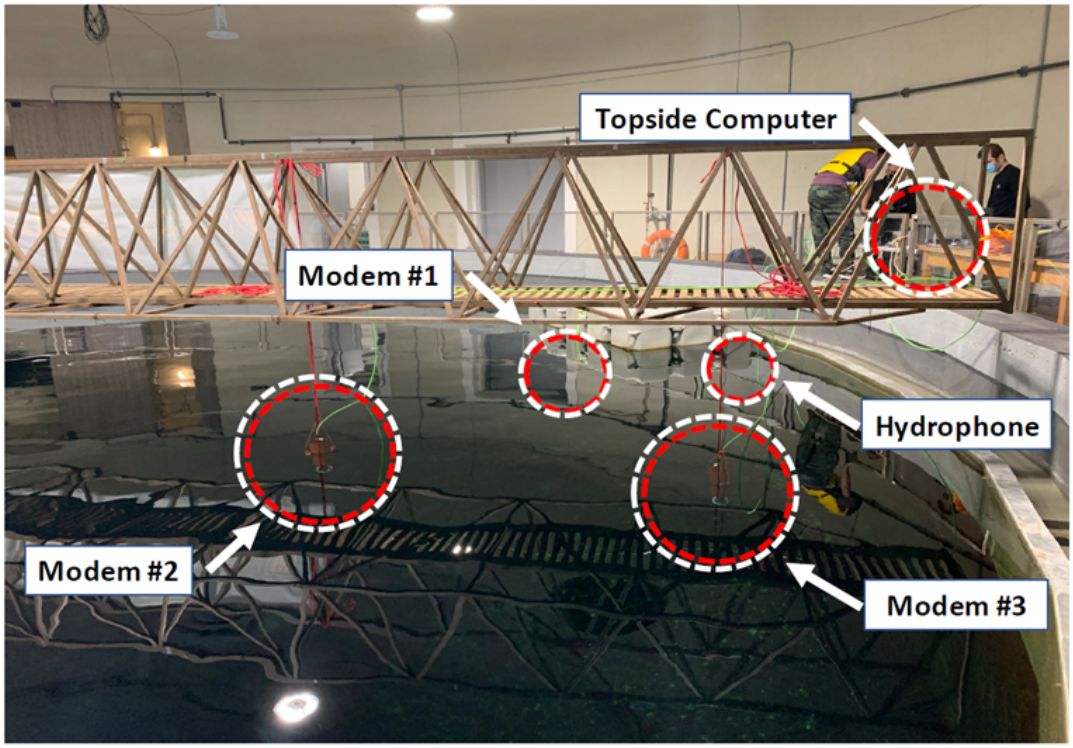

Figure 4.12: The three underwater network nodes (based on Subnero modems) and a passive hydrophone deployed in the Aquatron Pool Tank (controlled environment test and verification) to verify the designed and developed functionality and performance of the communicating network nodes.

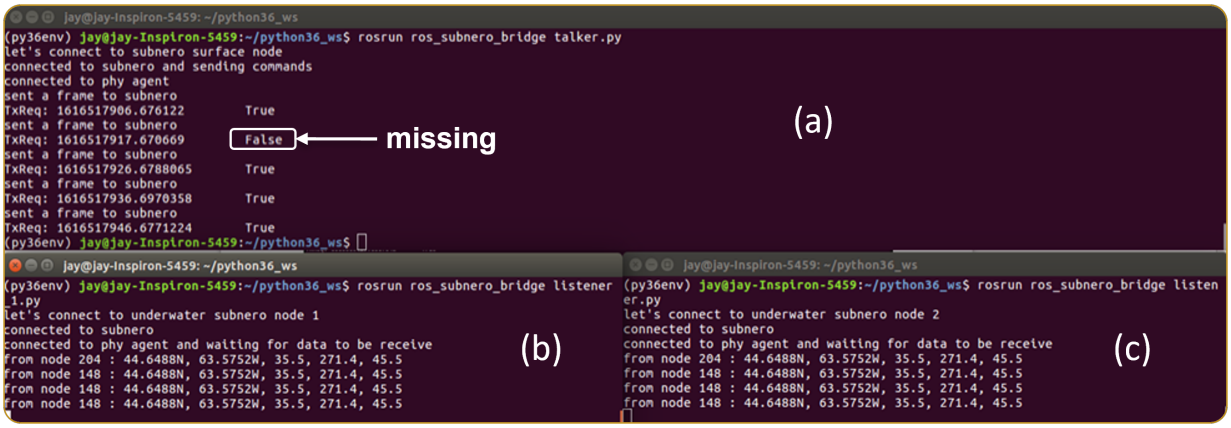

Figure 4.13: For the setup in Figure4.12five messages were periodically transmitted by the surface underwater network node at the Aquatron Pool Tank (controlled environment test and verification) as an experiment. The second of the five messages transmitted by theUSVunderwater node (top terminal) was dropped and thus not received by the two underwaterUUVnodes (bottom two terminals) due to the congested network link.

Figure 4.14: Frequency analysis of Figure4.132-minute experiment from hydrophone measurements show: (top) thePSDhas large amplitudes around the five transmitted signal's 24 kHz carrier - as expected, and (bottom) the spectrogram captures the received signals and correctly shows a gap in time where the second packet would have been were it not dropped. This hydrophone analysis corroborates the Figure4.13observations and verified the communications network performance at short ranges and in shallow water.

4.2.2 Challenges in the Aquatron Pool Tank Tests

It was anticipated there would be multi-path in the Aquatron Pool Tank (Figure3.26) due to its concrete structure and small dimensions (15 m diameter $\times$ 4 m depth). This was verified during experiments where it was noted that the underwater modems receive multiple reflections of a signal from a single transmission (Figure4.15).

In the controlled environment, three underwater network nodes were deployed in the Aquatron Pool Tank to emulate underwater communication scenarios. Successful communication between the surface node and the underwater nodes was demonstrated, as evidenced by the reception of custom messages containing location, kinematic, and geometrical data. Having achieved all that was meaningful for the communication system test and verification in a controlled environment, the next step was to transition to semi-controlled environment test and verification as shown in the Figure3.9.

Building upon the insights gained from the controlled environment, in-water testing in less controlled environments were initiated. The same experimental setup with the minimal three underwater network nodes necessary would be trialed through multiple series of deployments off the COVE jetties (semi-controlled environment). The underwater nodes would now be distributed over a much larger space which will vary in its depth,SVP,

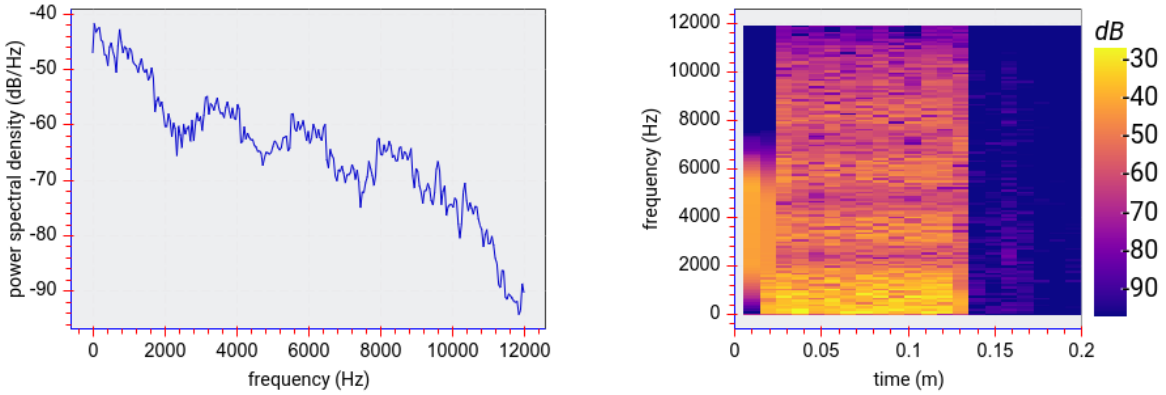

(a) (b)

Figure 4.15: Power distribution of received custom CDMA raw baseband signal with preamble (Figure4.6) shows the power (dB/Hz) decreases with increase frequency in the concrete Aquatron Pool Tank and where 2 kHz harmonics are likely multi-path as manifest in a: (a)PSD, and (b) spectrogram. As per Figure4.6theRSSIis strong and also manifested in the repeat columns (time slices each consisting of 248 chips) in the spectrogram.

underwater ambient, multi-path, etc. compared to a controlled environment.

4.3 Test and Verification in a Semi-Controlled Environment

Two main experiments were performed to verify network node capabilities in a more complex environment than the Aquatron Pool Tank.

The first was to verify full-duplex communications on a node to transmit and receive the same underwater message concurrently to show that this is possible as this is not possible with the typical popular half-duplex TDMA modulations and is still novel underwater. In half-duplex schemes the single channel is either transmitting or receiving.

The second test verified that the three deployed underwater nodes can be integrated into a full-duplex CDMA network that additionally is able to relay beyond line-of-sight.

4.3.1 Full-Duplex Verification with a Single CDMA Node

To verify the designed underwater communication network capabilities, full-duplex transmission / reception tests were conducted. August 4, 2022 was a sunny day with high ambient noise levels and low wave activity in-water at theCOVE. Full-duplex communication, where data transmission and reception can occur concurrently over two channels, was verified by transmitting a long 3+ seconds message and receiving reflections before the entire message was transmitted.

To achieve this, the surface node was deployed to a depth of 2.5 m, transmitting with a carrier frequency of 24 kHz within a 20-30 kHz band, bandwidth of 10 kHz for bandpass and 5 kHz for lowpass. A single modem (node) was deployed from jetty 1 at the COVE to transmit and receive the reflected signal with this channel.

These results from these full-duplex tests show that full-duplex underwater communications is feasible and indeed, achievable. However, the challenge lies in the receiver's ability to sample at the correct time to receive the signals accurately, where transmission and reception happen concurrently on two channels, timing synchronization is crucial to avoid interference between the transmitted and received signals. If the receiver samples the signal at the wrong time, it may not properly separate the transmitted signal from the reflected signals or noise, leading to errors in the received data.

This full-duplexCDMAchannel also facilitates exploring potential reflections (seabed, water surface, thermocline) to characterize the underwater channel. Not surprisingly, the underwater environment significantly impacts the full-duplexCDMAchannel performance. This highlights the importance of considering environmental factors and choosing appropriate signal and noise power levels to ensure reliable communications.

Interestingly, even when the signal power was below the noise level (signal power of -70 dB to -92 dB), the system still achieved a positive bit error rate and throughput. The robustness is attributed to theCDMAspread spectrum technique, which can mitigate the impact of noise and interference by spreading the signal energy over a wide bandwidth. The receiver can then employ sophisticated signal processing techniques, like matched filtering and decoding, to accurately recover the transmitted data even in noisy conditions.

Overall, the successful full-duplex tests provided valuable insights into the practical challenges and considerations of deploying a full-duplex node in the underwater environment. These findings guided the integration of multiple full-duplex nodes and contributed to the advancement of underwater communication systems at the COVE, which is presented and discussed next.

4.3.2 Integration of Multiple Full-Duplex CDMA Nodes

One underwater network node was deployed off of each of the three jetties at theCOVE (Figure4.16) —1 $\times$ surface node and 2$\times$ standalone underwater submerged nodes. The maximumCOVEwater depth of $\simeq$ 11 m was where the surface node was deployed (near the Stella Maris seabed platform).

The objective of this experiment was to relay a message from the surface node (address: 204) to the submerged node with address 93 via submerged node with address 148 through line-of-sight. Simulations for this experiment was performed for the optimal transmitter and receiver depths (Figures3.23,4.17). Based on this, all nodes were deployed at $\simeq$ 4 m depth to achieve the best channel by isolating from environment factors like the surface.

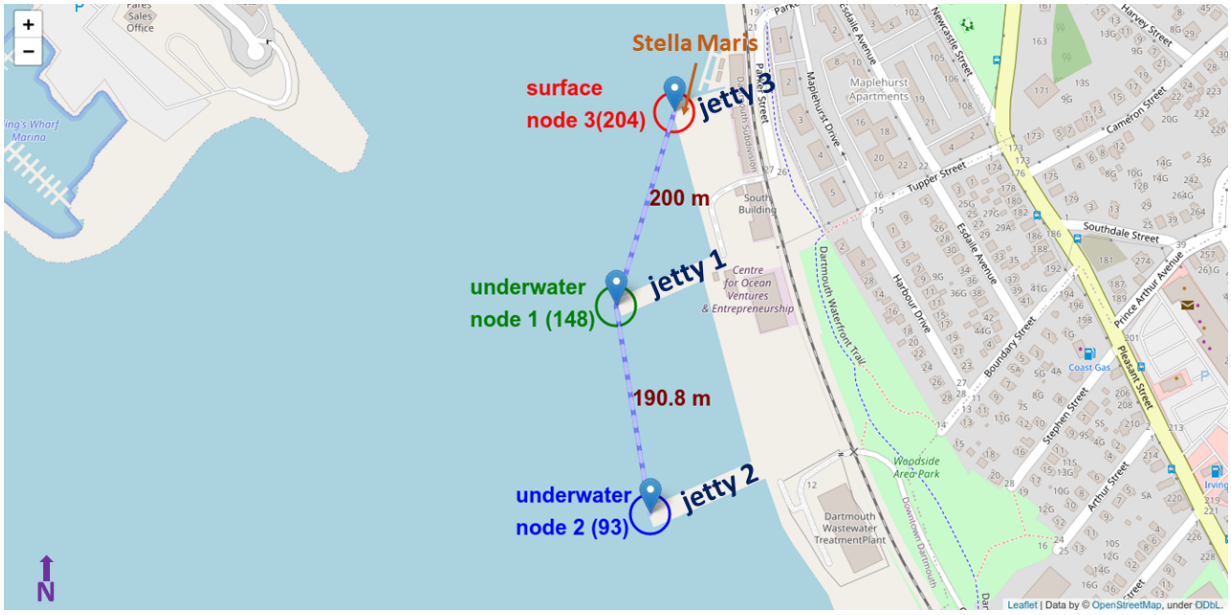

Figure 4.16: Experimental setup with 3 underwater network nodes deployed off the COVE jetties (semi-controlled environment) with 1× surface node (address 204) and 2× submerged nodes (addresses 148 and 93, respectively). All underwater network nodes were spaced $\simeq$ 200 m from the next modem off their respective jetties.

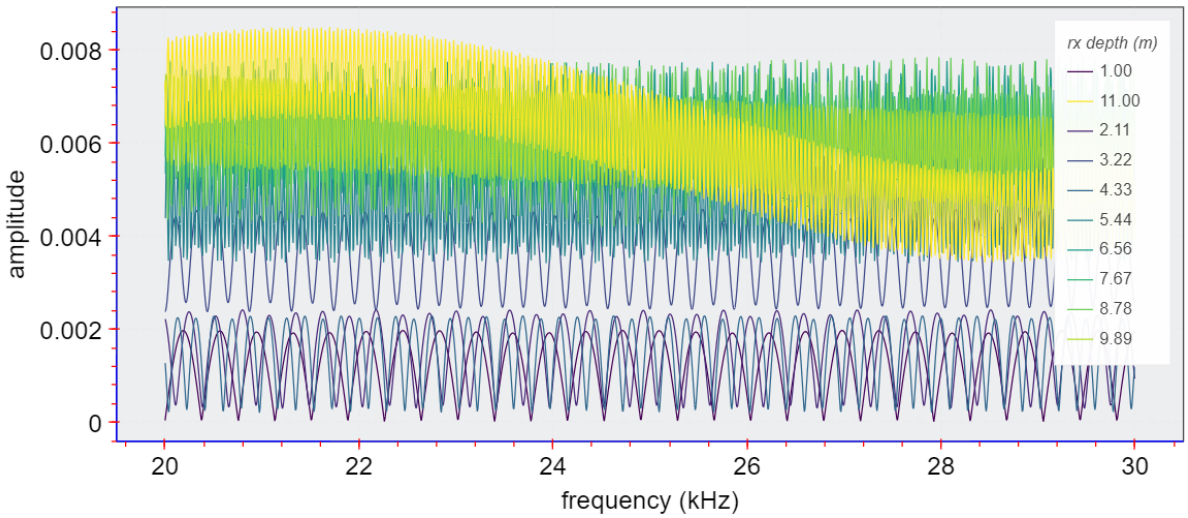

Figure 4.17: Simulation of Multi-frequency channel response to a 4 m depth transmitter at the COVE (semi-controlled environment) at variable range to the receiver at depths from $1 - 11$ m and from a horizontal range of 200 m. This characterizes the underwater water channel to determine where transmitters and receivers could be optimally placed in the water column. These results indicate 4 m is a good transmitter and receiver water depth.

Figure4.19illustrates a typical above-water experimental setup at theCOVE(semi-controlled environment) to support the underwater network nodes deployed off that jetty.

The central jetty node served as the network hub as all acoustic signals were accessible from here. Figure4.18is a typicalSSPmeasured by theCOVE's Stella Maris seabed platform on August 10, 2022 which was a test day.

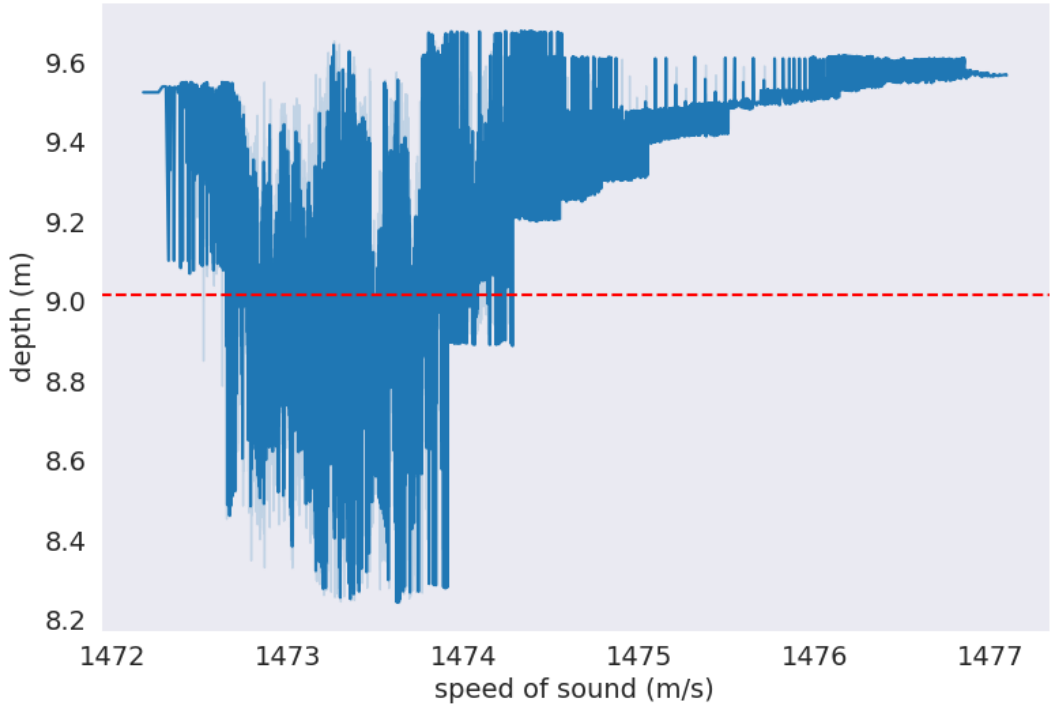

Figure 4.18: The sound speed profile (SSP) measured by theCOVE's Stella Maris seabed platform (near jetty 3 ≈ 9 m deep) on August 10, 2022. TheSSPprovides information on how the acoustic signals will travel and informs where receivers would be best placed. The red-dotted line is the mean depth. It serves as a reference to analyze and interpret observed acoustic propagation characteristics in the area.

A submerged node is deployed from the middle jetty and thus all nodes were accessible acoustically since there is noLOSbetween nodes 204 and 93 (Figure4.16). Figure4.16, Figure4.19and Figure4.20provide a complete picture of the experimental setup, depicting the location of all three deployed underwater network nodes. Node 1 was placed at a depth of 4.52 meters at the central jetty, while node 2 and the surface node were deployed at depths of 0.5 meters and 1.8 meters, respectively. These were suggested in Figure4.17as good depths in the underwater channel.

The underwater nodes and hydrophones were integrated into a network with separate wireless routers to create awireless distribution system (WDS)– a wireless LAN. The node

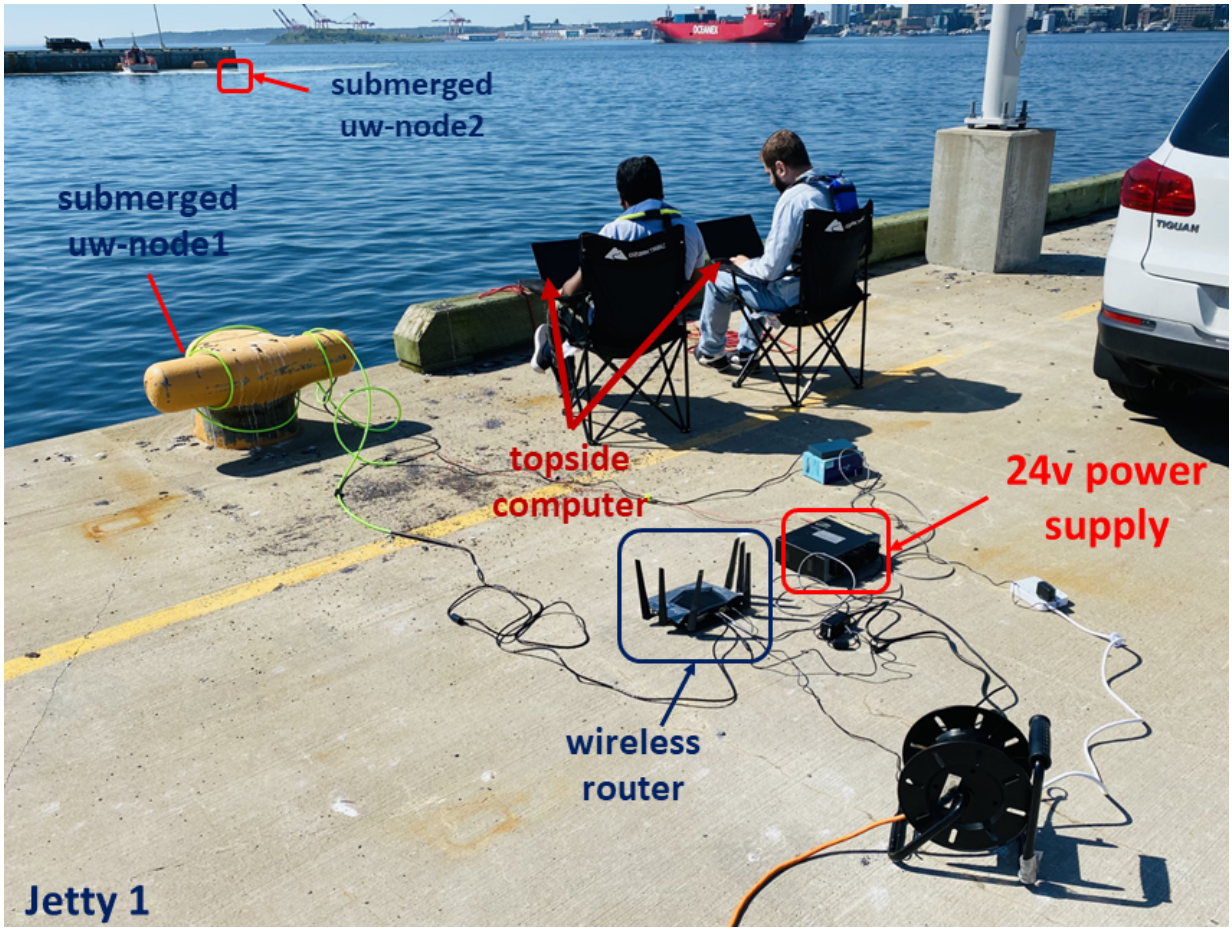

Figure 4.19: Typical above-water experimental setup at theCOVEon August 10, 2022 to support one of three underwater network nodes (not visible) deployed off jetty # 1.

placements and depths were determined through simulations (Figure4.17) and deployed as described in Table4.1.

Table 4.1: Roles and depths of the three deployed network communications nodes at the COVE (semi-controlled environment) for the multiple network nodes integration verification.

role	**location**	**node #**	**node address**	**depth (m)**
transmitter	surface	3	204	1.8
relay (rx then tx)	underwater	1	148	4.0
receiver	underwater	2	93	0.5

On the designated test day, August 10th, 2023, the carrier frequency was set to 24 kHz, with a band from 20 kHz to 30 kHz. The bandpass bandwidth was configured to 10 kHz, while the lowpass bandwidth was set to 5 kHz. The weather conditions that day were a

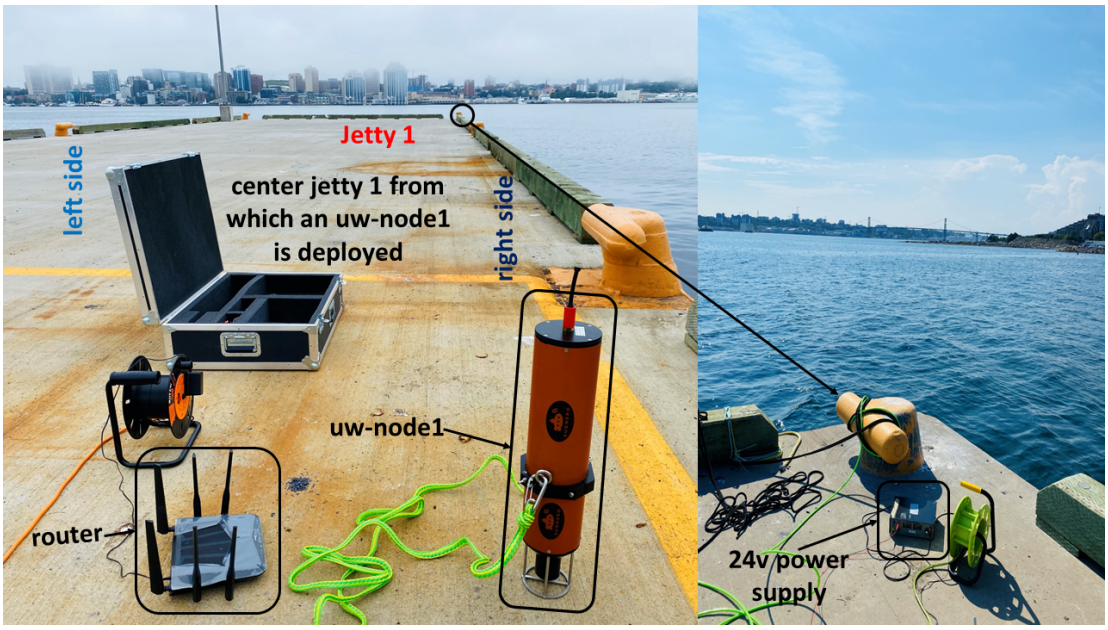

(a)

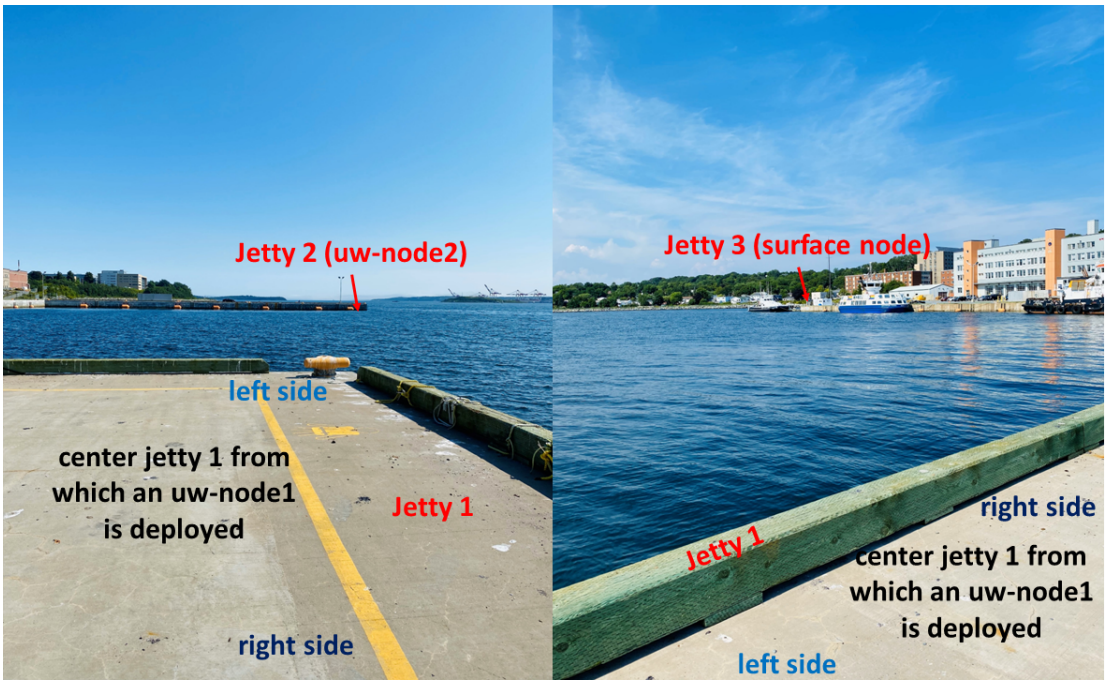

(b)

Figure 4.20: Relative arrangement of underwater network nodes deployed off the three COVE(semi-controlled test environment) jetties (Figure4.16): (a) central jetty 1 where submerged node 1 was deployed to 4.52 m depth; (b) jetty 2, located to the *left* of central jetty 1 deployed uw-node2 to 0.5 m. jetty 3, located to the right of central jetty 1 deployed a surface underwater node to 1.8 m depth. Left and right are referenced with the observer at a jetty looking out to sea.

combination of cloudy and sunny conditions with minimal to medium wave activity. This meant a high acoustic ambient.

The distance between the transmitting (node-3, address 204) and intended receiving (node-2, address 93) nodes was 390.9 m as measured by the Unetstack acoustic ranging functionality (Figure4.21).

In the experiment, a message was transmitted from the surface (node-3, address 204) to a submerged node (node-2, address 93). The transmitting node did not haveLOS to the intended receiving submerged node. Therefore, it had to be relayed via another submerged node (node-1, address 148). This emulates the condition where a command from above-water is sent to an underwater node and further, underwater relaying was necessary. As shown in, Figure4.22) the message was successfully transmitted from the surface node (address 204) to the intended underwater node (address 93) via another relaying underwater node (address 148) (Figure4.23) given the surface node was not in LOSof the intended receiving node.

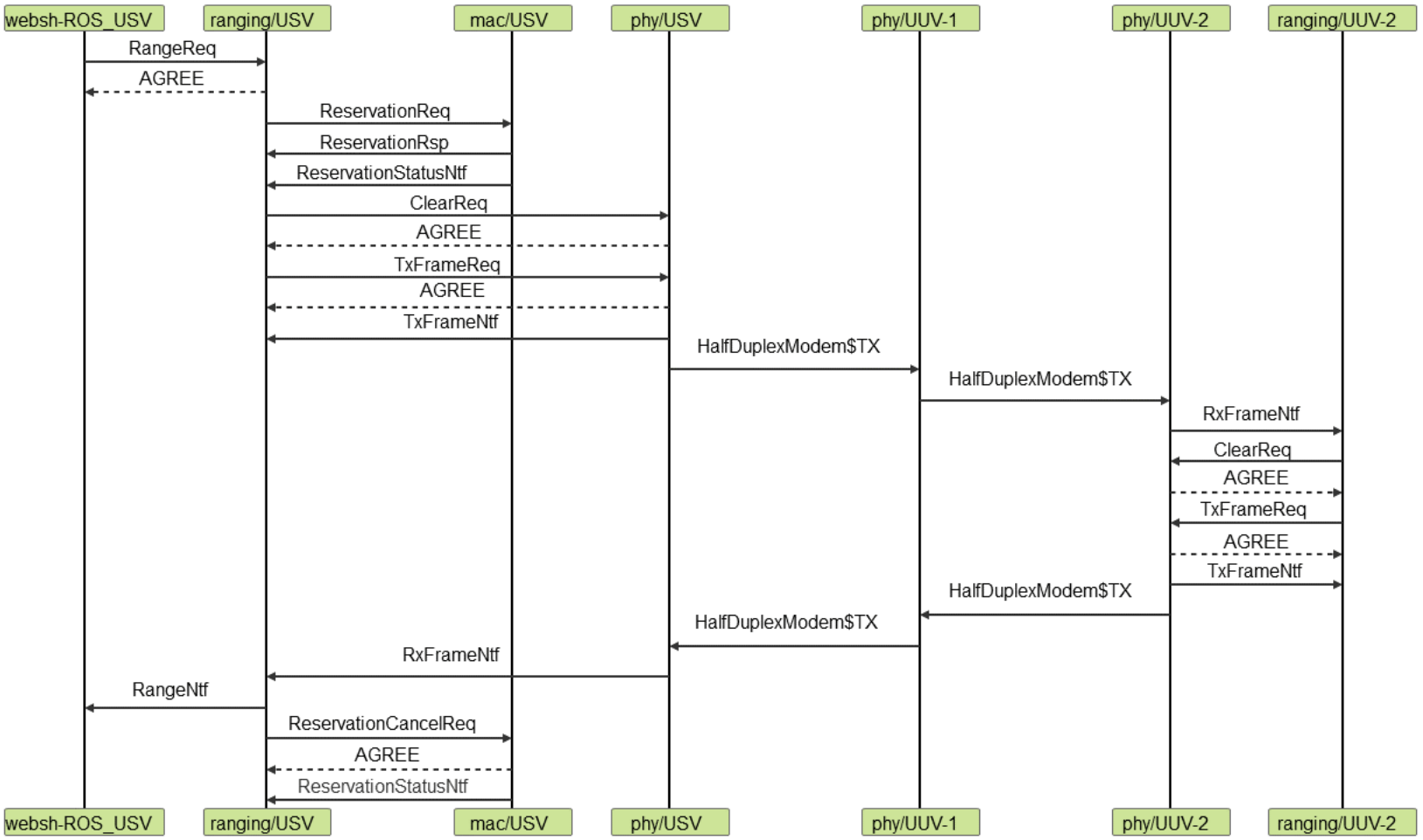

Figure 4.21: Unetstack network stack event trace when a ranging operation is initiated from the surface node (node 3) to submerged node 2 at theCOVE, as depicted in Figure4.16. This presents the communication process designed within the network stack, capturing every event and operation in the ranging.

Figure 4.22: With the three nodes deployed at the COVE (4.16), a message was successfully relayed from the surface node (node # 3) to a submerged node (node # 2) via another submerged node (node # 1). Node # 1 as the relay node made the transmission possible as there was noLOSbetween the transmitting and intended receiving node. This relay mechanism enables communication over longer distances and enables better coverage in underwater acoustic networks. The successful message relay demonstrates the effectiveness and robustness of the communication system under the tested conditions.)

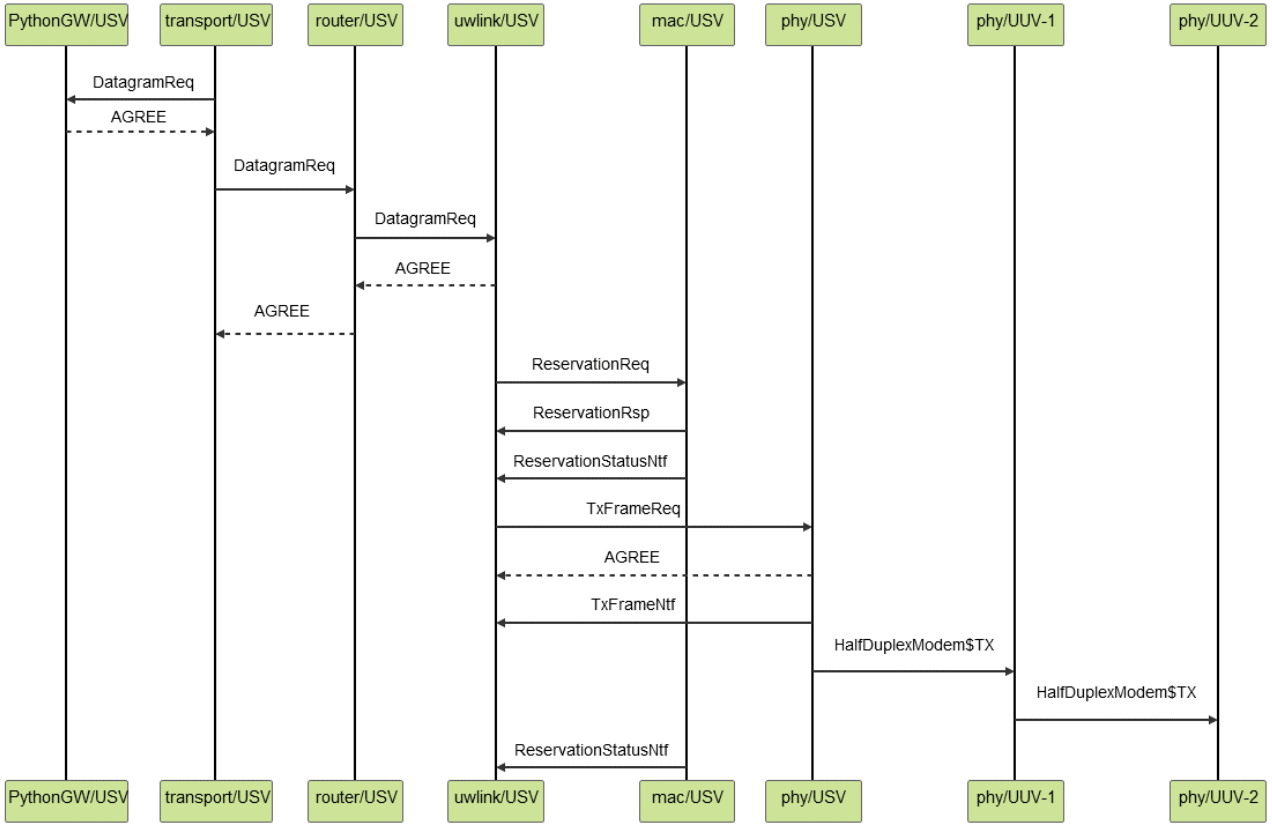

Figure 4.23: Unetstack network stack event trace when the *Hello* message is transmitted or broadcasted as a DataFrame. This presents the process within the designed network stack, showing the sequence of operations and interactions that occur at each node during the transmission of the *Hello* message.

For simplicity, all traces in Figure4.23and4.21, were initiated from aROSnode that utilized a Python Gateway, this plays a role in translating and managing communication between theROSnode, which is running Python code, and the underwater nodes, which might use different communication protocols or interfaces.

At theCOVE, a minimal number of three nodes were deployed, including a surface node and two standalone underwater submerged nodes. Despite the challenges posed by the depths and environment, the end goal of relaying information from the surface node to the submerged nodes, without directLOSconnectivity, was successfully achieved. Simulations and optimal depth configurations were employed to ensure better signal reception while considering external environment factors.

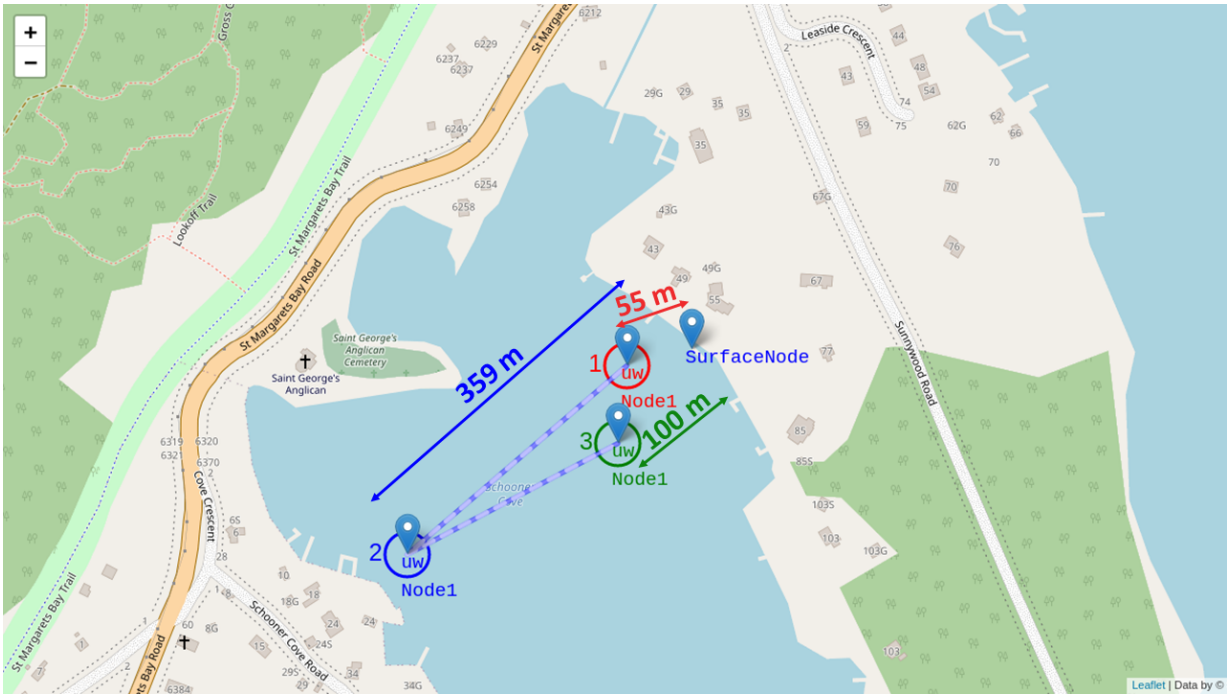

Figure 4.24: St. Margaret's Bay (uncontrolled environment) at 44.6802104 N, and 63.91634 W (farther from Halifax approaches) saw two underwater network nodes deployed. A surface underwater network node was deployed from the jetty and one submerged underwater network node was deployed at multiple stand-offs from the surface underwater network node. The one submerged underwater network node at 1, 2 and 3 was 55 m, 359 m and 100 m, respectively, from the surface underwater network node

However, due to the ship traffic (high underwater ambient) in the Port of Halifax and

the weather conditions in August 2022 (wind and waves contributing to underwater environment and deployed modem motions), another series of tests were planned and conducted at St. Margaret's Bay which is a more inland body of water and farther from the Halifax Harbour approaches.

4.4 Test and Verification in Uncontrolled Environments

Given the limited resources, only two underwater modems were deployed at St. Margaret's Bay to verify the communication system's performance. The surface node was deployed off the jetty (stationary) and the submerged underwater network node was towed by boat to different stand-offs, annotated as 1, 2 and 3 and were 55 m, 359 m and 100 m, respectively, from the deployed surface underwater network node(Figure4.24).

Throughout these experiments, challenges were encountered, necessitating adaptations and resulting in valuable observations. These findings will serve as the foundation for the Results chapter, where the collected data will be analyzed, and meaningful conclusions about the performance and capabilities of the underwater communication network will be drawn.

Chapter 5

Results and Discussions

[1]A. M. Bassam, J. Patel and M. L. Seto, "Kalman Filter-based Doppler Tracking and Channel Estimation for AUV Implementation", OCEANS 2021: San Diego – Porto, San Diego, CA, USA, 2021, pp. 1-8, doi: 10.23919/OCEANS44145.2021.9705878, [17].

The simulations (Chapter3) motivated the implementation and experimentation (Chapter4) in the form of multiple deployments in increasingly more complex environments. The results from these deployments will be presented in this chapter (Chapter5) and discussed to quantify the efficacy of the proposed novel communication system.

The next Chapter after this (Chapter6) summarizes the thesis contributions and draws conclusions on the novel communication system developed.

The proposed communication system's integration was successful and verified through controlled indoor tank (Aquatron) and jetty-side (COVE) experiments (Chapter4) to underwater ranges on the order of hundreds of meters. Larger ranges were not tested. The results show the system is viable and capable of achieving the intended objectives when implemented with theROSmiddleware as a robotic subsystem. The next step is to understand the performance of this as a whole communication system.

Section 5.1 addresses the semi-controlled environment deployment at theCOVE. Then, Section 5.2 addresses the results from the uncontrolled environment deployment at St. Margaret's Bay.

5.1COVE(semi-controlled environment)

5.1.1 Communication Systems Performance

Figures5.1and5.2presents the analysis to quantify the communication system's performance from the August 4 and 10, 2022 in-water trials at theCOVE, respectively. It illustrates the variation of throughput and channel quality with time. As well, Figure5.3 shows theBER,RSSI, andCFOwithSNRlevels (TableD.17).

Throughput and Channel Link Quality

The throughput is the average number of bits of user data received through the channel per unit time. The communication channel quality measures the mutual information between received and transmitted bits. Similar information is expressed in theBER. Link quality can be quantified as shown in Eq.5.1:

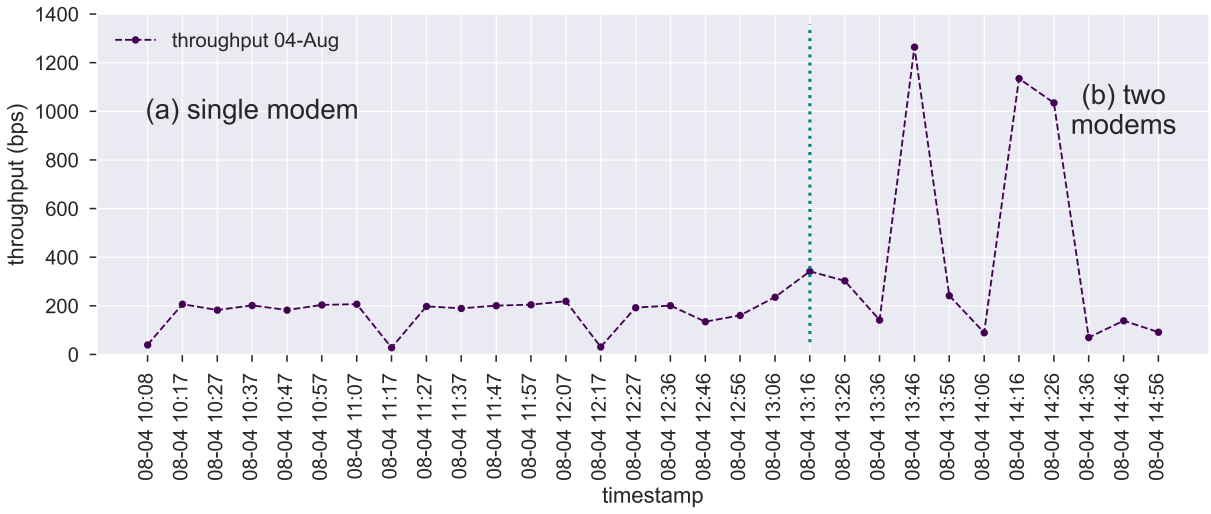

Figure 5.1: Proposed communication system performance from the Aug 4, in-water trials (COVE, semi-controlled environment, Figure4.16). Submerged node 1 transmits at 1418 bps in: (a) full-duplex mode to achieve throughput of 200 bps when there is no interference from the ferries (received messages at node 1 are shown); (b) operationally half-duplex mode to surface node 3 (jetty 3). The received throughput at surface node 3 (jetty 3) shows generally higher throughput. Soon after, the tied up boat departed. Despite strong interference the communication system still managed a full-duplex throughput of 200 bps and a maximum half-duplex throughput of 1250 bps. All received messages decoded correctly.

$$\textbf{channel quality} = \frac{total\ volume\ of\ data\ received}{volume\ of\ data\ transmitted} \times 100 \tag{5.1}$$

which accounts for dropped frames or packets. Figure5.1presents results from initial in-water semi-controlled environment tests at theCOVE. In-water on August 4, there was an unanticipated boat tied-up near submerged node 1 (the transmitting node) until 1345.

To make best use of available bandwidth underwater, a spreading factor of 8 was selected in theCDMA-encoded messages, and all subsequent experiments were conducted with this value. A solitary node was deployed off center jetty 1 to a depth of 2.5 m (COVE) to initially test the full-duplex channel characteristics.

Single Full-Duplex Node

On August 4^{th} from 1008 - 1307, only submerged node 1 (jetty 1) was deployed and

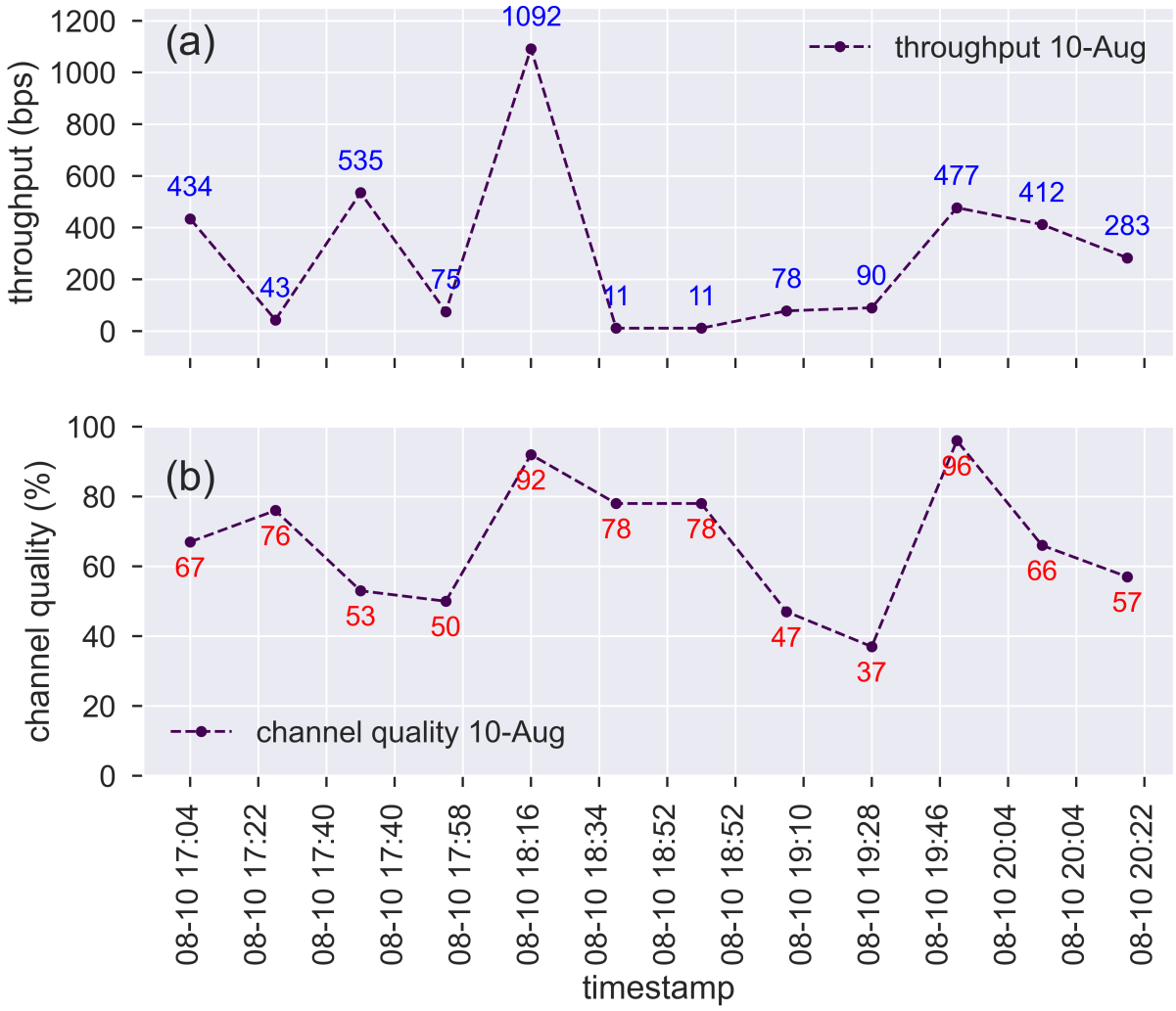

Figure 5.2: Proposed communication system performance for the August 10, 2022 in-water trials (COVE, semi-controlled environment, Figure4.16). (a) Each sample represents a message received at surface node 3 (jetty 3) transmitted (1418 bps) from submerged node 2 (jetty 2) via submerged node 1 (jetty 1) – i.e. signal path goes south to north. When there is no interference, the throughput is better on average than Figure5.1by a factor of 2 or more. (b) Channel quality at surface node 3 corroborates the better channel.

in full-duplex mode. It transmitted at 1418 bps and received its returns. The first noted return is the one that is $>$ 0.25 in the correlation of its preamble against the transmitted message's preamble. This test served to indicate the ambient noise level around jetty 1

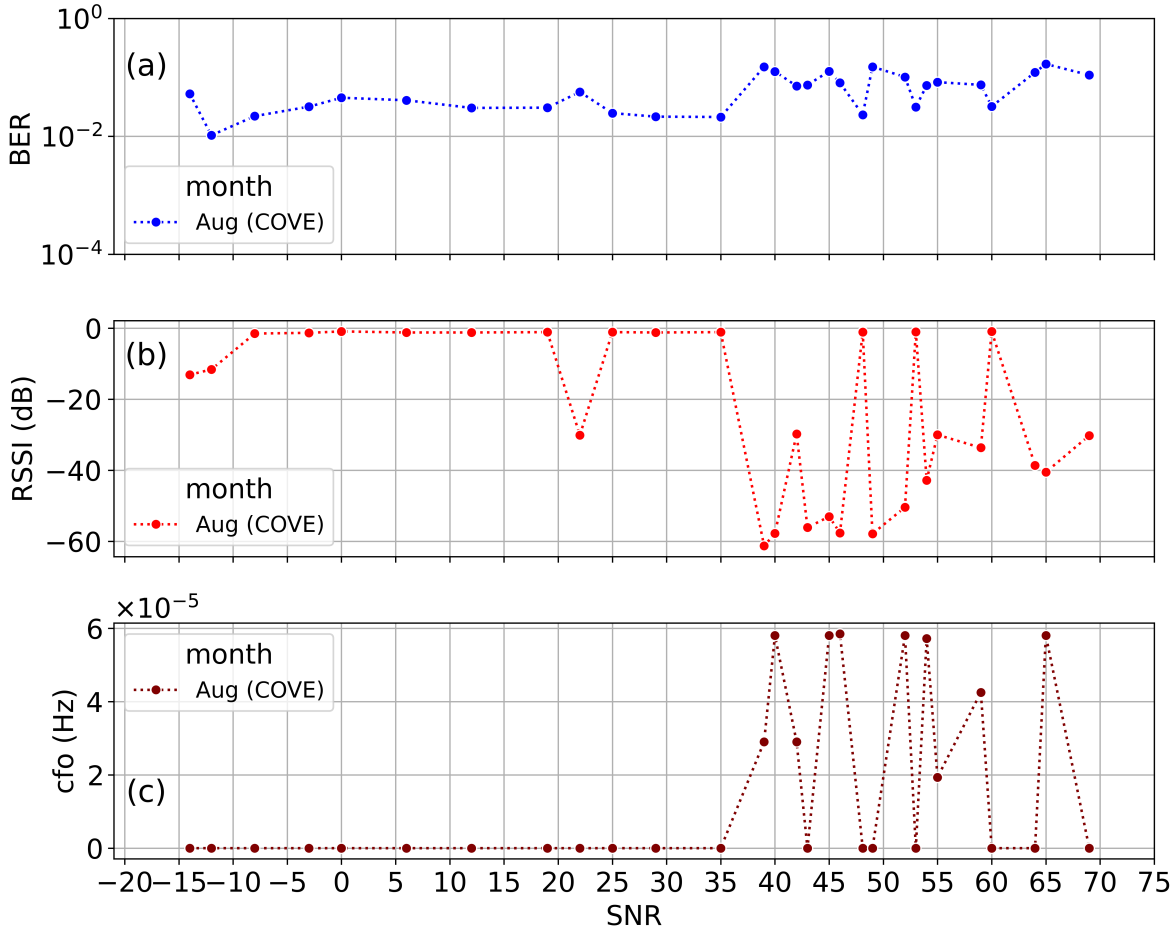

Figure 5.3: Proposed communication system performance for all in-water trials (COVE, semi-controlled environment, Figure4.16) in-water trials (Aug 4 and 10, 2022). Each sample represents a successfully received and decoded broadcasted message for:(a)BERdoes not increase withSNRas expected – unmeasured effects in the water; (b)RSSIvariations withSNR, emphasizing the significance of signal strength for reliable data transmission; and (c)CFOestimations, highlighting system robustness against frequency deviations.

(as transmitter and receiver are co-located) was -65 dB (TableD.13in appendix). The achieved throughput of 200 bps is notable because traditional full-duplex modems typically have a throughput of 80 bps at this location.

Note, there are receptions of very low throughput which occur when the ferry leaves

to cross from Dartmouth to Halifax (1008, 1117, 1217, 1336, 1436) which causes strong interference at jetty 1. This manifests as very low (11 bps) or near-zero throughput.

Two Operationally Half-Duplex Nodes

In Figure5.1from 1307 to 1456, submerged node 1 (jetty 1) broadcasted messages (1418 bps) to surface node 3 (jetty 3) as connectivity tests between two nodes (TableD.14). Note the throughput is generally higher, when there is no interference from ferries. As the transmit and receive nodes are two distinct nodes that are not co-located on the same modem.

The higher throughput at jetty 3 ($>$ 1000 bps to a maximum of 1265) is closer to the transmitted 1418 bps from jetty 1. What is noteworthy is that in a near-harbour environment the communication system is still able to receive and correctly decode received messages at surface node 3, albeit at lower throughput but superior to typical modems, when strong in-water noise sources are close to the transmitter.

Three Full-Duplex Nodes

Consequently, with this realization, the August 10 in-water trials instead started in the early evening when there was less marine traffic and colder water (Figure5.4) – both desirable conditions. For this set of in-water trials, transmissions (1418 bps) were from submerged node 2 (jetty 2) to surface node 3 (jetty 3) via submerged node 1 (jetty 1). This is over a longer distance than the earlier two-node experiment. When there is no interference, on average. the throughput at jetty 3 (Figure5.2a) increased by a factor of 2 over the case of Figure5.1with this much improved channel reflected in the strong channel link quality at jetty 3 (Figure5.2b, TableD.16).

Bit Error Rate, Received Signal Strength Indicator, Carrier Frequency Offset

Communication system performance measures likeBER,RSSIandCFOcan be gauged against theSNRwhich in this case is calculated as:

$$\text{SNR} = \frac{transmitted\ power}{noise\ power}. \tag{5.2}$$

The transmitted power was set by the modem power level (in dB), and the noise power was an on-going measurement of the ambient noise level (in dB). Note that all the power measurements reference of 1 Watt.

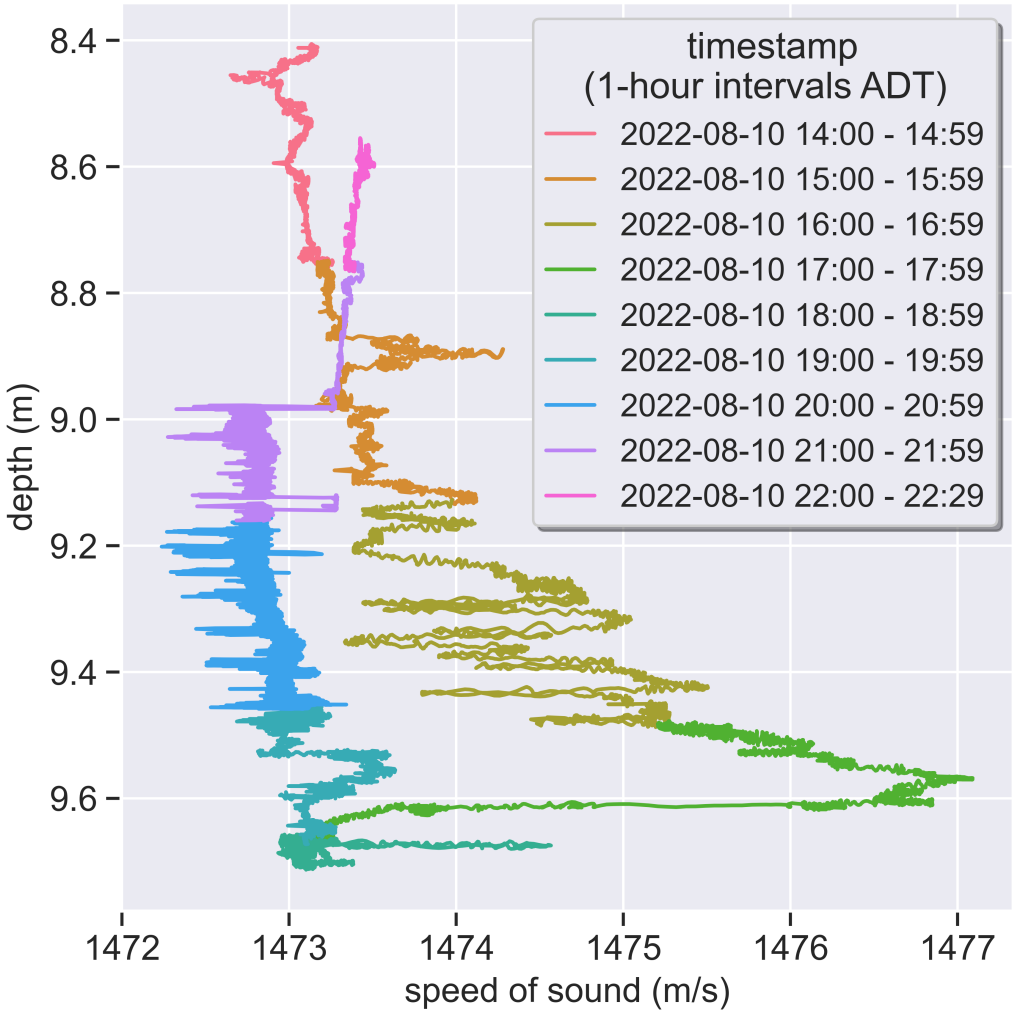

Figure 5.4: The sound speed profile measured at Stella Maris (COVE, near jetty 3) on August 10, 2022 between 14:00 and 22:30 ADT which is during the experimental hours.

The bit error rateBERis defined as:

$$\text{BER} = \frac{bits\ received\ with\ error}{bits\ transmitted}. \tag{5.3}$$

This is another measure of channel quality. It is desired that the BER be as low as possible.

The Received Signal Strength Indicator orRSSIis computed based on the received signal

strength amplitude. In underwater communications, this is the power level of the received acoustic signal in dB [92].

$$\text{RSSI} = transmit\ power + antenna\ gain - path\ loss. \tag{5.4}$$

The carrier frequency offsetCFOis a measure of the signal fidelity. It is based on the difference between the received carrier frequency and the transmitted carrier frequency. It can be estimated by analyzing the preamble or pilot sequences in the received signal compared to the transmitted signal's preamble. It is measured in Hz.

$$\text{CFO} = f_{c,Rx} - . \tag{5.5}$$

This is a measure of channel Doppler. It is desired that theCFObe as small as possible.

In general, as theSNRdecreases theBERincreases. This emphasizes the requirement for the maximum signal strength (power) possible. Therefore, a lowBERand a highRSSI is a measure of a receiver's resilience to noise withSNR.

However, Figure5.3a unexpectedly shows the opposite trend. The reason for this is explained in section5.3.4. Figure5.3b shows generally highRSSIup to an$SNR$of 35. This is also explained in section5.3.4. Discrepancies can be due to other interfering sources in the water column. Figure5.3c show theCFOis generally very small. This is consistent with a low-Doppler channel. This implies the outliers inBERandRSSIare not due to Doppler effects. Despite the inconsistentBERandRSSI, every received message was correctly decoded.

The analysis of theBER,RSSIandCFOperformance measures provided insight into how theSNRaffects the system's performance and underscored the importance of accurate channel characterization (BERandRSSI) and Doppler compensation (CFO). These findings facilitated a deeper understanding of the system's behavior in challenging underwater environments and contributed to the evaluation of theCDMAunderwater communication system's capabilities.

5.1.2 Communication Systems Performance Below the Noise Floor

The next analysis examined how far below the noise floor a broadcast could be and still be decoded by a receiver. Surprisingly, successful receptions were achieved below the

noise floor. Table5.1shows theSNRs range from high positive values (38 dB and 39 dB) to negative values as low as -47 dB.

Table 5.1: Given a noise floor of -72 dB the broadcast power was progressively dropped at submerged node 1 (jetty 1).

signal Tx power dB	**noise power dB**	**SNR at Tx**
-34	-72	38
-33	-72	39
-50	-72	22
-60	-72	12
-65	-72	7
-71	-72	1
-75	-72	-3
-80	-72	-8
-90	-72	-18
-100	-72	-28
-110	-72	-38
-119	-72	-47
-117	-72	-45
-117	-72	-45

The message depicted in Figure5.5,5.6and5.14is particularly noteworthy as it demonstrates the lowest node 1 (address 148) transmission power that can be achieved on a Subnero modem-based communication network. This is a testament to the system's resilience against the high underwater acoustic ambient. Figure5.5demonstrates that the measured noise power was -72 dB and the signal power transmitted from submerged node 1 (address 148), at the particular time was set to -119 dB. The peaks (circled) in the passband PSD of the custom dashboard represent the main frequency components of the transmitted signal. Given that the broadcasted bandwidth is about 10 kHz, the separation between the circled peaks is close to 10 kHz. These peaks are indicative of the primary frequencies where the energy of the signal is concentrated. The peak at 10 kHz is unrelated to this experiment. Figure5.6confirms the successful reception and decoding of the broadcasted transmission at surface node 3 (address 204). This confirmation includes information about the originating node's address and the content of the transmitted data.

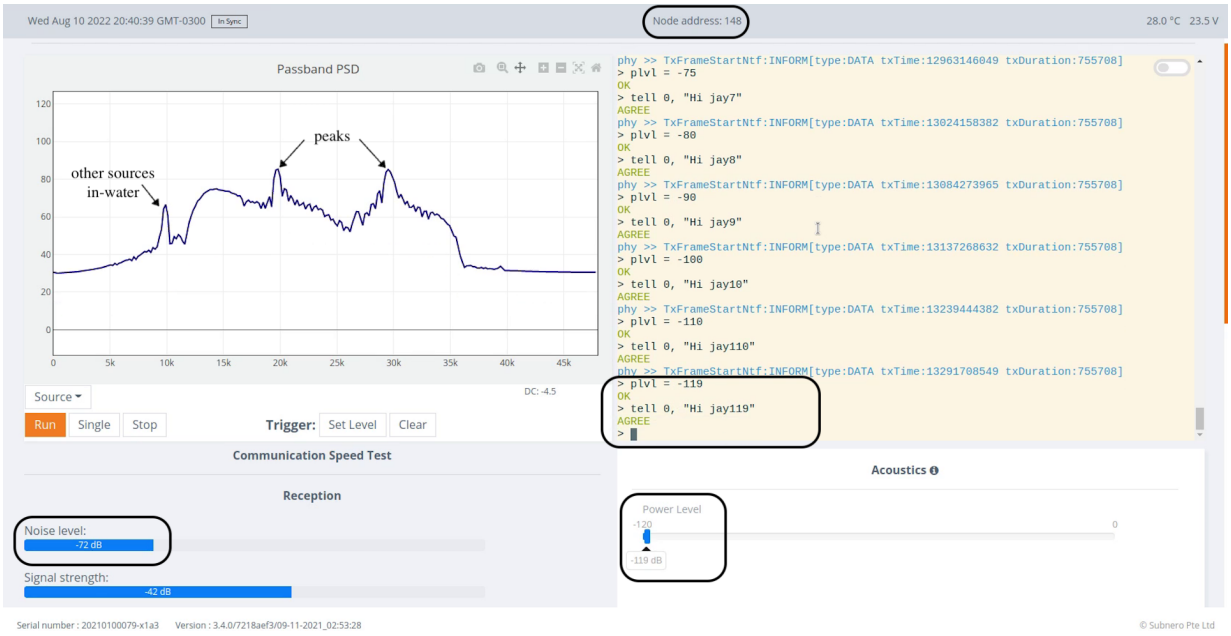

Figure 5.5: At the COVE (semi-controlled environment) with setup as in Figure4.16. The passband PSD is (custom dashboard) calculated at node 1 (address 148) for a dataframe broadcasted (transmitted) to the network from node 1 (148) to all nodes. This transmission achieved aSNRof -47 (measured in-water noise of -72 dB and a power level of -119 dB). Notably, the broadcasted bandwidth is 10 kHz (p-p) which is greater than classicalTDMA nodes. Notably, successful reception was achieved below the noise level, demonstrating the lowest limit of transmission power that can be configured on any Subnero-based node.

This range ofSNRs in Table5.1showcases the system's ability to maintain communication integrity across a wide spectrum of signal strengths. These results underscore the effectiveness of the developed nodes and the protocol used to maintain reliable underwater communications, even in the face of significant noise interference.

The spectrograms shown in Figures5.9to5.14are examples where dataframes were successfully received within the underwater deployed network at COVE. These transmissions were formed at submerged node 2 (jetty 2) and transmitted to surface node 3 (jetty 3) via submerged node 1 (jetty 1) over a wide range ofSNRs given a measured in-water noise level of -72 dB. The hydrophone was deployed at jetty 1 (near submerged node 1). The spectrograms are all generated from the hydrophone at jetty 1. For the runs here, 1 dataframe is the same as 1 message.

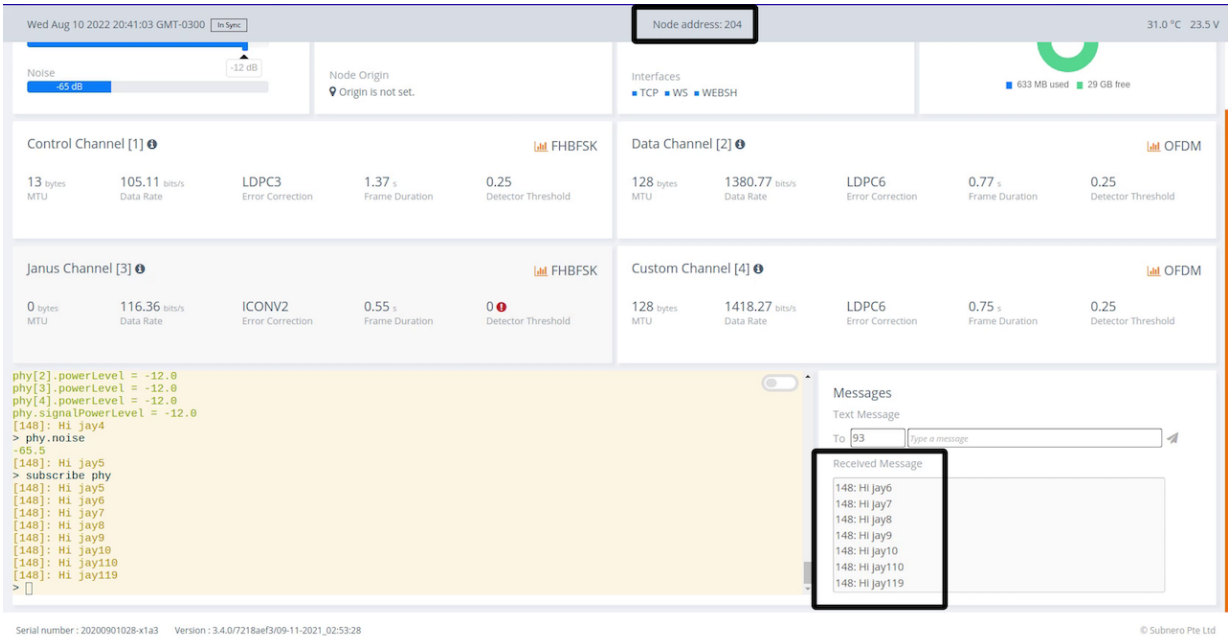

Figure 5.6: At the COVE (semi-controlled environment) with setup as in Figure4.16. A received broadcasted dataframe (Unetstack dashboard) at surface node 3 (address 204) from node 1 (address 148) broadcasted to all nodes. This reception achieved aSNRof -47, against a measured in-water noise of -72 dB and transmit power level of -119 dB. Notably, the reception was achieved a fair bit below the noise floor. This demonstrates the lowest transmission power possible on the Subnero-based network nodes.

In Figure5.9the hydrophone spectrogram showed the successful transmission of a dataframe from submerged node 2 and its reception at surface node 3. There are clearly Doppler effects (as highlighted). Nonetheless, the communication network correctly received and decoded the dataframe.

Figure5.10is a zoomed-in version of Figure5.9which highlights that the frame transmitted by surface node 2 (right) is comprised of a preamble (controlframe) concatenated to the dataframe. The originating node 2 requested an acknowledgement or receipt from surface node 3. The frame on the left is that acknowledgement as a transmission from submerged node 2 for surface node 3. The preamble was successfully decoded and thus Doppler effects were compensated. This verifies the preamble was correctly transmitted, decoded and applied towards compensation.

Figure5.11is an example of the Unetstack ranging agent in the modems which determines the distance between nodes using two-way-travel-time. This gives a fairly accurate range measure over long distances. Shown, are 2 rangings, The first ranges node 1 to node 3 and the second from node 2 to node 1. For the case of the second ranging, at $t = 24.2\ s$ submerged node 2 transmitted a Rangingframe to node 1. At $t = 25.0\ s$ the lighter blue line is the return from surface node 3. In second interval the pulse travelled at the speed-of-sound over double the range between the two nodes. Therefore, the range between nodes 2 and 1 was 190.8 m.

Figure5.12shows two broadcasts from node 1. The broadcast from node 1 (left) was performed with transmit power = -34 dB with the noise floor = -72 dB to yield an SNR of 38 dB (-34+72 = 38). Then, broadcast 2 was performed with a node 1 transmit power = -33 dB and the same noise floor = -72 dB to yield an SNR of 39. Both broadcasts went to nodes 2 and 3 however, they were only decoded at node 3 (relayed at node 2). The message was decoded correctly. This is not unexpected given an SNR of 38 dB. This case was the base line against further reductions in the node 1 transmit power. Table5.1shows the SNR with progressively lower node 1 transmit power.

Figure5.13similarly shows the case where the transmit power has dropped further to -80 and -90 dB resulting in SNRs of -8 and -18. This cases has clearly dropped below the noise floor and could be decoded correctly at the receiver at node 3.

In the semi-controlled environment of COVE (Figure4.16), an in-depth examination of the signal characteristics was conducted as shown in Figures5.7and5.8. The baseband PSDof control and data packets, transmitted from node 93 to node 204 with node 148 serving as an intermediate relay, was depicted in Figure5.7. These plots provided insights into the frequency distribution and power characteristics of the transmitted signals in the baseband range, emphasizing their spectral properties.

In these examinations, the baseband signal was identified as the unmodulated, original frequency spectrum of a signal. In thePSDplot, frequencies were found centered around 0, representing the DC component. The presence of negative frequencies signified the complex nature of the signal, encompassing both real and imaginary components.

Conversely, the passband signal, evident in Figure5.8, emerged from modulating the baseband signal onto a carrier frequency. ThePSDplot of this signal showcased a shift in frequency content to a higher range, revealing only positive frequencies. The frequencies displayed were determined by both the carrier frequency and the signal's bandwidth.

Figure5.8further depicted the baseband and passbandPSDof the successfully decoded received signal upon the reception of control and data packets on submerged node 1 (address 148) for relaying. Figure5.8afocuses on the control packet, while Figure5.8b shows the data packet, both intended for submerged surface node 3 (address 204).

Despite underwater challenges in a noisy and variable channel quality for a near-harbour environment like the COVE, the communication system was quite resilient and successfully decoded every sample it received. There were no corrupted received samples.

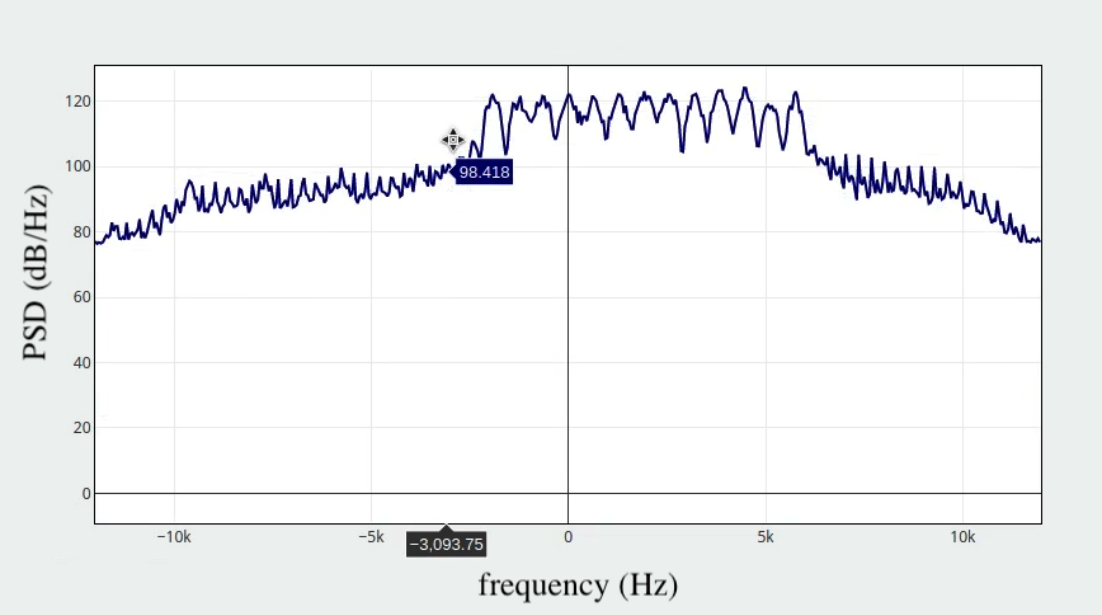

(a)

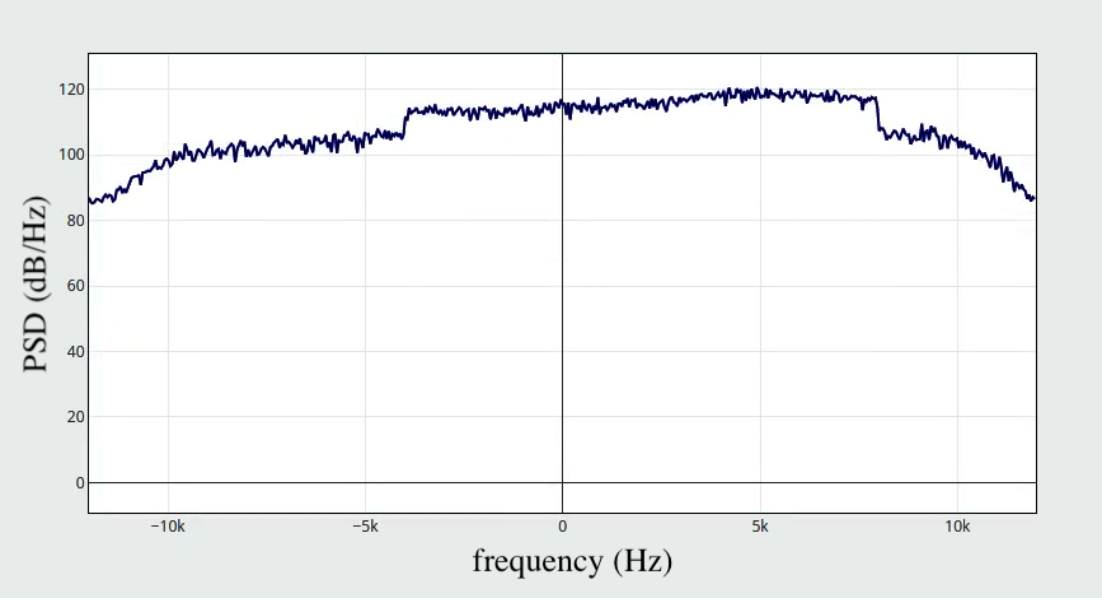

(b)

Figure 5.7: At the COVE (semi-controlled environment) with setup as in Figure4.16. BasebandPSDof the control packet transmitted from node 93 (jetty 2) to node 204 (jetty 3) via node 148 (jetty 1). Shown are the signals received at node 148 (data between -3 kHz to +8 kHz) using the custom dashboard for: (a) the preamble as apparent in the multiple peaks, contains a small amount of data and (b) the data which span 12 kHz arriving shortly after the preamble. The near-full available bandwidth is used by the system. This is a larger bandwidth than other systems.

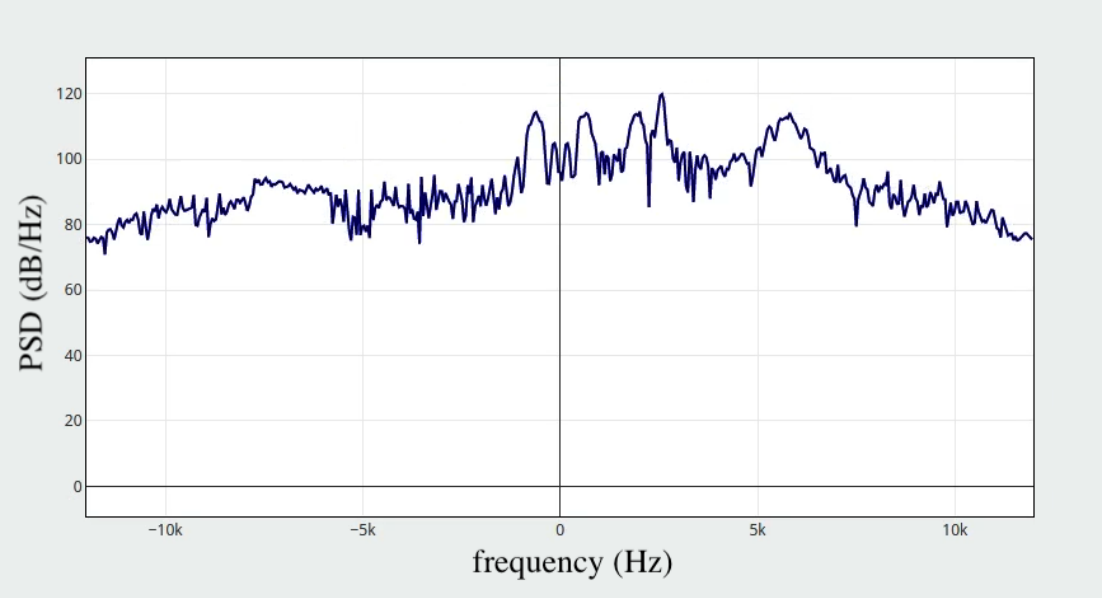

(a)

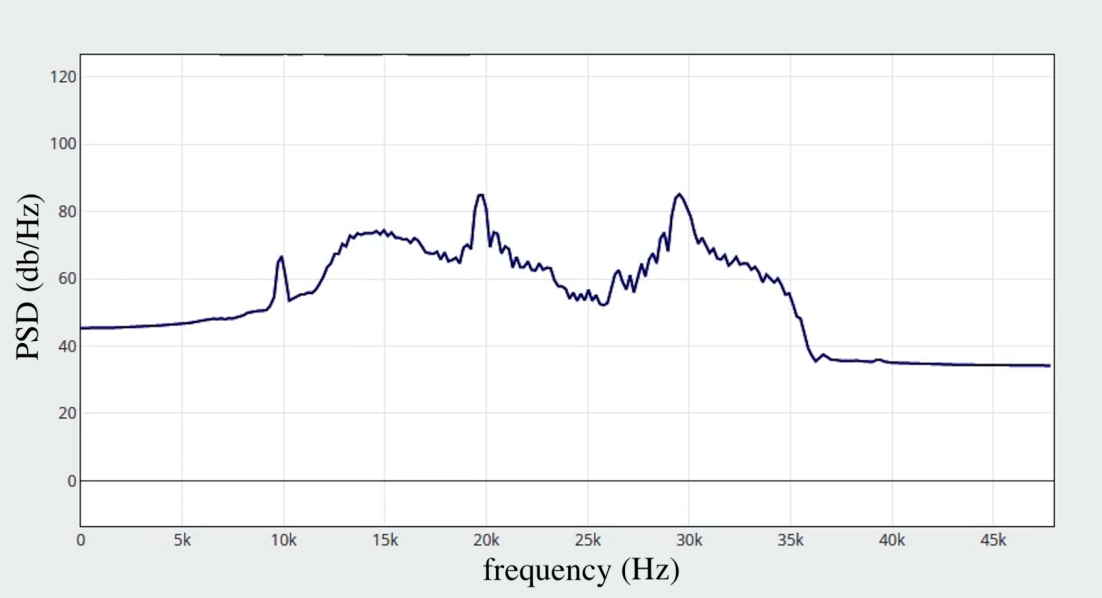

(b)

Figure 5.8: At the COVE (semi-controlled environment) with setup as in Figure4.16. Power spectral densities calculated with the custom dashboard for control packets received at node 148 (jetty 1) for control packets transmitted from node 93 (jetty 2) to node 204 (jetty 3) via node 148. Shown are the control packet: (a) baseband successfully decoded and (b) passband successfully decoded. As both baseband and passband were proven successfully decoded at the relay node, the correct messages were relayed to node 204. This is a consequence of node 148 also having the key to decode a message it did not need to decode.

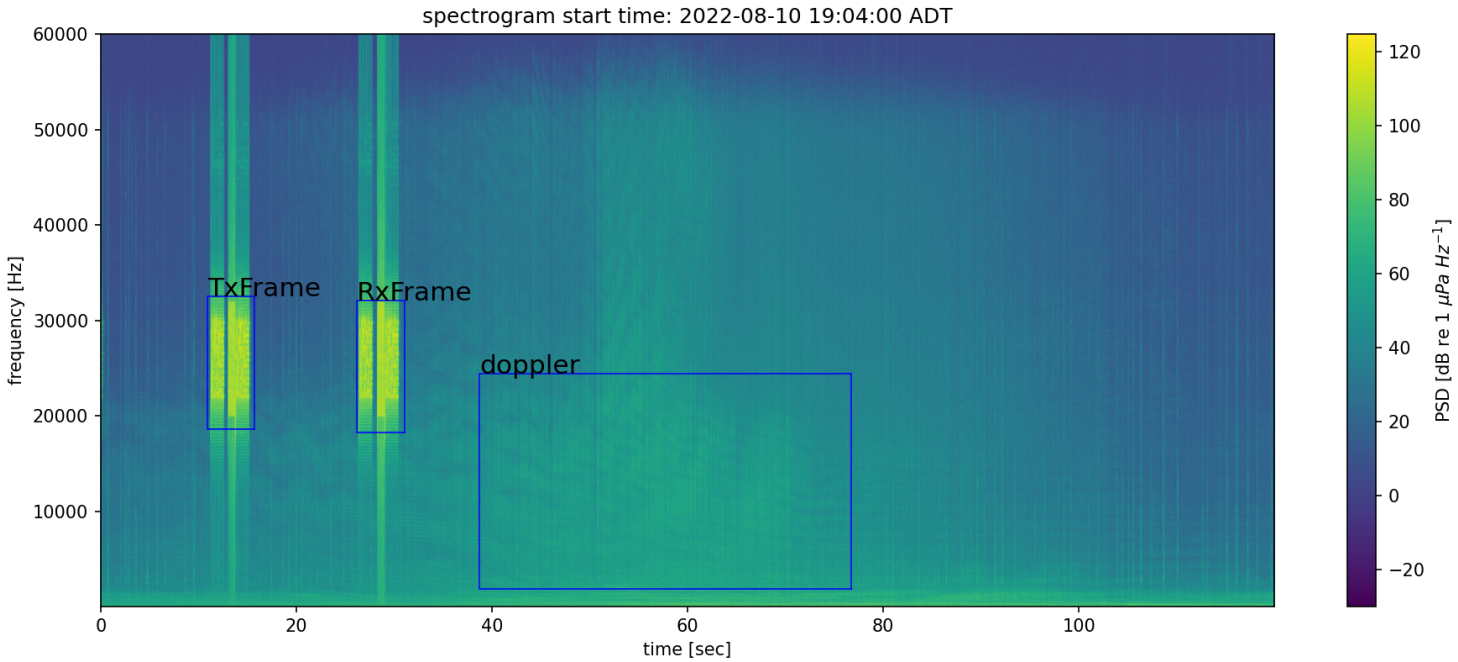

Figure 5.9: At the COVE (semi-controlled environment) with setup as in Figure4.16. Hydrophone recording at jetty 1 of dataframe transmission from submerged node 2 (93) to surface node 3 (204) via submerged node 1 (148). Note the presence of Doppler effects due to relative motion between transmitter, relay and receiver nodes. In the presence of Doppler, the communication system correctly received and decoded the dataframe at the receiver (not shown).

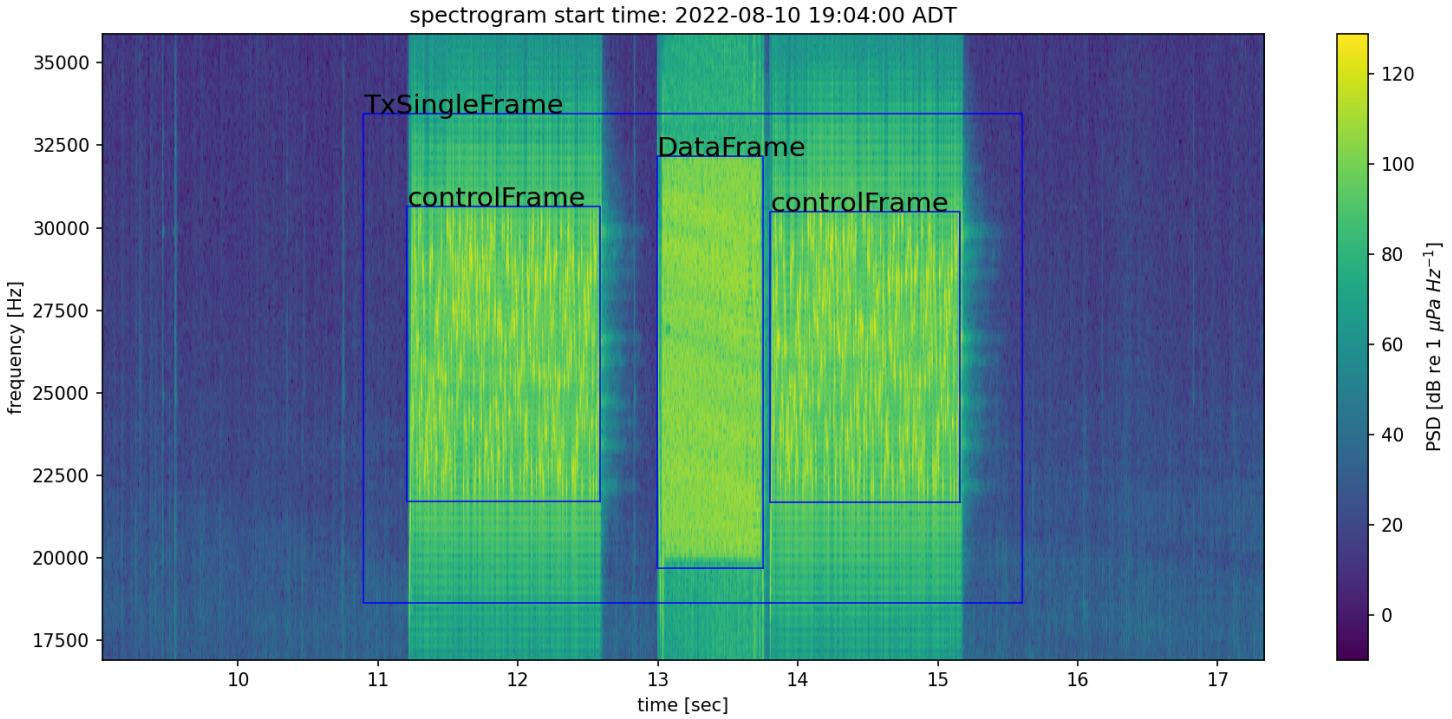

Figure 5.10: At the COVE (semi-controlled environment) with setup as in Figure4.16. Hydrophone recording at jetty 1 of dataframe transmission from submerged node 2 (93) to surface surface node 3 (204) via submerged node 1 (148). This is a zoomed in version of Figure5.9to highlight that at submerged node 2, a single frame was transmitted (left) comprised of a dataframe concatenated to a controlframe. The second control frame (right) was transmitted by surface node 3 to submerged node 2 as the ack bit was enabled on node 2 to verify the frame reception at surface node 3. This confirms that surface node 3 received the frame. The original transmitted frame from node 2 is not shown in this zoomed in version to show detail in the transmitted dataframe from submerged node 2.

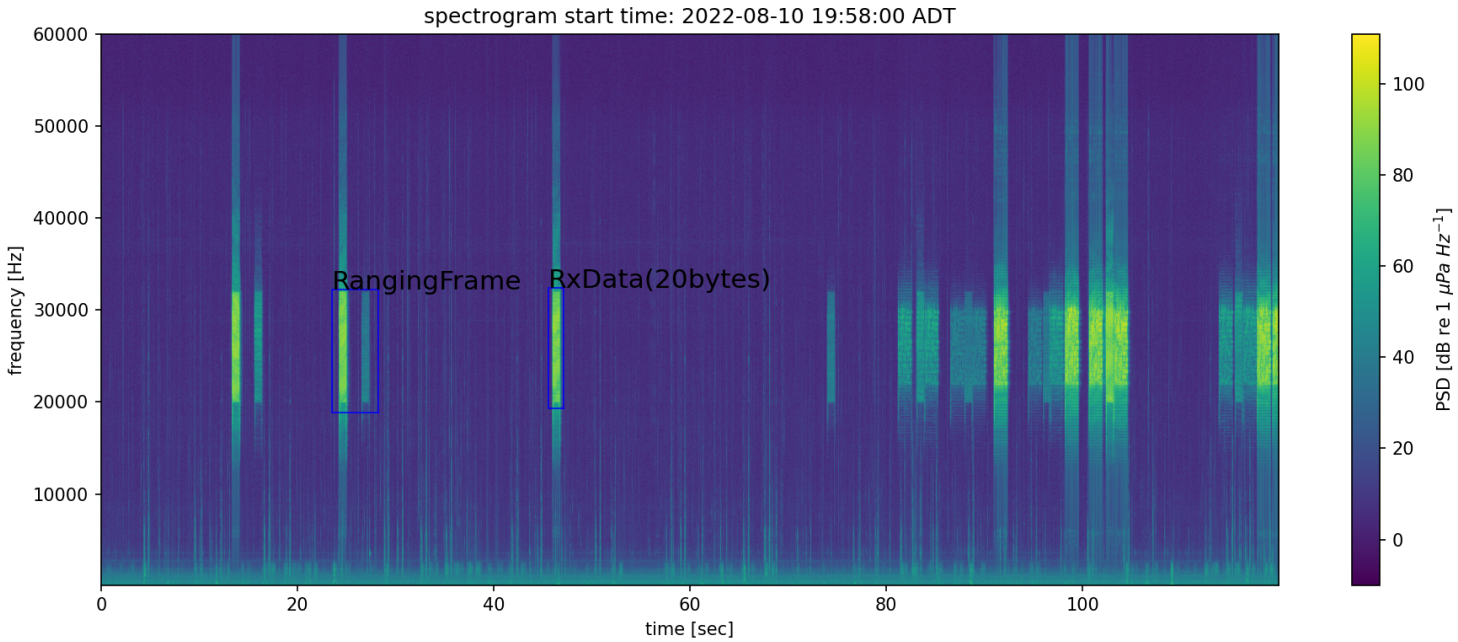

Figure 5.11: At the COVE (semi-controlled environment) with setup as in Figure4.16. Hydrophone recording at jetty 1 of Rangingframe transmission from submerged node 2 (93) to surface surface node 3 (204) via submerged node 1 (148). This transmission serves to determine the range or distance between submerged node 2 and surface node 3.

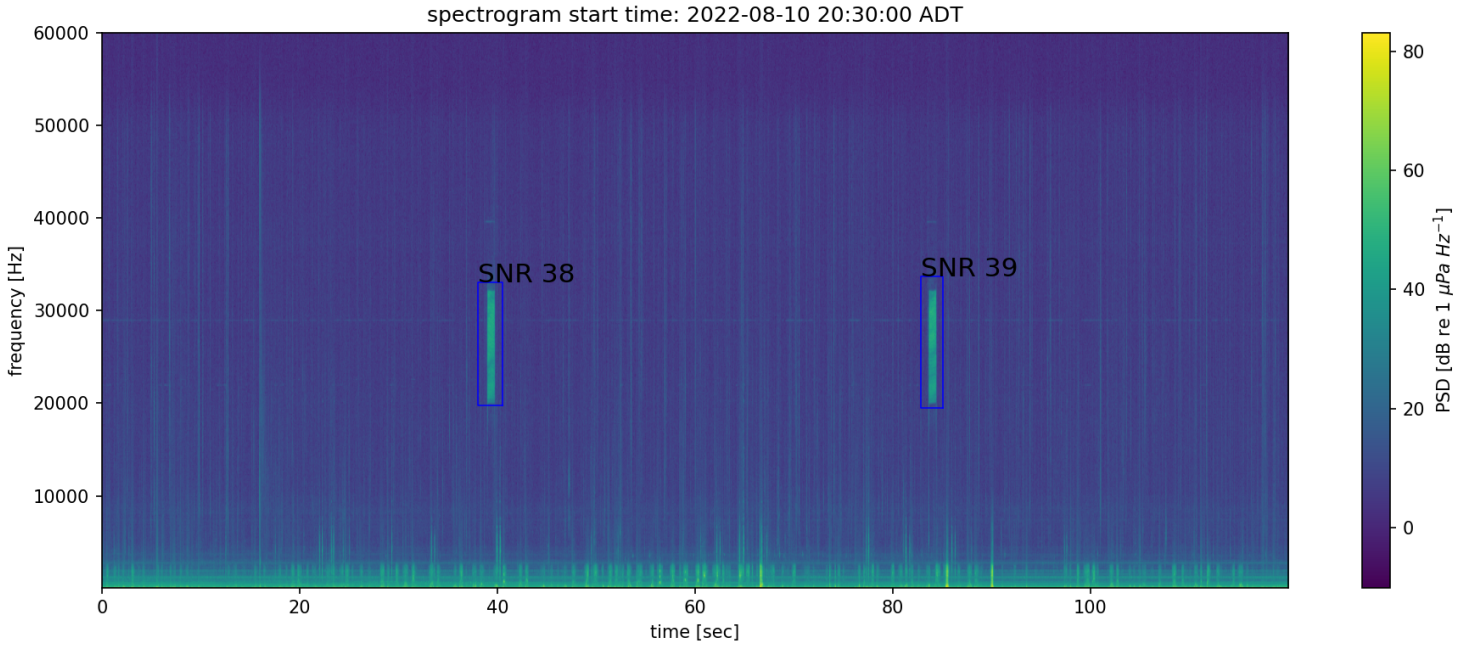

Figure 5.12: At the COVE (semi-controlled environment) with setup as in Figure4.16. Hydrophone recording at jetty 1 of a dataframe broadcasted twice to all nodes in the communication network. The noise floor is at -72 dB. The transmitted power for the broadcasts were -34 dB and -33 dB, respectively from left to right. Given this, the broadcast SNRs are 38 and 39. Two instances of a receive broadcasted dataframes in the network transmitted by the underwater node 1 (148) to surface node 3 (204) with in-water noise measured at -72 dB and theSNRs measured at 38 dB and 39 dB, respectively.

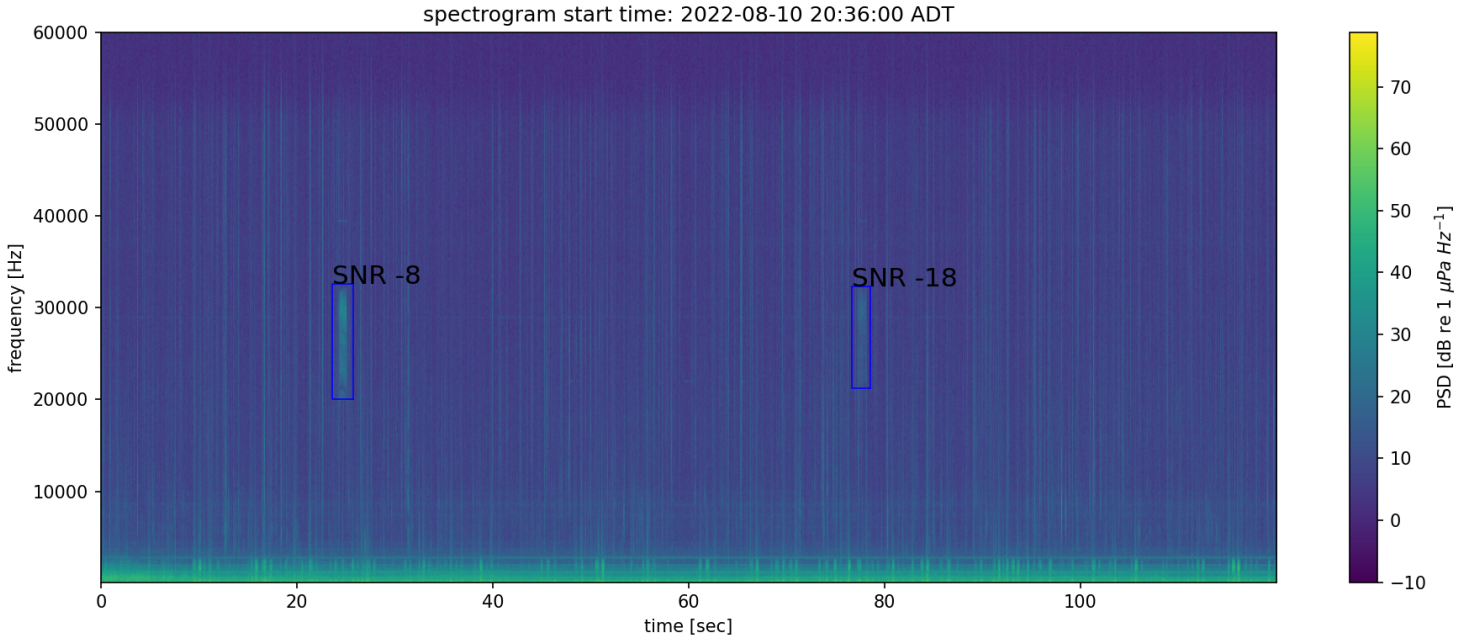

Figure 5.13: At the COVE (semi-controlled environment) with setup as in Figure4.16. Two instances of receive broadcasted dataframes in the network transmitted by the underwater modem node (148) to the surface node (204) where in-water noise was measured at -72 dB andSNRs were measured -8 dB and -18 dB, respectively. Notably, successful reception was achieved below the noise level.

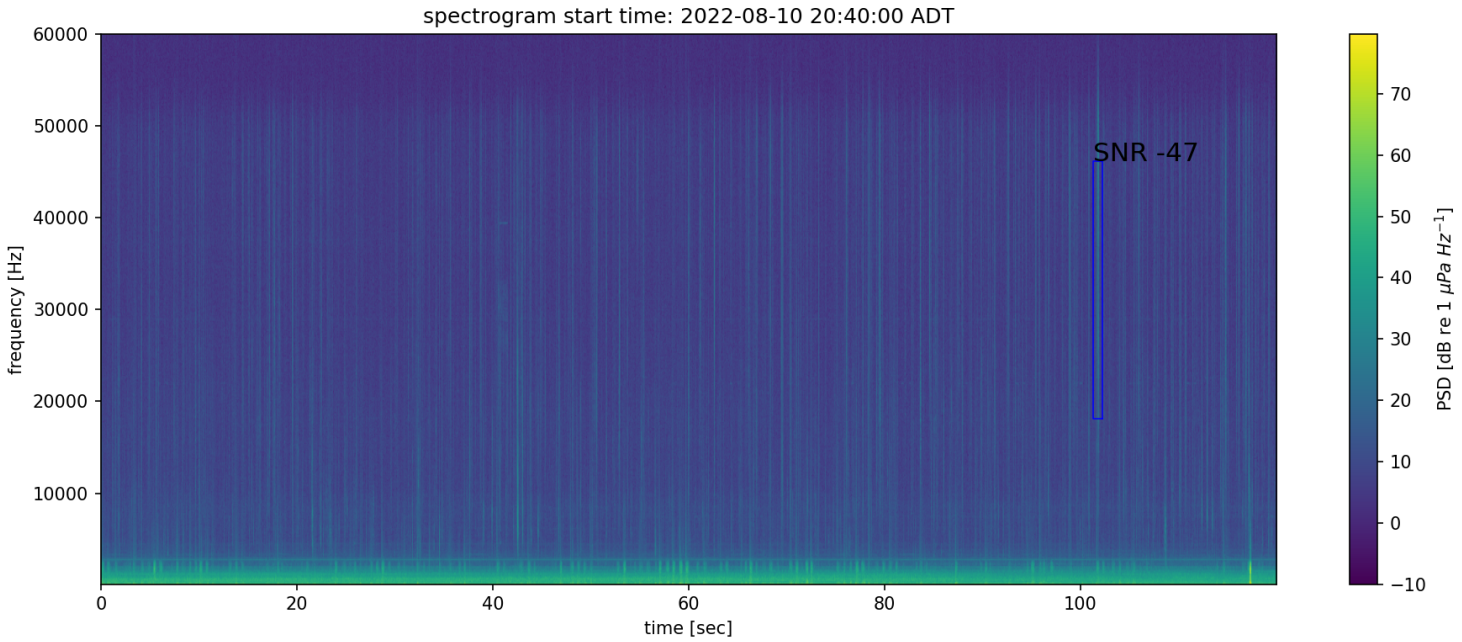

Figure 5.14: At the COVE (semi-controlled environment) with setup as in Figure4.16. A dataframe received in the network, transmitted from the underwater modem node (148) to the surface node (204). This transmission occurred atSNRof -47 dB, against a measured in-water noise of -72 dB. Notably, successful reception was achieved below the noise level, demonstrating the maximum low limit of transmission power that can be configured on any Subnero-based node.

5.2 St. Margaret's Bay (uncontrolled environment)

To overcome heavy underwater acoustic traffic challenges in the Halifax Harbour approaches and the transitional fall weather conditions towards characterizing the communication system, tests were also conducted at St. Margaret's Bay on October 12, 2022. Due to limited resources, only two nodes (modems) were deployed to evaluate the the communication system performance in an acoustically quieter environment. The surface node was deployed from the jetty to 2.5 metres depth. The submerged underwater node 1 was towed behind a boat to three different locations labeled 1, 2, and 3 as shown in Figure4.24. These locations were 55 m, 359 m, and 100 m from the surface node, respectively.

Figure5.15shows the channel conditions at St. Margaret's Bay as measured by a deployed sound velocity profiler from the surface to 3 m depth. The weather on the test day included sunny conditions with low to medium ambient noise, and little to no surface waves.

5.2.1 Communication Systems Performance

As it was at theCOVE, the communication system was characterized through the bit error rate and channel link quality in St. Margaret's Bay.

Bit Error Rate

The BER as a function of SNR was determined in simulations by averaging multiple runs for different SNR values until the threshold BER of 10^{-3} was achieved.

To evaluate the communication system performance, the theoreticalBERfor 3 nodes with spreading factors k = 8, 32, 64, 128 and 256 for both Walsh and M-sequence type encoding were simulated. The average of the simulation results is depicted in Figure5.16a. These results correctly show thatBERdecreases with increase spreading factor (k). This is because a higher spreading factor results in a wider spread spectrum, which provides increased resistance to interference and noise. Consequently, the system achieves better performance in terms ofBER, as the spreading factor increases. However, as the spreading factor increases, the system's throughput may decrease. This is because a higher spreading

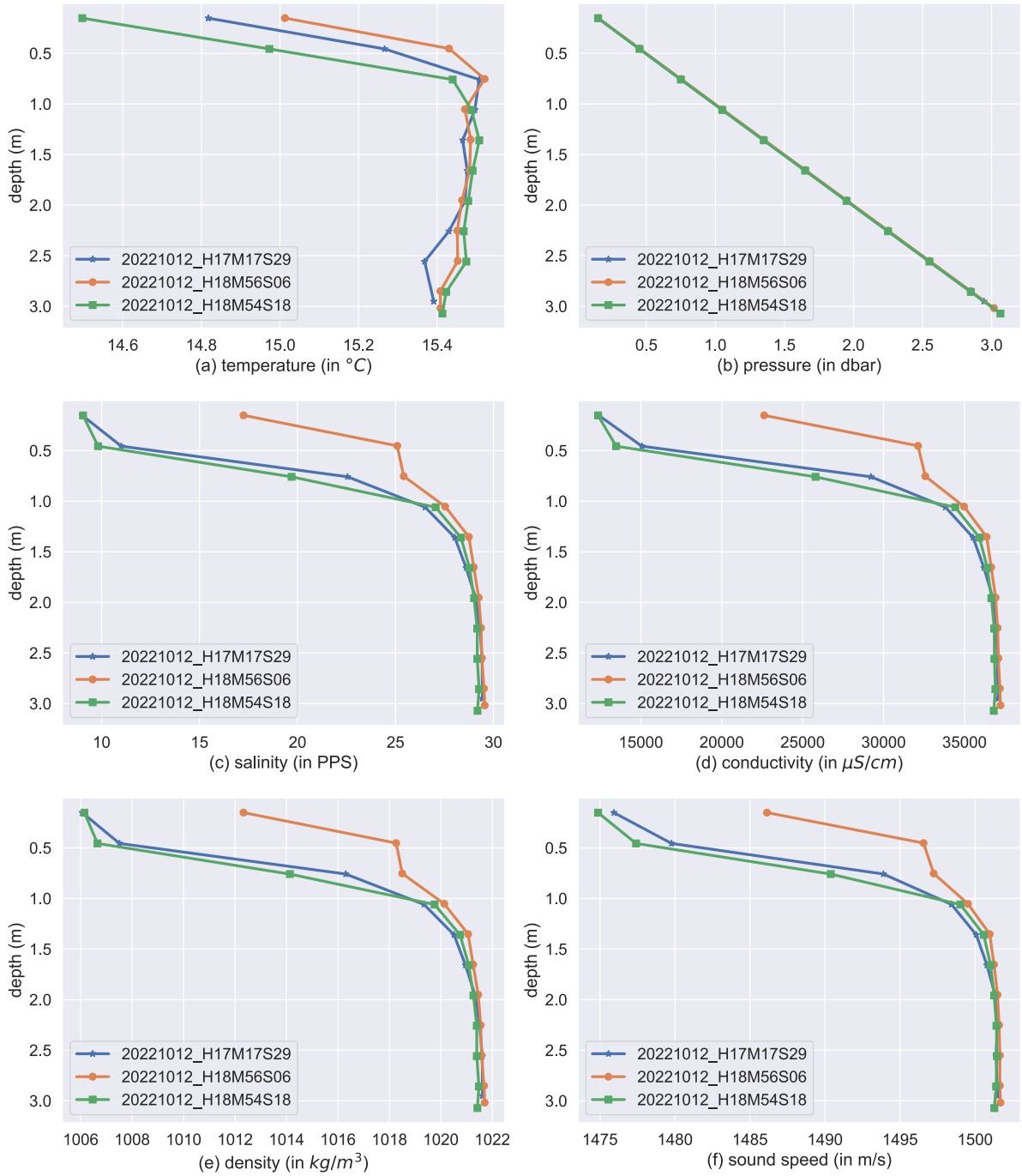

Figure 5.15: St. Margaret's Bay (uncontrolled environment, 44.6802104 N, 63.916349 W) underwater channel characteristics on the October 12, 2022 test day, over 3 AST times, with depth as a function of: (a) temperature; (b) pressure; (c) salinity; (d) conductivity, and (e) density. These all contribute to the depth variation with (f) sound speed. The later time (orange) at 18:56:06 shows departures from the earlier 17:17:29 (blue) and 18:54:18 (green). This discrepancy could be attributed to temporal shifts in the bay's thermocline or halocline, external noise sources, or transient meteorological conditions influencing the water column.

factor requires more bandwidth to transmit the same amount of information, resulting in a reduced overall throughput. This is the "near-far" effect, where nodes with stronger signals (near nodes) can interfere with nodes that have weaker signals (far nodes) when the spreading factor is increased. As a result, the system may experience a decrease in throughput as the spreading factor increases. Therefore, there is a trade-off between BER and throughput in CDMA systems, and the choice of spreading factor needs to be carefully considered based on the communication system requirements and constraints. Figure5.16b shows the experimentally derived BER curves.

$\frac{E_b}{No}$ is the ratio of energy per bit (E_b) to the spectral noise (No). $\frac{E_b}{No}$ is thus a measure of the SNR for a digital communication system measured at the receiver input. $\frac{E_b}{No}$ is a measure of the SNR here.

On the other hand, the experimental BER was determined by comparing the transmitted and received bits (Eq.5.3). Each deployed node was assigned a unique PN code which was known to all the network nodes. The agent on the Subnero modem firmware was taken as reference and developed an agent [17], was being used to compensate Doppler shifts up to a certain extent. The results of the experiments show the agent effectively resolved carrier frequency offsets in the range from 10^{-5} to 10^{-3}. The highest frequency offset that the agent resolved during the experiment was 1.7×10^{-4}.

The tests were unexpectedly impacted by noise from lawnmowers from the other side of the bay. This created outliers in the BER vs SNR in Figure5.16b.

Channel Quality

The motivation for progressing from theCOVEto St. Margaret's Bay was to have better channel quality with which to evaluate the communication system.

As shown in Figure5.17a,BERshows a near-constant trend asSNRincreases. This is unexpected behavior. TheBERfluctuates within a range, especially at higherSNR values, suggesting additional factors interfering with the characterization. This is due to known environmental factors such as lawnmowers operating on the other side of the bay; Figure5.17b,RSSIgenerally increases with increaseSNR. This is expected as better signal strength is associated with higherSNRs. Figure5.17c,CFOremains relatively constant across the range ofSNRvalues. This suggests that the system is quite robust against Doppler effects, as theCFOdoes not show significant variations.

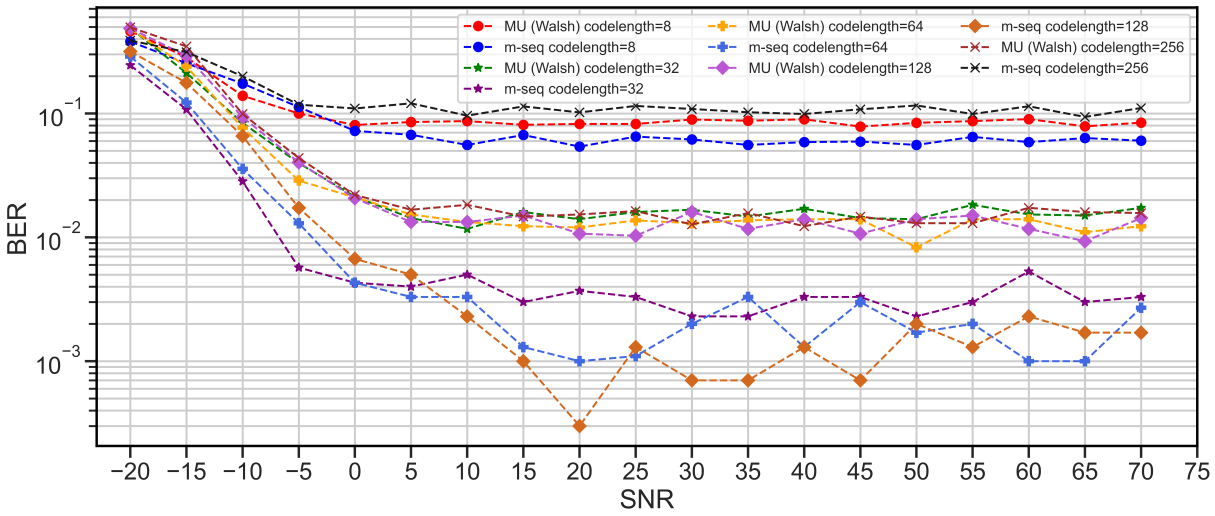

(a)

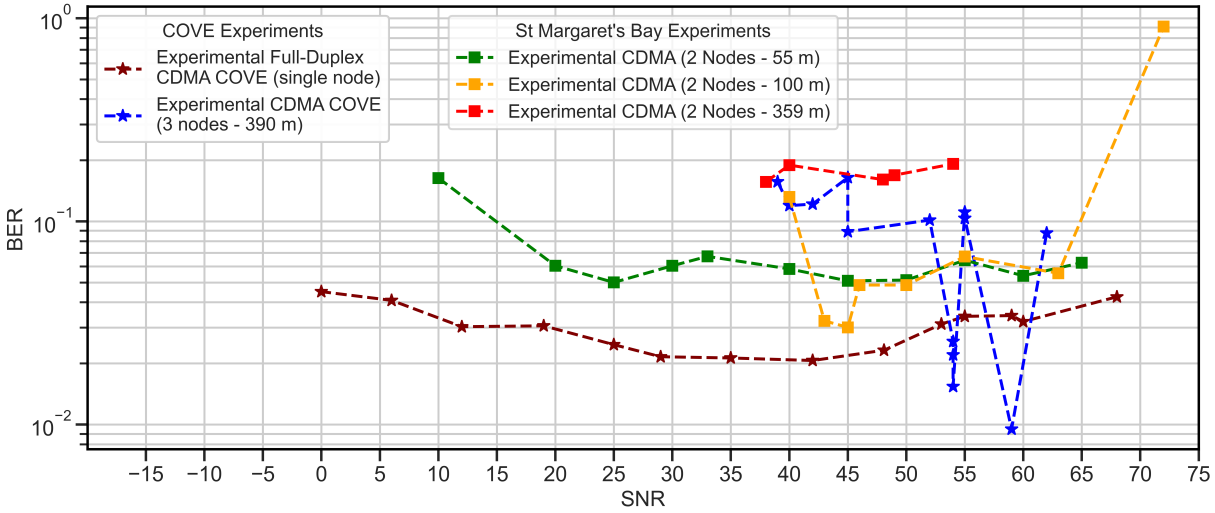

(b)

Figure 5.16: St. Margaret's Bay (uncontrolled environment)BERcomparison for different node configurations; (a) **theoretical** BER curves for spreading factors of $k = 8$, 32, 64, 128 and 256 with three nodes – $k = 8$ shows the most favorableBER; (b) **experimentally** derivedBERcurves for spreading factor 8 from in-water measurements. Observed outliers when the nodes are separated by 100 m likely due to lawnmowers from the other side of the bay.

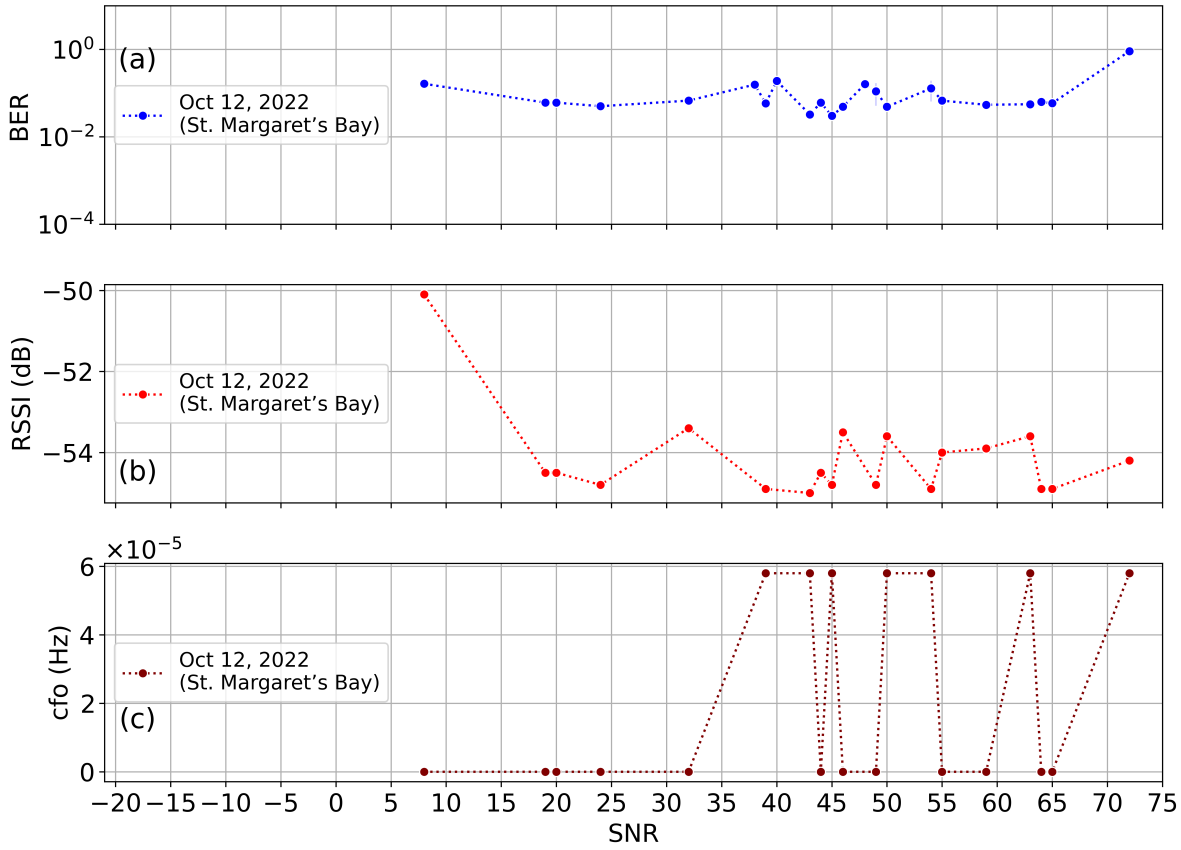

Figure 5.17: Proposed communication system performance for in-water trials (St. Margaret's Bay, uncontrolled environment, Figure4.24, Oct 12, 2022). Each sample represents a successfully received and decoded broadcasted message: (a) unexpectedly more-or-less constantBERtrend with increaseSNRdue to environment factors; (b) The positive correlation betweenRSSIandSNR, emphasizing the importance of signal strength for reliable data transmission; and (c) The relatively constantCFOacross differentSNRvalues, highlighting the system's robustness against frequency deviations.

post-processing

For this thesis, the Python packagepython audio spectrogram explorer (PASE)[62] was utilized extensively, but it was necessary to adapt it to the project requirements. With the adaptedPASEtools, underwater audio files recorded with the OceanSonics icListen HF Hydrophones (model 6089 and 6042) deployed at theCOVE(44.660762 ° N, 63.558304° W)

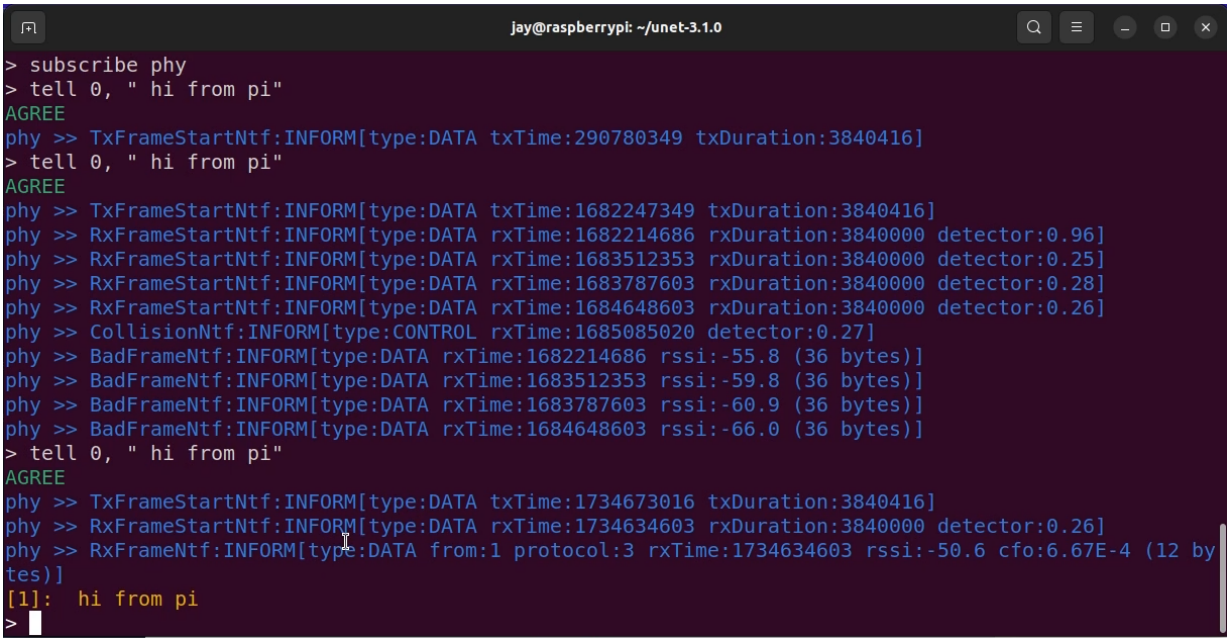

Figure 5.18: At St. Margaret's Bay (uncontrolled environment) with setup detailed in Figure4.24. The custom RPi node was strategically deployed (transmitter at 3m and receiver at 1 m depths) to where a message would be received and subsequently decoded in full-duplex mode. Hydrophone recordings at the St. Margaret's Bay jetty showed multiple (4) receptions of a transmitted message (*hi from pi*) from the RPi node. Notice, the initial transmissions faced decoding challenges (*CollisionNtf*), likely attributed to multipath. Contrary to this, the next transmission (*TxFrameStartNtf*) was received and correctly decoded. Notably, the custom RPi node was able to correctly decode subsequent messages in the presence of multipath.

and St. Margaret's Bay (44.679745° N, 63.916418° W), to 1.8 m depth, were plotted.

The data diversion mode was set to original data to ensure integrity of the logged acoustic signals were maintained. Spectrograms of logged acoustic signals (as *.wav* files) were generated with the modifiedPASEpackage to analyze the signal spectral content as a function of time.

Figures5.19to5.21displays the spectrograms of various transmission examples and received frames. They depict the signal spectral content over time and thus enables the identification and analysis of transmissions and receptions in the underwater acoustic network.

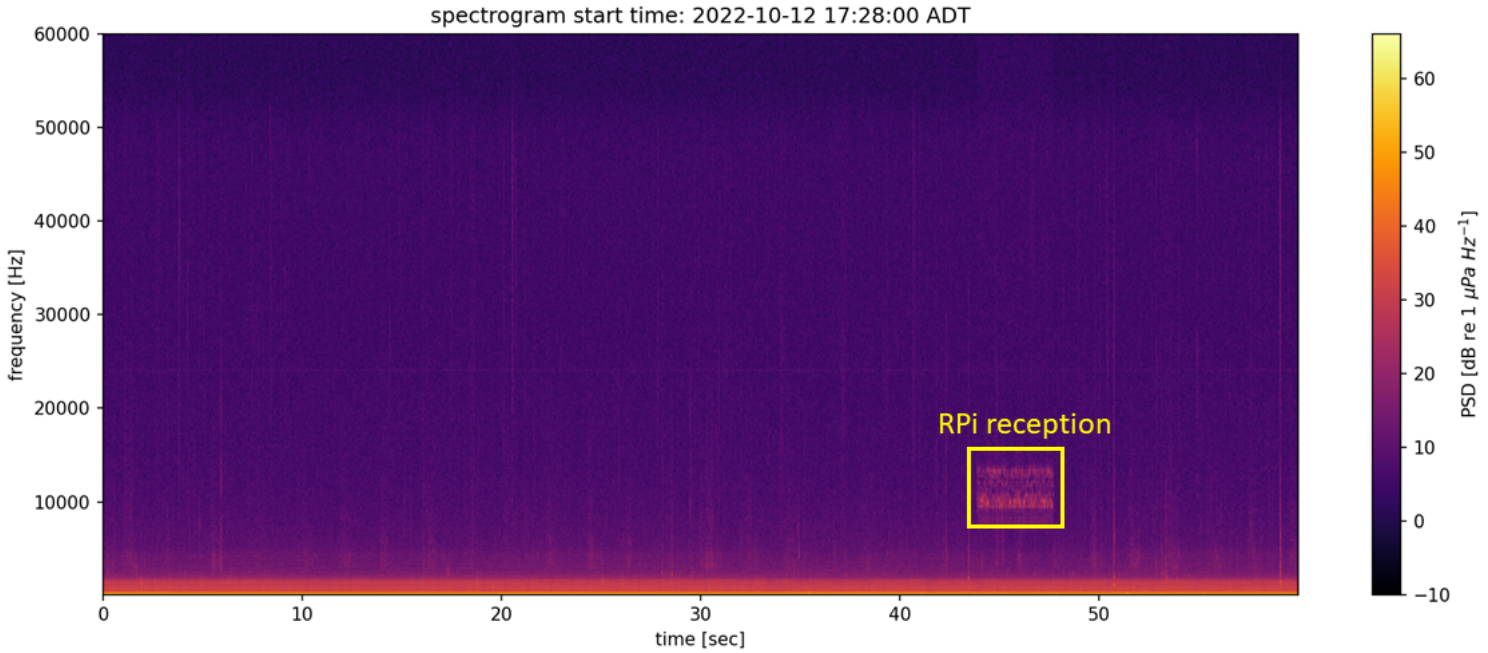

Figure 5.19: At St. Margaret's Bay (uncontrolled environment) with setup as in Figure4.24. Analysis from a hydrophone deployed near the jetty, captured the successful transmission (broadcasts) from the custom RPi modem in full-duplex mode. This received reference transmission is the foundation to compare successful detections against using correlations in time as it just exceeds the 0.25 threshold at 0.26.

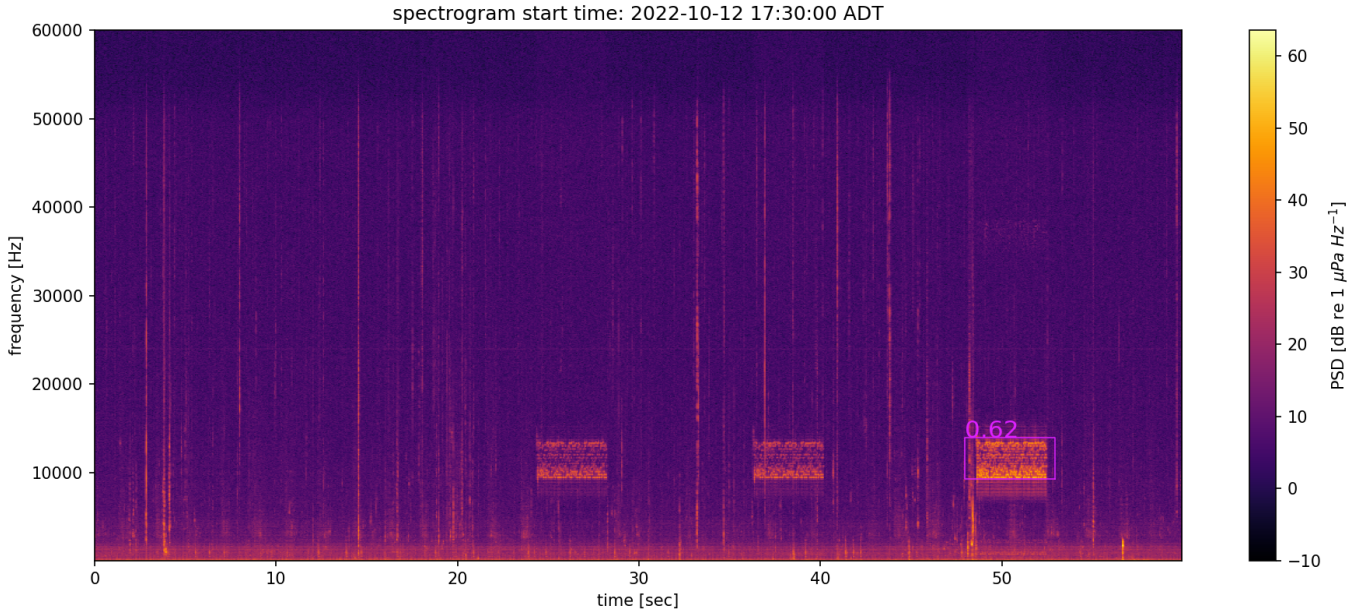

Figure 5.20: At St. Margaret's Bay (uncontrolled environment) with setup as in Figure4.24. Analysis from a hydrophone deployed near the jetty, captured the successful transmission from the custom RPi modem in full-duplex mode (Figure5.18). Each correlated reception is highlighted by a bounding box and bears its detection score above it (e.g. 0.62). The other 2 receptions did not achieve a high enough correlation score (0.25). This highlight's the RPi modem's ability to adapt to the Bay's ambient milieu.

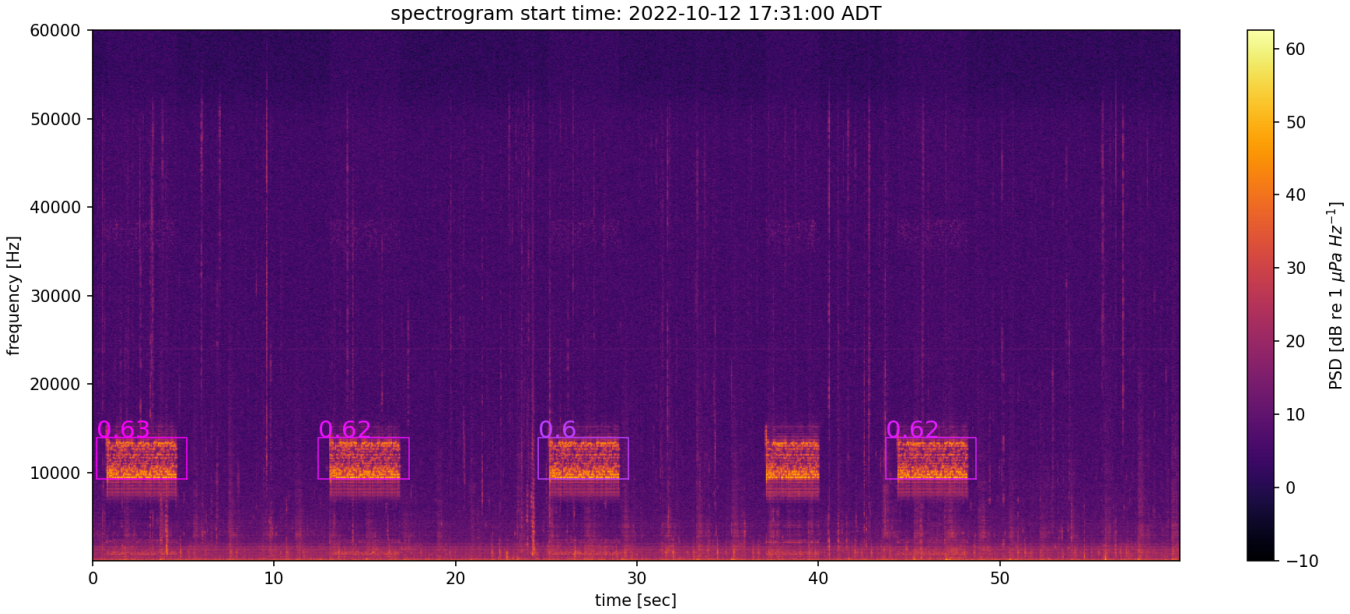

Figure 5.21: At St. Margaret's Bay (uncontrolled environment) with setup as in Figure4.24. Analysis from a hydrophone deployed near the jetty, captured multiple successful receptions from multiple transmissions (for which Figure5.18shows only 2 transmissions) using the custom RPi modem in full-duplex mode. The spectrogram shows the custom RPi modem's distinct receptions. Each signal, bounded by a box and annotated with its correlation score achieved a score that is $\geq$ the reference in Figure5.19.

Figures5.7ato5.7bshow the basebandPSDof messages transmitted from node 93 (jetty 2) and received at the intermediate relay node 148 (jetty 1). Note the data bandwidth of this communication system is nearly 12 kHz which is notably larger thanTDMA-based systems with the same carrier frequency by a factor of 2.

5.3 Experimental and Simulation Findings Analyzed as a Whole

In this section, the in-water measurements obtained from theCOVEand St. Margaret's Bay experiments was explored and analyzed as a whole. The data undergoes a series of analyses: correlation; regression; data filtering; descriptive statistics, and visualizations to extract insights from the communication system evaluation.

5.3.1 Data Overview

The in-water data was from measurements during underwater communication experiments and from data generated using aCDMAcommunication simulation model. Analyses on the datasets were applied to determine signalSNR,BER, and transmitted power. A dataset consisted of several panda dataframes [79] each representing communications performance metrics (e.g.,SNR,BER, throughput, channel quality, etc.) (AppendixD).

5.3.2 Data Statistical Analysis

The description statistics or statistical analysis for each dataframe calculates the mean, standard deviation, minimum, maximum, and quartiles forSNR,BER, throughput, channel quality andRSSItowards insights into their central tendencies and data spread. These descriptive statistics help characterize the data and provide a quantitative summary of the CDMAunderwater communication system's variables and measurements.

The key findings from the descriptive statistics include:

1. In the experimental dataframes, the meanSNRwas approximately 39.1 dB, with a standard deviation of 22 dB over a dynamic range of 95 dB. This is marginally acceptable. The meanBERwas around 0.0743, indicating a relatively low error rate which is more than acceptable.

2. The simulation dataframes exhibited similar statistics to the experimental ones, indicating that the simulation model captures the experimental measurements adequately

for the developed underwater communication system.

3. The datasets showed diverse trends between SNR and throughput, as well as SNR and channel quality. For the August data, there is a positive correlation between SNR and throughput, and a negative correlation between SNR and channel quality.

4. The dataframes of all in-water measurements from August 2022 (COVE) provided a broader overview. From this, the mean SNR was 42.0 dB, with a mean BER of 0.078. These results are quite good given a harbour environment.

5.3.3 Correlation Analysis

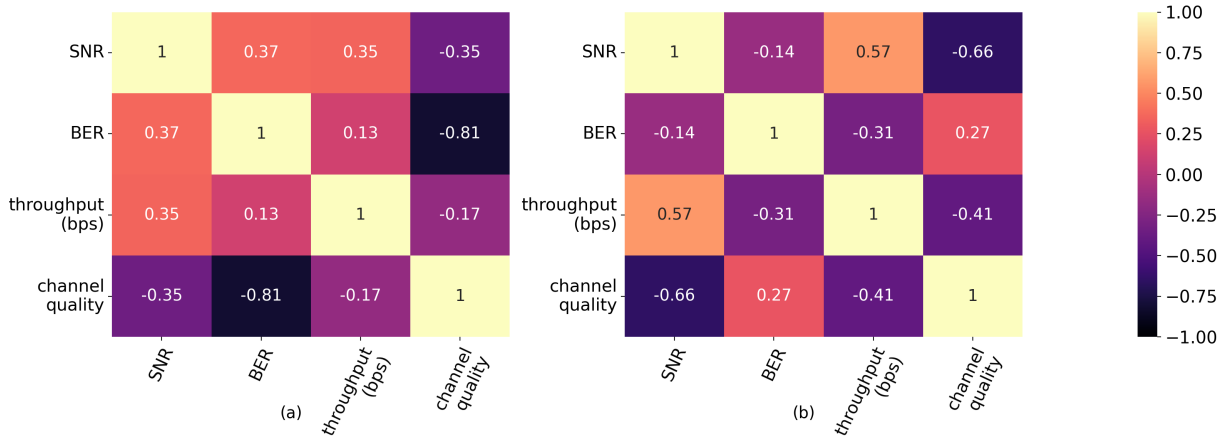

Figure 5.22: Heatmaps display the correlations among key performance metrics from the COVE and St. Margaret's Bay experimental datasets for the months of August and October, 2022. For the August dataset, there's a positive correlation between SNR and throughput, and a contrasting negative correlation between SNR and channel quality. In contrast, the October dataset reveals a stronger positive relationship between SNR and throughput, and an even more pronounced negative relationship between SNR and channel quality. This variation between the two months underscores the dynamic nature of underwater communication systems and the importance of consistent monitoring.

A correlation matrix was constructed to reveal the relationships across variables within dataframes in a dataset. The correlation matrix measures the strength and proportionality relationships between pairs of variables. Positive correlations indicate variables that tend to increase or decrease together, while negative correlations suggest an inverse relationship.

The correlation analysis, shown in the Figure5.22, revealed a moderate positive correlation betweenSNRandBER, which was counter-intuitive to the initial expectation of an inverse relationship. This suggested the possibility of a non-linear relationship between these two variables or the influence of other factors onBERthat are not captured bySNR alone.

The correlation analysis, shown in the Figure5.22, revealed several interesting findings:

1. For the August dataset, there was a positive correlation of approximately 0.37 betweenSNRandBER. There was also a positive correlation of approximately 0.35 betweenSNRand throughput, and a negative correlation of approximately -0.35 betweenSNRand channel quality.

2. For the October dataset, there was a negative correlation of approximately -0.14 betweenSNRandBER. The correlation betweenSNRand throughput was approximately 0.57, indicating a stronger positive relationship than in the August dataset. A strong negative correlation of approximately -0.66 was observed betweenSNRand channel quality.

This suggests factors other than theSNRimpact theBERlike channel quality. Channel quality can vary greatly due to environmental factors that cannot be controlled. To determine the non-linear relationships amongst these performance metrics, a regression analysis was performed to get a quantitative measure of the strength of the relationships.

5.3.4 Regression Analysis

The regression analysis usingordinary least squares (OLS)(Figure5.23), further confirmed the observations of Figure5.22. There exists a positive correlation betweenSNR andBER, as indicated by the positive slope. While the slope is numerically small (approximately 0.00085),SNRdoes have an influence onBER. The plot shows the actual BERvalues (in blue) and the predictedBERvalues (in red) based on theOLSregression. The intercept of the regression line is approximately 0.0391, which is the predictedBER whenSNRis zero. The model does not fit the measurements perfectly indicating there are factors other thanBERwhich have impact but are not captured bySNRalone. Other factors such as signal distortion, interference, or noise characteristics, may also need to be considered. These were not directly measured.

However, the discrepancies between the actual measurement points and theOLSregression lines suggest that the model may not capture all the intricacies of the data, pointing

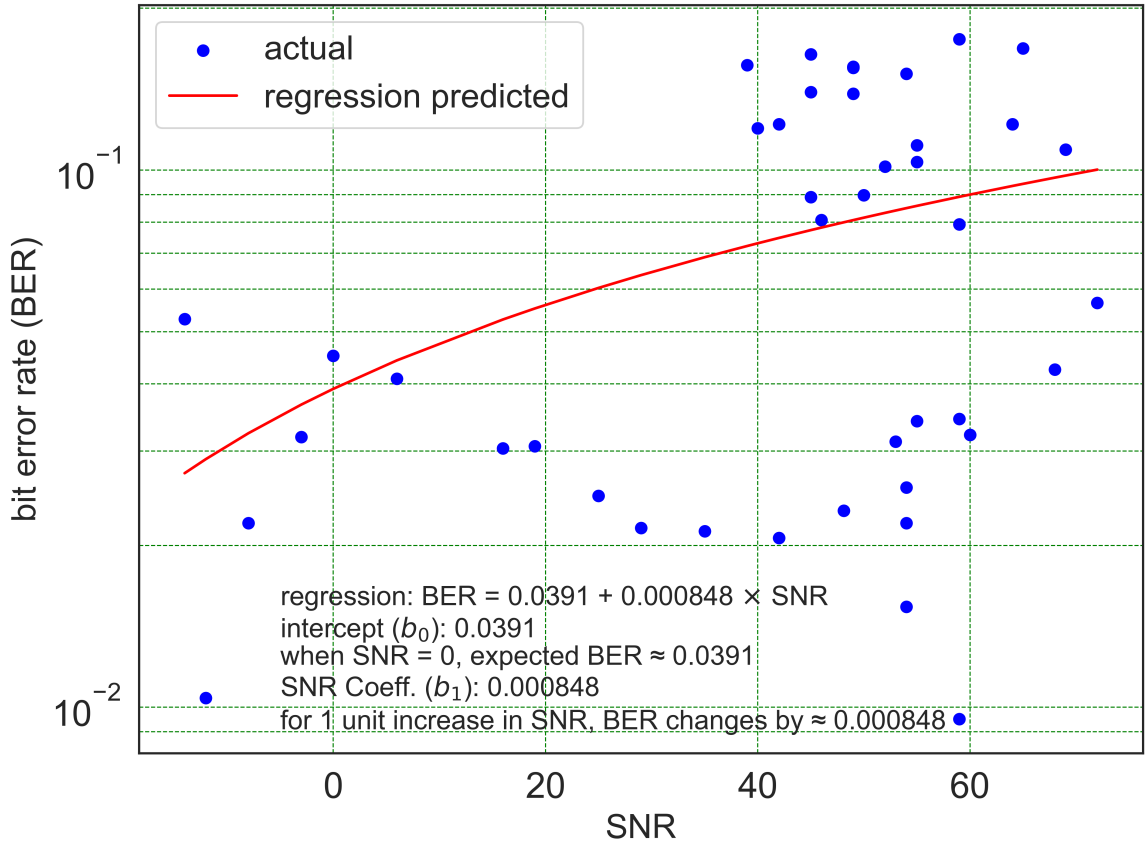

Figure 5.23: a regression analysis shows that there is a positive relationship betweenSNR andBER, as indicated by the positive coefficient ofSNR. However, the coefficient is very small (approximately 0.00085), suggesting that whileSNRdoes have an influence onBER, its impact is not profoundly strong. The plot shows the actualBERvalues (in blue) and the predictedBERvalues (in red line) based on the regression model.

to the possibility of other factors influencingBERbeyondSNR. On the other hand, the exponential regression fitting curves shown in Figure5.24, represented by the dashed lines, show a different trend and seem to fit the data more closely, especially for lower values of SNR. This impliesSNRis inversely proportional toBER, which is typical in communication systems. Both the August and October 2022 datasets follow similar trends, indicating that the underlying communication system behaviour is consistent across these months.

In the subsequent evaluation, as presented in Figure5.25, the performance of the proposed

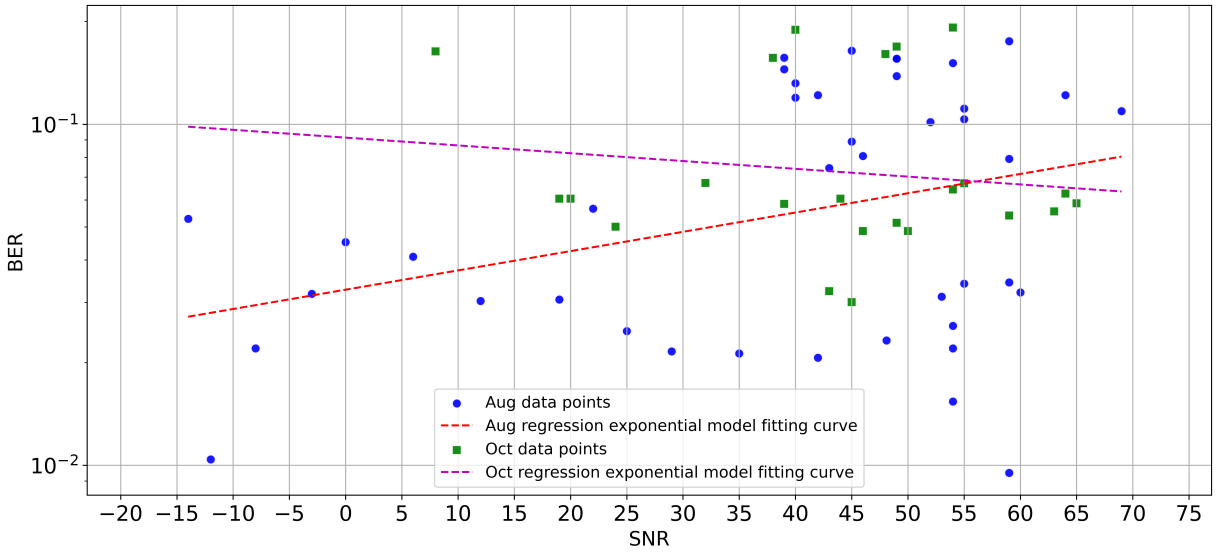

Figure 5.24: A comparison of exponential regression analyses for the August and October 2022 measurement highlights the negative relationship betweenSNRandBER. The August measurement points (in blue circles) and its exponential regression fitting curve (red dashed line) demonstrate a declining trend ofBERwith increasingSNR, which is consistent with typical communication system behaviours. Similarly, the October measurements points (green squares) and its exponential regression fitting curve (orange dashed line) exhibits a similar trend, albeit with some differences in the strength and nuances of the relationship. This representation underscores the similarities and disparities between the two months' datasets in terms of the impact ofSNRonBER.

communication system over two distinct periods - August (COVE, a semi-controlled environment) and October (St. Margaret's Bay, an uncontrolled environment) - is portrayed. The interplay betweenSNRandBERis consistently observed, reinforcing the notion that asSNRescalates,BERdeclines, indicating enhanced data fidelity. Notably, the October dataset manifests a marginally elevatedBERat analogousSNRlevels. This suggests the October environment was better. Furthermore, theRSSItrends confirm the anticipated positive correlation withSNR. However, theCFOmetrics, indicative of receiver-transmitter frequency synchronicity, exhibits mixed results, especially in October, flagging possible synchronization challenges. The blue shaded regions in the plots, describes the confidence intervals, offer a metric of the inherent uncertainty associated with the regression predictions, provides some insight into the data's variability and the regression's fidelity.

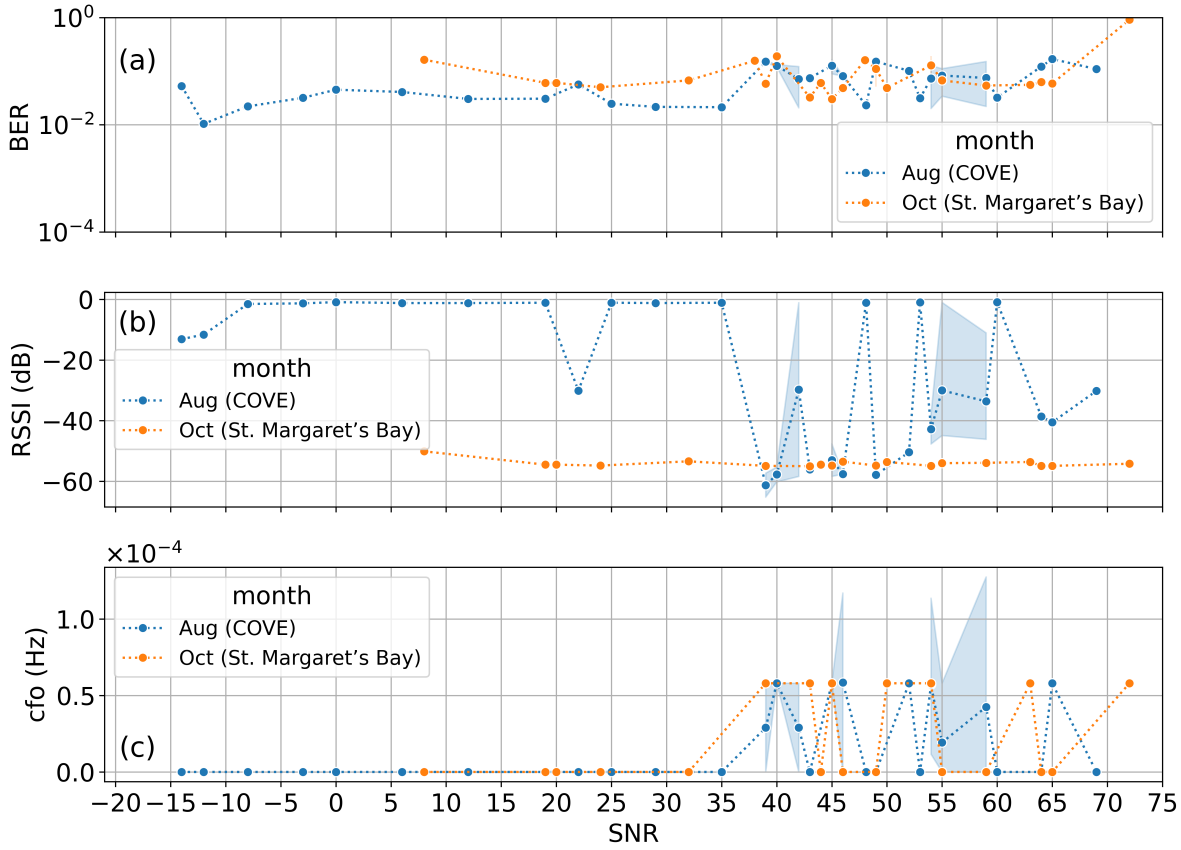

Figure 5.25: Performance evaluation of the proposed communication system, encompassing in-water meaurements from Aug 4 - Aug 10, 2022 (COVE, semi-controlled environment) and October 2022 (St. Margaret's Bay, uncontrolled environment). This representation highlights: (a) the system's ability to discern signals in the midst of environmental noise and interference; (b) accentuates the pivotal role of signal strength in ensuring unerring data transfer, and (c)CFOapproximations, signifying the system's resilience against unintended frequency drifts. The distinction between the two datasets, represented by varying hues, facilitates a comparative assessment, unveiling the system's versatility in diverse aquatic conditions.

5.3.5 Data Visualization

The exploration of the data also involved the creation of scatter plots (Figure5.26and 5.27).

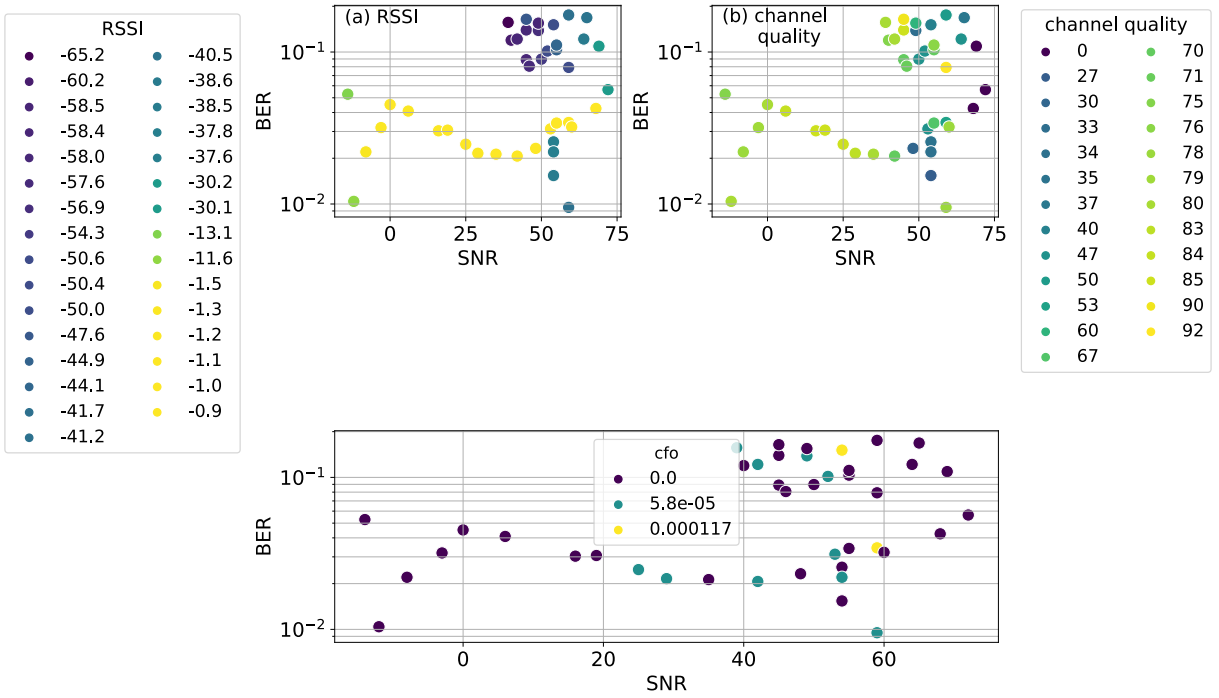

Figure 5.26: Relationship between the experimental measurement variables. One observes moderate downward trends that implies there are still a multiple measurements points that do not follow the trend with context toSNRandBER.

The key observations from the scatter plot include: all measurements points exhibit a downward trend, indicating that as theSNRincreases, theBERtends to decrease. This trend is consistent with expectations and demonstrates the impact of theSNRon the system performance. The experimental data points (circles, triangles, squares, and stars) generally lie above the simulation measurement points (crosses and pluses). This discrepancy may arise from factors such as noise, interference, and specific conditions in the experimental setup. Comparing specific data points, theBERvalues for the *Experimental CDMA (2 Nodes deployed 55 m apart at Saint Marget's bay)* and *simulation MU (Walsh) codelength=8* are relatively close. This suggests that the simulation model effectively represents the experimental system under those conditions.

Similarly, the BER values for the *Experimental CDMA (2 Nodes deployed at 100 m apart at St. Margaret's Bay)* and *simulation m-seq code length = 8* are also relatively close, supporting the validity of the simulation model for those parameters.

These observations indicate that increasing the SNR can lead to improved system performance by reducing the BER. This trend holds true for both the experimental measurements and simulation – considering various deployment scenarios and code lengths.

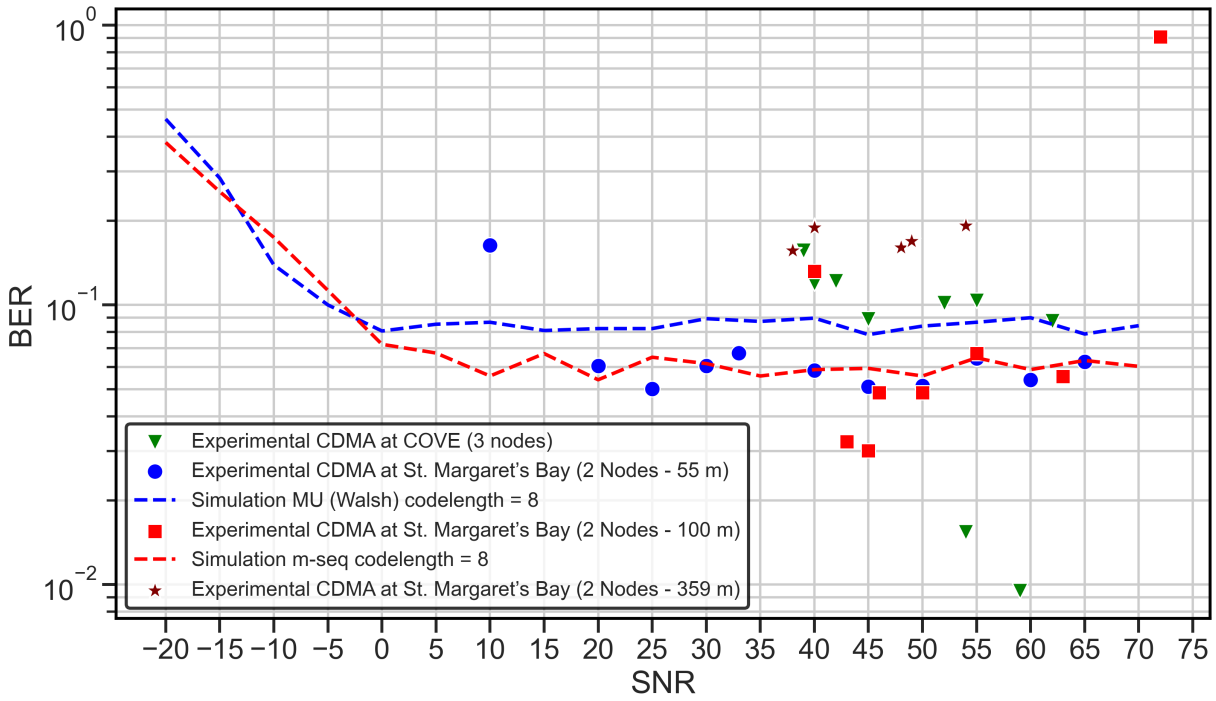

Figure 5.27: Comparison between the experimental measurements and their predictions from simulation for different deployments locations and CDMA code lengths, illustrates the relationship betweenSNRandBERin the communication system.

From the Figure5.27, revealed several interesting findings about the collected data and simulated data:

1. All data points show a downward trend, indicating that asSNRincreases, theBER tend to decrease. This is consistent with the negative correlations observed in the correlation matrix.

2. The experimental measurement points (circles, triangles, squares, and stars) are generally higher than the simulation ones (crosses and pluses). This could be due to various factors of real world attributes such as noise, interference, and the specific conditions of each deployment in the experimental setup.

3. The BER values for *Experimental BER – 2 Nodes deployed 55 m apart from each other in St Margarets bay* and *Simulation – BER (MU (walsh) codelength=8)* are relatively close to each other, suggesting the simulation model is a good representation of the experimental system for the specific conditions.

4. The BER values for *Experimental – 2 Nodes deployed at 100 m apart at St. Margaret's Bay* and *Simulation – BER (m-seq code length=8)* are also relatively close to each other, further supporting the validity of the simulation model.

5.3.6 Group Analysis

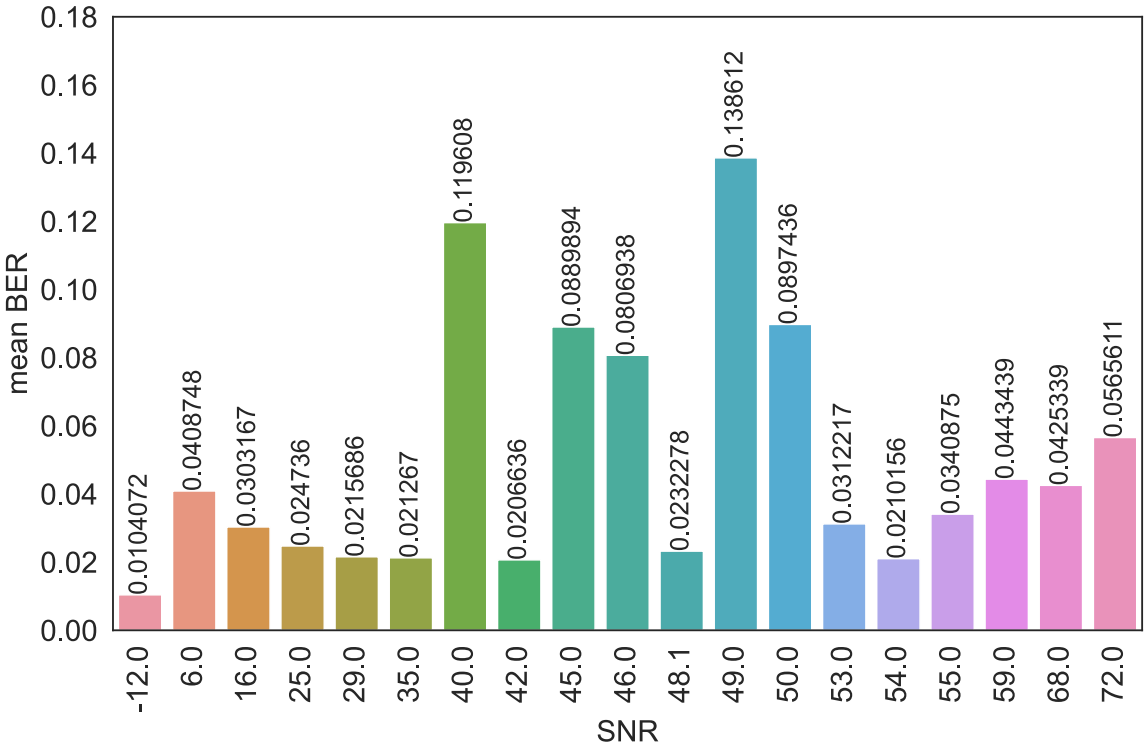

Figure 5.28: Grouped analysis showcasing the average (BER) against distinct (SNR) levels. each bar represents a specific SNR level, with its height illustrating the corresponding mean BER. This analysis is pivotal as it captures the tendency of BER to decrease with increasing SNR, emphasizing the inherent behavior of the proposed communication system. The visualization underscores the nuanced relationship between SNR and BER, offering crucial insights for system performance evaluations.

The group analysis plot shows a different view of the measurement points, highlighting the relationships between variablesBERandSNRand their distributions. This plot was particularly useful in identifying patterns and trends in the data, especiallyBER, Figure5.28can provide insights into how theBERvaries withSNR. For instance, if the mean BERis significantly different for differentSNRlevels, this might indicate thatSNRhas a strong effect onBER.

5.3.7 Result

1. The correlation analysis revealed a moderate positive correlation betweenSNRand BER, contrary to the initial expectation of an inverse relationship. This suggests the possibility of a non-linear relationship or the influence of other factors onBER. This aligns with the expectations for a communication system.

2. The regression analysis confirmed the positive relationship betweenSNRandBER, but the effect ofSNRonBERwas small due to unmodelled effects. This indicates thatSNRalone may not be sufficient to predictBERaccurately.

3. The data visualization of the relationships between variables and their distributions highlighted their correlations.

In summary, the data exploration and analysis provided valuable insights into the performance and characteristics of the proposedCDMAunderwater communication system. The analyses suggested that whileSNRis a relevant factor, it is not the only factor that impactsBER. Other factors, such as signal distortion, interference, or noise characteristics, should be considered. The correlation analyses revealed unexpected relationships between variables, highlighting the need for further investigation into the system's behavior. The regression analysis confirmed the limitations of usingSNRalone to predictBERaccurately. The data visualization techniques helped identify trends, patterns, and outliers within the data. The visualizations aided in understanding the relationships between different variables and the distribution of each variable. These findings contribute to a comprehensive understanding of the CDMA communication system, enabling further improvements and optimizations. Future work could involve an in-depth analysis with experimental measurements of these other factors and their impact onBERand system performance.

The experimental measurements summarized in TableD.17was analyzed to evaluate the performance of the proposed system. Various performance metrics, including throughput, channel quality,SNR, bit error rateBER,RSSI, andCFO, were included. Several

noteworthy trends and observations were identified upon analysis. For instance, a positive correlation between signal quality and error rates was observed as theSNRincreased, resulting in a decrease in theBER. Channels with better quality achieved higher throughput. Furthermore, a general decrease in theRSSIvalues was observed with increasing SNR, indicating a strong signal reception. Valuable insights into the performance characteristics of the system were provided by these results, contributing to the understanding of its behavior under different conditions.

The results presented in this chapter aligns well with the research objectives and questions defined in Chapter3. The results contribute significantly to the understanding of the CDMA underwater communication system's capabilities and provided a foundation for further analysis and future work discussion in Chapter6.

In the next chapter, this thesis concludes by summarizing the key findings, discussing their implications, and outlining potential areas for future research and development.

Chapter 6

Conclusion

This thesis presented a comprehensive analysis of the proposed communication system's performance characteristics, emphasizing the significance of signal quality, channel optimization, and signal strength in achieving high throughput and minimizing error rates. The in-water experiments reveal valuable insights, discussed next, into the system's performance, underscoring the need for robust and reliable communication links.

In comparison to previous research [13,14,29], this study delves deeper into the functionality and performance of Subnero modems. It provides practical insights into the application of these modems in real-world underwater environments, an area less explored in previous studies. In conclusion, this thesis contributes to the field by providing a comprehensive analysis of the communication system's performance characteristics, shedding light on the importance of signal quality, channel optimization, and signal strength. The findings offer practical insights for the design and optimization of communication systems, positioning Subnero's WNC3 series of smart devices, powered by UnetStack, at the forefront of cutting-edge underwater wireless communication technology. With their exceptional performance, dynamic configurability, and advanced networking and localization capabilities, these devices offer innovative and reliable solutions for underwater IoT and autonomous subsea inspections [57].

The research objective was to design and verify a communications network that spans above and below-water, uses bandwidth more efficiently than time-division multiple access methods, be full-duplex and secure against unauthorized access. Fulfilling each of these requirements is a contribution to underwater communications. Underwater communications is typically half-duplex and, to date, primarily uses time-division multiple access which engages the entire available network bandwidth for only one transmission, i.e. it does not use the bandwidth efficiently. The requirement for multi-domain (i.e., above and below water) enables multi-domain robotic collaborations. Such robotic collaborations are needed for e.g, in communicating underwater robot findings to above-water nodes, rapidly, for timely evaluation and decision-making. A use case is in the search for downed aircraft.

Towards these requirements, a novel code-division multiple access (CDMA) network was proposed, designed, modelled and verified in-water. The network was initially explored in simulations with tools like Network Simulator 3 (NS-3) and then Unetstack. Above-water, the use of CDMA is well-established. The novelty of this thesis was to successfully implement underwater CDMA nodes and then integrate them with above-water nodes. The challenge was to create an underwater receiver that can receive, process and interpret transmissions that embed information for multiple nodes as opposed to the usual single node.

CDMA takes the multiple signals, intended for multiple distinct nodes, and creates a composite signal based on an exclusive-OR between the individual signals and their respective spreaded code and spreads it over a larger spectrum than any individual signal contains. With this network protocol, multiple nodes can concurrently communicate over the same channel bandwidth. Multi-path is inherent in underwater communications and CDMA's ability to discriminate which "return" to respond to is an asset. In this way, the available bandwidth is used very efficiently. The transmitted composite signal is encoded and accessed through an a priori known key and thus, secure. With the key, individual receiver nodes access their component in the transmitted composite signal to decode and extract their portion.

At the receiver, the code chip rate (pulses-per-second) represents the PN (spreaded) code which is greater than the symbol rate (pulses-per-second) representing the data. Consequently, this creates a synchronization challenge. Precise synchronization between the received signal and its respective spreading code is necessary and more challenging – especially at high chip rates. This synchronization challenge was carefully addressed through the meticulous design of the receiver algorithm (SectionC.2). By implementing time synchronization techniques and optimizing the code tracking process, the demodulation of the spreaded signals was ensured – despite the limited signal sampling interval. This achievement significantly contributes to the system's reliable recovery of the original signal data.

Furthermore, the proposed receiver topology enhances the system's performance. It introduces an improved receiver topology which down-converts the spread spectrum signal to baseband using a common quadrature down-converter for more complex modulation schemes. This approach simplifies code sequence recovery and enables more efficient despreading. The receiver operates in two distinct modes: acquisition and tracking. During the acquisition mode, it diligently searches for the correct phase of the code sequence by progressively correlating with all possible phases. Once the phase is acquired, the receiver seamlessly transitions to tracking mode. Tracking mode maintains alignment with the original spreading code's amplitude to ensure the demodulation works.

In the realm of bit recovery, a system akin to a Costas loop is employed. This system involves vector rotation and time recovery, facilitated by a Gardner time error detector and a PI controller, all implemented in software. These components collectively contribute to the accurate recovery of the I and Q bit streams, further enhancing the system's performance and robustness.

To ensure the robustness and effectiveness of the proposed communication system, a

comprehensive validation and testing process was undertaken. This process involved modelling, controlled in-water verification, and real-world deployments in unstructured underwater environments. The outcome of the modelling indicates the proposed underwater communications system is feasible underwater. Following successful modelling, the next step was to perform controlled in-water verification at the Aquatron pool tank where the system was shown to be secure and can work in full-duplex mode.

To bridge the gap between controlled testing and real-world underwater deployments, the system was then deployed in semi-controlled environments. One such deployment was at COVE, Halifax Harbour, where environmental conditions are more dynamic than in controlled settings but still manageable.

The ultimate validation of the system involved real-world deployments in unstructured underwater environments. These deployments were at St. Margaret's Bay, where the system faced the challenges of unpredictable water conditions, varying depths, and potential interference. These deployments served as a critical test of the system's resilience and reliability in harsh, uncontrolled underwater settings. Throughout the verification and testing, the system consistently demonstrated its effectiveness and reliability as quantified through the BER, throughput, and minimal carrier frequency offset. It successfully transmitted data, maintained synchronization, and recovered information in a variety of underwater conditions. The system's ability to adapt to dynamic environments and perform reliably in both controlled and unstructured settings highlights its robust design and implementation. Serendipitously, it can operate below the noise floor which enhances its stealth which affords some security.

In summary, the comprehensive verification process, which encompassed modelling, controlled in-water verification, and real-world deployments, confirmed the system's readiness for practical applications in underwater communication. The successful transition from modelling to real-world testing highlighted the system's adaptability and its potential to address the challenges of underwater communication in dynamic environments. Future involves further refinement and potential deployment in specific underwater applications, such as collaborative multi-domain robotic missions or underwater monitoring and data collection. Following the detailed analysis and contributions presented in this thesis, attention is now turned to the horizon of future research. Built upon the foundation contributed by this thesis, several avenues are ripe for exploration with contributions. Potential directions that promise to further advance the field of underwater communication systems, leveraging the insights and findings from this study, are outlined in the following future work section.

6.1 Future Work

The research outcomes presented in this thesis has provided valuable insights into the performance characteristics and practical implications of the communication system. As with any study, there are several avenues for future research and development that can build upon the findings and further advance the field. This chapter explores potential areas for future work and suggests directions for continued investigation.

- Scalability, Robustness and Network Expansion

  The proposed underwater communication system operates as an ad-hoc network. Its design ensures some degree of redundancy, enabling it to maintain overall network functionality even if specific communication links fail. If one route fails due to node failure, another node could take over, assuming there are multiple routes for particular nodes, a condition that necessitates network density. However, scenarios with a limited number of nodes, or where the relaying node fails, present significant challenges for network recovery.

  In terms of managing increased traffic, the system's broadcast nature allows it to efficiently utilize available bandwidth amongst its users. Despite the potential for fluctuations in channel quality to impact the entire network, the system has demonstrated competency in traffic management.

  Overall efficiency while handling simultaneous communications from a large number of nodes has not been thoroughly tested due to resource limitations. However, it can be inferred from the principles of Code Division Multiple Access (CDMA) systems that there will be a soft capacity. Beyond this limit, network efficiency may degrade due to inter-user interference. In an underwater environment, this soft capacity is influenced by several factors including the spread spectrum technique used, the available bandwidth, the acoustic properties of the water measured by SVP, and the signal processing techniques implemented. It's important to note that the lower available bandwidth and the time-varying nature of underwater channels pose additional challenges for underwater CDMA systems. Additionally, the longer spreading factors can be explored for the proposed system to realise the effect of the same on the performance on the network (e.g. better filtering results).

  These points highlight potential areas of investigation that could verify and potentially enhance the network's scalability and robustness. Conducting more extensive experiments or modelling to determine the specific capacity limitations and performance characteristics of this underwater CDMA system may be a necessary future

step. The complexities outlined here illustrate the delicate balance required in designing underwater communication systems that maintain functionality and performance as they scale. Therefore, future work should focus on how to best optimize these systems as they expand.

In light of the intricate nature of designing underwater communication systems that can sustain functionality and performance as they grow, it becomes imperative for future research to concentrate on optimizing these systems as they expand. This includes exploring the possibility of assessing the efficiency of RSSI through testing a single transmission with an array of receivers. Such an approach may yield substantial enhancements in the strength of received signal amplitudes and warrants further investigation. This study adopts the standard equalization methods utilized by the Subnero modems for optimal performance on the default OFDM channel. Moving forward, there is significant value in examining alternative equalization techniques, including ZF, MMSE, and Machine Learning, especially when applied to configurations with multiple antennas [66].

- Power Optimization and Energy Efficiency

  Power consumption is a critical aspect of underwater communication systems, as energy resources are typically limited. Future work can explore strategies (e.g. RSSI based power control) and techniques to optimize power consumption and improve energy efficiency for the embedded nodes (operates on the battery generally). Investigating power management approaches, adaptive transmission power control, and energy harvesting techniques can enhance the sustainability and longevity of the communication system. By addressing power-related challenges, researchers can develop energy-efficient solutions that maximize the system's performance while minimizing its environmental impact.

- Environmental Variations and Adaptability

  Underwater communication channels exhibit fluctuations in environmental conditions, such as water temperature, salinity, and turbidity. Future research should focus on studying the system's adaptability to different environmental factors and addressing their impact on communication performance. By understanding how the system responds to changing conditions, researchers can develop adaptive algorithms, modulation schemes, and error correction techniques that improve communication reliability and throughput in various underwater environments. This research will enable the system to adapt to different operational scenarios (e.g. deep water) and enhance its robustness in challenging conditions.

- Further Field Testing and Validation

  While this study included an end-to-end practical deployments and field-testing at the COVE (11 m water depth, harbour environment), and St. Margaret Bay (16 m water depth), both are shallow water environments. Additional field-testing and verification in deep dynamic underwater environments is an essential next step. Conducting experiments in different geographic locations, in deeper water, different bottom cover, and other sound speed profiles, will provide a comprehensive understanding of the OFDM-CDMA performance under other operational conditions. This additional field-testing will enable further refinement and verification of the findings (Chapter 5), ensuring the communication system is reliable and effective over a wider range of operational conditions.

- Integration of Advanced Techniques and Technologies

  The field of underwater communication systems is continuously evolving, with advancements in acoustic signal processing, machine learning, and network protocols. Future work should explore the integration of these advanced techniques and technologies into the communication system. For example, leveraging machine learning algorithms for adaptive channel equalization, interference mitigation, and signal detection can enhance the system's performance in challenging underwater environments. Also more complex channel model can be adapted and validated for simulation and real time deployment conditions. Additionally, exploring the integration of emerging communication protocols and network architectures, such as software-defined networking in multiple domains, can further optimize the system's efficiency and flexibility.

By addressing these areas in future research, the communication system can be enhanced and expanded to meet the growing demands of underwater applications. The practical deployments and field testing conducted in this study lay the foundation for further advancements, and continued research in these areas will contribute to the development of robust and efficient underwater communication systems.

References

[1] *Wireless Communications: Principles and Practice, 2e.* Prentice Hall PTR, 1996.

[2]Docker. https://www.docker.com/, 2022.

[3]Network Simulator-3. https://www.nsnam.org/, Retrieved April 1, 2020.

[4]Jaltarang, ns-3 based underwater sensor network simulator. http://cse.iitkgp.ac.in/~smisra/swan/tre/jaltarang.html, Retrieved Feb 1, 2020.

[5]Ocean acoustics library. https://oalib-acoustics.org/, Retrieved Feb 1, 2020.

[6]Exercise unmanned warrior: an international exercise using autonomous tech to detect underwater mines. https://tinyurl.com/yk6tpnle, Retrieved March 20, 2020.

[7]Marc Greis Tutorials for NS-2. https://www.isi.edu/nsnam/ns/tutorial/, Retrieved Oct 2, 2020.

[8]Aqua-Sim – Obinet. https://obinet.engr.uconn.edu, Retrieved April 15, 2024.

[9]Subnero underwater modem. https://subnero.com/, Retrieved April 15, 2024.

[10]Mosa Ali Abu-Rgheff. 3 - fundamentals of spread-spectrum techniques. In Mosa Ali Abu-Rgheff, editor, *Introduction to CDMA Wireless Communications*, pages 153–194. Academic Press, Oxford, 2007.

[11]Abdel-Mehsen Ahmad, Michel Barbeau, Joaquin Garcia-Alfaro, Jamil Kassen, Evangelos Kranakis, and Steven Porretta. Doppler effect in the underwater acoustic ultra

low frequency band. In *ADHOCNETS 2017 : 9th International Conference on Ad Hoc Networks*, pages 3 – 12, Niagara Falls, Canada, September 2017. Springer.

[12]Michael A. Ainslie and James G. McColm. A simplified formula for viscous and chemical absorption in sea water. *The Journal of the Acoustical Society of America*, 103(3):1671–1672, 03 1998.

[13]Prasad Anjangi and Mandar Chitre. Model-based data-driven learning algorithm for tuning an underwater acoustic link. In *2018 Fourth Underwater Communications and Networking Conference (UComms)*, pages 1–5, 2018.

[14]Prasad Anjangi, Mandar Chitre, Manu Ignatius, and Chinmay Pendharkar. Distributed spatial diversity enabled receiver system for an underwater acoustic link. In *2021 Fifth Underwater Communications and Networking Conference (UComms)*, pages 1–5, 2021.

[15]N. Bahrami, N. Khamis, A. Baharom, and A. Yahya. Underwater channel characterization to design wireless sensor network by bellhop. *TELKOMNIKA Telecommunication Computing Electronics and Control*, 14:110–118, 2016.

[16]A. Bassam. *Pilot-Aided, Time-Domain Doppler Estimator, Tracker and Compensator for Doubly Dispersive Underwater Acoustic Channels Dominated by Wave Motion*. Phd's thesis, Dalhousie University, CA, 2020.

[17]Ali M. Bassam, Jay Patel, and Mae L. Seto. Kalman filter-based doppler tracking and channel estimation for auv implementation. In *OCEANS 2021: San Diego – Porto*, pages 1–8, 2021.

[18]K. Bektas. *Full-Duplex Underwater Networking Using CDMA*. Master's thesis, NAVAL POSTGRADUATE SCHOOL MONTEREY, CA, 2004.

[19]V. Bellec, R. Bøe, L. Rise, A. Lepland, T. Thorsnes, and L. R. Bjarnadóttir. Seabed sediments (grain size) of nordland vi, offshore north norway. *Journal of Maps*, 13:608 – 620, 2017.

[20]arlpy python tools by ARL. https://github.com/org-arl/arlpy, Retrieved January 8, 2021.

[21]W.S. Burdic. *Underwater Acoustic System Analysis*. Peninsula Publ., 2002.

[22]Gunilla Burrowes and Jamil Y. Khan. Short-range underwater acoustic communication networks. In Nuno A. Cruz, editor, *Autonomous Underwater Vehicles*, chapter 8. IntechOpen, Rijeka, 2011.

[23]A. Bury, J. Egle, and J. Lindner. Diversity comparison of spreading transforms for multicarrier spread spectrum transmission. *IEEE Transactions on Communications*, 51(5):774–781, 2003.

[24]Ivano Calabrese, Riccardo Masiero, Paolo Casari, Lorenzo Vangelista, and Michele Zorzi. Embedded systems for prototyping underwater acoustic networks: The desert underwater libraries on board the pandaboard and netdcu. *2012 Oceans*, pages 1–8, 2012.

[25]Leandro Calado, Orlando Camargo Rodríguez, Gabriel Codato, and Fabio Contrera Xavier. Upwelling regime off the cabo frio region in brazil and impact on acoustic propagation. *The Journal of the Acoustical Society of America*, 143(3):EL174–EL180, 2018.

[26]SonTek CastAway-CTD. Sound velocity profiler (CastAway-CTD E767-CA-CTD). *https://www.xylem.com/siteassets/brand/sontek/resources/specification/sontek-castaway-ctd-spec-sheet-2018.pdf*, Retrieved Jan 1, 2023.

[27]chilleas Anastasopoulos. gr-cdma. *https://github.com/anastas/gr-cdma*, Retrieved April 15, 2024.

[28]M. Chitre. *Underwater Acoustic Communications in Warm Shallow Water Channels*. Phd's thesis, National University of Singapore, Singapore, 2006.

[29]M. Chitre, R. Bhatnagar, M. Ignatius, and S. Suman. Baseband signal processing with unetstack. In *2014 Underwater Communications and Networking (UComms)*, pages 1–4, 2014.

[30]M. Chitre, R. Bhatnagar, and W. Soh. Unetstack: An agent-based software stack and simulator for underwater networks. In *2014 Oceans - St. John's*, pages 1–10, 2014.

[31]Mandar Chitre, Teong-Beng Koay, Grant Deane, and Gabriel Chua. Variability in shallow water communication performance near a busy shipping lane. In *2021 Fifth Underwater Communications and Networking Conference (UComms)*, pages 1–5, 2021.

[32]common underwater sounds. https://dosits.org/science/sounds-in-the-sea/what-are-common-underwater-sounds/, Retrieved Oct 2, 2020.

[33]Analog Devices. Adalm-pluto software-defined radio active learning module. https://www.analog.com/en/design-center/evaluation-hardware-and-software/evaluation-boards-kits/adalm-pluto.html, Retrieved April 15, 2024.

[34]H. Doukkali, S. Houcke, and L. Nuaymi. A cross layer approach with csma/ca based protocol and cdma transmission for underwater acoustic networks. In *2007 IEEE 18th International Symposium on Personal, Indoor and Mobile Radio Communications*, pages 1–5, 2007.

[35]Xiujuan Du, Meiju Li, and K. Li. Reliable transmission protocol for underwater acoustic networks. In *Computer and Network Security Essentials*, 2018.

[36]Fan Guanghui, Zhang Yonghuai, and Sun Haixin. A new code-division multiple access protocol for underwater acoustic network. In *2007 IET Conference on Wireless, Mobile and Sensor Networks (CCWMSN07)*, pages 56–59, 2007.

[37]fjåge - framework for java and groovy agents by ARL. https://github.com/org-arl/fjage, Retrieved January 8, 2021.

[38]The General bathymetric chart of the oceans (gebco 2019). https://www.gebco.net/data_and_products/gridded_bathymetry_data/, Retrieved May 20, 2020.

[39]Gnuradio. https://www.gnuradio.org/, Retrieved April 15, 2024.

[40]R. Gold. Optimal binary sequences for spread spectrum multiplexing (corresp.). *IEEE Transactions on Information Theory*, 13(4):619–621, October 1967.

[41]F. Guerra. The world ocean simulation system - WOSS. http://telecom.dei.unipd.it/ns/woss/, Retrieved Feb 20, 2020.

[42]F. Guerra. WOSS - the world ocean simulation system, github repository. https://github.com/MetalKnight/woss-ns3, Retrieved Jan 1, 2023.

[43]Gregory F. Gusberti. Spread spectrum modulation and demodulation. https://youtu.be/68Nua8gKdRU, Retrieved April 15, 2024.

[44]Heron usv simulation. https://github.com/heron/heron_simulator, Retrieved Jan 2019.

[45]Franz Heubach. *Long-Range Gravity-Aided Autonomous Underwater Vehicle Navigation*. Master's thesis, Dalhousie University, CA, 2022.

[46]R.P. Hodges. *Underwater Acoustics: Analysis, Design and Performance of Sonar*. Wiley, 2011.

[47]OceanSonics iCListen. Ocean Sonics icListen HF Hydrophone (SC2-ETH). https://oceansonics.com/products/iclisten-sj9/, Retrieved Jan 1, 2024.

[48]Manu Ignatius. Converting your laptop into a janus modem using unet. https://blog.unetstack.net/converting-your-laptop-into-a-janus-modem-using-unetaudio, Retrieved April 15, 2024.

[49]Hala Jodeh, Aisha Mikkawi, Ahmed Awad, and O. Othman. Comparative analysis of routing protocols for under-water wireless sensor networks. In *ICFNDS '18*, 2018.

[50]N. Koenig and A. Howard. Design and use paradigms for gazebo, an open-source multi-robot simulator. In *2004 IEEE/RSJ International Conference on Intelligent Robots and Systems (IROS) (IEEE Cat. No.04CH37566)*, volume 3, pages 2149–2154 vol.3, 2004.

[51]H. Kulhandjian, T. Melodia, and D. Koutsonikolas. Cdma-based analog network coding for underwater acoustic sensor networks. *IEEE Transactions on Wireless Communications*, 14(11):6495–6507, 2015.

[52]Acoustic Research Laboratory. unet-py. https://pypi.org/project/unetpy/, Retrieved April 15, 2024.

[53]W. Lee. Mobile communications design fundamentals: Lee/mobile. 1993.

[54]X. Li, J. Liu, L. Yan, S. Han, and X. Guan. Relay selection for underwater acoustic sensor networks: A multi-user multi-armed bandit formulation. *IEEE Access*, 6:7839–7853, 2018.

[55]Joseph C. Liberti and Theodore S. Rappaport. *Smart antennas for wireless communications : IS-95 and third generation CDMA applications*. Prentice Hall communications engineering and emerging technologies series. Prentice Hall PTR, Upper Saddle River, NJ, 1999.

[56]Joel Lindsay, Jordan Ross, Mae L. Seto, Edward Gregson, Alexander Moore, Jay Patel, and Robert Bauer. Collaboration of heterogeneous marine robots toward

multidomain sensing and situational awareness on partially submerged targets. *IEEE Journal of Oceanic Engineering*, 47(4):880–894, 2022.

[57]Subnero Pte. Ltd. White paper: Software defined underwater acoustic modems for communication, networking, navigation and monitoring. Technical report, January 2022.

[58]Hanjiang Luo, Kaishun Wu, Rukhsana Ruby, Feng Hong, Zhongwen Guo, and Lionel M. Ni. Simulation and experimentation platforms for underwater acoustic sensor networks: Advancements and challenges. *ACM Comput. Surv.*, 50(2), May 2017.

[59]Musa Morena Marcusso Manhães, Sebastian A. Scherer, Martin Voss, Luiz Ricardo Douat, and Thomas Rauschenbach. Uuv simulator: A gazebo-based package for underwater intervention and multi-robot simulation. In *OCEANS 2016 MTS/IEEE Monterey*, pages 1–8, 2016.

[60]Sukanta K. Hazra Manu Ignatius. Low-cost DIY underwater modem using cots components and unet audio. https://tinyurl.com/ynp6n88c, Retrieved April 15, 2024.

[61]Tin Win Maw. Integration of security and authentication agent inns-2 and leach protocol forwireless sensor network. 2014.

[62]Sebastian Menze. sebastianmenze/Python-Audio-Spectrogram-Explorer: PASE. https://github.com/sebastianmenze/Python-Audio-Spectrogram-Explorer, October 2022.

[63]Johannes Meyer, Alexander Sendobry, Stefan Kohlbrecher, Uwe Klingauf, and Oskar von Stryk. Comprehensive simulation of quadrotor UAVs using ROS and gazebo. In *Simulation, Modeling, and Programming for Autonomous Robots*, pages 400–411. Springer Berlin Heidelberg, 2012.

[64]Albert Armisén Morell. Chain simulation of ds-cdma communication systems. 2010.

[65]Nils Morozs, Wael Gorma, Benjamin T. Henson, Lu Shen, Paul D. Mitchell, and Yuriy V. Zakharov. Channel modeling for underwater acoustic network simulation. *IEEE Access*, 8:136151–136175, 2020.

[66]Ivy Y. Moutushi. *Simulations of Implementation of Advanced Communication Technologies*. PhD thesis, West Virginia University, Morgantown, West Virginia, 2023.

[67]D. Nams, M. L. Seto, and J. J. Leonard. On-line adaptation of underwater acoustic transmission rates to optimize communications for collaborative auv missions. In *OCEANS 2015 - MTS/IEEE Washington*, pages 1–8, 2015.

[68]Anand Nayyar and Valentina Emilia Balas. Analysis of simulation tools for underwater sensor networks (uwsns). In Siddhartha Bhattacharyya, Aboul Ella Hassanien, Deepak Gupta, Ashish Khanna, and Indrajit Pan, editors, *International Conference on Innovative Computing and Communications*, pages 165–180, Singapore, 2019. Springer Singapore.

[69]Open Robotics. ROS Index. https://index.ros.org/packages/, 2022.

[70]Jay Patel. Adalm-pluto-file-transfer & fm receiver plutosdr. *https://github.com/patel999jay/ADALM-Pluto-File-Transfer*, Retrieved April 15, 2024.

[71]Jay Patel. CDMA simulation. *https://github.com/patel999jay/CDMA_simulation*, Retrieved April 15, 2024.

[72]Jay Patel, Ali Bassam, and Mae Seto. Multi-uuv object detection, localization and tracking with secure, full-duplex communication networks. *Proceedings of Meetings on Acoustics*, 44(1):070037, 2021.

[73]Jay Patel and Mae Seto. CDMA-based multi-domain communications network for marine robots. In *Proceedings of the International Conference on Underwater Networks & Systems*, WUWNET'19, New York, NY, USA, 2019. Association for Computing Machinery.

[74]Jay Patel and Mae Seto. CDMA-based multi-domain communications network for marine robots. *The Journal of the Acoustical Society of America*, 148(4):2510–2510, 2020.

[75]Jay Patel and Mae Seto. Live rf image transmission using ofdm with rpi and plutosdr. In *2020 IEEE Canadian Conference on Electrical and Computer Engineering (CCECE)*, pages 1–5, 2020.

[76]Jay Patel and Mae Seto. Underwater channel characterization for shallow water multi-domain communications. *Proceedings of Meetings on Acoustics*, 40(1):070014, 2020.

[77]Plotly dashboards. *https://plotly.com/*, Retrieved April 15, 2024.

[78]Dario Pompili, Tommaso Melodia, and Ian F. Akyildiz. A CDMA-based medium access control for underwater acoustic sensor networks. *Trans. Wireless. Comm.*, 8(4):1899–1909, April 2009.

[79]Python Software Foundation. Python.org. The Python Software Foundation, 2022.

[80]Zeyad A. H. Qasem. *Robust Index Modulation Techniques for Underwater Acoustic Communications*. Phd's thesis, Xiamen University, China, 2021.

[81]Gang Qiao, Yunjiang Zhao, Songzuo Liu, and Muhammad Bilal. Dolphin sounds-inspired covert underwater acoustic communication and micro-modem. *Sensors*, 17(11), 2017.

[82]J. Ross, J. Lindsay, E. Gregson, A. Moore, J. Patel, and M. Seto. Collaboration of multi-domain marine robots towards above and below-water characterization of floating targets. In *2019 IEEE International Symposium on Robotic and Sensors Environments (ROSE)*, pages 1–7, June 2019.

[83]Toby Schneider. The dynamic compact control language. https://github.com/GobySoft, Retrieved April 15, 2024.

[84]Toby Schneider, Stephanie Petillo, Henrik Schmidt, and Christopher Murphy. The dynamic compact control language version 3. In *OCEANS 2015 - Genova*, pages 1–7, 2015.

[85]M. Stojanovic, J. Catipovic, and J. G. Proakis. Adaptive multichannel combining and equalization for underwater acoustic communications. *The Journal of the Acoustical Society of America*, 94(3):1621–1631, 1993.

[86]M. Tahiliani. Use Aqua-sim and Aqua3d. http://mohittahiliani.blogspot.com/2014/07/underwater-wsn-simulations-in-ns-2.html, Retrieved Feb 12, 2020.

[87]The Linux Foundation. The Linux Kernel Archives. Linux Kernel Organization, 2022.

[88]W.H. Thorp and D.G. Browning. Attenuation of low frequency sound in the ocean. *Journal of Sound and Vibration*, 26(4):576–578, 1973.

[89]William H. Thorp. Deep-ocean sound attenuation in the sub- and low-kilocycle-per-second region. *The Journal of the Acoustical Society of America*, 38(4):648–654, 1965.

[90]William H. Thorp. Analytic description of the low-frequency attenuation coefficient. *The Journal of the Acoustical Society of America*, 42(1):270–270, 1967.

[91]NS3 UAN. The UAN model for underwater network simulation. *https://www.nsnam.org/docs/models/html/uan.html*, Retrieved Feb 1, 2020.

[92]Unetstack 3.3.0 api. *https://unetstack.net/javadoc/3.3/overview-summary.html*, Retrieved Jan 1, 2023.

[93]Underwater networks handbook. *https://unetstack.net/handbook/unet-handbook_preface.html*, Retrieved April 15, 2024.

[94]unet-contrib. *https://github.com/org-arl/unet-contrib*, Retrieved April 15, 2024.

[95]Unetstack simulator. *https://unetstack.net/*, Retrieved April 15, 2024.

[96]Robert J. Urick. *Principles of underwater sound*. Peninsula Publishing, 3rd ed. edition.

[97]P. Vijayalakshmi and Vanitha Rajendran. Performance analysis of vbf protocol in underwater communication for anchoring nodes and moving nodes. 2017.

[98]Mathuranathan Viswanathan. *Digital Modulations using Python*. https://www.gaussianwaves.com, 2019.

[99]A. Viterbi. CDMA: Principles of spread spectrum communication. 1995.

[100]H. Wang, S. Wang, R. Bu, and E. Zhang. A novel cross-layer routing protocol based on network coding for underwater sensor networks. In *Sensors*, volume 17, 29 June 2017.

[101]Niaz Ahmedn Yi Lou. *Underwater Communications and Networks*. Springer Cham, China, 2022.

[102]Xiaohui Zeng, Zhaohui Luo, Fangjiong Chen, Hua Yu, Fei Ji, and Quanshen Guang. An ns-3 compatible emulation framework for underwater acoustic network. In *Proceedings of the Thirteenth ACM International Conference on Underwater Networks & Systems*, WUWNet '18, pages 31:1–31:5, New York, NY, USA, 2018. ACM.

[103]Yibo Zhu, Robert Zhong Zhou, James Peng Zheng, and Jun-Hong Cui. An efficient geo-routing aware mac protocol for underwater acoustic networks. In Jun Zheng,

David Simplot-Ryl, and Victor C. M. Leung, editors, *Ad Hoc Networks*, pages 185–200, Berlin, Heidelberg, 2010. Springer Berlin Heidelberg.

Appendix A

Publications

1.J. Lindsay, J. Ross, Seto, M., E. Gregson, A. Moore, Patel, J. , and R. Bauer **Collaboration of heterogeneous marine robots towards multi-domain sensing and situational awareness on partially-submerged targets** in IEEE Journal of Oceanic Engineering, vol. 47, no. 4, pp. 880-894, Oct. 2022.

2.Ali Bassam, Jay Patel and Mae Seto. **Kalman Filter-based Doppler Tracking and Channel Estimation for AUV Implementation** In Oceans 2021, San Diego, USA.

3.Jay Patel, Ali Bassam, Mae Seto. **Multi-UUV Target Tracking and Localization using secure, full-duplex communication system** In 6^{th} Underwater Acoustics Conference & Exhibition (UACE), 20-25 June 2021.

4.Jay Patel, Mae Seto. **CDMA-Based Multi-Domain Communications Network for Marine Robots** In Acoustics Virtually Everywhere - The 179^{th} Meeting of the Acoustical Society of America (ASA), 7-11 December 2020.

5.Jay Patel, Mae Seto. **Underwater channel characterization for shallow water multi-domain communications** In 2020 International Conference on Underwater Acoustics (ICUA). pp. 1–7, Sept. 2020.

6.Jay Patel, Mae Seto. **Live RF Image Transmission Using OFDM with RPi and PlutoSDR** In 2020 IEEE Canadian Conference on Electrical and Computer Engineering (CCECE), London, Canada, Sept. 2020.

7.Jay Patel, Mae Seto. **CDMA-based multi-domain communication network for marine robots** In Proceedings of the International Conference on Underwater Networks amp; Systems. WUWNET'19, Atlanta, GA, USA: Association for Computing Machinery, Oct. 2019.

8.J. Ross, J. Lindsay, E. Gregson, A. Moore, J. Patel, and M. Seto. **Collaboration of multi-domain marine robots towards above and below-water characterization of floating targets** in 2019 IEEE International Symposium on Robotic and Sensors Environments (ROSE), Ottawa, Canada, June 2019. **(Best Student Paper)**

Appendix B

System Model

This appendix was added due to the valuable suggestion of reviewers for additional background and details to justify the OFDM-CDMA approach which was a contribution of the thesis.

With advances in underwater communication, the imperative for robust and efficient data transmission systems is increasingly realized despite the challenging channel conditions. Challenges unique to the underwater communication channel include severe multipath propagation, significant Doppler shifts, and limited bandwidth. In response to these challenges, a hybrid communication system was proposed which combinedOFDM[28] withCDMAmedium access control to exploit the benefits of both to achieve notably more reliable underwater data transfer.

The OFDM-CDMA system architecture was crafted to encode and decode data through complex, yet coherent, processes that are resilient to the underwater channel challenges. The system model delineates a transmitter and receiver which ensures data integrity despite the channel.

At the core of the OFDM-CDMA system is the transmitter which employsindex modulation (IM)to distribute data into discrete groups, subsequently utilizing orthogonal spreading codes to minimize interference and enhance spectral efficiency. The receiver was designed to capture, process, and reconstruct the transmitted data with additional signal processing (FFT, IFFT, synchronization, channel estimation, pilots, etc.) to correct channel distortions and Doppler variations.

The mathematical model, integral to the system's functionality, is based on equations governing the signal's spreading, modulation, and demodulation. This model includes the discrete Fourier transform (DFT)and itsinverse discrete Fourier transform (IDFT), to convert data between the time and frequency representations, as needed to recover the transmitted message well.

Each component of the system's model is detailed in this Appendix. This includes the approach and mathematical foundation underpinning it. FiguresB.1, Algorithm1, and Algorithm2outline the functionality within the transmitter and receiver structures. The subsequent sub-sections describe the system's architecture and provides insight into the the hybridOFDM-CDMAapproach, adapted for the complex underwater acoustic channel.

B.1 Transmitter Structure

As mentioned earlier, the proposed transmitter (Algorithm1) encodes data using a hybrid approach that combinesOFDMwithCDMAtechniques. Let B bits be the transmitted data divided into G groups with m bits in each group, where $m = \frac{B}{G}$. TheIMis conducted within these m bits where the bits of each group $g \in \{1 \dots G\}$ are partitioned into two segments, $P_1^{(g)}$ and $P_2^{(g)}$.

Algorithm 1: Transmitter process

Data: Split the B input bits into G groups
for *each group* **to** g **do**
- Divide bits into two parts, $P_1^{(g)}$ and $P_2^{(g)}$.
- Map $P_1^{(g)}$ to a code $i(g)$ from a set of predefined spreading codes.
- Map $P_2^{(g)}$ to a modulated data symbol $s^{(g)}$ using an M-ary digital modulation scheme.
- Spread the modulated symbol $s^{(g)}$ over the spreading code $i(g)$.

Interleave the spreaded symbols to create the interleaved data block d.
Apply the inverse FFT-transform to d to get d'.
Insert a pseudo-noise (PN) sequence as a guard interval to d' to form the signal $\underline{S}(t)$.
Up-convert the signal $\underline{S}(t)$ for transmission through the underwater acoustic (UWA) channel.
Result: Passband signal $y(t)$; `/*Transmitted to UWA channel */`

The first segment, denoted $P_1^{(g)}$, identifies the index of the chosen spreading code $c_i(g)$ from a predefined set of orthogonal codes $\mathcal{C}$. The index, $i(g)$, ranging from 1 to n, is the spreading code allocated to the g^{th} group. This scheme utilizes orthogonal spreading codes to minimize interference and increase spectral efficiency, which is essential for data integrity in challenging transmission environments like underwater. The second segment, $P_2^{(g)}$, is translated into a modulated symbol $s^{(g)}$ using an M-ary digital modulation scheme, where the size of $P_2^{(g)}$ is given by $\log_2 M$, to ensure the modulated symbols are efficiently mapped to utilize the full spectrum. This approach, supported by an M-ary digital modulation, allows a diverse range of symbols to be used, each representing $\log_2 M$ bits of information, to optimize the data transmission rate.

For theCDMAcomponent, the system employs orthogonal Walsh codes [23], generated from W_n, and Gold codes. The W_n for $n = 4$ is shown in Eq.B.1:

$$W_n = \begin{bmatrix} 1 & 1 & 1 & 1 \\ 1 & -1 & 1 & -1 \\ 1 & 1 & -1 & -1 \\ 1 & -1 & -1 & 1 \end{bmatrix} \tag{B.1}$$

Each c_k corresponds to the k^{th} column of matrix W_n where $1 \leq n$. Gold codes, a class of constant amplitude zero auto-correlation sequences, are generated by circular shifts of a root sequence, offering excellent correlation properties for the system.

Each modulated symbol $s^{(g)}$ is spread using the corresponding spreading code $c_i(g)$, to create a spread sequence $x^{(g)}$. The modulated constellation symbols $u^{(g)}$ spreads over the spreading code $c_i(g)$, chosen based on the $P_1^{(g)}$ index bits, and can be written as in Eq.B.2.

$$\mathcal{X}^{(g)} = \left[x_1^{(g)}, \cdots, x_n^{(g)}\right]^T = \left[u^{(g)} c_i^{(g)}{}_{,1}, \cdots, u^{(g)} c_i^{(g)}{}_{,n}\right]^T \tag{B.2}$$

This sequence is then passed through the interleaver to mitigate error bursts, and subsequently transformed by the IFFT to create theOFDMdata block. Therefore, the OFDMdata block $M \times 1$ generated after obtaining $x^{(g)}$ of all (g) is given, after the system interleaver, as in Eq.B.3.

$$\bar{d} = \left[x_1^{(1)}, \cdots, x_1^{(g)}, \cdots, x_2^{(1)}, \cdots, x_2^{(g)}, x_n^{(1)}, \cdots, x_n^{(g)}\right]^T \tag{B.3}$$

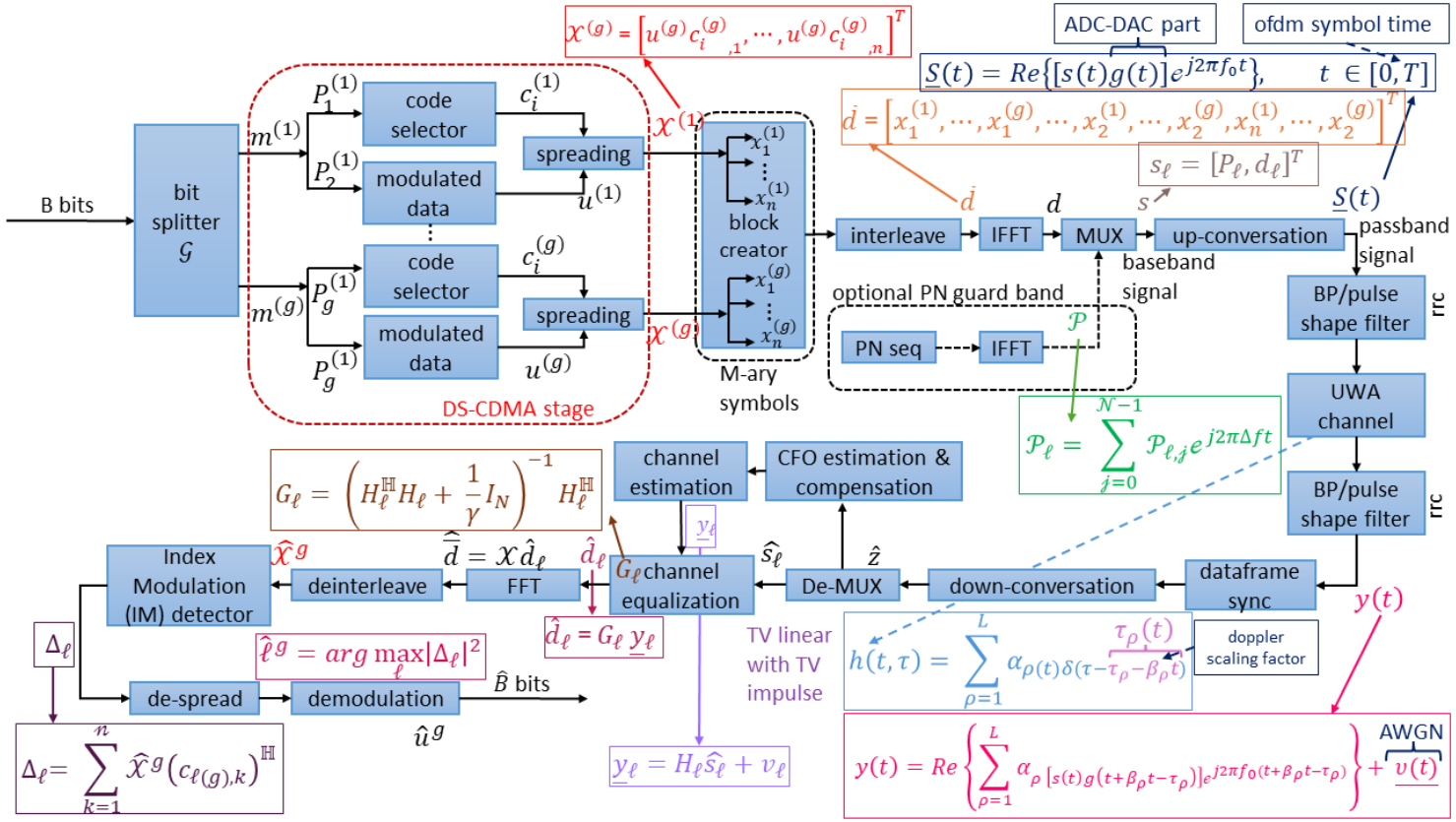

Figure B.1: Thesis underwater communication system / node using software-defined modems, based on [28,80].

This modulated sequence is prepared for the IFFT step which converts it from the frequency domain back to the time domain. Given $\bar{d}$, the IFFT output is denoted d and will be the time domainOFDMsymbol sequence for the insertion of aCP. The IFFT is expressed as in Eq.B.4:

$$d = IFFT\left(\bar{d}\right) \tag{B.4}$$

For the discrete time domainOFDM, the IFFT can be written as in Eq.B.5:

$$d\left[n\right] = \frac{1}{N}\sum_{k=0}^{N-1} \bar{d}_k \bullet e^{2\pi\frac{kn}{N}} \tag{B.5}$$

where $d\left[n\right]$ is the n^{th} sample of the discrete time domainOFDMsignal, n is the sample index and $\frac{1}{N}$ is the usual IFFT normalization. A cyclic prefix (CP) is appended to the OFDM symbol to guard against intersymbol interference (ISI) caused by multi-path propagation. This baseband signal is then upconverted for transmission through the underwater acoustic channel.

A PN sequence can also be added as a guard-band to avoid ISI. The P_ℓ after IFFT can be written as in Eq.B.6:

$$P_\ell = \sum_{j=0}^{\mathcal{N}-1} P_{\ell,j} e^{j2\pi\Delta ft} \tag{B.6}$$

where $\mathcal{N}$ is the PN length and Δf is the frequency spacing. Here, $\mathcal{N} \gg \quad L$ to avoid ISI, where L is the maximum number of underwater channel tap delay. So, at the multiplexer (FigureB.1) shows the signal can be expressed as in Eq.B.7:

$$s_\ell = \left[P_\ell, d_\ell\right]^T \tag{B.7}$$

where s_ℓ is the baseband signal and $N = M\text{x}N$ is the length of the baseband signal. Conventionally, theCPis added to remove the ISI with the advantages of a simpler receiver design that maintains the orthogonality of the sub-carriers. Therefore, Eq.B.7can be re-written as $s_\ell = \left[CP, d_\ell\right]^T$. Then, this up-converted baseband signal to passband can be expressed as in Eq.B.8:

$$\underline{S}(t) = \Re\left\{[s(t)\, g(t)]\, e^{j2\pi f_0 t}\right\}, \quad t \in [0, T] \tag{B.8}$$

where T is the OFDM symbol time, f_0 the carrier frequency, and $g(t)$ the ADC-DAC part. The filtering and pulse shaping are approximated as Eq.B.9:

$$g(t) = \begin{cases} 1, & \text{for } t \in [0, T] \\ 0, & \text{otherwise} \end{cases} \tag{B.9}$$

where root raised cosine (rrc) filters are used at the transmitter and receiver.

B.2 Underwater Channel Model

The underwater channel model is a time-varying linear system with a channel impulse response, as expressed in Eq.B.10:

$$h(t, \tau) = \sum_{\rho=1}^{L} a_\rho(t) \delta(\tau - \tau_\rho(t)) \tag{B.10}$$

where $a_\rho(t)$, $\tau_\rho(t)$, and $\delta(t)$ denote the time-varying amplitudes of path ρ, L multi-path delays, and the Dirac delta function, respectively. Now, every $\tau_\rho(t)$ has a Doppler shift given by Eq.B.11:

$$\tau_\rho(t) = \tau_\rho - \beta_\rho t \tag{B.11}$$

such that β_ρ is the proportional change per unit time in the observed frequency of a wave, due to the motion of the source and observer (the Doppler effect -DSF). Assuming all paths have the sameDSF, the time-varying channel is more completely described with the Doppler scaling factor, to also capture the relative motion between transmitter and receiver. Thus, Eq.B.10is more completely written as in Eq.B.12:

$$h(t, \tau) = \sum_{\rho=1}^{L} a_\rho(t) \delta(\tau - \tau_\rho - \beta_\rho t) \tag{B.12}$$

Algorithm 2: Receiver process

Data: Received passband signal $y(t)$; `/*Received signal with AWGN */`
Result: Recovered B bits
Down-convert the received signal $y(t)$;
Remove the guard interval and apply the FFT to retrieve the transmitted data block d';
Apply the FFT-transform to d' to de-interleave and retrieve the original data block d;
for *each group* g *in* d **do**
    De-spread the received symbols using the corresponding spreading code $i(g)$;
    De-map the symbols to retrieve the original bits $P_2^{(g)}$;
Combine the bits $P_1^{(g)}$ and $P_2^{(g)}$ for each group to reconstruct the original B bits;

B.3 Receiver Structure

The proposed receiver structure (algorithm2) for the underwater acoustic communication system captures the passband signal transmitted through the underwater acoustic channel, which captures multi-path Doppler effects. The passband signal $y(t)$ can be expressed as in Eq.B.13:

$$y(t) = \Re\left\{\sum_{\rho=1}^{L} a_\rho(t)\left[\underline{S}(t)g\left(t+\beta_\rho t-\tau_\rho(t)\right)\right]e^{j2\pi f_0\left(t+\beta_\rho t-\tau_\rho(t)\right)}\right\} + \underline{\upsilon}(t) \tag{B.13}$$

where $\underline{\upsilon}(t)$ is the passband's additive white Gaussian noise (AWGN). Based on Eq.B.13, the signal for each path is scaled in duration by T to approximately $\frac{T}{1+\beta}$, and a Doppler induced frequency shift $e^{j2\pi f_{\mathfrak{n}} t}$ which is experienced for each sub-carrier, where $f_{\mathfrak{n}}$ is the frequency spacing of each sub-carrier.

To mitigate Doppler effects, a custom preamble is sent at the beginning, and/or a post-amble at the end, of every frame for synchronization and to coarsely estimate the DSF. This received signal $y(t)$ is first cross-correlated with known preambles and/or post-ambles to estimate the length of the received signal $\mathcal{B}'$. Then, this estimated DSF can be calculated by comparing the length of the transmitted signal $\mathcal{B}$, which is known a priori, with the estimate in Eq.B.14:

$$\mathcal{B}' = \frac{\mathcal{B}}{\mathcal{B}'} - 1 \tag{B.14}$$

The receiver resamples the received signal at $(1+\mathcal{B}')f_s$, where f_s is the original sampling frequency at the transmitter. For the system, resampling is performed at the passband $y(t)$ to mitigate the DSF. Therefore, small timing errors are introduced in the conversion from the passband to baseband. These errors will be eliminated and compensated via CP inserted between the data and symbols. The received signal is down-converted to baseband and processed to remove the CP. The equalization is performed on the receiver side using an MMSE equalizer [98] expressed as in Eq.B.15:

$$G_\ell = \left(H_\ell^{\mathbb{H}} H_\ell + \frac{1}{\gamma} I_N \right)^{-1} H_\ell^{\mathbb{H}} \tag{B.15}$$

where $\gamma = /\sigma_n^2$ is the signal-to-noise ratio per symbol, H_ℓ the channel matrix, $H_\ell^{\mathbb{H}}$ its Hermitian transpose, and I_N the identity matrix. This is the alternative form of the MMSE equalizer taps for an end-to-end system delay. The signal $\underline{y}_\ell = H_\ell \widehat{s}_\ell + v_\ell$ is passed to the equalizer and the equalizer output $\hat{d}_\ell = G_\ell \underline{y}_\ell$ is then fed to the Fast Fourier Transform (FFT) to convert the signal into the frequency domain for further processing, and $\widehat{\bar{d}}$ is obtained after the FFT block.

The detection of the frequency domain data symbol is given by Eq.B.16:

$$\widehat{\bar{d}} = \mathcal{X} \hat{d}_\ell \tag{B.16}$$

The detected symbol vector in Eq.B.16is equivalent to the interleaved vector (Eq.B.3). The IFFT converts a complex frequency domain signal back to the time domain. This is needed to calculate $\bar{d}$ (Eq.B.3). The output of that is input to the deinterleaver (FigureB.1) to obtain $\widehat{\bar{d}}$ (EqB.16). Finally, apply the Maximum Radio Combining Detector [80] to detect the received information bits.

Every $\hat{\mathcal{X}}^g$ vector from each $\widehat{\bar{d}}_\ell$, of n-length corresponding to subgroup g, is de-spread by all possible spreading codes. The output of the IM detector is an ℓ - length code such that $\ell \in \{1, \cdots, n\}$ as given by Eq.B.17:

$$\Delta_\ell = \sum_{k=1}^{\mathfrak{n}} \hat{\mathcal{X}}^g \left(c_{\ell(g),k}\right)^{\mathbb{H}} \tag{B.17}$$

$P_1^{(g)}$ (Algorithm1) is detected by squaring the maximum absolute value of Δ_ℓ which is the output of the de-spreading operation (Eq.B.18):

$$\hat{\ell}^{(g)} = \arg\max_{\ell} |\Delta_\ell|^2. \tag{B.18}$$

Similarly, glsp2g (Algorithm1) can be detected using the same process as $P_1^{(g)}$. Then, $\hat{u}^g$ must be demodulated for the g^{th} group, to recover the original data bit, B.

B.4 Operational summary of the communication system

This section summarizes the communication system's operation, linking the mathematical models and algorithms described earlier to their practical implementation. Figure B.2shows the signal flow for the operations, while the enumerated list, below, details the corresponding mathematical equations.

1.spreading and modulation: $x^{(g)} = \left[s^{(g)} \bullet c_{i(g)}\right]^T$

2.OFDM symbol generation: $\widetilde{d} = IFFT\left(x^{(g)}\right)$

3.CP insertion and up-conversion:
$s = \mathrm{CP}_{\mathrm{insert}}\left(\widetilde{d}\right)$
$S(t) = \Re\left\{s(t) \bullet g(t) \bullet e^{2\pi f_c t}\right\}$

4.received signal processing:
$y(t) = downconvert\left(y(t)\right)$; and $\widetilde{r} = FFT\left(\mathrm{CP}_{\mathrm{remove}}\left(y(t)\right)\right)$

5.de-spreading and demodulation: $\hat{S}^{(g)} = \widetilde{r} \bullet c_{i(g)}^T$

6.channel estimation and compensation:
$\hat{h} = channelestimation\left(\widetilde{r}\right)$; and $\widetilde{r}_{equalized} = equalize\left(\widetilde{r}, \hat{h}\right)$

7.data retrieval: $B = \left(\widehat{P_1^{(g)}}, \widehat{P_2^{(g)}}, \cdots, \widehat{P_2^{(g)}}\right)$

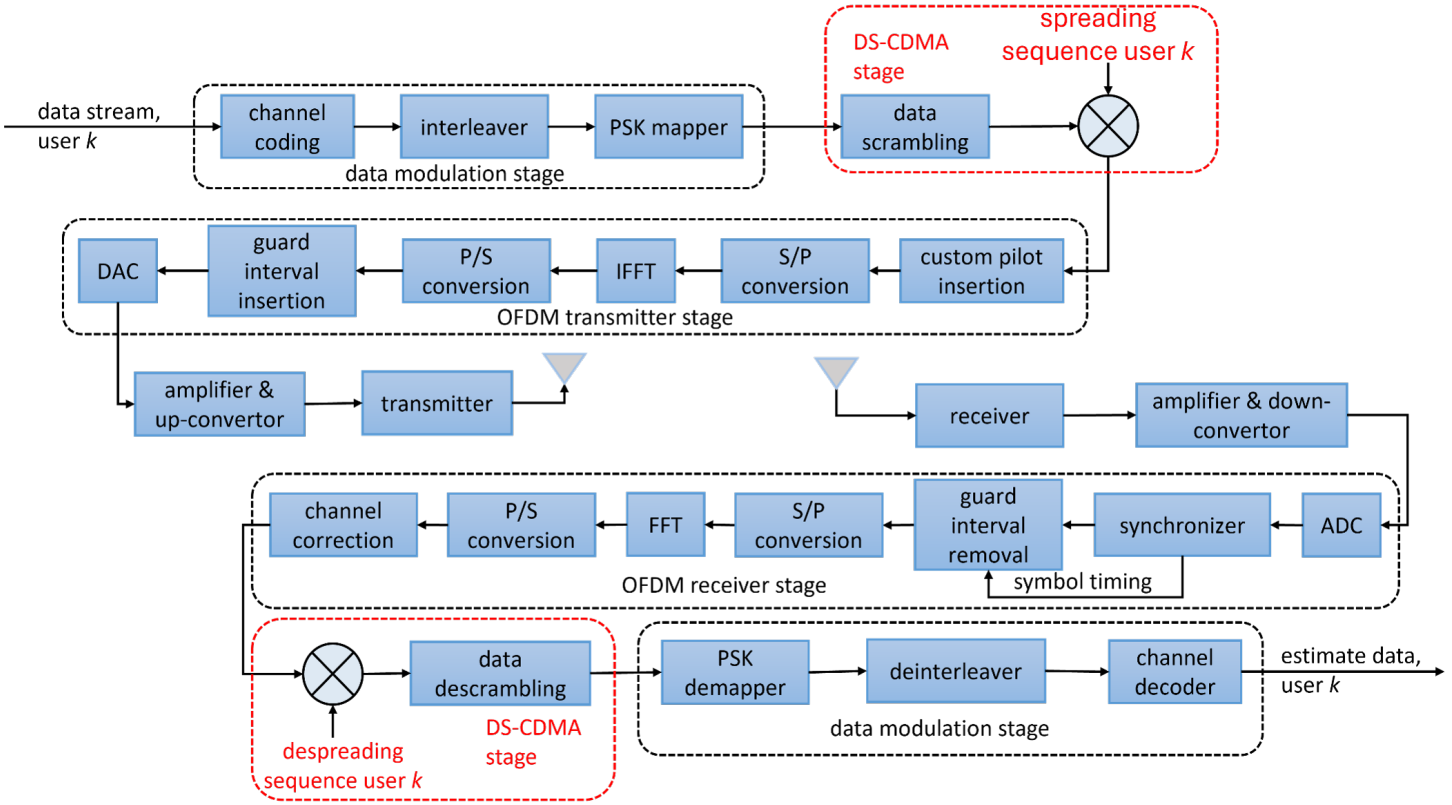

Figure B.2: Operational signal flow of the proposed hybrid OFDM-CDMA communication system, based on [28,80].

In the previous sections, the background was laid out for the mathematical models and algorithms that describe the proposed OFDM-CDMA communication system. As the focus shifts from these foundational aspects, it is important for the rationale behind the choice of the hybrid OFDM-CDMA solution to be contextualized. Attention now turns to the unique and harsh environment that is the underwater acoustic channel — a domain which challenges conventional systems in general. This sub-section aims to unravel these complexities and pave the way for a solution that is both innovative and pragmatic.

B.5 Challenges of CDMA in Underwater Acoustics

While CDMA is established for above-water channels, and confers many advantages, this is not the case for the underwater acoustic channel. For the same CDMA benefits in underwater acoustic channels, unaddressed challenges need solutions.

TableB.1summarizes these CDMA challenges when implemented underwater and motivate a solution beyond the basic CDMA.

The unique characteristics of the underwater acoustic channel, compared to above-water ones, means the application of conventional communication methods will not work. These characteristics are briefly presented next.

1. Signal propagation is affected by the variable temperature gradients, salinity, and depth, in contrast to above-water environments.

2. Multi-path propagation introduces delayed signal versions in the channel, complicating the detection and decoding efforts.

3. Doppler shifts, arising from relative motion between transmitter and receiver due to water currents, disrupt synchronization.

4. Bandwidth is limited due to frequency dependent attenuation which means signal carrier frequencies, and consequently bandwidth, are low (order of 10's of kHz). This demands efficient utilization strategies for the available bandwidth.

5. High ambient noise from anthropogenic and natural underwater activities reduces the operational signal-to-noise ratio.

These characteristics drive the requirement for a robust and adaptable communication strategy, one that builds on the established above-water CDMA towards more resilient architectures.

Table B.1: Underwater acoustic signal propagation challenges and CDMA approaches that justify its selection as the multiple access class to pursue in this thesis.

aspect	underwater acoustics challenge	CDMA approach	addressed in thesis
signal propagation	**Variable sound speed** due to conductivity, temperature, and water depth, propagates signals quite differently than in air.	**CDMA adaptation for underwater use:** inherent resistance to multi-path interference and support for multiple users without frequency division.	✓
multi-path propagation & delay spread	Significant effects from **signal reflections** due to sea surface and bottom, creating multiple delayed signal versions in the channel.	**Orthogonal-frequency division multiplexing (OFDM):** inherently handles multi-path effects through increase symbol timing.	✓
Doppler shifts	Caused by relative motion between transmitter and receiver which impacts **synchronization and signal demodulation**.	**Signal processing:** Mitigates issues like Doppler shifts through pilots which enhances CDMA's effectiveness.	✓
multi-user interference (MUI)	**Overlapping signals from multiple users** can lead to signal degradation, a challenge exacerbated by the underwater environment's dynamics.	**Error-correcting codes & advanced techniques:** Powerful error-correcting codes (e.g., LDPC, Turbo) and advanced multiple access techniques (e.g., OFDMA, NOMA) mitigate MUI effects.	✓
bandwidth limitation	**Limited bandwidth** due to frequency and range-dependent attenuation, challenges CDMA's spread-spectrum requirement for more bandwidth.	**Physical layer adaptations**: Adaptive modulation schemes and power control improves performance (e.g., hybrid CDMA).	✓
ambient noise	**Unique underwater noise problem**, due to natural and anthropogenic activities which degrade detection more than in above-water channels.	**Integration with other methods:** Combining CDMA with MIMO or sophisticated error correction codes to enhance performance.	×
near-far problem	**Signals from closer transmitters overwhelm farther ones**, due to range-dependent attenuation, which complicates signal detection.	**Power control mechanisms:** Advanced power control and management ensures signals arrive at the receiver with similar power levels, mitigating the near-far problem (i.e., RSSI-based system).	×

B.6 Introduction to Hybrid OFDM-CDMA

The hybrid OFDM-CDMA multiple access solution has shown potential [80] to address some of the TableB.1challenges.

B.6.1 Advantages of Hybrid OFDM-CDMA

The hybrid OFDM-CDMA multiple access protocol has the following strengths for underwater acoustic signal transmission at the cost of some complexity.

1.CDMA is inherently resistant to multi-path interference as it artificially spreads the signal over a larger bandwidth than the signal requires. Therefore, only a small part of the actual transmitted signal suffers fading at any given time.

2.Integration of OFDM mitigates multi-path effects through the use of a cyclic prefix (zero-padding) between consecutive OFDM symbols. This prevents the inter-symbol interference that occurs from multi-path.

The benefit of the hybrid OFDM-CDMA solution is summarized in TableB.1which shows how the challenges are addressed by OFDM-CDMA.

B.6.2 Hybrid OFDM-CDMA System Justification

The justification for the proposed hybrid OFDM-CDMA system are presented next.

1.The structure of the hybrid system adeptly uses the sparse bandwidth by distributing data across multiple sub-carriers to ensure optimal usage.

2.The hybrid system is resilient to the omnipresent noise through its inherent de-spreading to maintain the same SNR.

The benefits of the hybrid OFDM-CDMA solution, relative to other modulation ones, are summarized in TableB.2with the performance evaluated against multiple criteria. This justifies the hybrid OFDM-CDMA MAC pursued in this thesis.

B.6.3 Consolidation and Justification for the Selection of Hybrid OFDM-CDMA

To this point, the hybrid OFDM-CDMA system's theoretical basis and architecture were described and the technical merits were evaluated.

In the chapters preceding this appendix, the technical merits of the hybrid system were established, and attention accorded to the empirical verification of these merits. It was demonstrated, through analysis and experimentation, that the hybrid OFDM-CDMA system outperforms standard modulation solutions for the dynamic underwater environment.

Thus, the rationale for selecting the hybrid system is two-fold: firstly, it is rooted in theoretical rigour critically evaluated within the main thesis sections. Secondly, and most compellingly, it is the empirical evidence, presented through systematic in-water testing and analysis, that verifies the system's operational feasibility and scalability.

The detailed methodology, comprehensive experimentation, and results, which are presented in Chapters3,4, and5, serve to reinforce the choice of the hybrid OFDM-CDMA system. These sections collectively provide the argument for the developed OFDM-CDMA modulation solution.

This appendix, therefore, complements and explains the connection between the theoretical constructs and their practical execution as detailed in the thesis body. It is not intended to replicate the empirical data in their entirety but to guide the reader to where these can be found and how they substantiate the assertions made.

Consequently, the justification for the hybrid system is not solely based on the theoretical concepts formulated but also on the benefits shown. It integrates simulations and empirical verification to consolidate the argument for the hybrid OFDM-CDMA system as one that fulfills the thesis objective.

Table B.2: Comparison of direct-sequence spread spectrum (DSSS) with other modulation techniques against several underwater communication performance metrics

feature/ aspect	**BPSK with DSSS**	**QPSK with DSSS**	**hybrid OFDM-DSSS with QPSK**
spectral efficiency	Lower compared to QPSK. Transmits 1 bit per symbol.	Higher compared to BPSK. Transmits 2 bits per symbol, effectively doubling the data rate for the same bandwidth.	Further improved with OFDM which. uses multiple sub-carriers allowing for high data rates and thus more efficient bandwidth use.
BER performance	Comparable to QPSK with AWGN channels for given Eb/N0.	Comparable to BPSK with AWGN channels for a given Eb/N0, despite transmitting more data. .	Enhanced from combination of OFDM and DSSS, which improves signal robustness and leads to potentially better BER given appropriate coding.
bandwidth usage	Requires more bandwidth to achieve the same data rate as QPSK.	More efficient bandwidth usage, achieving higher data rates within the same bandwidth as BPSK.	Optimal bandwidth usage from OFDM. The system can adapt to channel conditions & allocate bits accordingly across sub-carriers.
complexity	Simpler to implement & demodulate due it being binary.	Slightly more complex as it must distinguish between 4 phase shifts. This complexity is manageable.	Higher complexity from DSSS and OFDM integration and thus, requires more signal processing for FFT/IFFT, synchronization & channel estimation.
power efficiency	Efficient for low data rate transmissions.	More efficient for higher data rates given the same bandwidth, considering the same BER levels.	Potentially more efficient from adaptive sub-carrier allocations and the ability to concentrate energy where most needed but requires careful design.
resilience	To noise and interference due to DSSS processing gain.	To noise and interference due to DSSS processing gain, with added advantage of higher data throughput.	Exceptionally so to noise from combination of DSSS and OFDM. Offers strong resistance to multi-path interference and frequency-selective fading.

feature/ aspect	BPSK with DSSS	QPSK with DSSS	hybrid OFDM-DSSS with QPSK
system design	Simpler system design, especially beneficial in noise-limited scenarios.	Requires more care for phase synchronization and symbol distinction but benefits from higher throughput.	More complex due to integration of DSSS & OFDM. Can customize to highly variable and dynamic channel conditions.
advantages	Simplicity and robustness, Lower complexity leads to potentially lower cost in simpler systems.	Higher spectral efficiency, better utilization of bandwidth, suitable for higher data rate applications without increasing bandwidth.	Maximum spectral efficiency and data rates. Adaptive to channel conditions. Robust against a wide range of interferences & fading. Suitable for high multi-path environments.
disadvantages	Lower spectral efficiency. Not as suitable for bandwidth-constrained applications requiring high data rates.	Increased complexity due to the need for accurate phase recovery. Potentially more susceptible to phase noise & synchronization issues.	Higher complexity and computational demands. Requires more sophisticated hardware & signal processing. Synchronization & channel estimation may be challenging.

B.7 Verification of Full-Duplex Communications

In underwater communication systems, the ability to operate in full-duplex mode - i.e., simultaneously transmit and receive signals in a channel, is advantageous for efficient and continuous data exchange - when necessary and possible. This section presents an analysis to show full-duplex operation of the Subnero underwater modems using the Unetstack framework. To illustrate full-duplex capabilities with UnetStack on the Subnero modem, the UnetAudio interface is used. UnetAudio emulates the modem's behavior, serving as a proxy to demonstrate the operational parallels in UnetStack's full-duplex communications (section 15.4 of [93]).

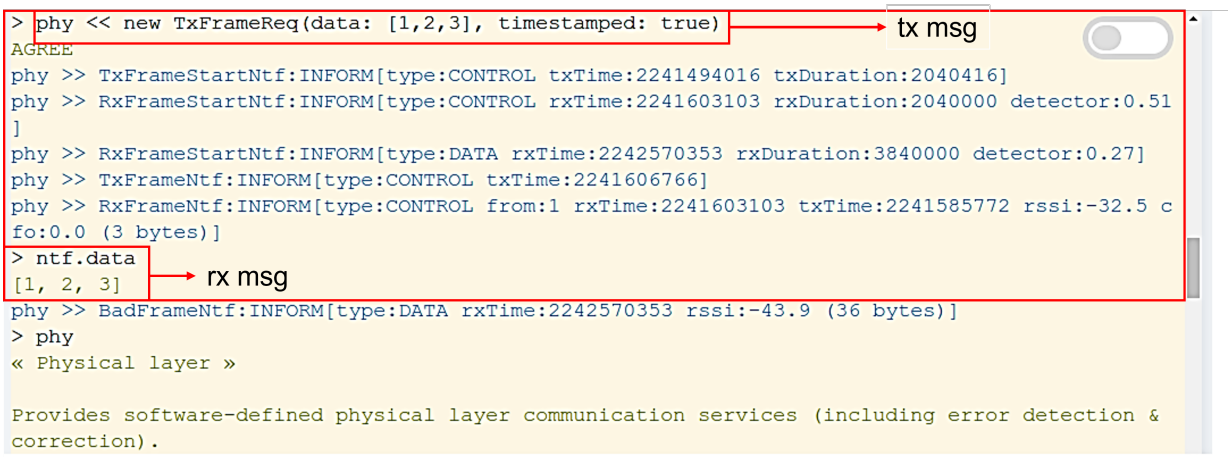

Figure B.3: Event logs from the UnetStack-based communication framework demonstrating full-duplex operations. The screenshot captures a mission sequence where a transmission request (*TxFrameReq*) with data [1,2,3] is timestamped, followed by notifications of *control* type transmission start (*TxFrameStartNtf*) and reception start (*RxFrameStartNtf*) for *control* and *data* types, with respective timestamps and durations indicating concurrent activity. The reception message (*ntf.data*) confirms the successful receipt of the transmitted data, verifying the system's full-duplex functionality.

To verify full-duplex communications, one must show transmission (Tx) and reception (Rx) can occur concurrently (FigureB.3). One way is to show there is an overlap in transmission and reception epochs. For example, the modem provides notifications of transmission start (*TxFrameStartNtf*) and end (*TxFrameNtf*), alongside corresponding notifications for reception start (*RxFrameStartNtf*) and end (*RxFrameNtf*). By examining the timestamps and duration of these events, one should see an overlap between the

transmission and reception epochs which indicates full-duplex operations.

An example for a typical notification in an experiment is shown in the screen capture of the modem signals the start of a data frame transmission (*TxFrameStartNtf*) with a *txTime* and a *txDuration*. Within that interval, the modem signals the start and end of data frame reception (*RxFrameStartNtf* and *RxFrameNtf*), annotated with *rxTime* and *rxDuration*. For full-duplex operation, the *txTime* plus *txDuration* must overlap with *rxTime* and *rxDuration*. This overlap was observed in the collected data, where *txTime* was recorded before the end of *rxTime rxDuration*, and vice versa, thereby demonstrating the concurrent transmission and reception.

B.7.1 Full-Duplex visualization

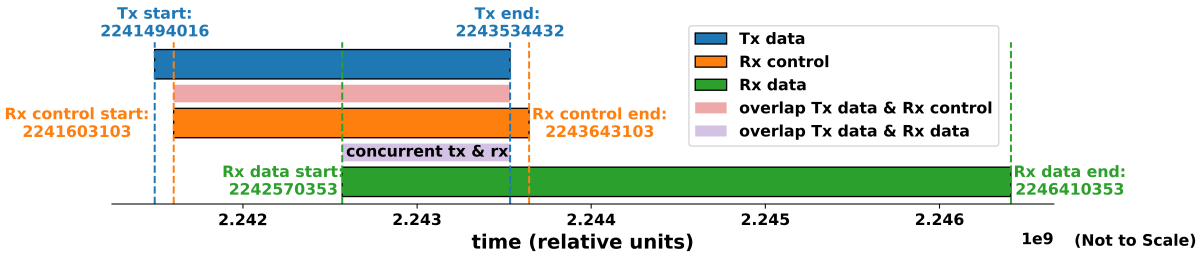

Figure B.4: Timing diagram of transmission and reception notifications for an experiment (times are in seconds since January 1, 1970 at midnight UTC) that show full-duplex operation with the overlap interval shown (in pink).

FigureB.4presents a timing diagram that visually shows full-duplex communication. The overlapping of the Tx and Rx periods, as denoted by the concurrent shaded area in pink, provides a clear visual representation of the modem's ability to perform simultaneous transmission and reception tasks.

The representation of time within the UnetStack framework, Unix epoch time, traditionally defined in seconds, is utilized in UnetStack for operations such as 1.hour.later and 2.minutes.later, which outputs a long integer representing the number of seconds since January 1, 1970, at midnight UTC (section 15.4 of [93]).

However, UnetStack also employs time in milliseconds for most Java and fjåge API calls [37], such as current TimeMillis(), WakerBehavior(), and TickerBehavior(). This granularity is further extended to microseconds for specific parameters within the physical

layer service, notably including time parameters such as *rxTime*, *recTime*, and *txTime*, as well as the synchronization time offset within the ranging agent service.

Given the use of microseconds for the physical layer service's time parameters in UnetStack, the *txTime* and *rxTime* are indicative of the precise moments of transmission and reception commencement, respectively. The fact that *txTime* preceded the end of the reception window, and *rxTime* occurred before the end of the transmission window, confirms the overlap. The timing diagram supports the conclusion of full-duplex operation within the UnetStack framework.

This distinction between seconds, milliseconds, and microseconds is of course important to interpret the timestamps and durations involved in transmission and reception events. It ensures the overlap is accurately calculated. However, the timings indicated in FigureB.4 do not require an the absolute time scale to confirm full-duplex operations.

Appendix C

Detailed examples of CDMA inUW-ASNs

As a continuation of the discussions presented in Chapter2, this appendix, is provided for a comprehensive exploration of CDMA technology, which is tailored specifically to the realm of underwater communication. Here, both theoretical concepts and practical implementations of CDMA are delved into, with the aim of bridging the gap between abstract understanding and real-world application being pursued. Through a series of examples, it is illustrated how CDMA facilitates secure, efficient communication in a shared underwater environment, with the inherent challenges posed by such a medium being addressed. Serving as an extension of the foundational knowledge presented in Chapter2, this appendix offers readers an enriched perspective on the potential of CDMA technology in enhancing marine communication systems.

C.1 Theoretic example

For this example, three users, A, B, and C, communicate with the same base station receiver/surface node/USV(R). The nodes' codes are shown below.

$$\begin{aligned}\mathbf{c_A} &= [\mathbf{1}, -\mathbf{1}, -\mathbf{1}, \mathbf{1}, -\mathbf{1}, \mathbf{1}]\text{user A}\\ \mathbf{c_B} &= [\mathbf{1}, \mathbf{1}, -\mathbf{1}, -\mathbf{1}, \mathbf{1}, \mathbf{1}]\text{user B}\\ \mathbf{c_C} &= [\mathbf{1}, \mathbf{1}, -\mathbf{1}, \mathbf{1}, \mathbf{1}, -\mathbf{1}].\text{user C}\end{aligned}$$

AssumeUUV A needs to communicate with surface node R, and the surface node R

is aware ofUUV A's code. For simplicity, assume the communication is synchronized, enabling the base station to know when to look for the codes. When A transmits a 1-bit, it sends its code as a chip pattern $[1, -1, -1, 1, -1, 1]$. Conversely, when A transmits a 0-bit, it transmits the complement of its code (the 1's and -1's reversed): $[-1, 1, 1, -1, 1, -1]$. At the base station, the receiver decodes these chip patterns.

In this simple example, if receiver R receives a chip pattern, $d = [d_1, d_2, d_3, d_4, d_5, d_6]$, and it intends to communicate with user u and knows u's code, $[c_1, c_2, c_3, c_4, c_5, c_6]$, the receiver performs the following electronic decoding function:

$$S_u(d) = d_1 \times c_1 + d_2 \times c_2 + d_3 \times c_3 + d_4 \times c_4 + d_5 \times c_5 + d_6 \times c_6.$$

where subscript u on S indicates the decoding function for user u.

Suppose user u is A and it sends a 1-bit, resulting in $d = [1, -1, -1, 1, -1, 1]$, the computation using S_A becomes:

$$\begin{aligned} S_A(1, -1, -1, 1, -1, 1) = (1 \times 1) + ((-1) \times (-1)) + ((-1) \times (-1)) \\ +(1 \times 1) + ((-1) \times (-1)) + (1 \times 1) = 6. \end{aligned}$$

If A sends a **0-bit**, which corresponds to $d = [-1, 1, 1, -1, 1, -1]$, the result is:

$$\begin{aligned} S_A(-1, 1, 1, -1, 1, -1) = (-1 \times 1) + (1 \times (-1)) + (1 \times (-1)) \\ (+((-1) \times 1) + (1 \times (-1)) + ((-1) \times 1) = -6. \end{aligned}$$

No matter the sequence of -1's and 1's in d, $S_A(d)$ will always fall within the range $-6 \leq S_A(d) \leq 6$. Moreover, the extreme values of 6 and -6 only occur when d is either A's code or its complement, respectively.

So. if S_A produces a $+6$ then 1 bit was received fromUUV A; if S_A produces a -6 then 0-bit was received fromUUVA; otherwise, assume another transmitter is sending information or there is an error. For example ifUUV B sends a 1-bit and it is received

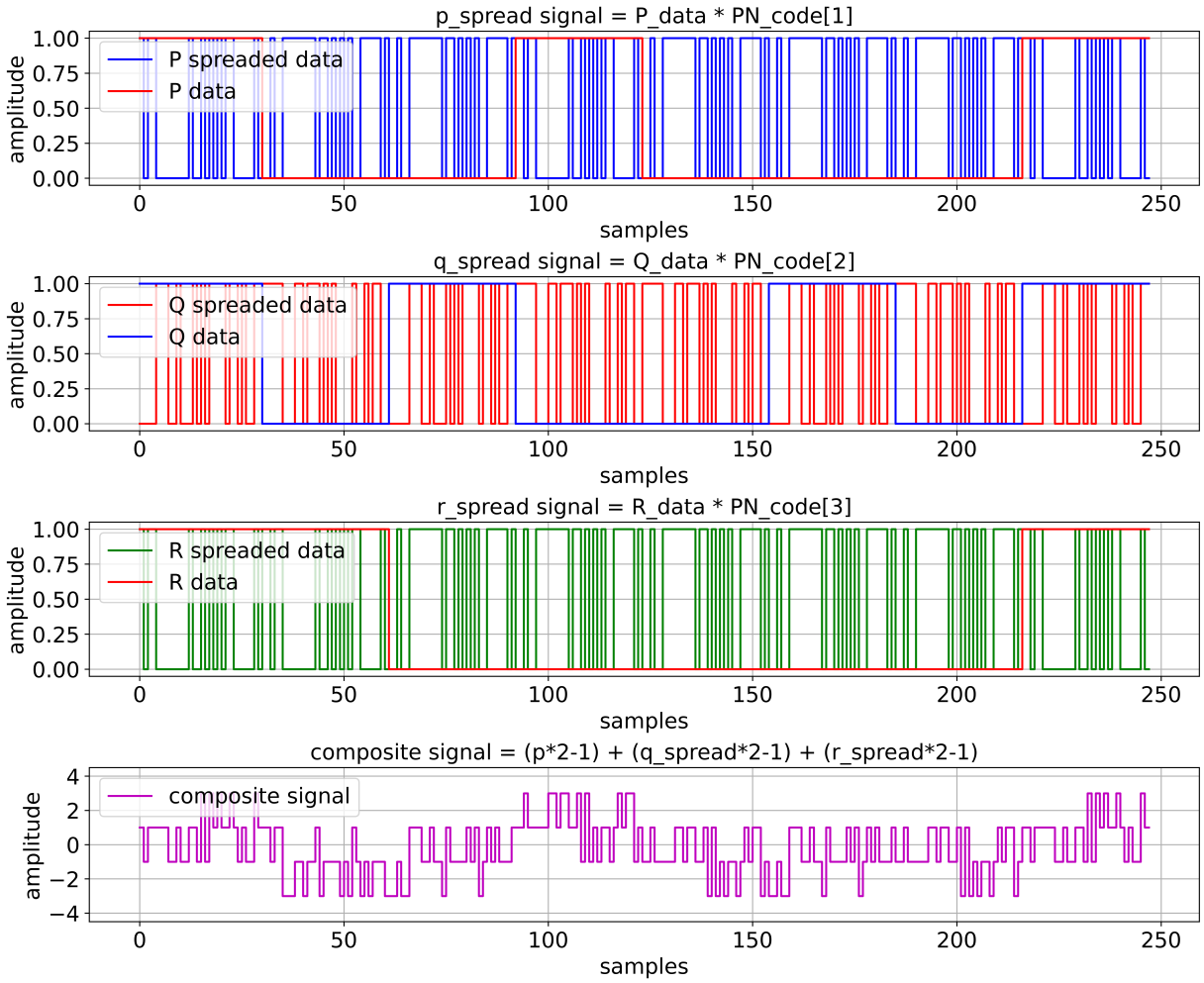

Figure C.1: Illustration of the CDMA signal generation and spreading process for three users. Each subplot shows the original data signal of a user and the result of spreading this signal with a unique PN code (in blue, red, and green for users p, q, and r, respectively). The fourth subplot shows the composite signal (in magenta), which is the sum of the spread signals of all three users.

with S_A, d becomes $[1, 1, -1, -1, 1, 1]$ and

$$S_A(1, -1, -1, 1, -1, 1) = (1 \times 1) + (1 \times (-1)) + ((-1) \times (-1)) \\ +((-1) \times 1) + (1 \times (-1)) + (1 \times 1) = 0.$$

Thus, the unwanted signal (from B) does not appear at all. It is easy to verify that if B had sent a 0-bit, the decoder would produce a value of 0 for S_A again. This means that if the decoder is linear and if A and B transmit signals S_A and S_B, respectively, at the same time, then $S_A(S_A + S_B) = S_A(S_A) + S_A(S_B) = S_A(S_A)$ since the decoder ignores B when using A's code. The codes of A and B that have the property, $S_A(c_B) = S_B(c_A) = 0$, are said to be orthogonal. Such codes are good but there are only a few of them with respect to the total combinations of 1's and -1's for the chip length.

C.2 Direct-Sequence Spread Spectrum (DSSS) Systems

In DSSS, a narrow-band signal containing a message of bandwidth – B_1 multiplied B_2, which is a signal with a larger bandwidth, also known as spreading signal.This signal has the essential features of DSSS in that:

- theBWof the spreading signal/composite signal is greater than theBWof the actual information signal B_1, and
- the spreading signal is independent of the information signal.

Consider an information/data signal $b(t)$ composed of a sequence of symbols, b_j, each of duration T_s. The data signal is given by Eq.C.1:

$$b(t) = \sum_{j=-\infty}^{\infty} b_j \Psi \left(\frac{t - jT_s}{T_s} \right) \tag{C.1}$$

where $\Psi(t/T)$ is the unit pulse function used in the baseband representation of the CDMA signal is defined by Eq.C.2:

$$\Psi(t/T) = \begin{cases} 1 & \text{for} \quad 0 \leq t < T \\ 0 & \text{for} \quad \text{otherwise.} \end{cases} \tag{C.2}$$

This signal is multiplied by a spreading sequence $a(t)$, is defined by Eq.C.3, composed

of an orthogonal sequence of chips, where a_i are the elements of the spreading code:

$$a(t)= \sum_{j=-\infty}^{\infty} \sum_{i=0}^{\mathcal{M}-1} a_i \Psi \left(\frac{t-(i+j\mathcal{M})T_c}{T_c} \right) \quad |a_i| = 1 \tag{C.3}$$

where T_c is the chip period, and $\mathcal{M}$ is the number of PN symbols in the sequence before the sequence repeats. It is noted that the chips spread and identify the signal, whereas the data symbols convey the actual information.

The multiplied signal, $a(t) \times b(t)$, is up-converted signal $s(t)$, given by Eq.C.4to a carrier frequency f_c as follows:

$$s(t)= b(t)\cos \omega_c t \tag{C.4}$$

For analysis purposes, the channel is ideal and the signal quality is not compromised so the received signal, $r(t)$ is given by Eq.C.5, is a weighted version of the transmitted signal with additive zero-mean white Gaussian noise, $\eta(t)$:

$$r(t)= As(t)+ \eta(t) \simeq Aa(t)b(t)\cos \omega_c t + \eta(t) \tag{C.5}$$

At the receiver, a local replica of the chip sequence, $a(t-\tau_0)$, is generated, where τ_0 is a random time offset between 0 and $\mathcal{M}T_c$, where $\mathcal{M}$ represents the number of PN symbols in the sequence before the sequence repeats. To de-spread the signal at the receiver, the local chip sequence must be delay-locked with the received signal. This means the timing offset, τ_0, must be set to zero.phase locked loop (PLL), can track the phase of a signal even if it changes over time, may be used to create a replica of the carrier, $\cos \omega_c t$. Using these two quantities, a decision statistic, Z_j calculated using Eq.C.6, is formed from multiplying the received signal by the local PN sequence and the local oscillator and integrating the result over one data symbol, according to calculation shown in the [55],

$$Z_j = Ab_j \left(\frac{T_s}{2} + \frac{1}{4\omega_c}(\sin 2\omega_c(j+1)T_s - \sin 2\omega_c jT_s) \right) + \tag{C.6}$$

Therefore, the energy per symbol of the signal component of the decision statistic, E_s, can be written as Eq.C.7,

$$E_s = \frac{A^2 {T_s}^2}{4}. \tag{C.7}$$

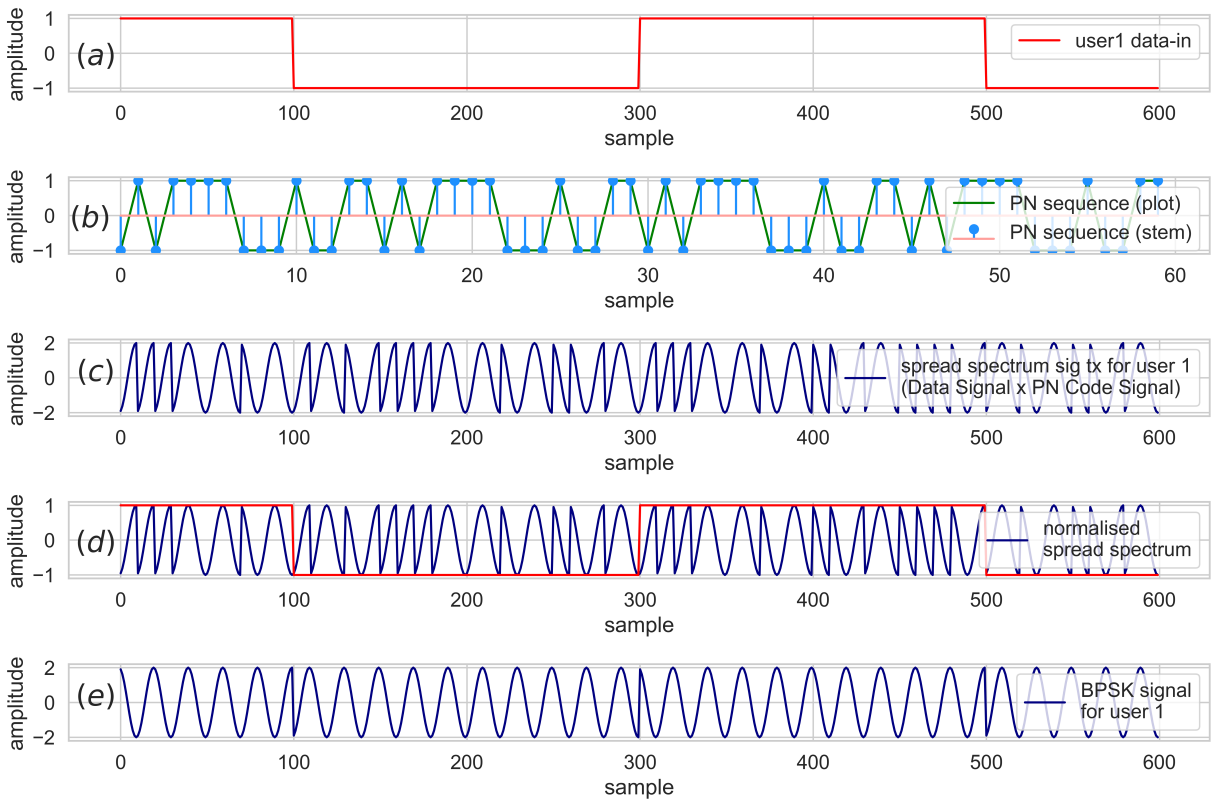

Figure C.2: This illustrates the process of generating a Binary Phase Shift Keying (BPSK) modulated Direct-Sequence Code Division Multiple Access (DS-CDMA) signal, (a) demonstrates the transformation of User 1's binary data. (b) presents the pseudo-random number (PN) sequence used for spreading. (c) represents the spread spectrum signal obtained by modulating the input data with the PN sequence. (d) The figure also highlights the comparison between the original data, the resultant spread spectrum signal, and the normalized spread spectrum signal. Finally, (e) it presents the original BPSK signal used for User 1. This visual representation provides a comprehensive view of the DS-CDMA technology, showcasing its ability to efficiently allow multiple users to coexist within the same bandwidth.

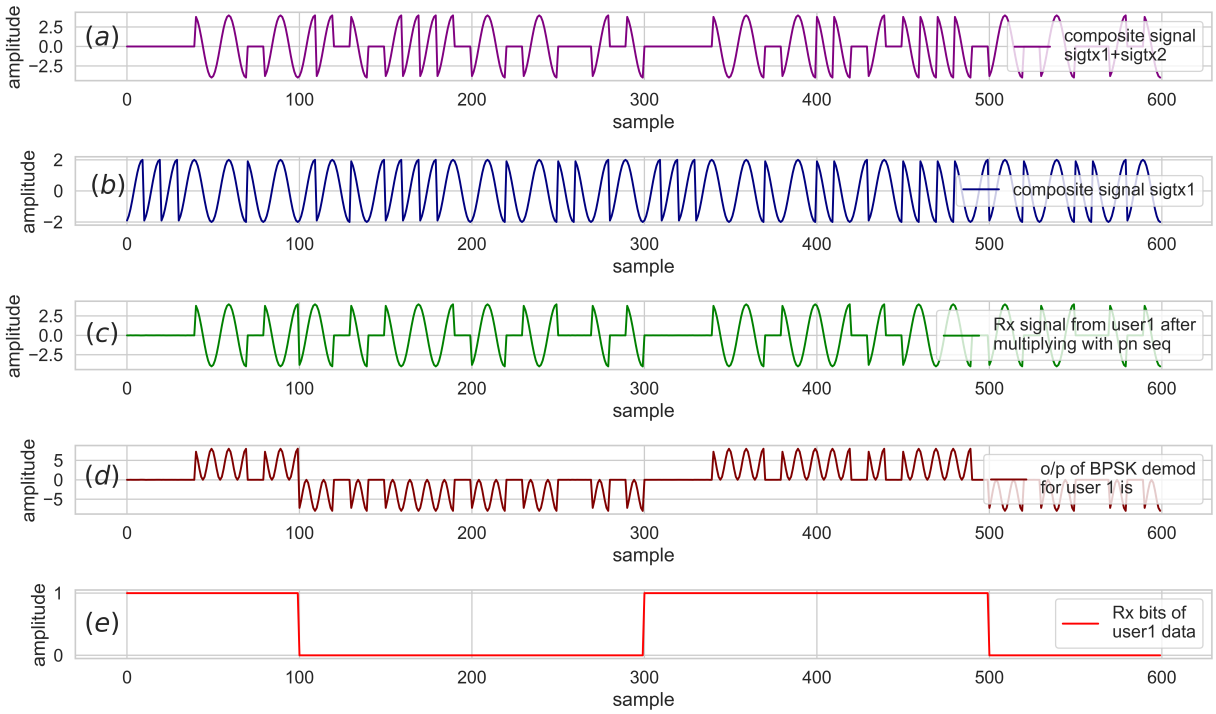

Figure C.3: Illustration the recovery process of a BPSK modulated DS-CDMA signal for User 1. (a) depicts the composite signal ($sigtx_1 + sigtx_2$), showing how signals from different users are combined in a DS-CDMA system. (b) isolates the sigtx1 component of the composite signal for comparison. (c) presents the received signal (rx_1) after multiplying with the PN sequence, representing the step of despreading in DS-CDMA. (d) shows the output of BPSK demodulation for User 1, highlighting the final stage of signal recovery. Finally, (e) displays the received bits ($rxbits_1$) of User 1 data, demonstrating the successful extraction of the original data. This step-by-step visualization provides a comprehensive understanding of DS-CDMA technology, showcasing its signal recovery process.

Assume transmitted symbols b_j are from a binary symbol set such that $b_j \in \{-1, 1\}$. Then, the energy per symbol, E_s, inC.7is the same as the energy per bit,. The bit error rate, P_e calculated using Eq.C.8, at the output of the matched filter receiver is given by:

$$P_e = Q\left(\sqrt{\frac{2}{N_0}}\right) \tag{C.8}$$

where $Q(x)$ is the standard Q-function, is the rate at which errors occur in a communication system, derived in Appendix B of [55] and N_0 represents the noise power per unit bandwidth and is typically expressed in units of watts per hertz ($\frac{W}{Hz}$) or decibels relative to one milliwatt per hertz ($\frac{dBm}{Hz}$). This bit error rate (P_e) as inC.8is the case with no spreading. Note, there is significant difference between Eq.C.7and Eq.C.8.

- the original signal is spread over a largerBWfor the same total power, the spectrum density of the signal can be very small makes it difficult for an eavesdropper to detect the signal. This is referred to aslow probability of detection (LPD),
- if there is no prior information about the PN sequence used, then it will be difficult to extract the information signal from the received signal. This is referred to aslow probability of interception (LPI).

CDMAmodulation is a special case of DSSS where the applied PN codes spread the data spectral content with the special properties discussed in2.1.3(Figure2.4). The binary data signal $m(t)$ is first multiplied by the high rate code sequence to acquire the energy spreading. The baseband signal $S_n(t)$, represented by Eq.C.9, is filtered to confine energy within the bandwidth defined by the code rate. The carrier modulation commonly used in spread spectrum is phase-shift keying (FigureC.4),

$$S_n(t) = m(t) \cdot C(t) \tag{C.9}$$

The baseband signal $S_n(t)$ is convolved with the impulse response of the spectrum-shaping filter $h(t)$ to yield $y(t)$ given by EqC.10:

$$y(t) = S_n(t) * h(t) \quad \text{where } * \text{ denotes convolution.} \tag{C.10}$$

Then, the bandpass signal $S_s(t)$, represented by Eq.C.11, becomes,

$$S_s(t) = [\, S_n(t) * h(t)] \cdot \cos S_s(t)t. \tag{C.11}$$

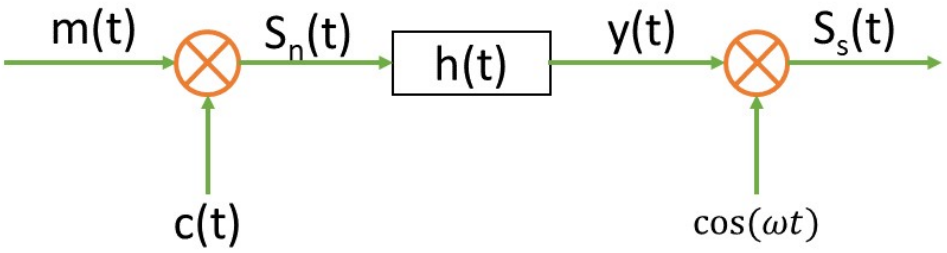

Figure C.4: Direct sequence spread-spectrum modulation system

The matched filter receiver is shown in Figure (C.5). The received bandpass signal $S_s(t)$ is converted to an equivalent complex lowpass signal $h_c(t)$ by mixing with a locally generated coherent carrier. The lowpass spread spectrum caused to collapse by multiplying $h_c(t)$ with a locally generated in-phase copy of the transmitted code sequence. The de-spread signal $B(t)$ is matched filtered and sampled.

The complex low-pass signal, represented by Eq.C.12, is given as:

$$h_c(t) = S_s(t) \cdot \cos S_s(t)t \tag{C.12}$$

The de-spread signal, represented by Eq.C.13, is recovered by:

$$B(t) = A(t) \cdot [C(t) * h(t)] \tag{C.13}$$

Finally, the output of the matched filter, represented by Eq.C.14, is given by:

$$D(T) = \int_{(K-1)}^{KT} [B(t) \cdot dt] \tag{C.14}$$

where K represents a positive integer value that denotes the symbol period or the number of symbols over which the integration is performed. It signifies the duration of the decision interval in terms of symbol periods and T represents the symbol duration, which is the time duration associated with each symbol in the communication system. It defines the interval of time over which the integration is conducted. The receiver decodes the data with this pattern: if $D(T) > 0$ then it decodes the binary **1** otherwise it decodes binary **0** [10].

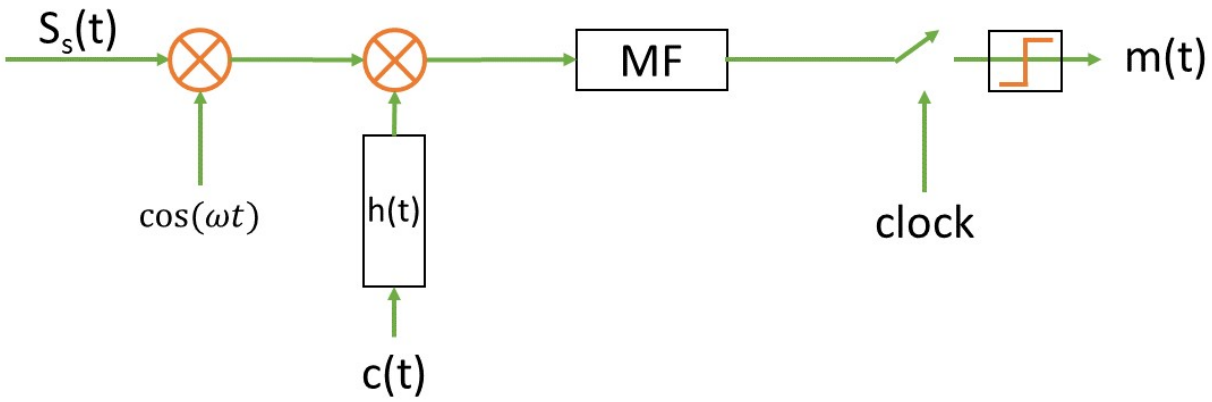

Figure C.5: Matched filter spread-spectrum receiver

C.2.1 The common receiver architecture and demodulation techniques inCDMAsystems

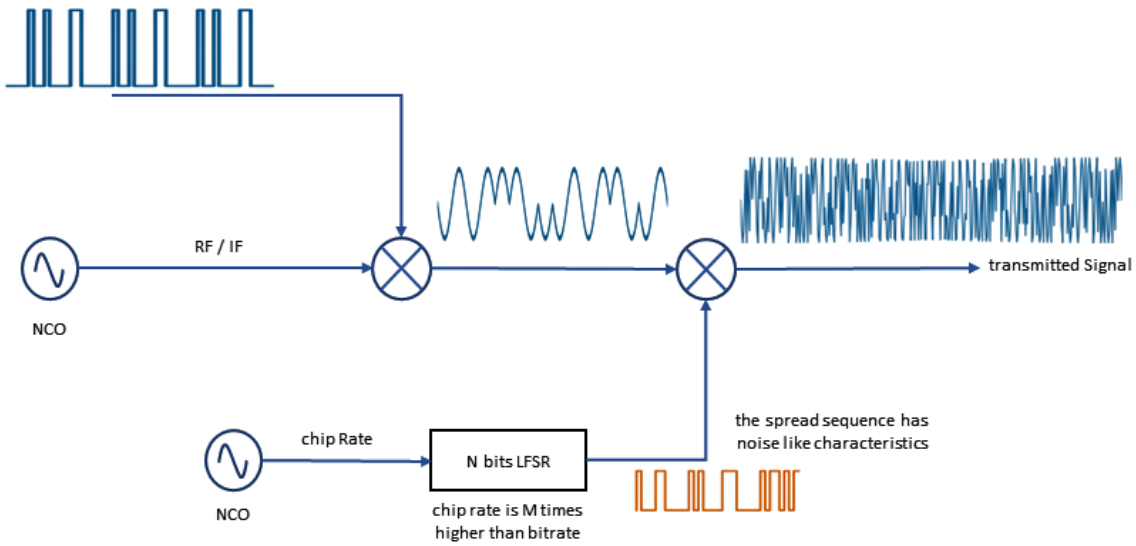

Figure C.6: CDMA BPSK Modulator

The modulation (FigureC.6), RF signal generator generates signal from the data bits and the bit string swaps theRForIntermediate frequency (IF)signal and theBPSK modulated signal is now modulated again using the code sequence, to generate the code

sequencelinear feedback shift register (LFSR)can be used that generates a sequence of n bits and this code sequence generates is clocked by anothernumerically controlled oscillator (NCO)which runs much faster rate than the actual bit rate. The output signal continues to be a binary phase shift modulated signal but now it is modulated by the data and also by code sequence and contains much more transitions of the phase in the output signal and has higher bandwidth, known as a spread spectrum signal (as in relation to a standard modulation, the spectrum of the data now is spread in a larger bandwidth) refer Figure2.8.

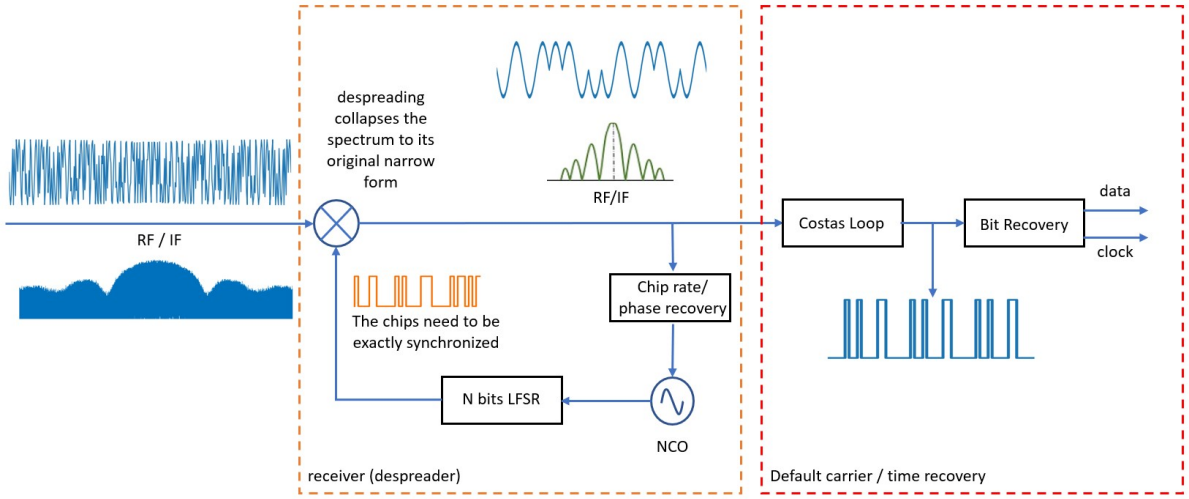

Figure C.7: CDMA BPSK demodulator

For the signal demodulation (FigureC.7) the modulation steps are reversed. To demodulate the spread-spectrum signal is to de-spread the signal to recover its original spectrum and therefore, the original data. The receiver must generate its own code sequence equal to that in the transmitter modulation and additionally generate its sequence exactly in-phase with the received sequence to revert the phase exactly in the same instants it was reversed in the transmitter then removing the code sequence nullifying the spreading effect. The receiver must detect whether it is generating the code sequence exactly in-phase, correct its own generator so it can de-spread the signal and the ideal output of the first mixer in the FigureC.7is theRFsignal modulated only with data. This occurs when the internal generated code sequence is exactly in-phase and exactly aligns with the code sequence used to spread the signal in the transmitter. The resulting de-spreaded signal has the original BPSKsignal and can be further applied to the blocks that may have costas loop to recover the bit string and also bit recovery/bit synchronizer to synchronize with the bit rate and generate the clock of the data.

At this stage, this receiver has two problems:

- it must run with a high sample rate to accommodate theRFsignal,
- it is difficult to recover the code sequence rate and phase, having it imposed on the RFsignal. It is easier to recover and synchronize the code sequence without the carrier present – which is to say the signal was already in the baseband.

A better receiver topology would be one where the spread spectrum signal enters a common quadrature down converter to down-converts the spread spectrum signal to baseband using the oscillator at the carrier frequency. Once the signal is in baseband, its easier to recover the chip rate to de-spread the signal and when de-spreading works efficiently, the signal component I and Q collapse to its original data spectrum and the IQ signal can follow through the costas loop and bit recovery/bit synchronizer. Receiver synchronize its own code sequence generator first using an acquisition phase (FigureC.8) where it acquire the phase of the code searching for all possible phase in a progressive way and once it locks the correct phase of code sequence, it follow the code tracking the difference and mis-aligning and correcting the NCO which generates the code sequence.

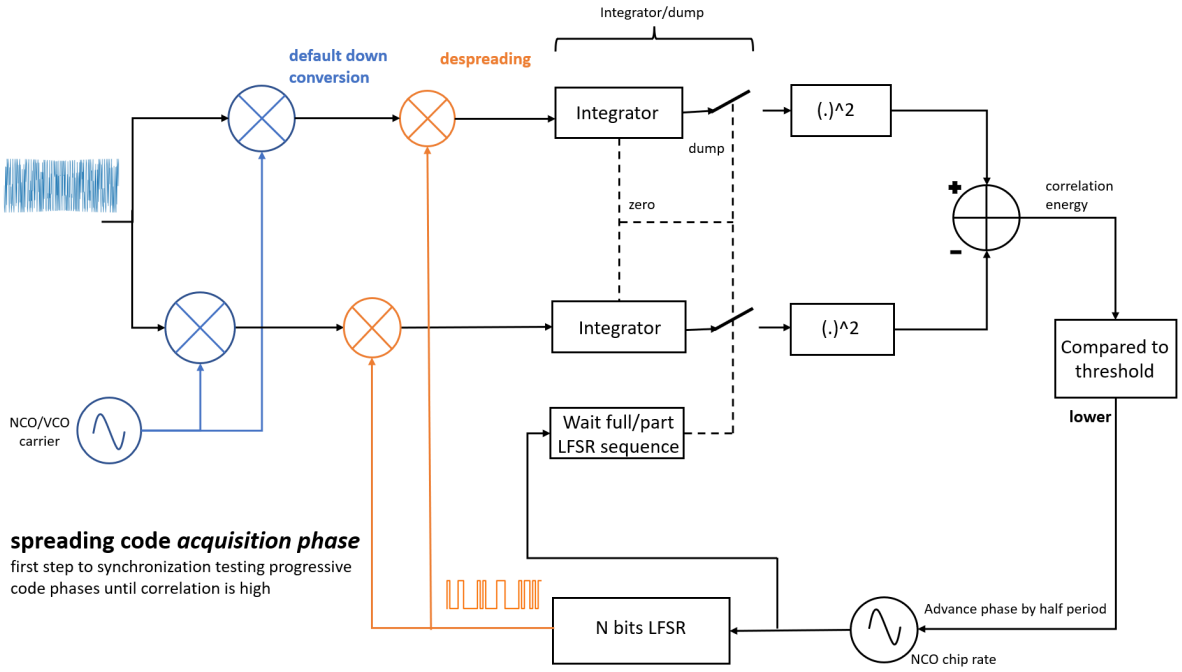

Figure C.8: spread spectrum receiver in acquisition mode

In acquisition mode, the RF signal is first down-converted with IQ mixer and then applied to de-spreading mixers, where a locally generated PN code sequence and then applied to a common correlator block where input signal is correlated with local replica of code sequence. Once the high correlation point is acquired when a local code sequence is aligned with the transmitted code sequence. This is the only point where there is a high probability of the correct data recovery and any misalignment of the local code sequence will generate a noise like signal with correlation zero and mean of the received signal is zero. After the de-spreading, two integrators are going to integrate the signal in the output of the de-spreading mixers. TheNCOgenerates the clock to advance the code sequence generator, and after generating full or partial code sequence, the result of the integrators dumped and the power of the integrators are being measured and decision has been taken if the correlation energy is weather lower than threshold or not. If it is lower than the threshold, the phase of theNCO, generating the chip rate, has been advanced. If the correlation energy is higher than the threshold, code sequence, that is being generated in the receiver, is in-phase with the code sequence received by the receiver and when this happens, receiver moved to tracking mode (FigureC.9) as it acquires the correct phase of the code sequence. This correlator also works as low pass filter, which constantly measures the output of these de-spreading mixers, the energy of IQ is high only if the signal is despreaded correctly otherwise its just a noise.

Now, the signal is only corrected for the small misalignment of the local code sequence with the received code sequence and for tracking, another topology needs to be added for tracking mode, which is nothing but the another pair of correlator for each arm in the receiver. so cleverly, two pair of code sequences are being generated but one is bit advance in time, also known as early code sequence & one is bit late in time, known as delayed code sequence and now at the correlator, again measure the energy of the both and gain the information if the receiver is running faster or the lower. This alignment will generate the positive or negative energy & again feed back to PI controller and that corrects the NCOgenerators inLFSRarms. FigureC.8looks like close-loop system but its a searching mode system, but the FigureC.9is a close-loop system that measures the deviations of the phase of the code sequence and its changing the rate of the twoNCOinLFSRarms.

Now, IQ dump bit streams can be recover using system such as costas loop so further extend the receiver with more blocks shown in the FigureC.10. This is not exactly a costas loop, but surely resembles a costas loop (with just I and Q inputs and signal is already in baseband) and a quadrature rotator that is implementing a common vector rotation using four mixers (pair of mixers for each IQ bit stream). The output of the PI controller in the vactor rotation block, can be directly connected to the input of the receiver with a DAV that generates a correction voltage that can fed directly into analog VCO in the input of

the receiver. This costas loop block will make Q bit stream to zero as BPSK signal only have the energy in the I component. Once the correct I and Q bit stream are collected, the same can further be processed by the Time recovery blocks (only I component needed for BPSK signal) using any time error detector such as garder time error detector and PI controller with its ownNCOgenerating signal with twice as the baud rate. This time recovery system will sample the signal exactly at the bit rate so at the output, 0 or 1 can be recovered [43].

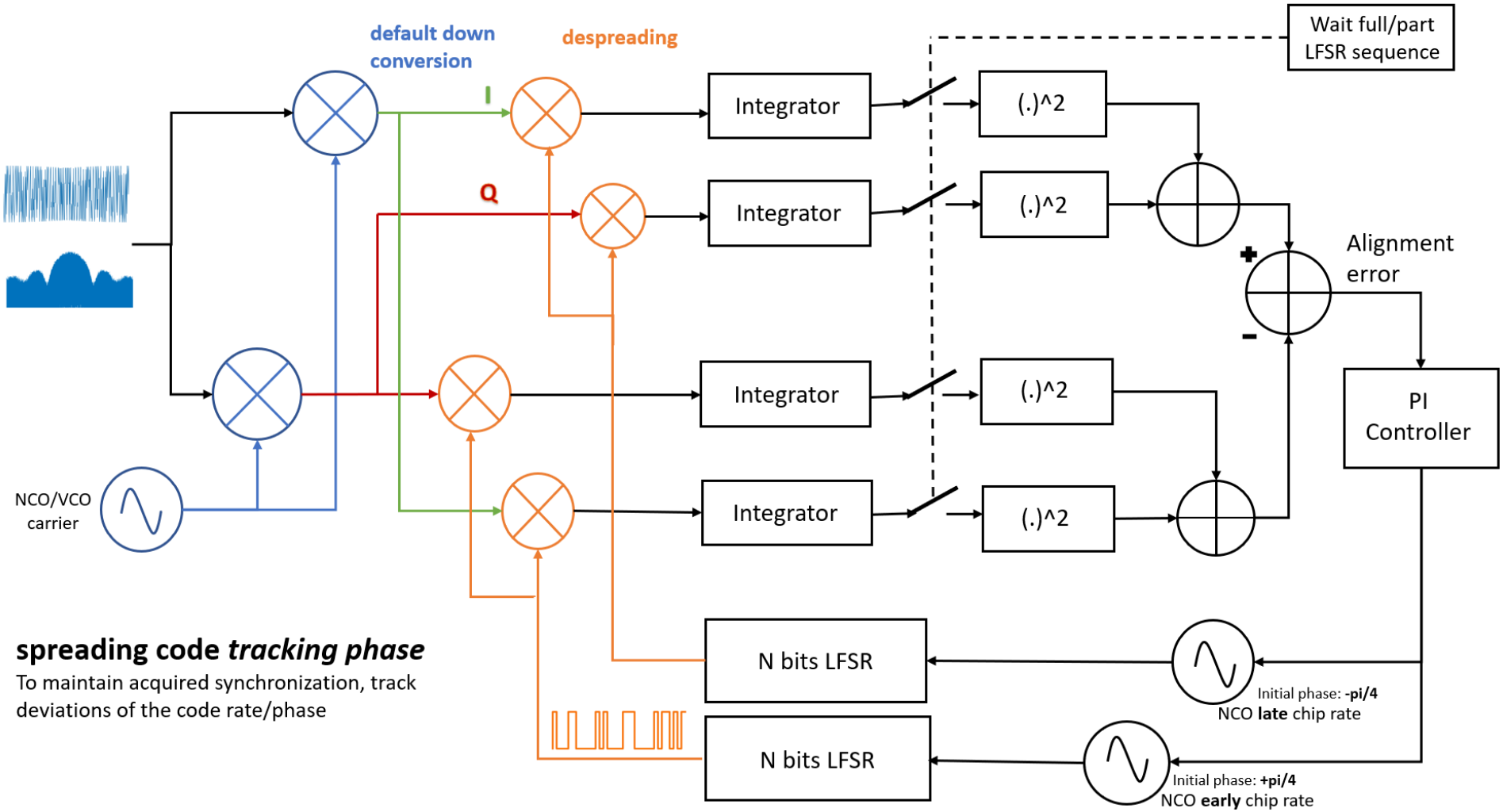

Figure C.9: spread spectrum receiver in tracking mode

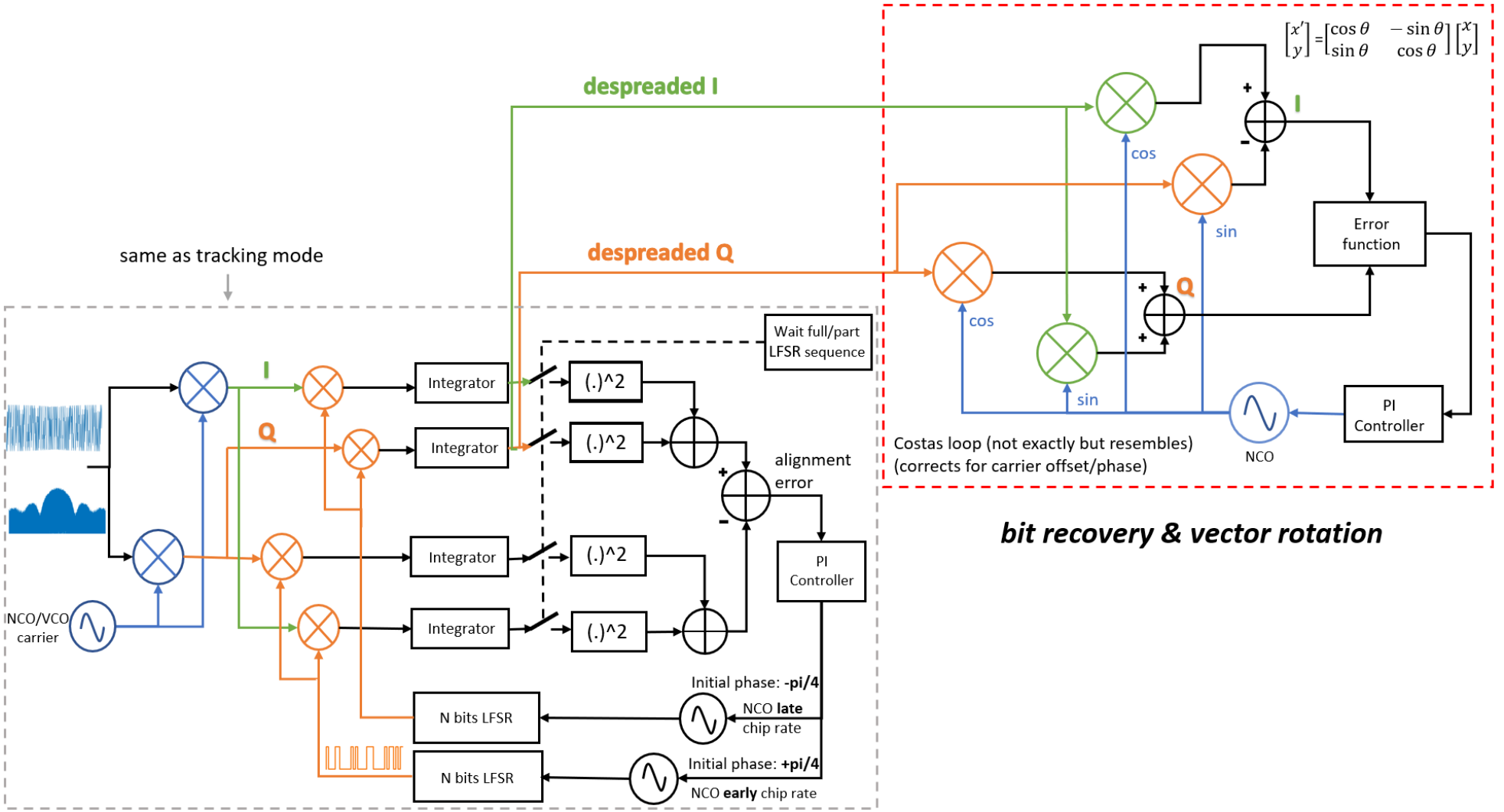

Figure C.10: spread spectrum receiver with a common vector rotation (resembles a costas loop)

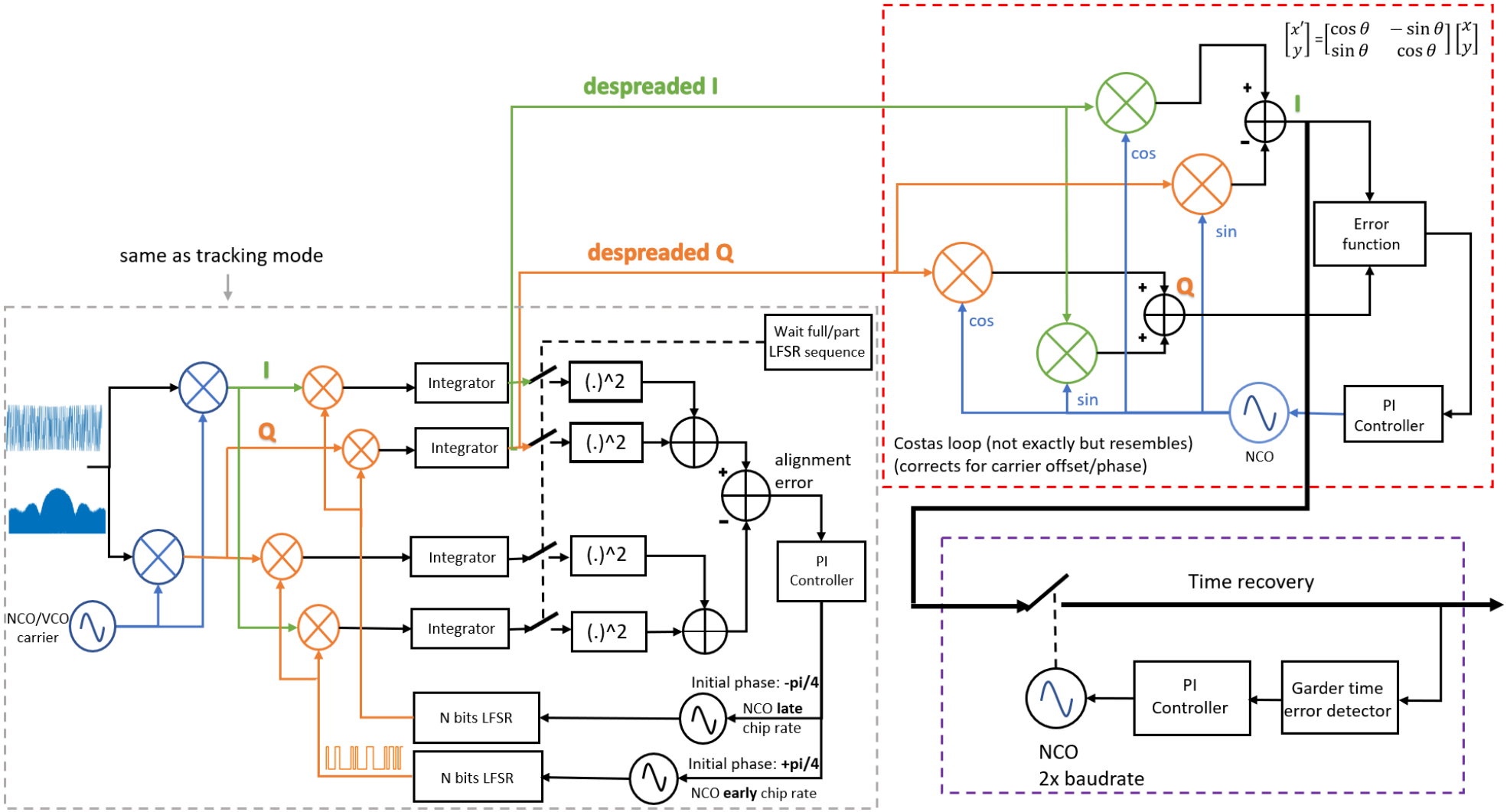

Figure C.11: spread spectrum receiver with a common vector rotation and time recovery blocks

C.3 Practical example

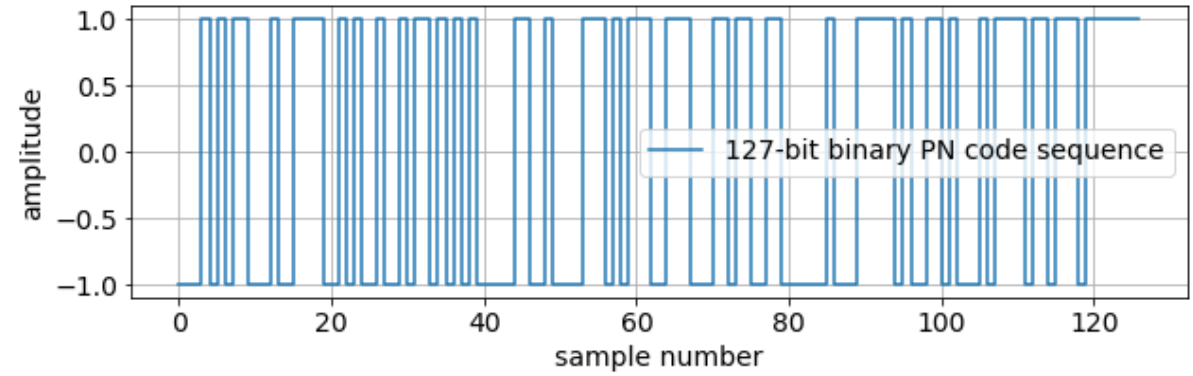

(a)

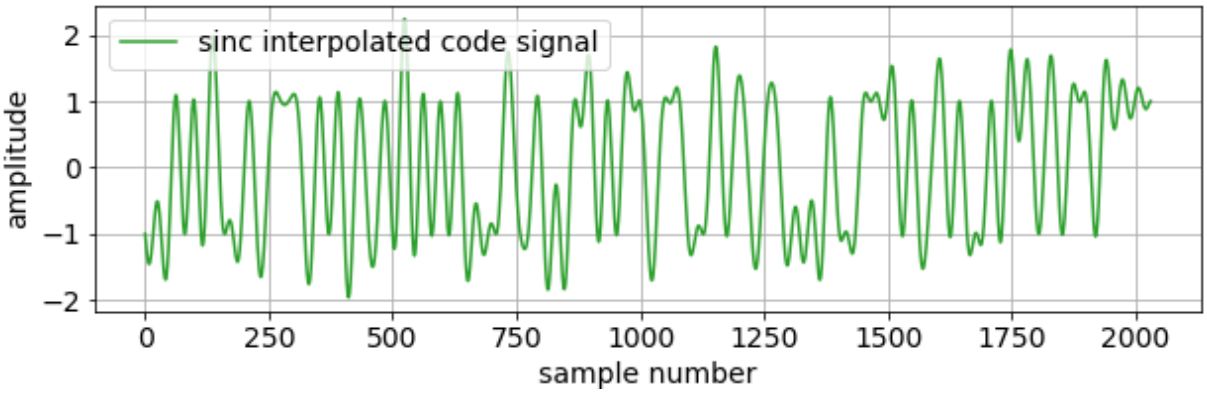

(b)

Figure C.12: (a) samples of 127-bit binary PN Code Sequence, (b) sinc interpolation of the code signal.

To do this first, right PN code-sequence (assume known at receiver) must be generated at receiver side. Assuming 127 bit binary PN code-sequence sequence with bit-mask of 120 and the initial seed value is 80 is used for the illustration purpose (FigureC.12). Assuming subnero modem's bandwidth is 10 KHz then $T_b = BW/$ chip length (e.g. 10 KHz/127 = 78.74), which can be discovered by measuring the spacing between frequencies.

For the testing purpose, a prototype modem is using computer sound card so bandwidth of the same would be around $\simeq$ 3 kHz and base-band sample rate is 48 kilo samples per

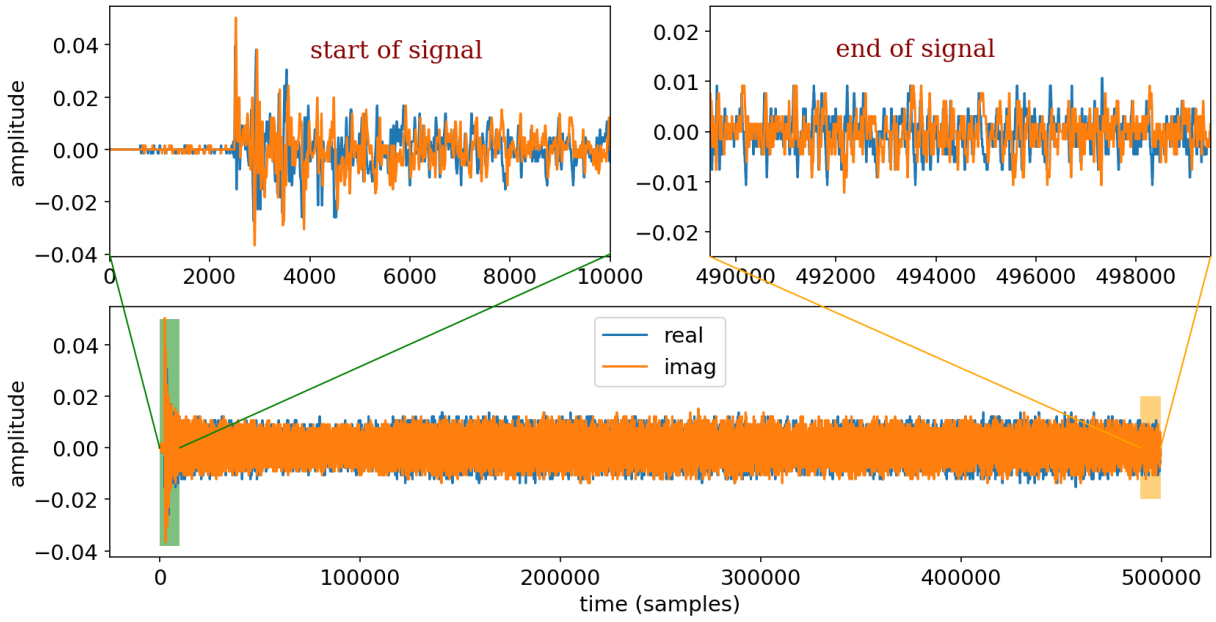

Figure C.13: samples of transmitted data signal, preamble is omitted for better visualization (zoomed in version)

second (symbol rate (T_b)). The number of samples/symbol is given by (48000/23.6 = 2033.8) samples/symbol. The symbol period can be calculated with the reciprocal of the symbol rate (T_b) (1/23.6 = 42.33 milliseconds —symbol rate is also referred to as baud rate.) so the one symbol period of code signal is $\simeq$ 42.33 milliseconds. If the signal is up-sampled by the factor of 16, it almost matches the $127 * 16 = 2032$ samples/symbol and interpolate with sinc function.

Now, the code signal is generated and extracted the baseband signal. The code-signal (built at receiver) cross-correlate with the extracted signal (received off underwater channel). correlation is a simple multiply and accumulate operation and cross-correlate is the code-signal slided forward by 1 sample against the received signal and correlate both. At some point the code-signal aligns with the received signal and at that point a nice spike is shown in the correlate plot (FigureC.14) and samples between correlation peaks are the received symbols. The first largest correlation peak is found and assume that that is the start of the received symbol and pick the next 2032 samples after the first highest peak and then assume that's the next peak and continue the process. After some point, signal will stop correlate with first correlation peak. As the perfect world do not exist and due

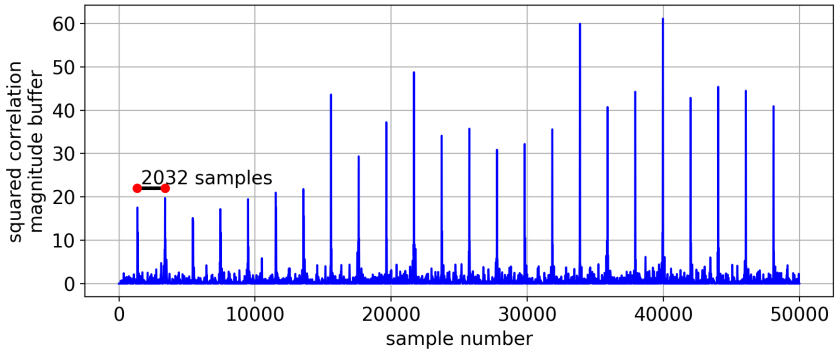

(a)

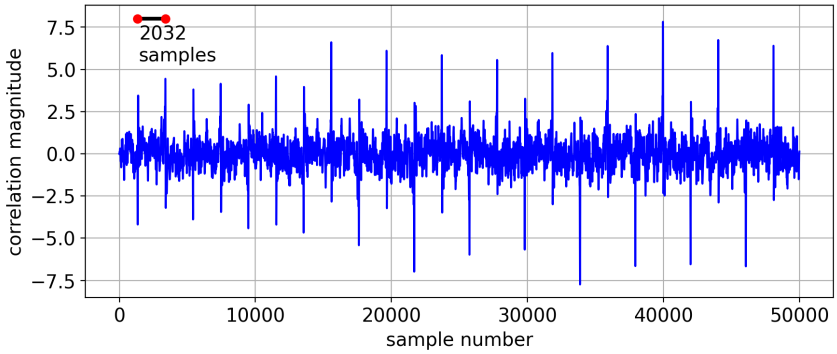

(b)

Figure C.14: (a) slice of the squared correlation magnitude buffer and (b) correlation magnitude buffer for the samples between 100k-150k samples range —this represents the points where the code-signal aligns with the base-band signal in this 50k sample-range. The large spikes, spaced approximately every 2032 samples indicate synchronization

to ambient noise and interference, so checking for the next highest peak at every probable alignment boundary, in this case the highest peak in the next probable alignment boundary (2032 + and - 200 samples).

To de-spread the signal - the code-signal just need to be multiply (i.e. its 2032 samples) with a slice of the received signal i.e. starting at a peak + the next 2032 samples (1 symbol period). Despreading the signal reveals the actual data signal m(t). The despread signal's spectrum can be examined in the FigureC.15, note the multiple frequency bursts and equi-distant tones/frequencies (refer FigureC.14) i.e. each tone is equidistant from the other by $\simeq$ 23.6 Hertz (or 1 symbol rate). An FFT of the real and imaginary components

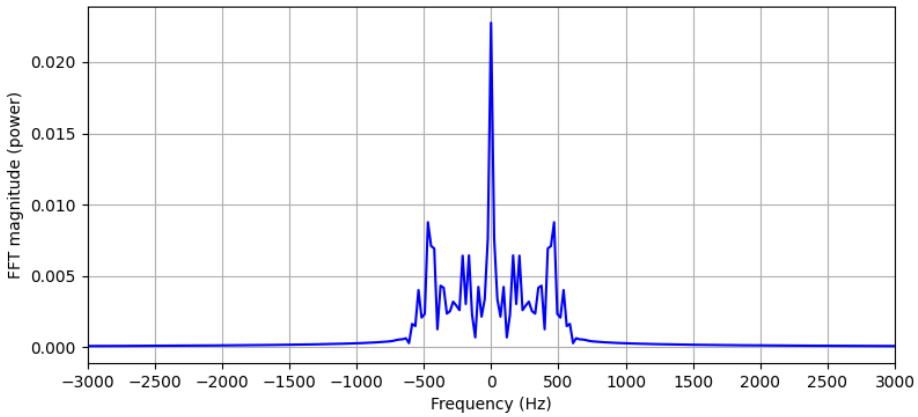

Figure C.15: FFT of the randomly chosen peak (in this case a first peak where correlation is strongest).

separately for each symbol and look for the frequency/tone with the highest energy content. That's the symbol, now decode/map the symbol to the actual data recovery. After the approximation, with sum % 16 <= 4 or >= 13, the symbols need to be hex decoded and the extracted symbols are as follows- $[15, 0, 3, 4, 9, 0, 8, 3, 4]$, remove the first and the last symbol from the sequence and hex decode the remaining (i.e. $0, 3, 4, 9, 0, 8, 3$) which gives 3444867 in decimal. That's the actual data transmitted.

Appendix D

Experimental data and tools used

This appendix presents a detailed account of the experimental setup, equipment, and methodologies adopted in the in-water verification exercises described in Chapter4. A pivotal aspect of ensuring the reliability and accuracy of our experiments lies in the meticulous selection and utilization of specific tools and equipment. Each piece of equipment used plays a crucial role in the successful execution of our experiments, underpinning the validation of the underwater communication protocols developed throughout this thesis. The descriptions provided here aim to offer comprehensive insights into the functionality and contribution of each tool and equipment piece, ensuring a clear understanding of the experimental environment and conditions.

D.1 Equipment and Tools Description

For the in-water verification described in Chapter4, a number of sophisticated tools and equipment was employed. These devices, ranging from advanced underwater modems to precise hydrophones, were integral to conducting the underwater communication tests. Their specifications and roles are enumerated below (refer to section4.2.1and Figure4.11):

1. **PC (Linux) with Python2, Python3, and UnetStack:** A Linux-based PC equipped with both Python2 and Python3 programming environments and UnetStack, a network simulation and development platform tailored for underwater communications [95].

2. **Subnero Underwater Modem (WNC-M25MSS3):** A floating modem designed for wireless underwater communication, capable of transmitting data up to 15,000 bits per second (bps) across frequencies ranging from 18 to 32 kHz. It features software-defined capabilities, including various modulation schemes (PSK, OFDM, FH-BFSK, FSK) and supports Janus standard for underwater acoustic communication. The modem is also designed for low power consumption and high Doppler resilience, making it suitable for dynamic underwater environments [9,57].

3. **Subnero Submerged Nodes (WNC-M25MSN3):** Two submerged nodes part of the Subnero's M25 series, these modems offer similar capabilities as the floating modem, designed for deployment beneath the water surface, facilitating robust underwater acoustic networking and data exchange [9,57].

4. **Ocean Sonics icListen HF Hydrophone (SC2-ETH):** A high-fidelity smart hydrophone capable of capturing a wide frequency range from 10 Hz to 200 kHz. It supports real-time data access, extensive data recording capabilities, and array formation for detailed underwater acoustic studies [47].

5. **Sound Velocity Profiler (SonTek CastAway-CTD E767-CA-CTD):** A compact, hand-deployable instrument for measuring sound speed profiles in the water column. It assists in understanding the underwater acoustic environment, crucial for optimizing communication system performance [26].

6. **Networking Equipment (Router and network switch):** Essential for setting up a local area network (LAN) to connect various components of the underwater communication system, facilitating data exchange and system integration.

7. **24 V DC power supplies:** Three units provided stable power to the underwater modems and other electronic components during the experiments, ensuring consistent performance throughout testing.

D.2 Experimental Data

Transitioning from the tools and equipment that formed the backbone of the experimental setup, this section is dedicated to the data collected during the in-water verification tests. The integrity of the research findings is heavily reliant on the accuracy and reliability of the experimental data collected. Represented by each dataset, a unique set of test conditions and outcomes significantly contributes to the understanding of the underwater

communication system's performance. The results from the comprehensive testing efforts are encapsulated in the following datasets, offering invaluable insights into the system's efficacy and areas for further improvement.

D.2.1 April 27, 2022 Testing

Some of the terms are defined as below :

1. **Noise** : measured ambient noise level (dB full scale).
2. **SNR**: It is calculated as follows: transmitted power / noise power. The transmitted power was determined from power level set on modem (in dB).
3. **RSSI(Received Signal strength Indicator)** : Received signal strength (dB full scale), it mentions that RSSI is a measure of the power level that an RF device, such as Wi-Fi, is receiving from the access point. In underwater communication contexts, RSSI would be the power level of the received acoustic signal.
4. **Signal fidelity** : Signal fidelity measures how well the received premable matches a transmitted preamble after passing through the channel.
5. **BER** : Divide the total number of bit errors by the total number of bits transmitted to calculate the Bit Error Rate.
6. **Commmunication quality** : Communication quality measures the mutual information between transmitted and received bits, and is estimated from bit error rate (BER) measurements before error correction.
7. **Throughput** : Throughput is the average number of bits of user data transmitted through the channel per unit time.
8. **Normalized Throughput**: The normalized throughput of the network is measured as the total number of bits of information successfully received by all nodes in the network per unit time, normalized by data rate.
9. **CFO(Carrier Frequency Offset)** : CFO is the difference between the received carrier frequency and the expected carrier frequency. CFO is estimated using known preamble or pilot sequences in the transmitted signal.

Testing Datasets

location : Aquatron, Dalhousie University (Figure3.26),
salinity : 28.2 at 19 °C, humidity : 22.8 %, temperature : 9.2 °C,
surface node (node address : 204) : at 2 m depth,
underwater node 1 (node address : 148) : at 1.6 m depth,
underwater node 2 (node address : 93) : at 2.36 m depth.

Table D.1: communication channel test results dataset 1

key	value
Noise Level (in dB)	-72
signal Strength	-19
signal Fidelity	61%
communication quality	40%
Throughput	1277 bps

Table D.2: testing dataset 1, Transmitted Frame : 10 from surface node, detection threshold : 0.25 on underwater node 1 (node address : 148)

	Frame 1	**Frame 2**	**Frame 3**	**Frame 4**	**Frame 5**	**Frame 6**	**Frame 7**	**Frame 8**	**Frame 9**	**Frame 10**
Detector Rx Thresh-old	0.6	0.53	0.56	0.58	0.57	0.61	0.58	0.55	0.6	0.57
RSSI	-19	-19.1	-19.2	-19	-19.1	-19	-18.9	-19	-19.2	-19.1
CFO	0.000058	0	0	0.000058	0.000058	0.000058	0.000058	0.000058	0.000058	0
BER	979/6630	991/6630	1007/6630	965/6630	953/6630	994/6630	972/6630	968/6630	993/6630	1011/6630
BER	0.147662	0.149472	0.151885	0.145551	0.143741	0.149925	0.146606	0.146003	0.149774	0.152489
Total Bytes Tx	128 bytes	128 bytes	128 bytes	128 bytes	128 bytes	128 bytes	128 bytes	128 bytes	128 bytes	128 bytes
Bad Frame	No	No	No	No	No	No	No	No	No	No

Table D.3: communication channel test results dataset 2

key	value
Noise Level (in dB)	-72
signal Strength	-19
signal Fidelity	61%
communication quality	40%
Throughput	1277 bps

Table D.4: testing dataset 2, Transmitted Frame count : 10 from surface node, detection threshold : 0.25 on underwater node 2 (node address : 93)

	Frame 1	**Frame 2**	**Frame 3**	**Frame 4**	**Frame 5**	**Frame 6**	**Frame 7**	**Frame 8**	**Frame 9**	**Frame 10**
Detector Rx Thresh-old	00.27	0.26	0.25	0.25	0.25	0.26	0	0	0	0
RSSI	-21.5	-21.5	-21.4	-21.5	-21.5	-21.7	0	0	0	0
CFO	NaN	0	0	0	NaN	NaN	NaN	NaN	NaN	NaN
BER	6630/6630	1191/6630	1114/6630	965/6630	6630/6630	6630/6630	6630/6630	6630/6630	6630/6630	6630/6630
BER	1	0.179638	0.168024	0.145551	1	1	NaN	NaN	NaN	NaN
Total Bytes Tx	133 bytes	128 bytes	128 bytes	128 bytes	133 bytes	133 bytes	0 bytes	0 bytes	0 bytes	0 bytes
Bad Frame	Yes	No	No	No	Yes	Yes	Not Re-ceived	Not Re-ceived	Not Re-ceived	Not Re-ceived

Table D.5: communication channel test results dataset 3

key	value
Noise Level (in dB)	-72
signal Strength	-19
signal Fidelity	61%
communication quality	40%
Throughput	1281 bps

Table D.6: testing dataset 3, Transmitted Frame count : 10 from surface node, detection threshold : 0.25 on underwater node 1 (node address : 148)

	Frame 1	**Frame 2**	**Frame 3**	**Frame 4**	**Frame 5**	**Frame 6**	**Frame 7**	**Frame 8**	**Frame 9**	**Frame 10**
Detector Rx Thresh-old	00.56	0.6	0.61	0.58	0.59	0.54	0.54	0.58	0.56	0.55
RSSI	-19	-19	-19	-19	-19	-19	-18.9	-18.9	-19	-18.8
CFO	0	0.000058	0.000058	0.000058	0.000058	0.000058	0	0.000058	0.000058	0.000058
BER	980/6630	932/6630	994/6630	963/6630	970/6630	959/6630	986/6630	952/6630	977/6630	980/6630
BER	0.147813	0.140573	0.149925	0.145249	0.146305	0.144646	0.148718	0.14359	0.14736	0.147813
Total Bytes Tx	128 bytes	128 bytes	128 bytes	128 bytes	128 bytes	128 bytes	128 bytes	128 bytes	128 bytes	128 bytes
Bad Frame	No	No	No	No	No	No	No	No	No	No

Table D.7: communication channel test results dataset 4

key	value
Noise Level (in dB)	-74
signal Strength	-22
signal Fidelity	25%
communication quality	31%
Throughput	317 bps

Table D.8: testing dataset 4, Transmitted Frame count : 10 from surface node, detection threshold : 0.25 on underwater node 2 (node address : 93)

	Frame 1	**Frame 2**	**Frame 3**	**Frame 4**	**Frame 5**	**Frame 6**	**Frame 7**	**Frame 8**	**Frame 9**	**Frame 10**
Detector Rx Thresh-old	0.25	0.25	0	0	0	0	0	0	0	0
RSSI	-21.7	-21.6	-21.4	-21.5	-21.5	-21.7	0	0	0	0
CFO	NaN	0	0	0	NaN	NaN	NaN	NaN	NaN	NaN
BER	6630/6630	1217/6630	1114/6630	965/6630	6630/6630	6630/6630	6630/6630	6630/6630	6630/6630	6630/6630
BER	NaN	0.18356	NaN	NaN	NaN	NaN	NaN	NaN	NaN	NaN
Total Bytes Tx	133 bytes	128 bytes	0 bytes	0 bytes	0 bytes	0 bytes	0 bytes	0 bytes	0 bytes	0 bytes
Bad Frame	Yes	No	Not Re-ceived	Not Re-ceived	Not Re-ceived	Not Re-ceived	Not Re-ceived	Not Re-ceived	Not Re-ceived	Not Re-ceived

Table D.9: communication channel test results dataset 5

key	value
Noise Level (in dB)	-72
signal Strength	-19
signal Fidelity	59%
communication quality	39%
Throughput	1281 bps

Table D.10: testing dataset 5, Transmitted Frame count : 10 from surface node, detection threshold : 0.25 on underwater node 1 (node address : 148)

	Frame 1	**Frame 2**	**Frame 3**	**Frame 4**	**Frame 5**	**Frame 6**	**Frame 7**	**Frame 8**	**Frame 9**	**Frame 10**
Detector Rx Thresh-old	00.26	0.53	0.53	0.58	0.59	0.51	0.56	0.56	0.54	0.52
RSSI	-19	-19	-18.9	-18.9	-19	-18.9	-18.9	-18.9	-18.9	-18.8
CFO	0.000058	0	0	0.000058	0.000058	0.000058	0.000058	0.000058	0.000058	0.000058
BER	982/6630	976/6630	1009/6630	939/6630	973/6630	933/6630	975/6630	977/6630	1028/6630	1044/6630
BER	0.148115	0.14721	0.152187	0.141629	0.146757	0.140724	0.147059	0.14736	0.155053	0.157466
Total Bytes Tx	128 bytes	128 bytes	128 bytes	128 bytes	128 bytes	128 bytes	128 bytes	128 bytes	128 bytes	128 bytes
Bad Frame	No	No	No	No	No	No	No	No	No	No

Table D.11: communication channel test results dataset 6

key	value
Noise Level (in dB)	-74
signal Strength	-22
signal Fidelity	26%
communication quality	0%
Throughput	0 bps

Table D.12: testing dataset 6, Transmitted Frame count : 10 from surface node, detection threshold : 0.25 on underwater node 2 (node address : 93)

	Frame 1	**Frame 2**	**Frame 3**	**Frame 4**	**Frame 5**	**Frame 6**	**Frame 7**	**Frame 8**	**Frame 9**	**Frame 10**
Detector Rx Thresh-old	0.26	0	0	0	0	0	0	0	0	0
RSSI	-21.7	0	0	0	0	0	0	0	0	0
CFO	NaN	NaN	NaN	NaN	NaN	NaN	NaN	NaN	NaN	NaN
BER	6630/6630	6630/6630	6630/6630	6630/6630	6630/6630	6630/6630	6630/6630	6630/6630	6630/6630	6630/6630
BER	1	NaN	NaN	NaN	NaN	NaN	NaN	NaN	NaN	NaN
Total Bytes Tx	133 bytes	0 bytes	0 bytes	0 bytes	0 bytes	0 bytes	0 bytes	0 bytes	0 bytes	0 bytes
Bad Frame	Yes	Not Re-ceived	Not Re-ceived	Not Re-ceived	Not Re-ceived	Not Re-ceived	Not Re-ceived	Not Re-ceived	Not Re-ceived	Not Re-ceived

D.2.2 Aug, 2022 Testing

Table D.13: Aug 4, 2022 full-duplex single node configuration experimental data

noise power(dB)	signal power(dB)	SNR	BER	Throughput (in bps)	channel quality	RSSI
-68.0	0	68.0	0.042534	40	75	-0.9
-68.0	-5	60.0	0.032127	207	80	-0.9
-64.0	-5	59.0	0.034389	183	78	-1.0
-65.0	-10	55.0	0.034087	202	79	-1.0
-68.0	-15	53.0	0.031222	183	80	-1.0
-68.1	-20	48.1	0.023228	204	84	-1.1
-67.0	-25	42.0	0.020664	207	85	-1.1
-65.0	-30	35.0	0.021267	28	85	-1.1
-64.0	-35	29.0	0.021569	198	85	-1.2
-65.0	-40	25.0	0.024736	190	83	-1.1
-64.0	-45	19.0	0.030618	201	80	-1.1
-67.0	-55	12.0	0.030317	205	80	-1.2
-68.0	-62	6.0	0.040875	219	75	-1.2
-64.0	-64	0.0	0.045098	31	70	-0.9
-67.0	-70	-3.0	0.031825	193	80	-1.3
-64.0	-72	-8.0	0.022021	201	85	-1.5
-68.0	-90	-12.0	0.010407	135	90	-11.6
-68.0	-92	-14.0	0.052790	161	70	-13.1
-70.0	-92	22.0	0.056561	236	71	-30.1

Table D.14: Aug 4, 2022 two node configuration experimental data, Note that channel quality measured is at Receiver.

noise power(dB)	signal power(dB)	SNR	BER	Throughput (in bps)	channel quality	RSSI	
-74	-30	43	0.074359	342	35	-56.1	
-66	-20	46	0.080694	303	32	-57.6	
-74	-25	49	0.155656	142	30	-58.0	
-74	-20	54	0.151131	1265	37	-50.0	
-74	-15	59	0.175264	242	33	-41.7	
-74	-15	59	0.079186	90	60	-50.6	
-74	-10	64	0.121719	1135	47	-38.6	
-74	-5	69	0.109201	1035	47	-30.2	
-74	-25	49	0.138487	70	47	-56.9	
-74	-25	49	0.154902	139	40	-58.5	
-74	-35	39	0.144987	92	43	57.3	

Table D.15: Aug 8, 2022 two node configuration experimental data

noise power(dB)	signal power(dB)	SNR	BER	Throughput (in bps)	channel quality	RSSI	CFO	
-70	-5	65	0.168326	88	35	-40.5	0.000058	
-66	-20	46	0.080694	303	32	-57.6	0.000117	
-74	-25	49	0.155656	142	30	-58.0	0.000000	
-74	-20	54	0.151131	1265	37	-50.0	0.000000	

D.2.3 Oct, 2022 Testing

Table D.16: Aug 10, 2022 three node configuration experimental data

noise power(dB)	signal power(dB)	SNR	BER	Throughput (in bps)	channel quality	RSSI	CFO	
-67	-12	55	0.103469	434	67	-44.9	0.000058	
-63	-11	52	0.101508	43	76	-50.4	0.000058	
-56	-11	45	0.164253	535	53	-47.6	0.000058	
-68	-13	55	0.111161	75	50	-44.1	0.000000	
-67	-13	54	0.025641	1092	92	-37.8	0.000058	
-70	-25	45	0.088989	11	78	-58.4	0.000058	
-72	-30	42	0.121719	11	78	-58.4	0.000058	
-72	-32	40	0.119608	78	47	-60.2	0.000058	
-72	-33	39	0.156712	90	37	-65.2	0.000058	
-71	-12	59	0.009502	477	96	-41.2	0.000170	
-66	-12	54	0.022021	412	66	-37.6	0.000058	
-67	-13	54	0.015385	283	57	-38.5	0.000170	

Table D.17: experimental data, combining all trial data from month of Aug

Throughput	channel quality	SNR	BER	RSSI	CFO
40	75	-14.0	0.053	-13.1	0.000e+00
207	80	-12.0	0.010	-11.6	0.000e+00
183	78	-8.0	0.022	-1.5	0.000e+00
202	79	-3.0	0.032	-1.3	0.000e+00
183	80	0.0	0.045	-0.9	0.000e+00
204	84	6.0	0.041	-1.2	0.000e+00
207	85	16.0	0.030	-1.2	0.000e+00
28	85	19.0	0.031	-1.1	0.000e+00
198	85	25.0	0.025	-1.1	0.000e+00
190	83	29.0	0.022	-1.2	0.000e+00
201	80	35.0	0.021	-1.1	0.000e+00
205	80	39.0	0.157	-65.2	5.800e-05
219	75	40.0	0.120	-60.2	5.800e-05
31	70	42.0	0.021	-1.1	0.000e+00
193	80	42.0	0.122	-58.4	5.800e-05
201	85	45.0	0.140	-58.0	0.000e+00
135	90	45.0	0.164	-47.6	5.800e-05
161	70	45.0	0.089	-58.4	5.800e-05
1236	71	46.0	0.081	-57.6	0.000e+00
142	30	48.1	0.023	-1.1	0.000e+00
1265	37	49.0	0.156	-58.0	0.000e+00
242	33	49.0	0.139	-56.9	0.000e+00
90	60	49.0	0.155	-58.5	0.000e+00
1135	47	50.0	0.090	-54.3	1.170e-04
1035	47	52.0	0.102	-50.4	5.800e-05
70	47	53.0	0.031	-1.0	0.000e+00
139	40	54.0	0.151	-50.0	0.000e+00
88	35	54.0	0.026	-37.8	5.800e-05
209	34	54.0	0.022	-37.6	5.800e-05
434	27	54.0	0.015	-38.5	1.170e-04
43	67	55.0	0.034	-1.0	0.000e+00
535	70	55.0	0.103	-44.9	5.800e-05
75	76	55.0	0.111	-44.1	0.000e+00
1092	53	59.0	0.034	-1.0	0.000e+00
11	50	59.0	0.175	-41.7	0.000e+00
12	92	59.0	0.079	-50.6	0.000e+00
78	78	59.0	0.010	-41.2	1.170e-04
90	78	60.0	0.032	-0.9	0.000e+00
0	47	64.0	0.122	-38.6	0.000e+00
0	37	65.0	0.168	-40.5	5.800e-05
0	35	68.0	0.043	-0.9	0.000e+00
0	40	69.0	0.109	-30.2	0.000e+00
0	42	72.0	0.057	-30.1	0.000e+00

Table D.18: Experimental data from St. Margret's Bay where two nodes were placed 55 m apart; one remained stationary while the other was towed by a boat.

Timestamp	SNR	channel quality	BER	RSSI	Throughput	CFO
17:49	8	71	0.163499	-50.1	12	0.000000
17:52	32	60	0.067270	-53.4	12	0.000000
17:53	24	68	0.050075	-54.8	15	0.000000
17:54	19	68	0.060483	-54.5	14	0.000000
17:55	20	68	0.060483	-54.5	14	0.000000
17:56	39	54	0.058371	-54.9	12	0.000058
17:57	44	74	0.060483	-54.5	23	0.000000
17:59	49	68	0.051433	-54.8	13	0.000000
17:59	54	69	0.064404	-54.9	13	0.000058
18:00	59	40	0.053997	-53.9	22	0.000000
18:01	64	45	0.062594	-54.9	18	0.000000
18:02	65	48	0.058673	-54.9	20	0.000000

Table D.19: Experimental data from St. Margret's Bay where two nodes were placed 100 m apart; one remained stationary while the other was towed by a boat.

Timestamp	SNR	BER	channel quality	Throughput	RSSI	CFO
16:10	40	0.13194	NA	NA	-55.3	0.000058
16:12	43	0.032407	NA	NA	-55	0.000058
16:13	45	0.030093	NA	NA	-54.8	0.000058
16:15	46	0.048611	NA	NA	-53.5	0
16:16	50	0.048611	NA	NA	-53.6	0.000058
16:17	55	0.06713	NA	NA	-54	0
16:20	63	0.055556	NA	NA	-53.6	0.000058
16:21	72	0.909722	NA	NA	-54	0.000058

Table D.20: Experimental data from St. Margret's Bay where two nodes were placed 359 m apart; one remained stationary while the other was towed by a boat.

Timestamp	SNR	BER	channel quality	RSSI	Throughput	CFO
16:51	38	0.156561	NA	NA	NA	NA
16:53	40	0.189291	NA	NA	NA	NA
16:56	48	0.160633	NA	NA	NA	NA
17:01	49	0.168929	NA	NA	NA	NA
17:06	54	0.192006	NA	NA	NA	NA

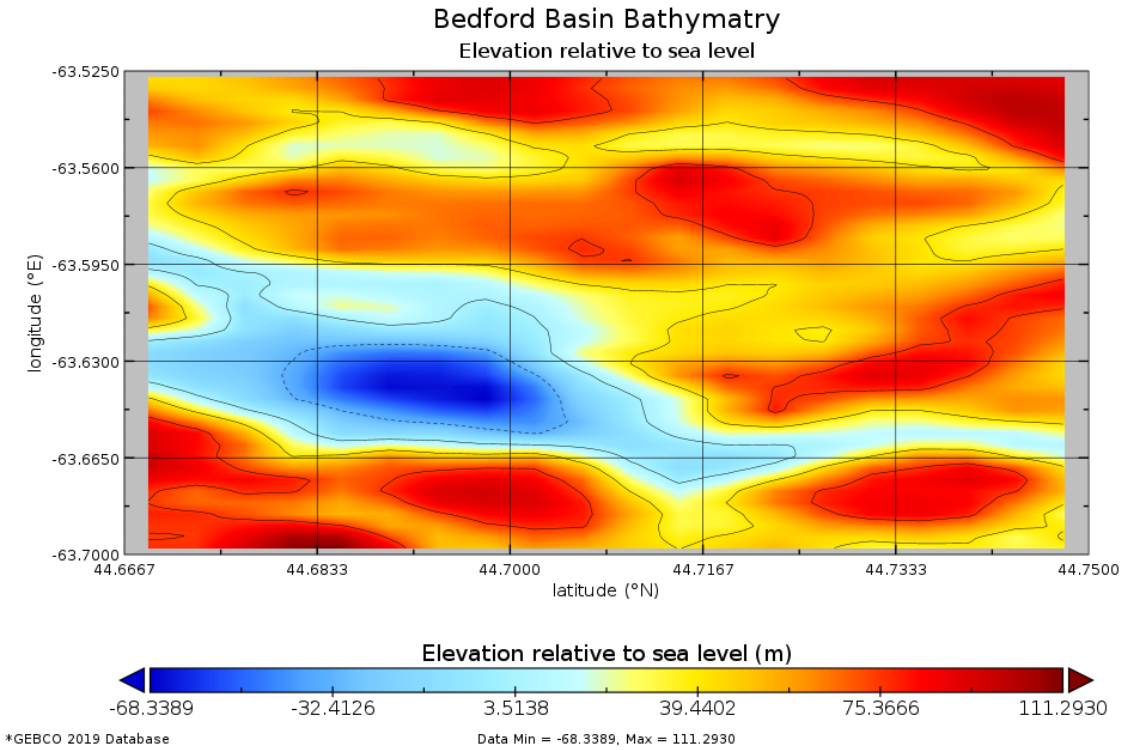

Figure D.1: Bedford Basin Bathymetry fromGEBCO2019 database, elevation relative to sea level (Halifax approaching near N-44.74834442138672, S-44.66629028).

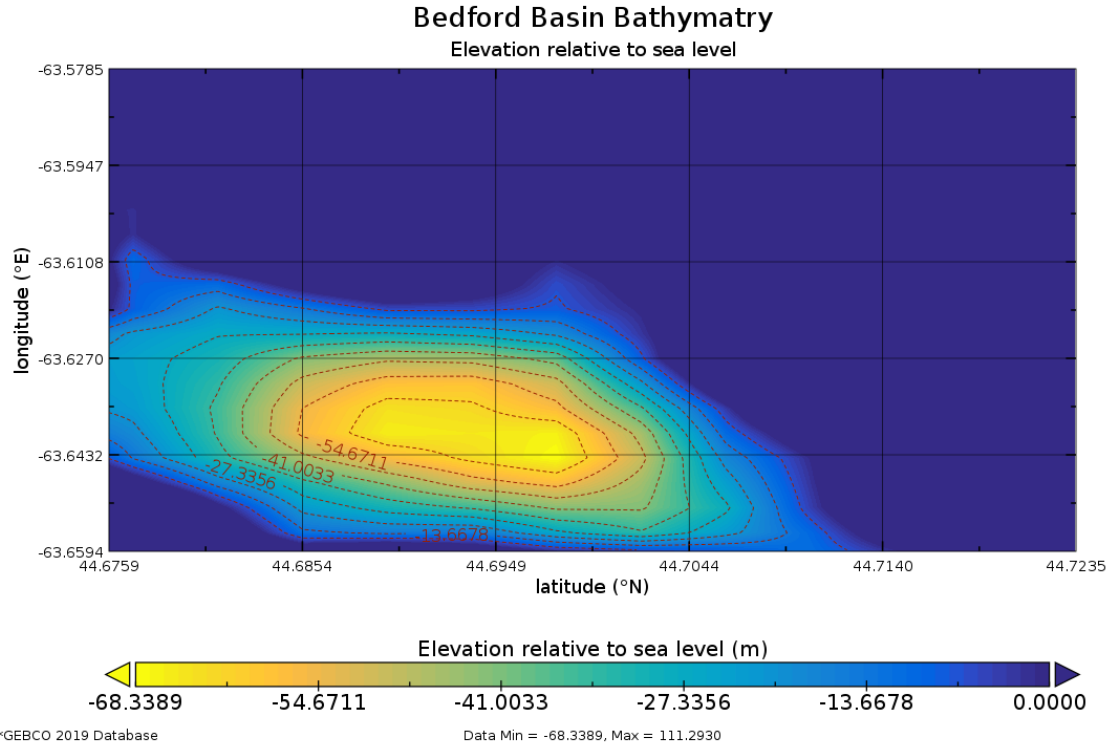

Figure D.2: Contours – Bedford Basin Bathymetry fromGEBCO2019 database, elevation is not shown here for better visualization (Halifax approaching near N-44.74834442138672, S-44.66629028).